Dissertation
submitted tothe
Combined Faculties for the Natural Sciences and for Mathematics
of the Ruperto-Carola University of Heidelberg, Germany
for the degree of
Doctor of Natural Sciences

presented by

MSc., Livia Marrone
born in: Palermo, Italy
Oral-examination: 28th November 2017

Plasticity of a prefrontal microcircuit during social defeat

Referees: Dr. Paul Heppenstall
Prof. Christoph Schuster

Abstract

The prefrontal cortex (PFC) is a critical brain area for behavioral flexibility and plays an important role in moderating social behavior and decision making in response to a changing environment. Our lab recently demonstrated that inhibition of projections from the PFC to the dorsal periaqueductal grey (dPAG), a structure involved in defensive behavior, elicits social avoidance in mice. Furthermore, in the PFC of animals which underwent social defeat, the amplitude of the synaptic response to mediodorsal thalamus (MDT) stimulation is significantly decreased (Franklin et al, 2017). The aim of this study was to investigate the molecular mechanisms underlying the weakening of the PFC and the acquisition of social avoidance after the defeat. Using translating ribosome affinity purification (TRAP), we demonstrated that social defeat induces differential changes in excitatory and inhibitory neuronal subpopulations of the PFC. No significant gene expression changes were detected in glutamatergic ($Camk2a^+$) neurons. $Pvalb^+$ interneurons, instead, showed decreased expression of genes related to presynaptic release and neuronal excitability and Sst^+ interneurons showed increased expression of genes related to cytoskeleton and axonal growth. Using reporter mice expressing green fluorescent protein (GFP) exclusively in Sst^+ neuronal boutons, we confirmed that these neurons make increased presynaptic contacts in PFC layer I after social defeat, consistent with the observed gene expression changes. In the meantime, we investigated postsynaptic plasticity in glutamatergic PFC-dPAG neurons using a novel tool that exploits SNAP-tag technology to label surface α-amino-3-hydroxy-5-methyl-4-isoxazolepropionic acid receptors (AMPARs) *in vivo* after behavior. Using this tool we found that PFC-dPAG neurons of defeated mice downregulate surface AMPARs at layer I excitatory inputs, the precise region where Sst^+ neurons show increased inhibitory contacts. Selective pharmacogenetic inhibition of Sst^+ neurons during social defeat was sufficient to impair the acquisition of social avoidance, arguing for a potential role of Sst^+ inputs in facilitating layer I PFC excitatory synaptic plasticity. In conclusion, we examined transcriptional, structural, and synaptic plasticity mechanisms occurring in the PFC in response to social defeat and identified an essential role for Sst^+ neurons in the acquisition of social avoidance behavior. Furthermore, we established a novel technique to image synaptic plasticity by *in vivo* labeling of surface AMPA receptors that will have broad application in behavioral circuit neuroscience research.

Zusammenfassung

Der präfrontale Cortex (PFC) ist eine Gehirnregion, die entscheidend für die Anpassungsfähigkeit des Verhaltens ist und eine wichtige Rolle bei der Wahl der Verhaltensstrategie in Abhängigkeit einer sich verändernden Umwelt spielt. Vor kurzem hat unsere Forschungsgruppe gezeigt, dass die Inhibierung von Neuronen, die vom PFC in das periaquäduktale Grau (*dorsal periaqueductal grey*, dPAG), einer Struktur im Gehirn, die in das Verteidigungsverhalten involviert ist, projizieren, das Vermeiden von sozialen Interaktionen (*social avoidance*) auslöst. Zudem ist bei einer Stimulation durch den mediodorsalen Thalamus (MDT) das exzitatorische postsynaptische Potential im PFC in Tieren signifikant verringert, die zuvor eine traumatisierende soziale Interaktion (*social defeat*) hatten (Franklin et al., 2017). Das Ziel dieser Studie ist es, die molekularen Mechanismen zu untersuchen, die nach einer traumatisierenden sozialen Interaktion (*social defeat*) die Schwächung des PFC und den Erwerb sozialen Vermeidungsverhaltens (*social avoidance*) verursachen. Unter Verwendung der *translating ribosome affinity purification* (TRAP) Methode konnten wir zeigen, dass *social defeat* spezifische Veränderungen in bestimmten exzitatorischen und inhibitorischen Klassen von Neuronen des PFC induziert. In der Klasse der exzitatorischen Camk2a^{+} Neuronen wurden keine signifikanten Genexpressionsunterschiede gemessen. Bei Pvalb^{+} Interneuronen hingegen ist die Expression von Genen verringert, die mit der präsynaptischen Freisetzung von Neurotransmitttern oder der Erregbarkeit von Neuronen assoziiert werden können und in Sst^{+} Interneuronen sind Gene höher exprimiert, die mit dem Zellskelett oder dem Wachstum von Axonen assoziiert sind. Mit Hilfe einer transgenen Maus, die grün fluoreszierendes Protein (*green fluorescent protein*, GFP) ausschließlich in den präsynaptischen Endigungen der Sst^{+} Neuronen exprimiert, wurde im Einklang mit den beobachteten Genexpressionsveränderungen gezeigt, dass diese Neuronen in Folge eines *social defeat* eine höhere Zahl an präsynaptischen Endigungen in der Schicht I des PFC aufweisen. Des Weiteren haben wir mit einer neuen, auf der SNAP-tag Technologie basierenden Methode die postsynaptische Plastizität in exzitatorischen Neuronen untersucht. Bei dieser Methode werden die in der Zelloberfläche lokalisierten AMPA Rezeptoren (*α-amino-3-hydroxy-5-methyl-4-isoxazolepropionic acid*) in vivo markiert und nach dem Verhaltensexperiment werden diese Rezeptoren ex vivo visualisiert. Mit dieser Methode konnten wir bei Mäusen nach einer traumatisierenden sozialen Interaktion (*social defeat*) in der Schicht I des PFC eine verringerte Anzahl der in

der Zelloberfläche lokalisierten AMPA Rezeptoren, die zu den PFC-dPAG Neuronen gehören, beobachten. Die Schicht I ist genau die Region, in der Sst^+ Neuronen eine erhöhte Anzahl inhibitorischer präsynaptischer Endigungen aufweisen. Die spezifische pharmakogenetische Inhibierung von Sst^+ Neuronen während eines s*ocial defeat* stört die Induzierung des sozialen Vermeidungsverhaltens (*social avoidance*). Dies spricht für eine mögliche Rolle von Sst^+ Neuronen in Bezug auf die Plastizität der exzitatorischen Synapsen in der Schicht I des PFC. Zusammenfassend haben wir Plastizitätsmechanismen auf der Ebene der Morphologie, der Transkripte und der Synapsen untersucht, die als Reaktion auf eine traumatisierende soziale Interaktion (*social defeat*) im PFC auftreten. In diesem Zusammenhang spielen Sst^+ Neuronen eine essentielle Rolle beim Erwerb sozialen Vermeidungsverhaltens (*social avoidance*). Darüber hinaus haben wir ein neues Verfahren etabliert, bei dem in der Zelloberfläche lokalisierte AMPA-Rezeptoren in vivo markiert werden und welches es ermöglicht, die synaptische Plastizität zu visualisieren. Dieses Verfahren bietet den Neurowissenschaften weitreichende Einsatzmöglichkeiten bei der Erforschung von C*ircuits* und Verhalten.

Table of contents

Table of figures

Table of abbreviations

AAV	Adenoassociated Virus
AMPAR	α-Amino-3-hydroxy-5-Methyl-4-isoxazole Propionic Acid Receptor
ASD	Autism Spectrum Disorder
BG	Benzylguanine
BLA	Basolateral Amygdala
CAMK2A	Calcium/calmodulin-dependent protein Kinase 2a
CG	Cingulate
CSPG	Chondroitin Sulfate Proteoglycan
dPAG	Dorsal Periaqueductal Grey
DRN	Dorsal Raphe Nucleus
HSPG	Heparan Sulfate Proteoglycan
HSV	Herpes Simplex Virus
IL	Infralimbic
LFP	Local Field Potential
LTD	Long Term Depression
LTP	Long Term Potentiation
MDD	Major Depressive Disorder
MDT	Mediodorsal Thalamus
mEPSP	Miniature Excitatory Postsynaptic Potential
NAc	Nucleus Accumbens
NMDAR	N-Methyl-D-Aspartate Receptor
PFC	Prefrontal Cortex
PL	Prelimbic
PTSD	Post-traumatic Stress Disorder
PVALB	Parvalbumin
SCZ	Schizophrenia
SST	Somatostatin
TRAP	Translating Ribosome Affinity Purification
vHPC	Ventral Hippocampus
VTA	Ventral Tegmental Area
WFA	Wisteria Floribunda Agglutinin

Introduction

The prefrontal cortex

Anatomy and connections

The prefrontal cortex (PFC) is commonly defined as the cortex of the anterior pole of the mammalian brain: in humans it is organized in a dorsolateral portion (dlPFC), that is located in front of the motor cortex, and an orbital and ventromedial portion (vmPFC), that is located in front of the limbic cortex (Fuster, 2008). Similarly to the rest of the cortex, neurons in the PFC are distributed along different layers, but unlike other cortical regions, this laminar organization is not homogenous: only the most anterior and lateral areas contain a clear layer IV (granular cortex); while moving more posteriorly the layer IV becomes progressively more rudimentary (dysgranular cortex) and is absent in the most posterior and medial areas (agranular cortex) (Wallis, 2012). Different layers target different brain regions: projections to subcortical areas arise from the deep layers V and VI, while cortico-cortico connections are mainly made by neurons in the superficial layers II and III (Douglas & Martin, 2004).

The PFC is the most recently evolved part of the nervous system and increases both in size and complexity of its organization with phylogenetic development (Fig.1). In rodents, the equivalent of the human PFC is identified, through connectivity studies, as the cortical region receiving massive inputs from the mediodorsal thalamus (MDT) (Guldin, Pritzel, & Markowitsch, 1981; Uylings & van Eden, 1990). Based on this evidence, also the rodent PFC is organized in a medial part (mPFC) and a lateral orbital part (OFC); but differently from primates, it consists uniquely of agranular cortex. Despite the absence of layer IV, the layer II/III is demarcated from layer V and VI by a band of thalamocortical fibers in deep layer III (Cruikshank et al., 2012).

The mouse mPFC (the object of this study, from now on named simply PFC) is divided in several subregions including (from most dorsal to most ventral) cingulate (CG or AC), prelimbic (PL) and infralimbic (IL) cortex (Fig.2). Despite having high overlap, their afferent and efferent projections distribute differently throughout the brain, allowing to distinguish the three subregions (Hoover & Vertes, 2007; Vertes, 2004).

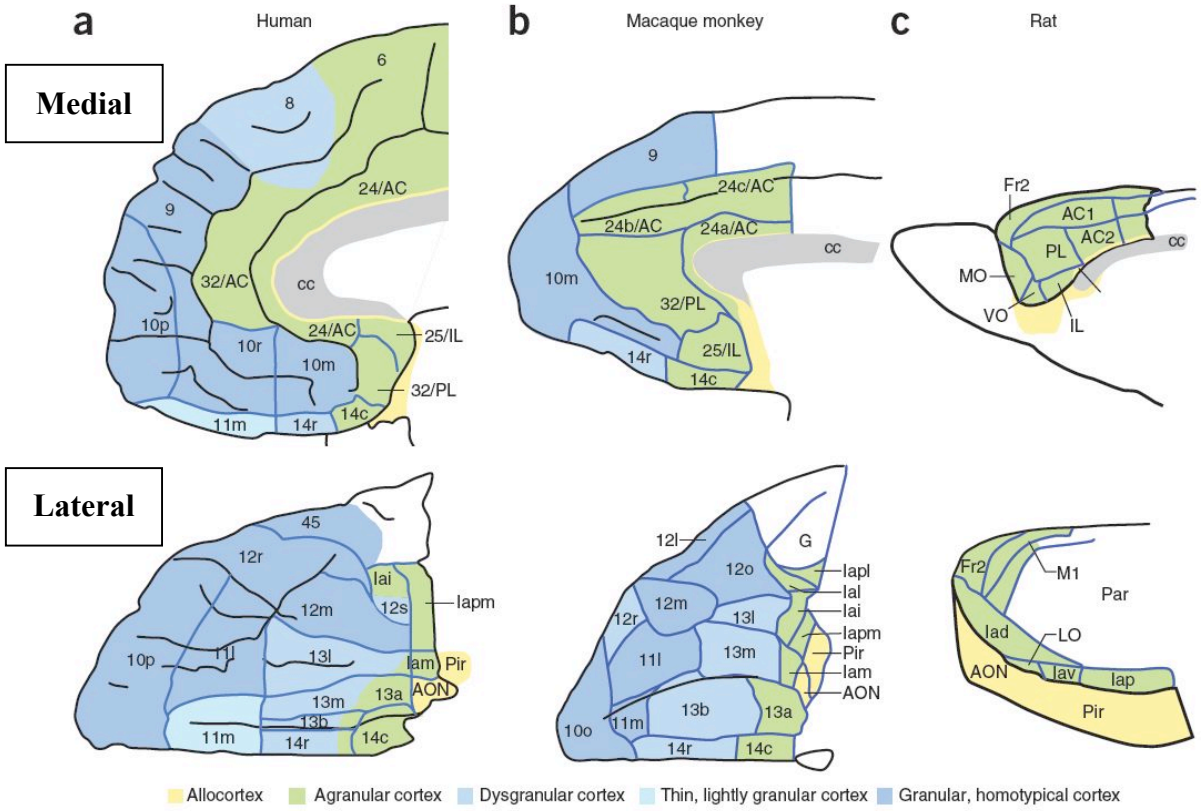

Figure 1. Comparative anatomy of PFC in mammals. *As taken from Wallis, 2012*. Schematic sagittal view of human **(a)**, monkey **(b)** and rat **(c)** medial (above) and lateral (below) PFC. AC, anterior cingulate area; AON, anterior olfactory nucleus; c, caudal; cc, corpus callosum; Fr2, second frontal area; I, insula; i, inferior; Ia, agranular infralimbic cortex; IL, infralimbic cortex; l, lateral; LO, lateral orbital area; m, medial; M1, primary motor area; MO, medial orbital area; o, orbital; p, posterior; Par, parietal cortex; Pir, Piriform cortex; PL, prelimbic cortex; r, rostral; s, sulcal; v, ventral; VO, ventral orbital area.

Regarding the inputs, while the CG receives predominantly sensory-motor afferents from cortical and thalamic regions; a gradual shift from cortical to limbic inputs, such as the basolateral and basomedial amygdala and the hippocampus (Vertes, 2004), is observed when moving more ventrally. As to the outputs, the PL massively projects to regions such as the nucleus accumbens, the insular cortex and the basolateral part of the amygdala, that are poorly targeted by the IL. The IL, indeed, preferentially targets other limbic regions, such as the basomedial amygdala, the medial and lateral preoptic nucleus, the lateral septum, the dorsomedial hypothalamus and other hypothalamic nuclei. This different distribution of inputs and outputs among CG, PL and IL reflects the roles of the different subregions. CG and PL are indeed involved in guiding attention and goal directed decision making, in homology to the human dlPFC (although mouse PL has also been suggested to be homologous to the human vmPFC area 32/AC, (Wise, 2008)), while IL has a prominent role

in viscero-autonomic activity and emotion regulation, in homology to the human vmPFC (Vertes, 2006).

Finally, the three mPFC subregions are also strongly reciprocally interconnected, with the exception of the IL, that receives considerably fewer inputs from the other mPFC regions (Vertes, 2004).

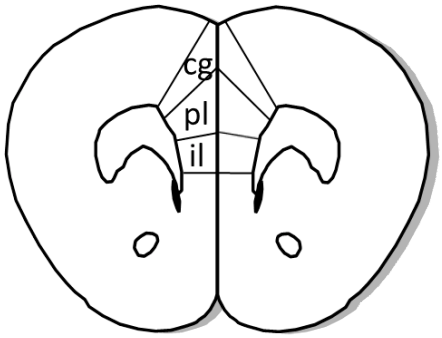

Figure 2. Schematic coronal view of mouse PFC and its subregions. *Adapted from Paxinos & Franklin, 2012*. cg, cingulate cortex; pl, prelimbic cortex; il, infralimbic cortex

Function

The first speculations about PFC function date back to late 1800s, when Phineas Gage, a railroad construction foreman, survived an accident in which a large iron bar pierced his skull, destroying great part of his frontal lobe. While Gage physically recovered from the accident, his personality was completely changed: he had lost the balance between his rationality and his instincts and, from being a very responsible, smart and well-balanced person, he had become impulsive, irreverent and vulgar, *"capricious and vacillating, devising many plans of future operations, which are no sooner arranged than they are abandoned in turn for others appearing more feasible"* (Harlow, 1993).

The personality change of Gage was due to the extensive damage of the PFC (Damasio, Grabowski, Frank, Galaburda, & Damasio, 1994; Ratiu, Talos, Haker, Lieberman, & Everett, 2004): indeed, through its numerous afferent and efferent projections this region plays an essential role in integrating environmental stimuli and experiences to direct our behavior, thought and emotion in an appropriate manner. This ability to keep in mind the right information, in order to use it to regulate behavior, is referred to as working memory (Goldman-Rakic, Cools, & Srivastava, 1996) and is strongly related to processes of decision making and strategy switching. Patients with lesions of the frontal lobe, indeed, show deficits in tasks requiring to switch strategies when a previously learned rule is no longer successful

(Aron, Monsell, Sahakian, & Robbins, 2004; Milner, 1963). Loss of cognitive flexibility is also present in psychiatric disorders such as schizophrenia, where a progressive thinning of the grey matter of the dlPFC is observed, as long as the psychosis develops (Cannon et al., 2016).

As evidenced by Phineas Gage case and other more recent clinical studies (Salas et al., 2016), the PFC also exerts a very important role in the inhibitory control of instinctive behaviors and, more generally, in regulating emotions. In this regard, it has been shown that in individuals suffering from post-traumatic stress disorder (PTSD), the gray matter in both vmPFC and anterior cingulate is significantly reduced (Kühn & Gallinat, 2013).

Actually, decision making and emotion regulation are not independent functions: for example, patients with a focal lesion of the vmPFC and an evident defect in emotion regulation (e.g. excessive anger, irritability, emotional outbursts) tend more often to take irrational decisions in the Ultimatum game, a laboratory model of economic decision making (Koenigs & Tranel, 2007). Also, in patients suffering from major depressive disorder (MDD), where PFC dysfunction is thought to play a major role (Kang et al., 2012), depressed mood and anhedonia are accompanied by defects in attention and working memory (Murrough, Iacoviello, Neumeister, Charney, & Iosifescu, 2011).

Local microcircuit

The local PFC network consists of excitatory pyramidal projection neurons (80–90% of the total population) and inhibitory local GABAergic interneurons (10–20% of the total population). Pyramidal neurons can be classified in pyramidal tract (PT) neurons and intratelencephalic tract (IT) neurons. PT neurons are located only in layer V and VI, they are thick tufted and target only subcortical regions, while IT neurons are located in both layer II/III, V and VI, they are thin tufted and target contralateral cortex or striatum (Dembrow & Johnston, 2014). These two subclasses of projecting neurons respond also differently to neuromodulators: for example, while serotonin inhibits PT neurons via 5-HT_{1A} receptor, it excites IT neurons via 5-HT_{2A} receptor (Avesar & Gulledge, 2012). Both of these subclasses of projection neurons are targeted by GABAergic interneurons, but PT neurons receive stronger inhibition from one interneuron subclass, namely $Parvalbumin^{+}$neurons (A. Lee et al., 2014).

Interneurons can indeed be classified in several subtypes, the two prominent and most well-known subtypes are Parvalbumin (Pvalb)$^+$ and Somatostatin (Sst)$^+$neurons.

Pvalb$^+$ neurons are targeting perisomatic regions of pyramidal neurons, blocking the output of these cells, while Sst$^+$neurons target the dendrites, blocking the input of these cells. Electrophysiologically, Pvalb$^+$neurons, thanks to electrical coupling and chemical synapses, have a high level of synchronization, a high firing rate and are narrow spiking; Sst$^+$ neurons are more heterogeneous: about one third is narrow spiking with a high firing rate and the rest are wide spiking with a low firing rate (Kvitsiani et al., 2013). Pvalb$^+$ and Sst$^+$neurons have also been classified based on their morphology and targets. Based on that, two main subtypes of Pvalb$^+$ neurons are identified as basket cells, with a highly branched, inter and intralaminar axonal arbor, making synapses onto soma and proximal dendrites, and chandelier cells, actually more abundant in frontal cortices (Taniguchi et al., 2013), with a mainly local axonal arbor, that makes synapses on the axon initial segment (or spike initiation zone) of pyramidal neurons. In the same way, Sst$^+$neurons can also be classified as the so called Martinotti cells, spread in all layers, but targeting selectively the apical tufts of pyramidal neurons in layer I, and non-Martinotti cells, located mainly in deeper layers, branching their axon in layer II/III and V. Many of these Sst$^+$non-Martinotti neurons inhibit Pvalb$^+$ interneurons, exerting in this way a disinhibitory action on pyramidal excitatory neurons (Pfeffer, Xue, He, Huang, & Scanziani, 2013).

Using a reward foraging task, Kvitsiani et al.demonstrated that Sst$^+$ and Pvalb$^+$ interneuron types can encode specific behavioral variables in the PFC. In this behavioral test, mice were trained to go back and forth between a reward zone and a trigger zone (where they could trigger a new reward): while Pvalb$^+$ neurons fired at the moment of the reward exit, narrow spiking Sst$^+$ neurons uniformly suppressed their activity when mice entered the reward zone. By contrast, wide spiking Sst$^+$ interneurons did not show homogeneous activity dynamics, demonstrating that Sst$^+$neurons are a highly heterogeneous subpopulation (Kvitsiani et al., 2013).

Recently, a third small subclass of inhibitory interneurons has been characterized, that is positive for the Vasoactive Intestinal Polypeptide (Vip). In the PFC it has been shown that these Vip$^+$interneurons send inhibitory connections to other interneurons, in particular to those positive for Sst (Pi et al., 2013).

Excitatory-inhibitory balance in the PFC

A normal balance between excitation and inhibition is required for a proper functioning of the PFC and also of other brain regions. For example, in mouse models for frontotemporal dementia and amyotrophic lateral sclerosis, it seems that excitotoxicity in motor cortex plays a role in neurodegeneration. In this case excitotoxicity is due to Sst^+neurons hyperactivity, which induces an excessive inhibition of $Pvalb^+$interneurons, leading then to excitotoxicity of layer V projecting neurons (W. Zhang et al., 2016).

In the PFC, when the excitatory-inhibitory balance is perturbed with an elevated stimulation of pyramidal neurons, this leads to altered social preference (Yizhar et al., 2011). Actually, several studies in both humans and mice demonstrated that an alteration of this balance in the PFC is correlated with disorders that are characterized by a social dysfunction, such as major depressive disorder and schizophrenia, even if the contribution of this imbalance to the social component is not clear yet (Bicks, Koike, Akbarian, & Morishita, 2015; Soumier & Sibille, 2014; Zikopoulos & Barbas, 2013).

In the dlPFC of schizophrenic patients, lower levels of glutamic acid decarboxylase 67 (GAD67), an enzyme required for GABA synthesis, are detected, and this deficit has been shown to be prominent in $Pvalb^+$basket cells (Curley et al., 2011), which also show decreased density of axon terminals in layer III (D. A. Lewis, Cruz, Melchitzky, & Pierri, 2001). In the meantime, pyramidal neurons spine density in layer III is decreased (Kolluri, Sun, Sampson, & Lewis, 2005), a phenomenon that is hypothesized to result in lower network excitation and to be the cause for the reduced feedback inhibition from $Pvalb^+$basket cells. As a consequence, the newly established excitatory/inhibitory balance at lower level impairs the generation of the so called gamma oscillations that are required for normal cognitive processing (Cho, Konecky, & Carter, 2006; David A. Lewis, Curley, Glausier, & Volk, 2012). Interestingly, in this regard, recent studies in mice in which the activity of $Pvalb^+$ interneurons was impaired, confirmed that their role is necessary to support working memory and cognitive flexibility, but not for other behavioral domains normally altered in schizophrenia, such as sensitivity to psychostimulants and also social preference (Murray et al., 2015).

As to depressive disorders, in the PFC of depressed patients, it was observed a decreased number of GABAergic interneurons, but not $Pvalb^+$ interneurons (Rajkowska, O'Dwyer, Teleki, Stockmeier, & Miguel-Hidalgo, 2007). However, decreased excitation of $Pvalb^+$

neurons has been observed in mice that are susceptible to learned helplessness, a model of stress induced depressive behavior. In the same study, resilient mice were turned into susceptible by inhibition of these interneurons (Perova, Delevich, & Li, 2015).

As to Sst^+interneurons, some findings showed that their number and *Sst* mRNA are reduced in the dlPFC of both schizophrenic and depressed patients (Morris, Hashimoto, & Lewis, 2008; Tripp, Kota, Lewis, & Sibille, 2011). Findings about depression are corroborated by studies in mice where it has been shown that, following chronic unpredictable stress, these neurons have a deregulation of eIF2 signaling for protein translation and that mice that are knockout for *Sst* show a high behavioral emotionality, as measured by several anxiety and depression related behavioral tests, that however, do not include any social measurement (L. Lin & Sibille, 2015). The same behavioral measurements were oppositely regulated when PFC Sst^+ neurons were acutely inhibited, resulting in increased behavioral emotionality, or chronically inhibited, resulting in decreased behavioral emotionality (Soumier & Sibille, 2014).

Dissecting the roles of PFC circuitry

Tools for manipulation of neural circuits

In the recent years, the role of specific brain circuits has started to be elucidated thanks to a combination of viral approaches with optogenetics and pharmacogenetics, that allowed to artificially manipulate their activity (Gordon, 2016; Riga et al., 2014).

Both optogenetic and pharmacogenetic tools take advantage of the introduction of genetically encoded exogenous proteins to drive neuronal depolarization or hyperpolarization. Optogenetics uses opsins, proteins that are able to modulate neuronal firing upon illumination, in the timescale of milliseconds. One of the most famous opsins used in this context is channelrhodopsin-2 (ChR2), a cation channel that induces action potential firing upon illumination with blue light, while the chloride pump Halorhodopsin (NpHR) or the proton pump Archaerhodopsin (Arch) are widely used to inhibit action potential. Light is delivered in the target brain structure where the opsins are expressed through a laser or LED device coupled to a thin optical fiber implanted in the skull (Fenno, Yizhar, & Deisseroth, 2011).

Pharmacogenetics, instead, uses engineered proteins that respond to unique inert chemical ligands that do not have any pharmacological activity *per se* in the CNS. One example are

Designer Receptors Exclusively Activated by Designer Drugs (DREADDs), engineered versions of muscarinic receptors, that can be selectively activated by binding of the inert ligand clozapine N-oxide (CNO), delivered intraperitoneally. Among DREADDs, hM3D is the engineered version of the G_q coupled M3 muscarinic receptor, and induces neuronal depolarization upon CNO binding, putatively through the closing of KCNQ potassium channels, that normally act as outwardly rectifying channels for depression of neuronal excitability (Alexander et al., 2010). hM4D is the engineered version of the G_i coupled M4 muscarinic receptor and induces neuronal hyperpolarization upon CNO binding, through activation of G-protein inwardly rectifying potassium channels (GIRKs) (Armbruster, Li, Pausch, Herlitze, & Roth, 2007). Notably, it has recently been shown that CNO is not able to enter the brain, and that metabolically derived clozapine, arising from CNO administration, is instead the actual *in vivo* DREADD actuator (Gomez et al., 2017).

In both optogenetics and pharmacogenetics the expression of these proteins can be reached through the use of transgenic animals or the injection of viral vectors in the regions of interest. Cell specificity and circuit specificity can be reached by the use of Cre-dependent constructs and retrograde viruses expressing Cre, respectively. Retrograde viruses are able to infect neurons entering their axonal terminals and are then transported through the axons to the soma of the infected neuron, so that Cre expression (in this case) is detectable in the afferent neurons of the infected region (Boender et al., 2014). Examples of retrograde viruses that are used for this aim are some serotypes of adenoassociated virus (AAV) (Christoffel et al., 2015), herpes viruses (HSVs) (Antinone & Smith, 2010) and canine adenovirus (CAV) (Boender et al., 2014).

Both opsins and DREADDs are expressed also at the level of axonal terminals, so that it is also possible to manipulate projections to specific output regions implanting the optic fiber (or a cannula for local CNO administration (Stachniak, Ghosh, & Sternson, 2014)) only in correspondance of the output region of interest.

Although sharing many similarities, the main difference between the two techniques is that optogenetics, despite having much more precise temporal resolution than pharmacogenetics, has the disadvantage that the manipulation can affect also fibers of passage projecting to more distal regions, as the optogenetic activation of chloride or proton pumps is believed to act by blocking action potential propagation (Tye et al., 2011).

PFC circuitry and top-down control of subcortical structures

When used in rodent models in specific behavioral contexts, these manipulation tools, together with electrophysiological recordings, have helped to dissect the role of the extensive network of connections of the PFC with many other cortical and subcortical regions of the brain (Riga et al., 2014).

In the context of working memory, for example, afferents from both ventral hippocampus (vHPC) and mediodorsal thalamus (MDT) demonstrated to play an essential role. The vHPC-PFC circuit is indeed required for encoding and formation of the memory, but not for its maintenance and retrieval (Spellman et al., 2015), that are instead mediated by the connection with the MDT. In particular, MDT-PFC projections are supporting working memory maintenance, while PFC-MDT pathway supports its retrieval in order to take a consequent action (Bolkan et al., 2017).

The PFC is also the hub that connects cortical and subcortical networks of mammalian brain. The dynamic interaction between these two networks is indeed required to guarantee the correct balance between higher order cognitive activities, such as attention and decision making, and the generation of instinctive behaviors and rapid emotional responses. In the normal non-stress conditions the PFC exerts an executive control on the subcortical network; but in stress conditions and several psychiatric disorders the amygdala takes the control, switching from a top-down to a bottom-up control of the system, with an increased generation of negative emotions and reactivity to threats (Arnsten, 2009; Murrough et al., 2011). In line with this top-down regulation of subcortical structures, acute activation of $Thy1^{+}$PFC cells, pyramidal neurons projecting to limbic structures, is actually sufficient to get an antidepressant response in naïve animals (Kumar et al., 2013).

Strong reciprocal connections exist between the PFC and the amygdala, especially its basolateral portion (BLA), playing an important role in the context of the evaluation of threats. Animals that are able to discriminate an aversive and a neutral condition have indeed a higher synchrony between the PFC and the BLA (Likhtik, Stujenske, Topiwala, Harris, & Gordon, 2013). Interestingly, the PL and IL connections to the amygdala play an opposite role in the context of fear conditioning, a behavioral paradigm where mice learn to associate aversive events to specific auditory cues. The acquisition of the aversive memory is associated to increased activity of BLA neurons projecting to the PL (Senn et al., 2014) and PL activation of amygdalar targets is necessary for fear memory retrieval (Do-Monte,

Quinones-Laracuente, & Quirk, 2015). In contrast, increased activity of BLA neurons projecting to the IL is observed during extinction of previously learned fear (Senn et al., 2014), that can also be promoted by IL activation itself (Milad & Quirk, 2002).

In the context of extinction it is important to notice that the PL integrates inputs from the BLA together with inputs from the vHPC: in particular, vHPC has been shown to reduce fear after extinction by inhibiting PFC responsiveness to the BLA (Sotres-bayon, Sierra-mercado, Pardilla-delgado, & Quirk, 2013).

Another region that is controlled and reciprocally connected with the PFC is the nucleus accumbens (NAc); a striatal structure that is very well known for its role in the context of reward, motivation and appetitive behavior. Motivational disorders, such as addiction and depression, are indeed associated with reduced glutamatergic transmission of PFC into NAc (Kalivas, 2009; Lüthi & Lüscher, 2014). The NAc seems to integrate the information from the PFC with information from other inputs. For example, it has been shown that during decision making, PFC activation inhibits responses of NAc to hippocampal and thalamic projections and the same happens when PFC-NAc circuit is artificially activated (Calhoon & O'Donnell, 2013). This observation attributes a regulatory role of PFC onto synaptic transmission from hippocampal and thalamic inputs into NAc.

Among the other subcortical targets implicated in motivated behaviors are the dorsal raphe (DRN), the ventral tegmental area (VTA), that both share reciprocal connections with the PFC, and the lateral habenula (LHb). Regarding the VTA, the functional role of the PFC-VTA circuit has not yet been explored with manipulation experiments, but this projection is likely to play a role in aversive experiences. Indeed, it has been shown that the postsynaptic strength on dopaminergic VTA neurons projecting to the PFC (the same neurons that are actually targeted by the PFC) is increased by aversive experiences (Lammel, Ion, Roeper, & Malenka, 2011). Finally, regarding PFC-DRN and PFC-LHb projections, these two seem to play an opposite role in a rodent model for behavioral despair, called forced swim test (FST), which correlates with motivational active adaptation to challenging environments, and that is used for evaluation of antidepressant drugs. In this behavioral paradigm, photoactivation of terminals in DRN induces behavioral activation, while photoactivation of terminals in LHb induces immobility (Warden et al., 2012) demonstrating the existence in the PFC of different subpopulations that, if activated, can drive opposite behavioral responses.

Social behavior

PFC and social behavior

Social behavior consists of several aspects, including knowledge of self and other (such as social memory, recognition and empathy), group dynamics (e.g. formation of social hierarchies) and social motivation (the desire to seek social contact). Human PFC regulates all of these aspects and its disruption is thought to play an essential role in the pathophysiology of psychiatric disorders, such as autism spectrum disorder (ASD) and schizophrenia (SCZ), where clear deficits in social cognition are detectable (Bicks et al., 2015).

This finding is confirmed by convergent research on animal models. Indeed, several behavioral paradigms are used in rodents to study social behavior. Social preference test, for example, is a common test used to assess social motivation, especially in ASD mouse models: in this paradigm mice choose to explore a chamber with a conspecific animal or a chamber with an object (Moy et al., 2004). To study social recognition and memory, the same two chambers are used to let mice choose between a familiar mouse and a novel conspecific (Thor & Holloway, 1982). In these tests, a natural wildtype shows usually a higher propensity for a social conspecific instead of an object, and for a novel mouse, instead of a familiar one. In social preference test, single neuron recording in the PFC showed that a subset of PFC neurons increase their activity when mice approach the social conspecific compared to an inanimate object (E. Lee et al., 2016). Evidences that associate social recognition (the ability to recognize a familiar mouse) to PFC in rodents are still lacking, even if functional connectivity between the PFC, HPC and amygdala seems to be required to consolidate social recognition memory (Tanimizu et al., 2017).

Another typical rodent social behavior is something that can be clearly observed directly in their home cage, when more mice are housed together: the formation of hierarchies and dominance relationships. A common behavioral paradigm that is used to study this behavior is the tube test in which two mice are invited to enter a tube by the two opposite ends: normally after some time one mouse (the “loser”) is forced back out of the tube by the dominant one. Using this test, an enhanced efficacy of the synaptic transmission in the PFC has been linked to a more dominant behavior (F. Wang et al., 2011).

It has to be noted that social behavior, in particular social motivation, can change and be adapted in response to experiences. For example, various form of stress are known to highly increase the risk for the development of depressive disorders (Cohen, Janicki-Deverts, & Miller, 2007), such as major depressive disorder, where social withdrawal and interpersonal difficulties are among the most common and disabling features (Hames, Hagan, & Joiner, 2013). One of these experiences is social stress, that is mimicked in mice by the social defeat behavioral paradigm, a model that is frequently used to study depression and anxiety associated behaviors. In social defeat, experimental mice are attacked and defeated by an aggressive conspecific. In the most common chronic version of this test, this event is repeated for 10 days, resulting in several depressive and anxious behaviors, that include a decreased social interaction and increased avoidance (Golden, Covington, Berton, & Russo, 2011). Using this model, it has been shown that optogenetic stimulation of PFC has an antidepressant effect on previously defeated mice. Indeed, mice that were laser stimulated did not show any decrease in social interaction and sucrose preference (a measure of anhedonia) compared to untreated defeated animals. However, the same stimulation had no effect on anxiety measurements (Covington et al., 2010).

Role of PFC circuitry in social motivation

In the recent years the role of distinct PFC circuits has started to be dissected also in the context of social behavior. As previously mentioned, PFC is strongly connected with several structures involved in motivation, such as the VTA and NAc. Dopaminergic afferents from the VTA to the PFC fire less in mice which underwent social defeat (Chaudhury et al., 2013) and 5 days- repeated optogenetic stimulation of PFC projecting VTA neurons neurons are sufficient to reverse social avoidance in previously defeated animals, through increased firing frequency of the circuit (Friedman et al., 2014). Interestingly, this activation has no effect on naïve mice (Gunaydin et al., 2014), implying that activity of these projections does not have a direct effect on social behavior. Regarding PFC-NAc connection, the rapid optogenetic activation or inactivation of this circuit in already defeated mice has no effect on their social interaction, while chronic disruption of the circuit through the use of tToxins induces increased social avoidance in mice that underwent a subthreshold social defeat (Christoffel et al., 2015). Interestingly, stimulation of the same projections is sufficient to reverse social avoidance and anhedonia when these are induced by local PFC administration of cholecystokinin (a neuropeptide normally released in PFC during defeat stress with anxiogenic effects). Conversely, stimulation of PFC-BLA projections in the same situation

has no effect on social avoidance and anhedonia but reverses the appearance of anxiogenic effects (Vialou et al., 2014).

Also PFC-DRN circuit has a role in social motivation, but this is in contrast with antidepressant and pro-behavioral activation role of PFC-DRN projections in forced swim test shown by Warden et al. in 2012. Indeed, studies from Olivier Berton's lab have dissected the organization of this connection and found an opposite effect on social avoidance. In particular, they demonstrated that PFC projections synapse onto GABAergic inhibitory neurons of DRN, which in turn strongly inhibit serotonin release from serotonergic neurons (Challis et al., 2013; Challis, Beck, & Berton, 2014). Repeated optogenetic inhibition of PFC-DRN projections during the social defeat days results in decreased social avoidance on the social interaction testing day, compared to untreated defeated animals. Conversely, repeated optogenetic inhibition of the same projections in non-defeated animals results in increased avoidance on social interaction testing day, compared to untreated controls (Challis et al., 2014). However, manipulation of this circuit directly on the social interaction day did not affect the previously learned social avoidance behavior, implying that PFC-DRN projections are important for the "learning" of social avoidance and not for the expression of social behavior itself.

In this regard, a recent work from our lab, using a subchronic social defeat procedure that induces social avoidance, but not generalized changes in depressive and anxiety behaviors, identified the PFC projections to the dorsal part of the periaqueductal grey (dPAG) as an important driver of social behavior (Franklin et al., 2017). Dorsal PAG is a brainstem region whose activity elicits the expression of defensive behaviors, such as flight and freezing (Carrive, 1993; Tovote, Esposito, Botta, Chaudun, & Jonathan, 2016). Subchronic social defeat seems to decrease the functional connectivity between PFC and dPAG and pharmacogenetic inhibition of this circuit mimics the effects of the defeat, inducing social avoidance in naïve animals. This behavioral effect is accompanied by an increased activity of dorsomedial and dorsolateral PAG, as evidenced by increased cFos levels, similarly to what observed in untreated animals after the defeat, suggesting that inhibition and weakening of this pathway causes a disinhibition of the dPAG (Fig. 3). However, the acquisition of the defeated phenotype is not accompanied by any change in the evoked synaptic responses of PFC to dPAG stimulation, but postsynaptic changes could be occurring in the PFC itself (see"Experience dependent plasticity in the PFC").

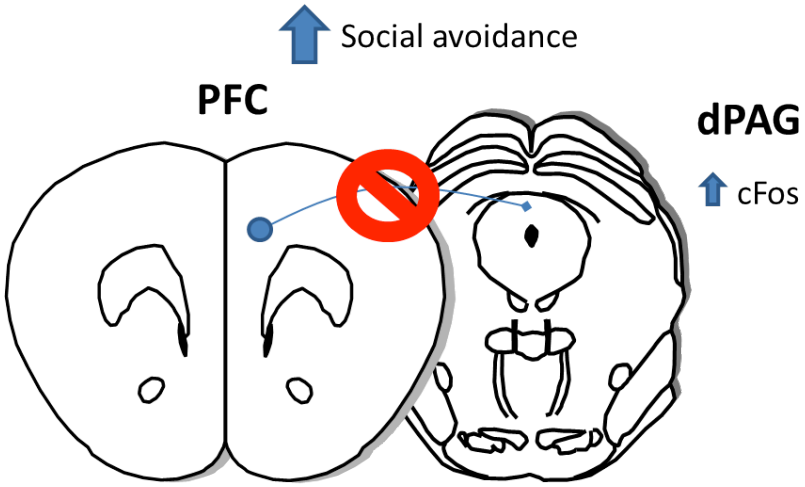

Figure 3. PFC exerts inhibitory control on dPAG driven social defensive behavior. Inhibition of PFC-dPAG circuit induces social avoidance and increases cFos in dPAG (see text for more details) (Franklin et al., 2017).

Synaptic plasticity

Mechanisms of Hebbian and homeostatic plasticity

The mammalian brain is an extremely plastic organ, as it has the ability to change and adapt its structure and function in response to life experiences, thereby modifying our thoughts and behavior. The basis of brain remodeling resides in synapses, the specialized junctions that mediate the communication between neurons, and is called synaptic plasticity. Thus, synaptic plasticity is the ability to change synaptic strength (namely the efficacy of synaptic transmission) in response to changes in synaptic activity.

The two main forms of synaptic plasticity are Hebbian and homeostatic plasticity. Hebbian plasticity is the most well studied, it was proposed for the first time by Donald Hebb in 1949 (Hebb, 1949) and is at the basis of important processes such as learning and memory. Hebbian plasticity requires correlated firing of the presynaptic and the postsynaptic neuron to occur and it is a positive feedback process. Basically, when activity in a synapse is increased this synapse will become stronger (a phenomenon called long term potentiation; LTP) and it will be easier to be excited and to undergo further potentiation. On the other hand, when activity in a synapse is decreased, this synapse will be weakened (a phenomenon called long term depression; LTD) and less and less prone to be excited. This type of plasticity is known to be induced rapidly, to persist for a long time (from hours to months) and to be input specific, meaning that it is confined to active synapses (Citri & Malenka, 2008).

Homeostatic plasticity has been discovered more recently: this plasticity works as a compensatory negative feedback mechanism that acts to maintain network stability. This means that, in conditions of elevated excitability, homeostatic mechanisms reduce synaptic strength; while, in response to chronic activity suppression, there will be an increase in synaptic gain (Pozo & Goda, 2010; Turrigiano & Nelson, 2000). These processes are important in the prevention of excitotoxicity and of synaptic silencing and loss. In contrast to Hebbian plasticity, homeostatic changes are believed to be slowly induced and to act globally at the level of all the synaptic inputs in a given neuron. However, there are several evidences that argue against that. For example, in the cerebellum it has been demonstrated that LTP changes induced by motor learning in single synapses are counterbalanced by compensatory weakening of specifically neighboring synapses (K. J. Lee et al., 2013).

LTP and LTD are triggered rapidly through the glutamate N-methyl-D-aspartate (NMDA) receptors. NMDA receptors are voltage dependent ion channels that contribute little to basal synaptic activity, because the ion flow is blocked by a Mg^{++} ion. In basal synaptic transmission, the response to glutamate is mainly driven by the ionotropic α-amino-3-hydroxy-5-methyl-4-isoxazole propionic acid (AMPA) receptors: when glutamate binds AMPARs, this leads to entrance of Na^{+} ions, leading to membrane depolarization of the postsynaptic spine. This membrane depolarization, together with glutamate binding, leads to removal of the Mg^{++} ion from the NMDA receptors and consequently to receptor opening. As NMDA receptors are also permeable to Ca^{++}, the opening of these channels leads to both Na^{+} and Ca^{++} entrance. High levels of Ca^{++} can trigger LTP, through Ca^{++}binding to the low affinity calcium/calmodulin-dependent protein kinase II (CaMKII) that is upstream a series of signaling cascades that elicit reinforcement of synaptic strength. In contrast, low levels of Ca^{++} (over a more prolonged period of time) trigger the opposite event, LTD, through preferential binding to the calcium/calmodulin-dependent phosphatase calcineurin, that has high affinity for calcium and is upstream a series of events eliciting weakening of synaptic strength (Citri & Malenka, 2008). Molecular mechanisms for induction of homeostatic plasticity are less clear, even if it has been demonstrated that both β3-integrin and the pro-inflammatory cytokine TNFα are required for its induction, both *in vitro* and *in vivo* (Cingolani et al., 2008; Kaneko, Stellwagen, Malenka, & Stryker, 2008; Stellwagen & Malenka, 2006). However, experimental evidence has been provided that TNFα may act as a permissive rather than instructive factor and more studies will be required to clarify this process (Steinmetz & Turrigiano, 2010).

In both plasticity types, increased or decreased synaptic strength is then expressed through changes at both presynaptic and postsynaptic level. At the presynaptic level, synaptic strength is determined by the increase in the neurotransmitter release probability. This seems to be mediated, both in Hebbian and homeostatic plasticity, by an increase in the number of Voltage Gated Calcium Channels (VGCC) in the active zone and an increase in the ready releasable pool of synaptic vesicles, both processes mediated by two proteins, named RIM and Rab3 (Han, Kaeser, Südhof, & Schneggenburger, 2011; Müller, Pym, Tong, & Davis, 2011; Tsetsenis et al., 2011).

At the postsynaptic side, both expression of Hebbian and homeostatic plasticity involve changes in AMPAR trafficking. AMPARs main function is exerted in dendritic spines, the postsynaptic components of synapses, but they are not localized only there. Indeed, AMPARs are translated both in soma and dendrites (Grooms et al., 2006) and can be transported by both lateral diffusion through the membrane and exocytosis or endocytosis through endocytic vesicles (Chater & Goda, 2014). Both processes can mediate increased or decreased levels of AMPARs on the membrane of dendritic spines. While increased levels of spine surface AMPARs are associated to increased postsynaptic strength, removal of AMPARs from spine surface is associated to weakening of the synapse (Huganir & Nicoll, 2013). When AMPARs are transported onto spine membrane in response to activity, the speed of their surface diffusion is reduced and they are captured in the so called postsynaptic density (Bats, Groc, & Choquet, 2007) (Fig.4).

These phenomena have been observed in both Hebbian and homeostatic plasticity, but some differences exist. AMPA receptors are indeed composed by 4 different subunit types: GluA1, GluA2, GluA3 and GluA4 (the latter being expressed only early in development (Luchkina et al., 2014)). Under physiological conditions synapses contain GluA2-GluA3 heterodimers, that are constitutively recycling between spine membrane and synaptic vesicles, and GluA1-GluA2 heterodimers, whose transport between membrane and synaptic vesicles is instead activity dependent (Shi, Hayashi, Esteban, & Malinow, 2001). As GluA2 is impermeable to calcium, these AMPARs allow only entrance of sodium ions. In both Hebbian and homeostatic plasticity, increases in synaptic strength involve an increased insertion of GluA1-GluA1 homodimers, which are permeable to calcium and contribute to further potentiate synaptic strength. Actually, in LTP, GluA2-lacking AMPARs are the first incorporated into the synapse, and will then be replaced with GluA2-containing receptors (Plant et al., 2006), to

stabilize LTP without allowing further calcium entrance. Recent studies demonstrated that these GluA1 homodimers are necessary also for the expression of homeostatic plasticity (Thiagarajan, Lindskog, & Tsien, 2005). However, it's been shown that GluA2 is required for the expression of homeostatic plasticity (Gainey, Hurvitz-Wolff, Lambo, & Turrigiano, 2009), while GluA1 is only required for Hebbian phenomena (Zamanillo et al., 1999). Once AMPARs are transported into synapses, they are stabilized by the interaction with the protein stargazin and PSD-95 (Bats et al., 2007). This interaction is important both to favour immobility of AMPARs in the postsynaptic density and also to promote their synaptic accumulation (Opazo et al., 2010). However, knocking out PSD-95 does not have any effect on LTP induction and expression, but impairs homeostatic phenomena (Sun & Turrigiano, 2011).

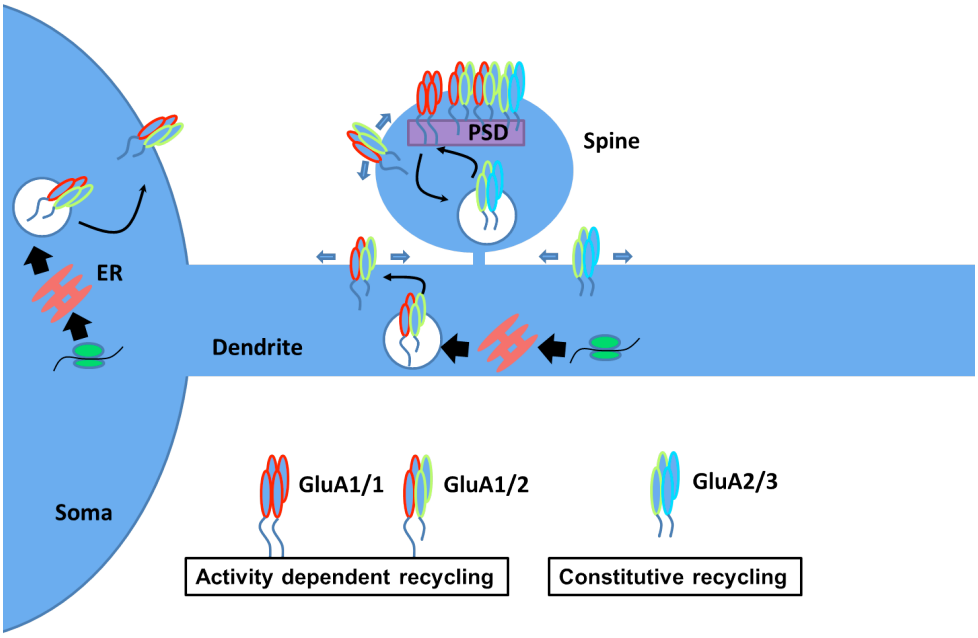

Figure 4. Localization and trafficking of AMPA receptors. AMPARs are translated both in soma and dendrites and are transported to spine membranes through both membrane diffusion and vesicular exocytosis. Depending on their subunit composition they can recycle with the membrane in either a constitutive or activity-dependent manner (see text for details).

Interestingly, synaptic plasticity involves also structural changes. First of all, spine size correlates with both the amount of AMPARs (Matsuzaki et al., 2001) and electrical strength of the synapse (De Roo, Klauser, & Muller, 2008). Also the dendritic branching and the shape of spines can change, with mushroom spines associated to a higher synaptic strength than thin spines (Haas, Li, & Cline, 2006; Yuste & Bonhoeffer, 2001). At the presynaptic

level, a larger postsynaptic density is matched by a larger active zone, with more synaptic vesicles ready for release (Murthy, Schikorski, Stevens, & Zhu, 2001).

In the long term, synaptic plasticity is expressed also through changes in transcription and translation (Alberini, 2009; Buffington, Huang, & Costa-Mattioli, 2015). These processes and their timing have been studied more extensively for LTP, where it is made a clear distinction between the early phase of LTP, consisting in its induction and lasting approximately 1h, an intermediate phase, lasting approximately 8h and relying on local protein synthesis, and a late phase, lasting over 8h and requiring new mRNA transcripts and protein synthesis, also known as the maintenance phase (Bliim, Leshchynska, Sytnyk, & Janitz, 2016).

At the transcriptional level a critical transcription factor is cAMP response element-binding protein (CREB), that is activated through phosphorylation of its Ser-133 residue, downstream the cAMP-PKA pathway (Dash, Hochner, & Kandel, 1990). CREB is considered critical in LTP and memory formation: mice that are knockout for the α and Δ isoform of CREB show, indeed, impaired memory and LTP (Bourtchuladze et al., 1994). CREB regulates the expression of several immediate early genes: one example is Arc/Arg3.1. Arc/Arg3.1 is transcribed in the nucleus and translated directly in the dendrite, its expression is induced by high glutamate stimulation and it plays a role in cytoskeletal rearrangement, facilitating AMPAR endocytosis (Chowdhury et al., 2006), a mechanism which is at the basis of its important role in homeostatic plasticity (Shepherd et al., 2006).

Regulation of translation is also essential for long term-changes of synaptic strength. One player of this process is Eukaryotic Initiation Factor 2α (eIF2α), a translation initiation factor whose phosphorylation (commonly reduced in response to stimuli that increase synaptic strength (Costa-Mattioli, Sossin, Klann, & Sonenberg, 2009)) is known to reduce the formation of the initiation complex and thereby the ability of the cell to synthesize new proteins (Pavitt, Ramaiah, Kimball, & Hinnebusch, 1998). Also, in several forms of Hebbian plasticity, such as long term LTP, it has been shown activation of the mechanistic target of rapamycin complex 1 (mTORC1) pathway (Buffington et al., 2015). mTORC1 controls translation of synaptic proteins through both phosphorylation of eIF4E–binding proteins (4E-BPs) and p70 S6 kinases (S6K1/2). Briefly, 4E-BPs phosphorylation leads to increased translation initiation rates, while S6 kinases promote translation through phosphorylation and activation of eIF4B (a cofactor of eIF4A), eukaryotic elongation factor 2 kinase (eEF2K), and ribosomal protein S6 (Ma & Blenis, 2009). Interestingly, mTORC1 pathway is known to

inhibit and to be inhibited by the glycogen synthase kinase-3 β (GSK3β), that plays a key role in LTD, where it is implicated in AMPARs internalization (Bradley et al., 2012; Peineau et al., 2007).

Finally, translation regulation is important also in homeostatic plasticity: indeed it seems that chronic silencing of synaptic inputs (which results in general increase of homeostatic synaptic strength) increases the dephosphorylated, active form of the translation elongation factor eEF2, which, in turn, results in dendritic protein synthesis (Sutton, Taylor, Ito, Pham, & Schuman, 2007).

Methods to detect synaptic plasticity

Electrophysiology is considered the best method to study plasticity, especially *in vitro*. In brain slices, for example, miniature Excitatory Postsynaptic Potential (mEPSP) is frequently used to measure synaptic strength. mEPSP is the spontaneous current that corresponds to the response of the postsynaptic cell to the release of a single molecule of neurotransmitter (independently on presynaptic action potential (that is blocked by tetrodotoxin)) (Fatt, & Katz, 1952). Changes in mEPSP frequency can be due to either changes in presynaptic release probability at existing sites (changes in vesicular pool or vesicular turnover rate) or in the number of functional synaptic sites (more dendritic spines or new synapses onto already established spines); while changes in amplitude are attributed to the presence of less AMPA receptors, or to AMPARs with lower conductance, on the postsynaptic side (postsynaptic plasticity) (Queenan, Lee, & Pak, 2012). *In vivo,* evoked local field potential (LFP) can instead be used to measure the strength of synaptic response of a brain region to the stimulation of another region (Tamura et al., 2011). However, the overall limitations of electrophysiology are due to lack of specificity in targeting a certain cell type and, in the case of *in vivo* LFP, also to the lack of cellular and intracellular resolution. The advent of optogenetics brought some improvement in these two areas. Indeed, ChR2 stimulation in brain slices was used in combination with other techniques (e.g.glutamate uncaging in presynaptic neurons or Ca^{++} imaging in the postsynaptic neuron) to study in specific cell types and with single synapse resolution the dynamic processes that occur upon artificial LTP induction (Schoenenberger, Schärer, & Oertner, 2011). However, these optogenetic methods are more suitable for the study of the basal mechanisms of plasticity, than to detect natural changes in synaptic strength that are occurring *in vivo*.

In this regard, structural plasticity is relatively easier to visualize. Quantifications of spine density, dendritic morphology and timing of spine dynamics are commonly used both in slices and in *vivo* to detect plasticity occurred during particular behavioral tasks. Sparse neurons can be filled with a fluorophore, either using common transgenic lines (e.g. *Thy1*::GFP) or iontophoresis techniques, and imaging can be done directly on fixed slices after sacrifice, or directly *in vivo* by the use of two photon *in vivo* imaging, for example to study spine stability (Holtmaat, Randall, & Cane, 2013).

Actually, two photon *in vivo* imaging, thanks to its high resolution, allowed to adapt also other techniques, aimed at plasticity detection, to *in vivo* use in the mouse brain. For example, in the recent years, several genetically encoded synaptic activity indicators have been developed. Among these, Calcium indicators, that respond to Calcium entrance with increased fluorescence, such as GCamPs, are the most well known, even if their functioning is more adequate for activity than plasticity measurements (Bozza, McGann, Mombaerts, & Wachowiak, 2004; M. Z. Lin & Schnitzer, 2016).

Other indicators of synaptic activity and plasticity are genetically encoded pH indicators or synaptophluorins. Synaptophluorins are synaptic proteins fused with mutated forms of GFP or other fluorophores, that are excitable only at a neutral pH, while becoming dark ("ecliptic") at an acidic pH (Miesenböck, De Angelis, & Rothman, 1998). The difference in the pH is important in the context of synaptic transmission, because the vesicular lumen of both synaptic vesicles for neurotransmitter release and endosomes for postsynaptic receptor trafficking has a pH around 5.5. The most famous pHluorin is SEP, a mutated form of GFP, that has been fused to several presynaptic proteins, such as synaptophysin and vGlut1, and also postsynaptic receptors, such as AMPARs and NMDARs subunits (M. Z. Lin & Schnitzer, 2016). AMPAR fused SEPs (SEPGluA1 and SEPGluA2) are the most suitable to detect plasticity events: in this case an increased SEP fluorescence would report an increased level of spine surface AMPA receptors, reflecting a higher synaptic strength (Roth, Zhang, & Huganir, 2017) (Fig.5).

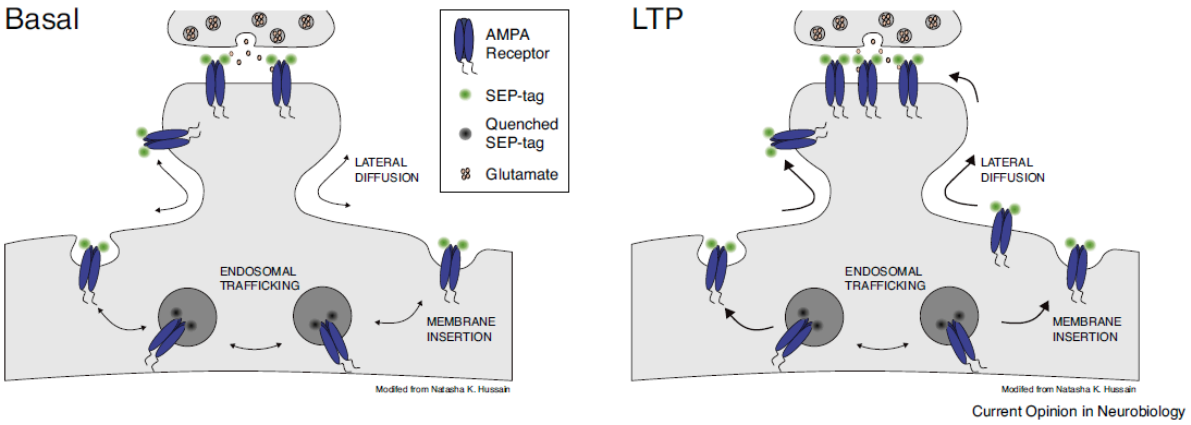

Figure 5. Use of SEP fused AMPA receptors to study synaptic plasticity. *As taken from (Roth et al., 2017).* SEP fluorescence is quenched at the acidic pH of endocytic vesicles, so that SEP fused AMPARs in endocytic vesicles are not visible, while surface exposed AMPARs are at a neutral pH and can be excited. After LTP, more AMPARs are transported onto spine surface and SEP fluorescence will consequently increase

Actually, some studies have started to demonstrate the potentialities of these tools in studying not only *in vitro* induced, but also behavioral induced plasticity.

In 2011, using SEPGluA1 and SEPGluA2 imaging on brain slices from somatosensory cortex, Malinow's group demonstrated that sensory experience, modulated by trimming or leaving intact mouse whiskers, bidirectionally regulates surface levels of SEPGluA1 and 2. Following sensory experience, surface GluA1 was increased on specific inputs, while following whisker trimming, surface GluA2 was increased globally on the entire dendritic arbor (Makino & Malinow, 2011). This study nicely showed AMPARs trafficking dynamics in different types of plasticity (Hebbian vs. homeostatic), but also it was the first study to use surface AMPA receptor imaging as a readout of *in vivo* induced plasticity, even if imaging was carried on acute brain slices.

In a similar manner, Huganir's group in 2015 used SEPGluA1 imaging, combined with two photon microscopy, to image AMPAR dynamics directly *in vivo* in the mouse somatosensory cortex. Using this method, it was shown that acute whisker stimulation elicited temporary or permanent increase in surface SEPGluA1, repectively, in dendritic shaft and spines (Y. Zhang, Cudmore, Lin, Linden, & Huganir, 2015).

As evidenced also by this latter study, though giving a great advantage (to follow synapse dynamics *in vivo* over time), one overall limitation of two photon *in vivo* microscopy is the low penetrance of this technique, that does not reach deep brain regions, and the necessity of head-fixing animals, that limits choice for behavioral studies.

Finally, as plasticity involves also changes at transcriptional and especially translational level, gene expression can also be used for its investigation. In this regard, it is interesting to notice that 2550 mRNAs have been identified that are localized in dendrites and axons (Cajigas et al., 2012) and local translation at the synaptic level is required for long term plasticity (Jung, Gkogkas, Sonenberg, & Holt, 2014). For this reason it would be useful not to lose dendritic RNAs when studying gene expression in contexts where plasticity is supposed to occur, something that could happen for example when cells or nuclei are isolated with FACS cell sorting.

Combining cell type specificity with dendritic RNA isolation is possible using the Translating Ribosome Affinity Purification (TRAP) technique: here GFP is fused to the L10A ribosomal protein and translated mRNA is isolated by anti-GFP mediated ribosomal immunoprecipitation. Cell type specificity is given by the possibility of expressing this construct in a Cre-dependent manner, or under specific promoters, thanks to the existence of specific mouse knock-in lines (Heiman, Kulicke, Fenster, Greengard, & Heintz, 2014; P. Zhou et al., 2013).

Experience dependent plasticity in the PFC

The PFC displays remarkable plasticity during the life course. Several types of experiences, including drug addiction and learning of tasks that implicate working memory, can cause some synaptic remodeling in the PFC (Kolb & Gibb, 2015); but stress is probably the most well known for having an impact on its structural and functional plasticity (McEwen & Morrison, 2013).

Stressful experiences seem to exert time-dependent effects onto the PFC. Acute stress enhances working memory and facilitates LTP in the PFC through increased surface levels of both AMPAR and NMDAR subunits (Yuen et al., 2009). On the contrary, chronic stress has detrimental effects on cognitive abilities and causes a decrease in postsynaptic glutamatergic transmission, through decreased levels of both total and surface AMPARs and NMDARs, that are increasingly degraded by the ubiquitin/proteasome system (Yuen et al., 2012).

Actually, a vast literature exists regarding the effects of chronic restraint stress on PFC structural plasticity in rodents. This type of stress has been shown, indeed, to reduce both spine density and apical dendritic branching in layer II/III PL and CG pyramidal neurons and the decreased branching in stressed mice was also predictive of an impaired ability to shift

attention (Liston et al., 2006; Radley et al., 2006). Interestingly, BLA projecting layer II/III PFC neurons are resistant to this remodeling (Shansky, Hamo, Hof, McEwen, & Morrison, 2009) and all alterations in dendritic branching of layer II/III neurons are totally reversible with recovery, but only in young animals (Bloss, Janssen, McEwen, & Morrison, 2010). Also layer V neurons undergo morphological changes after chronic stress. In the IL they present apical dendritic retraction (restored only in proximal dendrites after recovery), but no changes in the spine density (Goldwater et al., 2010); while in PL and CG they present dendritic retraction selectively in layer I (apical tuft) and decreased spine density in the distal tuft (Liu & Aghajanian, 2008). At the functional level the stress-induced dendritic retraction in IL is accompanied by an impairment in catecholaminergic facilitation of LTP, that is restored after recovery (Goldwater et al., 2010), while in the PL and CG it is accompanied by decreased excitatory post-synaptic response to serotonin and orexin (*in vitro* observations) (Liu & Aghajanian, 2008). These structural findings are also corroborated by studies in humans: a loss of spine synapses, together with decreased expression levels of genes related to synaptic function, are observed in the dlPFC of individuals with major depressive disorder (Kang et al., 2012).

The molecular mechanisms at the basis of these morphological alterations have only recently started to be identified. First of all, decreased expression and function of Brain-derived neurotrophic factor (BDNF) and of the mTORC1 pathway have been observed in stress and depression and have been hypothesized to be at the basis of the synaptic loss (Duman, Aghajanian, Sanacora, & Krystal, 2016). BDNF is a neurotrophic factor that is required for activity dependent formation and maintenance of synapses. The expression of its mutated form ($BDNF^{Val66Met}$ allele), results in a block of the processing and release of mature BDNF and causes atrophy of PFC neurons in mice (Aghajanian, 2013). mTORC1 signaling, as previously said, is important for synaptic plasticity and in the regulation of translation of synaptic proteins. In the PFC of depressed individuals, together with a reduced expression of mTORC1 signaling proteins, it has been found also an increased expression of REDD1, a negative regulator of the mTORC1 pathway. Mutant mice with a deletion in the gene encoding for REDD1 are resilient to the effects that chronic unpredictable stress has on behavior and synaptic and mTORC1 signaling, while overexpressing REDD1 in the PFC is sufficient to get both neuronal atrophy and anxiety and depressive behaviors (Ota et al., 2014). To demonstrate the key role of the mTORC1 pathway in depression is also another study which shows that manipulations of S6K1 in the PFC can bidirectionally control

depressive behavior. Constitutive expression of S6K1 led to antidepressant effects on stressed animals, while decreased activity led to prodepressive effects, such as increased immobility in the forced swim test (Dwyer, Maldonado-Avilés, Lepack, DiLeone, & Duman, 2015).

Although these studies did not include social forms of stress, some evidences exist that correlate PFC remodeling with adaptation of social behavior. Indeed, different studies showed that chronic social defeat increases levels of ΔFosB (Vialou et al., 2014), a very stable transcription factor that is induced by long-term changes in the brain (McClung et al., 2004), and reduces myelination in the PFC (Lehmann, Weigel, Elkahloun, & Herkenham, 2017).

Moreover, work from our lab recently demonstrated that in animals which underwent 3 days defeat the amplitude of the *in vivo* evoked postsynaptic response of PFC to MDT stimulation is decreased (Fig.6), suggesting the occurrence of postsynaptic plasticity mechanisms underlying the development of social avoidance (Franklin et al., 2017). This finding is interesting in light of the recent discovery that optogenetically induced long term potentiation and depression of MDT projections to PFC induce, respectively, increased and decreased social dominance (T. Zhou et al., 2017) and that dominant animals have increased AMPARs currents in PFC layer V pyramidal neurons (F. Wang et al., 2011).

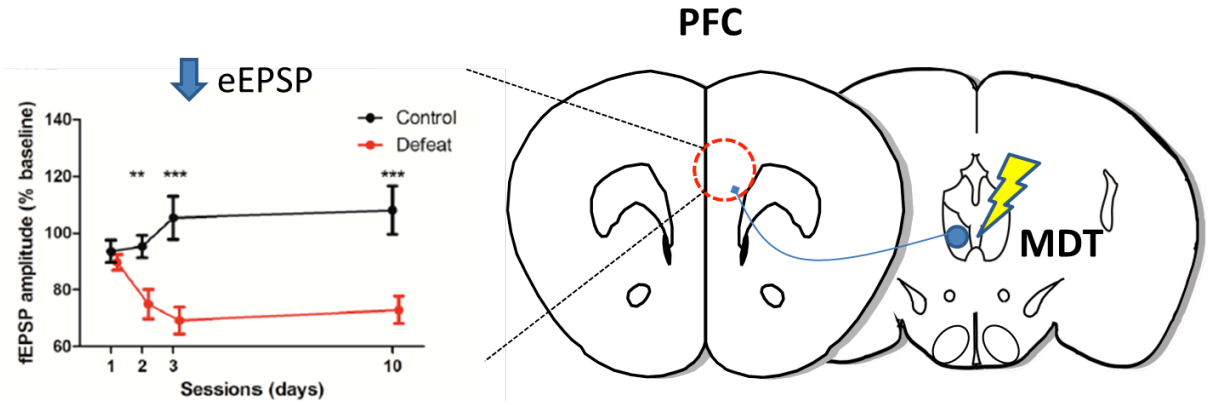

Figure 6. Decreased PFC postsynaptic response to MDT stimulation after social defeat. In defeated animals the amplitude of PFC evoked EPSP in response to stimulation of MDT is substantially decreased, at least until 1 week after the last defeat event (Franklin et al., 2017).

Aim of the project

PFC dysfunction and alterations in PFC excitatory-inhibitory balance have been recognized in disorders with a very strong social component, such as schizophrenia and depression. Also, from human and rodent studies, PFC is known to be very plastic and sensitive to stressful experiences. However, synaptic plasticity of this region in response to social traumatic experiences has been investigated only marginally. Our lab recently demonstrated that PFC-dPAG circuit is functionally disconnected in socially defeated mice and that inhibition of this circuit induces social avoidance. Moreover, PFC response to the stimulation of its main afferent, the mediodorsal thalamus (MDT), is strongly decreased in socially defeated animals (Franklin et al., 2017). These data raised the hypothesis that social defeat is inducing postsynaptic plasticity in the PFC of these animals.

To our knowledge, no studies examined the molecular plasticity of specific PFC efferents and subpopulations in response to social defeat and how this remodeling is contributing to the formation of social avoidance. For this reason, the main aim of this project was to examine synaptic plasticity in the PFC that is underlying the behavioral adaptation to social defeat. To do so, we used a social defeat paradigm that induces selectively changes in social behavior and we carried our analyses one day after the last defeat. Seen the importance of a correct excitatory-inhibitory balance for the physiology of this region, we focused on the different cell types of PFC microcircuit and integrated our findings with the study of plasticity in PFC-dPAG neurons, the main drivers of social behavior. The final scope was to use this information to reverse the behavioral plasticity induced by the defeat.

Additionally, in order to investigate postsynaptic plasticity in specific neuronal types, a second aim of this project was to set up a technique that allowed to label surface AMPA receptors after the behavioral challenge and to image them on fixed slices. Indeed, existing tools used for this aim require less convenient procedures, such as *in vivo* two photon imaging or *ex vivo* preparation of acute slices (Huganir & Nicoll, 2013; Makino & Li, 2013). In order to do so, we exploited the SNAP-tag technology, that was well established for *in vitro* and other *in vivo* preparations (Gautier et al., 2008; Yang et al., 2015), and we set it up for *in vivo* labeling in the mouse brain and subsequent imaging on fixed slices. Further, we validated the use of this novel technology in our study, to investigate functional plasticity in the PFC-dPAG circuit.

Materials and Methods

Animals

All experimental procedures were performed in accordance with protocols approved by Italian Ministry of Health. All experiments were carried on adult (3-6 months old) male mice. Mice were maintained in a temperature and humidity controlled facility on a 12-h light–dark cycle (lights on at 7:00) with food and water provided *ad libitum*. Wild type C57 BL6/J animals were obtained from EMBL local colony and CD1 animals were purchased as adult retired breeders from Charles River laboratories.

The following knock-in and transgenic lines were used:

Line	**Used as**	**Origin**
Thy1::GFP-M	Homozygous	(Feng et al., 2000)
CamK2a::Cre	Heterozygous	(Minichiello et al., 1999)
Sst::Cre	Heterozygous or homozygous	Jackson Lab. Stock 013044
Pvalb::Cre	Homozygous for breeding	Jackson Lab. Stock 008069
RC^{fsTRAP}	Homozygous for breeding	Jackson Lab. stock 022367
Flp deleter	Heterozygous for breeding	(Farley, Soriano, Steffen, & Dymecki, 2000)
*RC::*FPSit	Heterozygous for breeding	(Niederkofler et al., 2016)

Table 1. List of mouse lines.

CamK2a::TRAP, *Pvalb*::TRAP and *Sst*::TRAP were obtained crossing respectively *CamK2a*::Cre, *Pvalb*::Cre and *Sst*::Cre with RC^{fsTRAP} and were used in double heterozygosity. *Sst*::SypGFP mice were obtained crossing *Sst*::Cre mice with *RC*::LSL-SypGFP (obtained crossing *RC*::FPSit with Flp deleter animals) and used in double heterozygosity.

Molecular cloning of SNAPGluA1 constructs

For pCDNA- tdTomT2ASNAPGluA1, SNAP was inserted in place of SEP in the following intermediate vector that had been previously obtained in the lab: pCDNA-

tdTomT2ASEPGluA1. Briefly, to obtain this intermediate vector, tdTom had been PCR amplified by another plasmid owned by the lab, using the following primers:

Fw: 5' ATGGTGAGCAAGGGCGAG 3'

Rev: 5' CCGG GAATTC (EcoRI restriction site) AGGGCCGGGATTCTCCTCCACGTCACCGCATGTTAGAAGACTTCCTCTGCCCTC (T2A reverse complement) CTTGTACAGCTCGTCCATGC 3'

SEPGluA1 had been PCR amplified from another vector, pCALNL-SEPGluA1, kindly donated by Robert Malinow, using the following primers:

Fw: 5' CCGG GAATTC (EcoRI restriction site) ATGCCGTACATCTTTGCCTTT 3'

Rev: 5' CCGG CTCGAG (XhoI restriction site) TTACAATCCTGTGGCTCCCA 3'

The two fragments tdTomato and SEPGluA1 had been ligated and then inserted in a pCDNA3 expression vector (carrying the CMV promoter) previously cut with PsiI and XhoI and then ligated with tdTom-SEPGluA1 to get pCDNA- tdTomT2ASEPGluA1.

SEP was then excised using AgeI and NheI to obtain a 754bp excised sequence and a 9594bp long vector to be used for following ligation. SNAP was PCR amplified from the commercial vector pSNAPf (New England Biolabs) using the following primers:

Fw: 5' CCGG ACCGGT (AgeI restriction site) TTTCTAGGTGCGGTTGTGGGTGCCAATTTCCCTAGG (missing part of GluA1) ACCGACAAAGACTGCGAAATG 3'

Rev: 5' CCGG GCTAGC (NheI restriction site) ACCCAGCCCAGGCTTGCC 3'

The PCR product (~500bp) was then digested with AgeI and NheI to obtain sticky 5' and 3' ends and ligated with the previously opened vector (9594bp). In this way SNAP was inserted following the signal peptide of GluA1.

For pENTR1a- tdTomT2ASNAPGluA1, Gateway® pENTR™1A Vector (11813-011, Life Technologies) was cut in the multiple restriction site by EcoRI and XmnI and ligated with the tdTomato-T2A fragment mentioned above. Afterwards, pENTR1A-tdTomT2A was cut by EcoRI and XhoI to get the opened vector (~3700bp) and pCDNA- tdTomT2ASNAPGluA1

was cut by the same enzymes to get the SNAPGluA1 insert (3288bp) and the two fragments were ligated together.

After first experiments also 5'UTR and 3'UTR ends of the GluA1 gene were included in the vector: they were cut from the original Malinow's pCALNL-SEPGluA1 and inserted into our pENTR1a- tdTomT2ASNAPGluA1 vector. *(Note: insertion of the UTR ends was done by Angelo Raggioli, post-doc technician in the lab).*

Viral vectors

AAV-*hSyn*::SNAP; AAV-*hSyn*::GPI-SNAP and AAV-*hSyn*::GPI-Halo were produced in our lab (both cloning of DNA construct and viral packaging). AAV-*hSyn*::DIO-hM4DmCherry-WPRE was purchased from UNC Vector Core. For the HSV *hEF1α*::LSL-tdTom-T2A-SNAPGluA1, the cloned pENTR1a- tdTom-T2A-SNAPGluA1 sequence described above was sent to Rachael Neve at MIT McGovern Institute for Brain Research Viral Core Facility, who cloned and packaged it in an HSV vector already containing the hEF1α promoter, the Lox-STOP-Lox sequence, WPRE and polyA.

Behavioral tests

Social defeat and interaction

All behavioral testing occurred during the animal's light cycle. CD1 aggressive animals were screened for aggressive behavior placing them in the homecage of C57 wild type animals for 3 minutes. Only CD1s attacking for 3 consecutive days were used in the following behavioral tests. Social defeat was performed as previously described (Franklin et al., 2017). Briefly, mice were singly housed 3 to 7 days before the beginning of the paradigm. They were then subjected to 3 days repeated social defeat in their homecage by a different aggressive CD1 mouse each day. The daily social defeat protocol included 5 minutes of habituation to the room (the cage lid was removed), 5 minutes of sensory contact with the aggressor, that was placed in the mouse homecage behind a wire mesh barrier, allowing for approach and investigation from the resident, and finally, removal of the barrier and 10 minutes of social defeat, during which the resident mouse was repeatedly attacked by the aggressor. Control animals underwent the same protocol, except for the 10 minutes attacks, which were replaced by 10 additional minutes of sensory contact through the wire mesh barrier.

Social interaction was carried in a similar manner, but consisted only of 5 minutes of habituation and 5 minutes of sensory contact behind the wire mesh barrier.

Behavioral scoring

Avoidance during the 5 minutes barrier was automatically scored using Viewer III (Biobserve). To monitor avoidance time, the part of the homecage that did not contain the wire mesh barrier with the aggressor, was virtually divided in two equal zones, called approach and avoidance zone, in respect to the distance from the barrier. Time spent investigating during the first 3 minutes of the barrier period was quantified manually on the recorded video using The Observer XT11 (Noldus Information Technology, Wageningen, Netherlands) or Solomon Coder (version beta 17.03.22).

Stereotactic surgeries and perfusion

Prior to surgery mice were anesthetized with isoflurane (3-3.5%) in oxygen and then placed in a stereotactic frame (KOPF Instruments), where anesthesia was maintained by continuous administration of 1.5-2% isoflurane in oxygen by nose. For all surgeries the skull surface was exposed and aligned. All injections were performed using a glass capillary. The volume injected per region was 0.2-0.3 µl of viral solutions or 0.1-0.2 µl of cholera toxin subunit B Alexa 647/555 (CTB 647 and CTB 555, Life Technologies). After release of viral solutions or CTB the capillary was left in place for 10 minutes before removal. All antero-posterior (AP) and lateral (L) coordinates were calculated from bregma and dorso-ventral (DV) coordinates were calculated from brain surface, apart for dorsal PAG where DV coordinates were calculated from the skull. The used coordinates were AP: 1.71 mm, L: ±0.5 mm, DV: 1.5mm for PFC; AP: -4.2 mm, L: -1.18 mm, DV: 2.36 mm, -26° angle for dPAG; AP: 1.42 mm, L:-1.33 mm, DV: 3.5 mm for NAcc; AP: 1.85 mm, L: ±2.8, DV: 2.65 for insula. Only for pharmacogenetics experiments, half of the viral solution (AAV-*hSyn*::DIO-hM4DmCherry-WPRE) was released at 0.75 depth in the PFC and another half at 1.5 depth in the PFC, to enlarge the infection site. For i.c.v. delivery, a single 26-gauge stainless steel guide cannula (4 mm projection from pedestal, PlasticsOne) was implanted into lateral ventricle (AP: -0.2 mm, L: 1.15 mm, DV: 2 mm) and secured to the skull with dental cement (Duralay). Cannula was closed with a fitting dummy that projected 0.2 mm outside of the guide. After all surgeries skin was sutured and animals were placed on a heatpad for recovery. For all experiments involving stereotactic surgeries, the viral, tracer or cannula

location was always checked on serial coronal mouse brain sections at the end of the experimental procedures. Only mice with right locations were included in the study.

Western Blot

After cervical dislocation the whole prefrontal cortex was quickly manually dissected on a glass surface previously refrigerated with liquid nitrogen evaporation. Each PFC was homogenized in lysis buffer using a tissue homogenizer and a syringe and then incubated for 1h at 4°. One part of the lysate was then directly used for protein estimation with a Pierce BCA Protein Assay Kit (Thermo Scientific) in a standard spectrophotometer and the remaining part was added with equal volume of protein loading buffer, boiled at 95°C for 5', aliquoted and frozen at -80°C for subsequent use. 40 μg protein per sample were then used for Western Blot procedure. Samples were run on a 12.5% resolving gel and then transferred on a PVDF Membrane (Immobilon-P, Millipore). Membranes were blocked in 5%BSA TBS-T RT for 6h and then incubated with primary antibodies against the phosphorylated proteins at 4° o.n. The day after, membranes were incubated 1h RT with secondary antibody, (HRP linked anti rabbit, 1:20000, Amersham) and developed using Amersham ECL Western Blotting Detection Reagents (GE Healthcare). Imaging was done in a Chemidoc MP Imaging System (Biorad). Membranes were then stripped with Restore PLUS Western Blot Stripping Buffer and, after 1h 30 blocking, they were incubated with primary antibodies against the total proteins o.n. at 4°C and the same procedure described above was followed. Then, again, membranes were stripped and blocked for the last time for 1h 30 and incubated with antibody against GAPDH o.n. at 4°C and the same procedure was followed. Image densitometry was performed using Fiji.

Protein	**Code (Cell Signaling)**	**Concentration**
pS6 (Ser235/236)	2211S	1:1000
pAkt (Ser473)	#9271S	1:500
pGSK3β (Ser9)	9336S	1:500
p-eIF2α (Ser51)	9721S	1:500
S6 ribosomal protein	2217S 5G10	1:3000

Akt	#9272	1:1000
GSK3β	9315S	1:3000
eIF2α	9722S	1:1000
GAPDH	2118S	1:5000

Table 2. List of antibodies used in Western Blot

Buffers and Reagents for Western Blot

Lysis buffer

150mM NaCl

50mM Tris-HCl (pH 8.0)

1% NP-40

Protease inhibitors (cOmplete™, EDTA-free Protease Inhibitor Cocktail, Roche)

Phosphatase inhibitors (PhosSTOP™, Roche)

Running buffer 10X

250mM Tris base

1.92M Glycine

1% SDS

Transfer buffer 10X

250mM Tris

1.92M Glycine

(in Transfer Buffer 1X include 20% Methanol)

TBS 10X

200mM Tris-HCl pH 7.6

1.5M NaCl

(In 1X TBS-T add 1% Tween)

Blocking buffer:

5% BSA in 1X TBS-T

Loading buffer (Laemmli 2X)

10% w/v SDS

20% Glycerol

120mM Tris-Cl pH6.8

Bromophenol blue 0.02%

Translating Ribosome Affinity Purification (TRAP)

After cervical dislocation, the whole prefrontal cortex was quickly manually dissected on a glass surface previously refrigerated with liquid nitrogen evaporation. Prefrontal cortices from 3 mice of the same group were pooled together in each single sample for profiling of Parvalbumin$^+$ neurons, while each sample was made by the PFC of a single mouse for both Somatostatin$^+$ and CamK2a$^+$ neurons profiling experiments. The subsequent TRAP procedure was performed as previously described (Heiman et al., 2014). The RNA quality and amount was checked in a 2100 Bioanalyzer instrument using a RNA 6000 Pico Kit (Agilent Technologies). Only samples with an RNA integrity number (RIN) over 7.0 and a total amount of RNA of 1 ng minimum were used for subsequent microarray procedure.

Microarray analysis

Microarray procedures (MoGene 2.0 st, Affymetrix) were performed by EMBL GeneCore Facility at EMBL Heidelberg following a low input protocol for RNA amplification. Respectively, 5 ng, 2.8 ng and 1 ng were used as initial RNA starting amount for *CamK2a*::TRAP, *Pvalb*::TRAP and *Sst*::TRAP samples. Obtained CEL files were processed in GenePattern to originate a .gct expression file using AffyST Expression File Creator module. RMA and quantile normalization was applied and expression values were log converted. PCA was carried to identify presence of outliers. One outlier was excluded after PCA from each of the three experiments, ending up to 4 samples for sensory and 5 for defeated for *CamK2a*::TRAP experiment, 3 samples for sensory and 4 for defeated for *Sst*::TRAP experiment and 2 samples for sensory and 3 for defeated for *Pvalb*::TRAP experiment (where each *Pvalb*::TRAP sample was coming from a pool of three animals). The dataset was then collapsed using Median of probes and specificity of TRAP procedure was verified by checking the expression levels of several reference genes (see results). Following this quality control, gene expression data were filtered this way: only genes for which at least one sample had a log expression value of 6.5 (for CamK2a and Pvalb) or 7 (for Sst) were kept for the subsequent analyses. To check for statistical significance, the Comparative Marker Selection GenePattern module, with 0 permutations, was run on the data set. Several genes with a p-value below 0.05 (classical t-test) were identified, but none of them presented a False Discovery Rate (FDR) <0.05. We then ran a Gene Set Enrichment Analysis using GSEA Preranked module. For each of the three experiments, genes were ranked according to the t-test score returned by the comparative marker selection analysis. All parameters were

left as default, apart “minimum gene set size: 10”; “1000 permutations by gene set”. The following gene sets databases were used: KEGG, Reactome, Biocarta and all Gene Ontology databases. Only enriched Gene Sets with an FDR<0.05 were used to carry a Leading Edge Analysis, using the designed module contained in the GSEA software, to get a list of all genes that were leading the enrichment in the sensory or defeated group. This list of genes was filtered to get only genes that by themselves had a logFoldChange>0.27 (Fold Change>1.2) and a p-value <0.05 and these genes were used to create a network and visualize protein-protein interactions using STRING in Cytoscape. For each protein-protein interaction STRING provides a confidence score. Score goes from 0 to 1 and indicates the likelihood that an interaction is biologically relevant. Score is computed taking into account seven types of evidences: experiment, pathway database, textmining, coexpression, neighborhood, fusion, phylogenetic co-occurrence (Szklarczyk et al., 2017). For the present work, networks were created using a minimum confidence score of 0.4 (intermediate confidence).

Transfection and SNAP-tag labeling of HEK cells

HEK293T cells were cultured in DMEM (Gibco) medium additioned with 10%FBS and penicillin/streptomycin 50 µg/ml. Cells were transfected using polyethylenimine (PEI) transfection protocol. Briefly, transfection solution was prepared in DMEM (without serum): DNA (the pCDNA- tdTomT2ASNAPGluA1) and PEI (1mg/ml) were mixed in a ratio 1:3.5 (DNA µg/ PEI µl) and the solution was incubated for 15’ at RT. Cells were incubated with the transfection solution 37° o.n. (solution/ fresh complete medium: 1/10). Before proceeding to SNAP-tag labeling, cells were checked for tdTomato expression under an optical microscope. Transfected cells were incubated with 5µM of SNAP-Cell 505 or SNAP-Surface Alexa 488 (New England Biolabs), dissolved in complete medium, at 37° for 30’ and washed 3 times with complete medium before imaging.

SNAP-tag labeling on fixed brain slices

Mice were deeply anesthetized with Avertin 2.5% (Sigma-Aldrich) and perfused transcardially with PFA 4% in PB 0.1M pH 7.4; brains were then postfixed in PFA 4% overnight and then cut in PBS 1x by vibratome (Leica Microsystems) in serial coronal sections (50µm). Slices were washed for 15 minutes in PBS Triton 0.3%. Slices were then incubated with either the BG substrate SNAP-Surface Alexa Fluor 647 or SNAP-Cell 647-SiR (1µM, New England Biolabs) in PBS Triton 0.3% for 30’ RT with gentle shaking. After

that, 3x15' washes in PBS Triton 0.3% were done before staining with DAPI (5µg/ml, Molecular probes).

SNAP-tag or Halo-tag labeling *in vivo* in the mouse brain

For tagging of surface exposed SNAP (or Halo) fused proteins, a cannula was implanted in the lateral ventricle at least 1 week before the labeling. SNAP-Surface Alexa Fluor 647 (New England Biolabs) or HaloTag Alexa Fluor 488 ligand (Promega) was diluted up to 150 µM in PBS 1X (1:6.5 of the original dilution of reagents) on the day of the injection and kept in ice. Injection was performed with a Hamilton Syringe inserted in an infusion pump (SP210 iwz, World Precision Instruments). A total of 1 µl of 150 µM ligand was injected through the guide cannula in the ventricle of the awake mouse with a constant flow rate of 1 µl/min. The injector (0.3 mm projection from the guide) was left in place for another 1-2 minutes after the end of the ijection to allow diffusion of the substrate. Guide cannula was then closed with dummy and the animal was perfused 1h later.

For tagging of intracellular SNAP fused proteins SNAP-Cell 647-SiR (0.1 µl, 1mM in DMSO) was injected directly in the tissue with a stereotactic surgery procedure and the capillary was left in place for 10 minutes. The animals were perfused 1h after the removal of the capillary.

Immunostainings

In order to carry all the staining procedures mice were deeply anesthetized with Avertin 2.5% (Sigma-Aldrich, St Louis) and perfused transcardially with PFA 4% in PB 0.1M pH 7.4 one day after the last defeat. Brains were then post-fixed in PFA 4% overnight at 4°C. For long-term storage, brain slices were kept in PBS 1X with 0.02% sodium azide (Sigma Aldrich) and washed three times with PBS 1X just before starting free floating staining procedures. For all stainings, all primary and secondary antibodies were dissolved in blocking solution and application of secondary antibodies was always preceded and followed by 3 washes with PBS 1X. 15 minutes DAPI (5 µg/ml, Molecular Probes) staining was carried before the last wash before mounting. Slices were finally mounted on SuperFrost Plus slides (Thermo Scientific) and coverslipped with Mowiol.

Immunofluorescence for ΔFosB and pS6

After post-fixation brains were moved in sucrose 30% (in PBS 1X) for cryoprotection, where they were left until they sank. Brains were then frozen in isopentane (Sigma-Aldrich) and cut

by cryostat (Leica Microsystems) in 40 μm thick slices. Slices were blocked in blocking solution (BSA or Normal Goat Serum 5%, Triton-X 0.1%) for 1h and then incubated overnight with primary antibody (anti NeuN 1:500, mouse, Millipore and anti FosB, 1:1000, goat, Santa Cruz Biotechnology or anti-phosphoS6 (Ser235/Ser236), (1:200, rabbit, Cell Signaling) o.n. 4°C. Slices were then incubated for 1h with secondary antibodies Alexa 647 Donkey anti-Mouse, Alexa 488 Donkey anti-Goat (for ΔFosB) or Alexa 488 Goat anti-Rabbit (for pS6), (1:800, Thermo Fisher Scientific).

Immunohistochemistry for pCREB

For pCREB immunohistochemistry brains were cut by cryostat as just described. Slices were quenched for 15' in 3%H_2O_2 (Sigma Aldrich), 10% CH_3OH (Sigma-Aldrich), then washed 3 times with PBS-Triton 0.1% and blocked for 1h in PBS-Triton 0.1% before o.n. incubation at 4° with anti-pCREB Ser133 (1:1000, rabbit, Millipore). On the following day biotinylated Goat anti Rabbit (1:200, Vectastain) was used for 1h, followed by 1h 30 incubation with Avidine Biotin Elite (ABC kit, Vectastain), following manufacturer's instructions. Staining was then developed with 3,3′-Diaminobenzidine (DAB) 0.05% H_2O_2 0.03%. Developing reaction in H_2O_2 was blocked with rinses in PBS 1X. Slices were then mounted on SuperFrost Plus slides (Thermo Fisher Scientific), allowed to dry overnight, dehydrated with increasing alcoholic concentrations and mounted in Permount Mounting Medium (Fisher).

tdTomato amplification

For SNAPGluA1 experiments, after post-fixation brains were cut by vibratome in 70-100 μm thick slices. Slices were blocked in blocking solution (NGS 5% Triton X 0.3%) for 1h and then incubated with an anti RFP antibody (1:500, rabbit, Rockland Immunochemicals) o.n. 4°C to amplify tdTomato signal. As a secondary antibody, Alexa 546 Goat anti-Rabbit was used.

GFP amplification

For reconstruction of pyramidal neurons from *Thy1*::GFP animals, post-fixed brains were cut by vibratome in 250 μm thick slices. Slices were permeabilized with Triton 0.5% for 1h30' and then blocked in blocking solution (NGS 5% Triton 0.3%) for 1h. GFP signal was then amplified with an anti GFP antibody (1:600, rabbit, Invitrogen) with o.n. incubation at 4°C. As a secondary antibody Alexa 488 Goat anti-Rabbit (1:800, Thermo Fisher) was used.

Perineuronal net staining

For perineuronal net staining, post-fixed brains were cut by vibratome in 50 μm thick slices. Slices were blocked in blocking solution (NGS 5% Triton 0.3%) for 1h and then incubated with an anti-Parvalbumin antibody (1:1000, mouse, Millipore) and with the biotinylated lectin Wisteria Floribunda Agglutinin (WFA) (1:500, B-11355, Vector Laboratories) o.n. at 4°C. On the following day, slices were incubated for 1h with Alexa 647 Goat anti Mouse (1:800, Thermo Fisher) and Alexa 546 Streptavidin (1:600, Thermo Fisher).

Image acquisition and analysis

Dendritic arborization and spine density of PFC-dPAG neurons

Images were acquired at a laser resonant scanning confocal microscope (Leica TCS SP5 Resonant). For dendritic reconstruction a 40x oil objective was used (z-step 0.46 μm, zoom 1.7X). Each image resulted by stitching at least 6 adjacent stacks (minimum 80 μm thick) together in a single merged tilescan. To be included in the analysis, the GFP positive neurons had to be positive for CTB647 and the soma had to be located at least 35 μm below the edge of the stack. Neurons were reconstructed manually in Neurolucida (v7). Layers were drawn manually using as references the distribution of DAPI staining and the two colours CTB staining identifying layer V neurons projecting to the dPAG (CTB647) and layer II/III neuron and layer V neurons projecting to the NAcc. All the analyses (total and layer specific dendritic length, branching and Sholl analysis) were carried in Neurolucida Explorer.

For spine density analysis a 63x oil objective was used (z-step 0.13 μm, zoom 5X). Dendrite was traced and spines were counted manually in Neurolucida along the z-stack and both dendritic length and spine number were quantified using Neurolucida explorer.

SNAPGluA1 enrichment

Images were acquired at a laser scanning confocal microscope (Leica TCS SP5), using a 63x oil objective and a 5x magnification (z-step 0.38 μm). Apical tuft images were all taken from the proximal part of the apical tuft (starting about 3 μm after the first bifurcation). Anti-RFP antibody use was due to otherwise very high bleaching of endogenous Tomato signal: no differences in antibody penetration were observed (probably also due to the fact that Tomato positive neurons were very sparse, so the antibody did not tend to remain stuck at the edges of the slices (data not shown)). Care was anyway taken to avoid the edges and also the 10-20 deepest μm of the slices (that were 70-100 μm thick). Images came from at least 3 different

brain slices and no discrimination between cingulate, prelimbic and infralimbic cortex was made. For each animal 6-9 oblique dendrites and 3-8 apical proximal tufts images were acquired. Animals with a very low infection degree had none or very few retrogradely labeled neurons and were excluded from the analysis. Analysis was done in Fiji, as described in "Image and data analysis of SNAPGluA1 results".

Synaptophysin-GFP

Images were acquired at a laser scanning confocal microscope (Leica TCS SP5), using a 63x oil objective and a 4x magnification. Stacks had all the same volume (4.16 µm, z-step 0.38 µm). For each animal 6 images were acquired from 3 different slices (6 emispheres) for either cingulate, prelimbic or infralimbic cortex. Layer I was recognized using DAPI staining; while cingulate, prelimbic and infralimbic cortex were recognized visually using as a reference the upper corner between motor and prefrontal cortex, the fornix or corpus callosum, and, for caudal slices, the beginning of the ventricle (considered as the lower boundary of the infralimbic cortex). Number of boutons and bouton volumes were quantified automatically by using the Surface function in Imaris 8. Number of boutons was then divided by the total volume of the image (15701 μ^3) to get bouton density.

Perineuronal net

Images were acquired at a laser scanning confocal microscope (Leica TCS SP5), using a 40x oil objective. Stacks had a fixed volume (10 µm, z-step 0.5 µm). Always the first 10 µm from the edge of the slice were acquired. Cingulate, prelimbic and infralimbic cortex (six pictures per region, from 3 different slices) were identified as described above. Analyses were done manually on the z-stack in Fiji. $Pvalb^+$, WFA^+ and $Pvalb^+$ /WFA^+ neurons were manually identified. A region of interest (ROI) was manually drawn, separately for each channel, around each Parvalbumin positive neuron and around each WFA positive neuron and mean intensity of the ROI was quantified.

Other immunostainings

For ΔFosB, pCREB and pS6 stainings, images were acquired with a 10X objective at a widefield microscope (Widefield Leica DMI 6000 B) with a motorized xy stage that allowed to obtain a tilescan of the entire brain slice. Numbers of $pCREB^+$; $pS6^+$/ $NeuN^+$ or $\Delta FosB^+$/$NeuN^+$ cells were quantified in a semiautomated manner using Fiji. Images were thresholded and then ROIs were drawn around cg, pl and il cortex according to the Mouse Brain Atlas (Franklin and Paxinos, 2008). In each ROI, numbers of cells were counted using

fixed parameters for the “Analyze particles” tool and colocalization was examined using the “Image calculator” tool. Colocalization masks were visually checked.

Image and data analysis of SNAPGluA1 results

All of the analyses were carried in Fiji in a semi-automated manner. Intensity measurements were done along the Z-stack. Three different ROIs were used for spines (circular, 1 μm diameter), shaft (squared, 0.5 μm x 0.5μm) and background (squared, 1 μm x 1 μm). ROIs for spines were placed manually around each spine, in a way to contain both tomato and SNAPGluA1 signal, on the z-section where the spine size (identified by tomato) was the largest. For the background, at least 6 ROIs per picture were used, that were manually placed avoiding autofluorescent spots. For the shaft, at least 10 ROIs per picture, distributed along the entire dendritic shaft, were used and manually placed on the z-section where tomato brightness was the highest. Care was taken to avoid regions where perpendicular spines were present. ROIs of spines, shafts and backgrounds were extracted and mean pixel intensity was obtained for both channels from both the z-section where the ROI was placed and also the 3 consecutive previous and following z-sections. The mean pixel intensities from these 7 consecutive sections were then averaged to obtain the final value for the specific ROI. The 6 background values measured from the same picture were averaged to obtain a unique background value and the same was done for the 10 shaft portions. For each image and channel it was then obtained one final intensity value for the shaft, one for the background and one for each spine.

Both shaft and spines Tomato and SNAPGluA1 mean intensity values were background subtracted. Spine size was estimated dividing the mean intensity for spine Tomato by the mean intensity of shaft Tomato, to normalize for the degree of expression of the HSV in the single neuron:

$$\text{Spine size} = \frac{\text{Spine Tom intensity}}{\text{Shaft Tom intensity}}$$

Surface GluA1 content per spine was estimated dividing the mean intensity of spine GluA1 by the mean intensity of shaft GluA1, to normalize for the efficiency of the BG labelling. Shaft GluA1 intensity depends, indeed, on both the efficiency of the BG labeling and the level of expression of the virus in the single neuron (data not shown):

$$\text{Spine surface GluA1} = \frac{\text{Spine GluA1 intensity}}{\text{Shaft GluA1 intensity}}$$

As a measure of spine potentiation (surface GluA1 enrichment) Spine surface GluA1 was divided by the spine size.

$$\text{Spine GluA1 enrichment} = \frac{\text{Spine surface GluA1}}{\text{Spine size}}$$

All data were log transformed to make distributions normal and fitting in the used statistical model (see "Statistical analyses").

Statistical analyses

All statistical analyses were carried in GraphPad Prism 5, apart Pvalb/WFA intensity and SNAPGluA1 experiment, that were carried in JMP Pro 12.1. Graphs are represented as either dot plots, with mean ± SEM, or classical box plots and cumulative probability plots for the SNAPGluA1 experiment, where cumulative probability plots indicate the probability (y axis) of being above or below a particular value for the observed measurement (x axis). All used statistical tests are described in figure captions, apart those for microarray analysis, which are described above (see "Microarray procedure and analysis").

For SNAPGluA1 experiment; spine size, spine surface GluA1 and spine GluA1 enrichment for each spine were log converted and analyzed using a mixed model where behavior and experimental batch were considered the fixed effects and animal and dendrite (nested in animal) were the random effects.

Results

Social defeat induces changes in translation-related plasticity markers eIF2α and GSK3β in the whole PFC

To start to explore if social defeat was inducing any molecular plasticity in the PFC, we examined the levels of some transcriptional and translational markers of plasticity one day after the last defeat. As expected, animals undergoing 3 days social defeat increased significantly their social avoidance, as measured in the 5 minutes interaction preceding the defeat, compared to controls which just had a sensory contact with the aggressor (Fig.7).

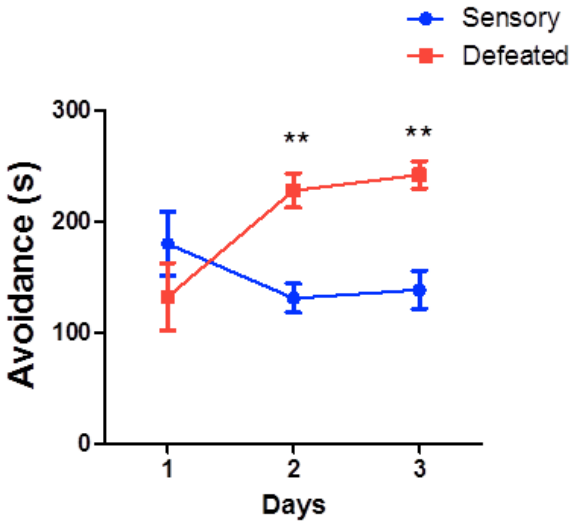

Figure 7. Social avoidance progression during a 3 days social defeat paradigm. While sensory contact only slightly decreases levels of social avoidance, defeated animals become progressively more avoidant during the three days (defeat, p=0.029; day x defeat, p=0.0001). Data were analyzed by two way ANOVA RM plus Bonferroni post hoc analysis. N=10; ** p<0.01

We then conducted an immunofluorescence (IF) against the two plasticity related transcription factors ΔFosB (Fig. 8g) and pCREB (the activated version of CREB) (Fig. 8h), and the ribosomal protein pS6 (Fig. 8i), activated by phosphorylation by S6K1 (Costa-Mattioli et al., 2009; Dwyer et al., 2015). We found that pS6, but not pCREB and ΔFosB, was significantly decreased in the cingulate and prelimbic part of the prefrontal cortex (Fig. 8d, e and f). We also tested for the same markers other important regions for instinctive behavior, namely the ventromedial hypothalamus (VMH) dorsomedial and ventrolateral part (Silva et al., 2013) and the PAG dorsal regions (Fig. 8b and c), but no significant effects were found in there, except for some subregional differences (Fig. 8, see legend).

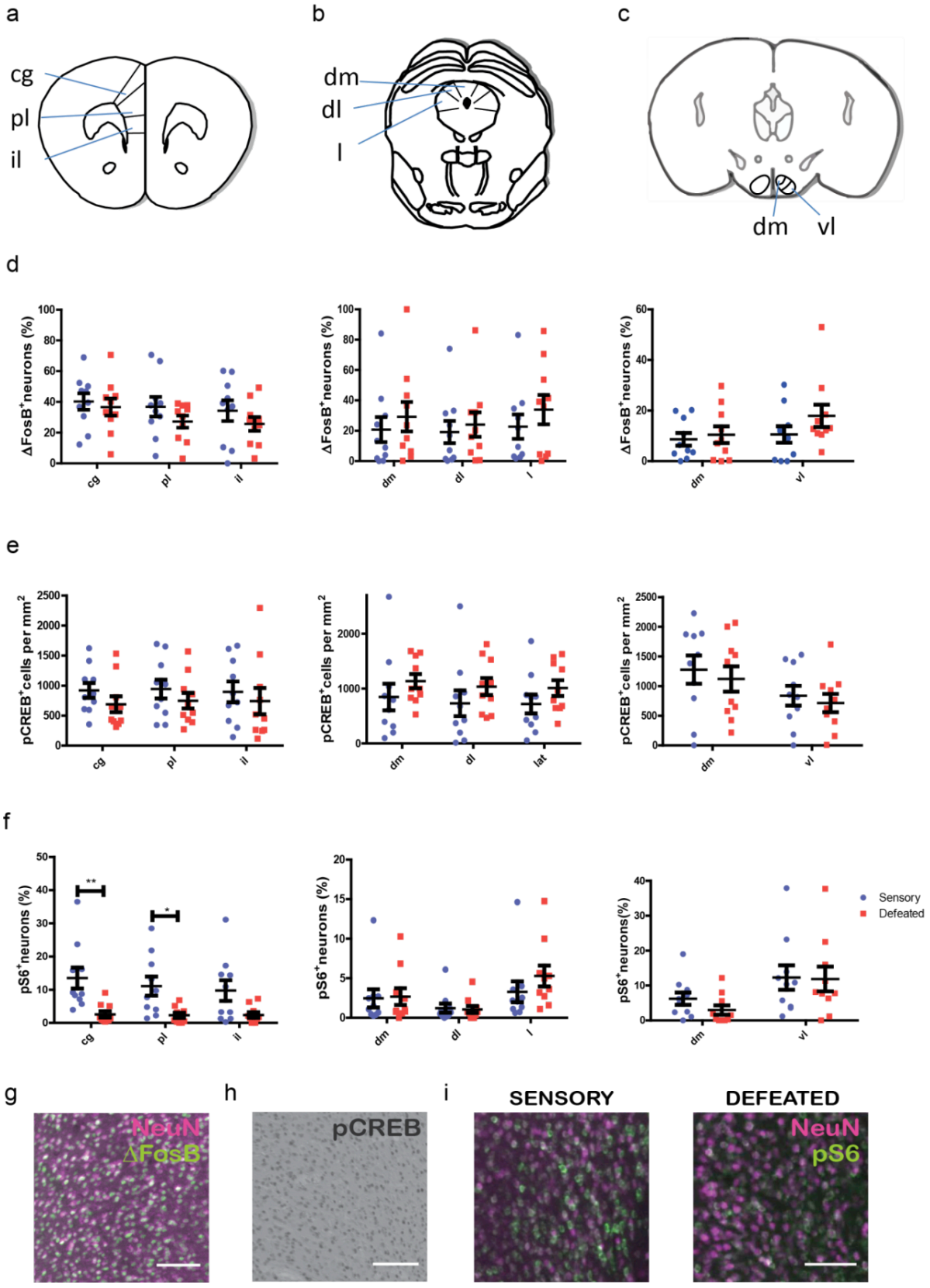

Figure 8. Social defeat induces a decrease of pS6 levels selectively in the PFC but no other changes in the plasticity markers ΔFosB and pCREB. Schematic representation of coronal slices of the analyzed regions: **(a)** PFC (cg=cingulate, pl=prelimbic, il=infralimbic); **(b)** dPAG (dm=dorsomedial, dl=dorsolateral, l=lateral) and **(c)** VMH (dm=dorsomedial, vl=ventrolateral). **(d)** From left to right: percentages of ΔFosB+/NeuN+ cells are

unchanged after the defeat in PFC, dPAG and VMH, but vary by region in PFC (region, p=0.0263) and VMH (region, p=0.0461). **(e)** From left to right: density of pCREB+cells is unchanged after the defeat in PFC, dPAG and VMH but varies by region in dPAG (region, p=0.0393) and VMH (region, p=0.0001). **(f)** Left: pS6 +/NeuN+ cells are significantly decreased in PFC (defeat, p=0.0057); middle and right: pS6 +/NeuN+ are changing only by region in dPAG (region, p<0.0001) and VMH (region, p=0.0124). Representative images of PFC staining for **(g)** ΔFosB, **(h)** pCREB, **(i)** pS6. All analyses were done by two way ANOVA RM plus post-hoc Bonferroni corrections. N=10 animals. ** p<0.01, * p<0.05 Scale bars are 50μm

Seen the role of pS6 in the context of translation, we extended the analysis to some signalling molecules that are related to synaptic protein synthesis (Fig. 9a). To this aim, we used Western Blot to analyze again pS6, Akt, an upstream marker of the mTORC1 pathway, eIF2α and GSK3β. Contrarily to Akt and S6, eIF2α and GSK3β are both inactivated by phosphorylation. Decreased phosphorylation of EIF2α is observed in plasticity, while active GSK3β inhibits Akt-mTORC1 pathway and seems to promote AMPAR internalization in LTD (Peineau et al., 2007). Furthermore, p-eIF2α and non phosphorylated GSK3β are also markers of endoplasmic reticulum (ER) stress, a pathway activated in several neurological disorders (Klann & Dever, 2004). Finally, GSK3β levels seem to be altered in depression and to be normalized by ketamine (Li & Jope, 2010; Piochon, Kano, & Hansel, 2016).

Unexpectedly, we could not replicate our IF result for pS6, that did not show any change neither in its total nor phosphorylated levels in the whole PFC of defeated animals (Fig. 9h and i). This could be due to the fact that changes observed in the IF were related to high intensity $pS6^{+}$neurons (see Methods) and could be too subtle to be detected by Western Blot. Also Akt, that is upstream pS6 signaling, did not show any change in either its total or phosphorylated levels (Fig. 9d and g). Instead, both the levels of total GSK3β and total eIF2α were significantly increased in the PFC of defeated animals (Fig. 9b and c) even if no changes were detected in their phosphorylated counterparts (Fig. 9e and f), making difficult to draw conclusions about their activation state. These results suggest that ER or translational stress could be occurring in the PFC of defeated animals.

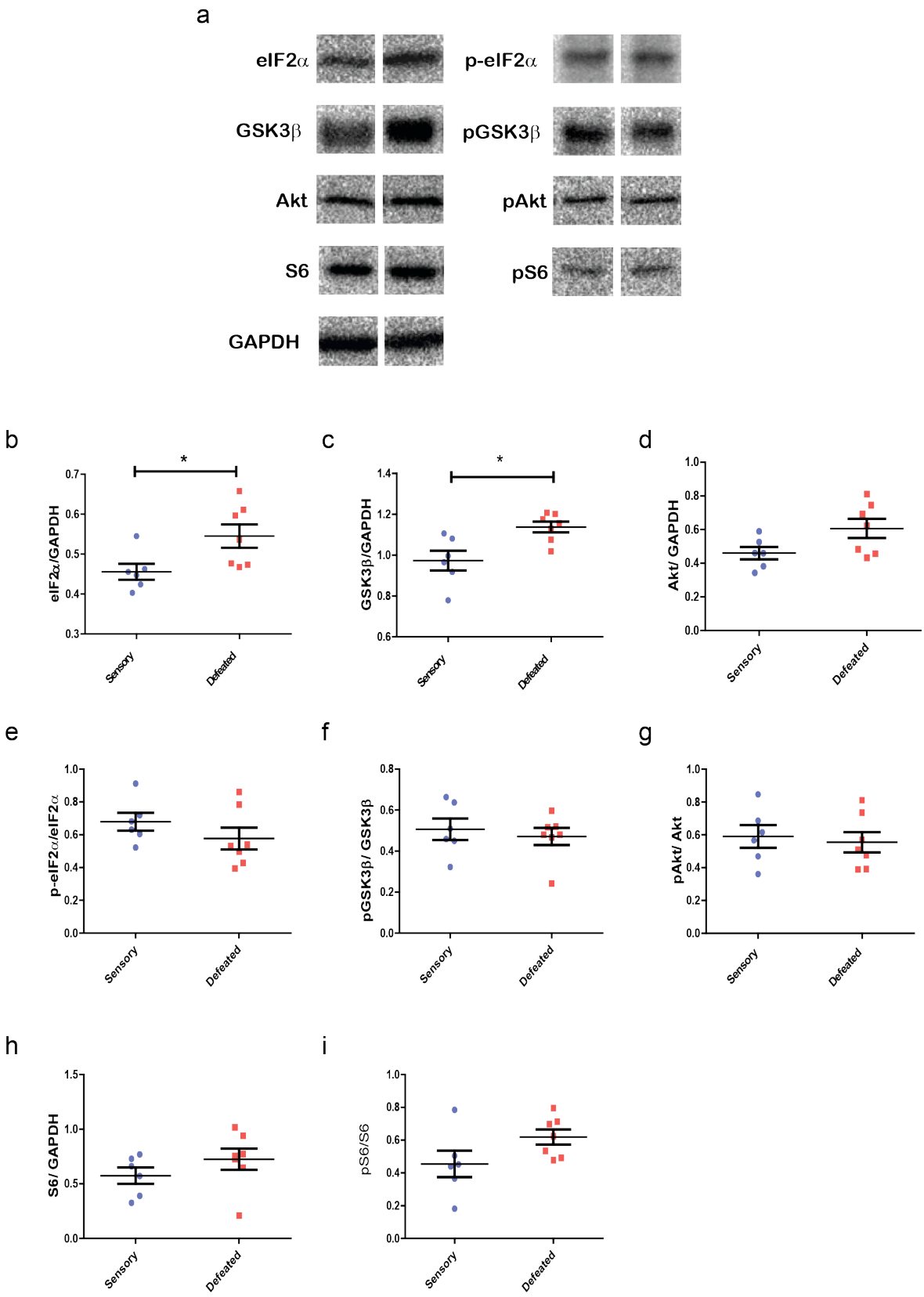

Figure 9. Increased expression of proteins related to ER/translational stress after social defeat. (a) Representative WB images. **(b)** Total eIF2α and **(c)** total GSK3β are increased in defeated animals. No changes are observed in **(d)** total Akt, **(e)** phosphorylated eIF2α, **(f)** phosphorylated GSK3β, **(g)** phosphorylated Akt, **(h)** total S6 and **(i)** phosphorylated S6. Data were analyzed by t-test. N=6 sensory, 7 defeated. *$p<0.05$

Setup of TRAP technique in the PFC to study translational remodelling of different neuronal types

As social defeat demonstrated to alter some translational markers of plasticity; in order to understand the contribution of the different prefrontal cortical cell types to the behavioral (and molecular) acquisition of the defeated phenotype, Translating Ribosome Affinity Purification (TRAP) technique was used. TRAP allows to isolate the RNA bound to ribosomes (namely translated mRNA) from a specific cell type (Heiman et al., 2014). In order to use this technique we used conditional knock-in animals (*RC*::LSL-L10A-EGFP) that express an EGFP fused version of the ribosomal protein L10A in response to Cre (P. Zhou et al., 2013). Only Cre expressing cells of these mice contain EGFP labeled ribosomes and EGFP immunoprecipitation allows to isolate them together with the bound mRNA, that can be used for following applications.

We crossed *RC*::LSL-L10A-EGFP animals with *CamK2a*::Cre, *Sst*::Cre and *Pvalb*::Cre animals, to get, respectively, only labeled ribosomes from the glutamatergic ($CamK2a^+$), and the two prominent GABAergic subpopulations ($Somatostatin^+$ and $Parvalbumin^+$.) As also evidenced by endogenous L10A-EGFP fluorescence (Fig. 10a, c and e), these three subpopulations have a very different abundance in the PFC, so we carried pilot experiments to set up the number of mice to pool and the concentration of affinity matrix to use for the immunoprecipitation, to get enough (>1ng) and good quality (RNA Integrity Number (RIN) > 7) RNA for subsequent procedures. PFC lysate from a single animal was sufficient to get enough and good quality RNA from *CamK2a*::TRAP (72 ng, RIN: 9.2; Fig. 10b) and *Sst*::TRAP (4 ng, RIN: 8.3; Fig. 10d) animals. For *Pvalb*::TRAP, instead, it was necessary to pool PFCs from 3 animals (24 ng, RIN: 9; Fig. 10f). The concentration of the affinity matrix used was the same described in Heiman et al., 2014 for *CamK2a*:: TRAP animals, half of that for *Sst*::TRAP animals and ¼ of that for *Pvalb*::TRAP animals. For all the three pilots, unremarkable amount of RNA was obtained from EGFP immunoprecipitation at the same conditions from PFCs of WT control animals (2.4 ng, 0.6 ng and 6 ng respectively for WT controls of *CamK2a*, *Sst* and *Pvalb*::TRAP), indicating a high signal to background ratio of the technique (Fig. 10b, d and f), due to low levels of contaminating aspecific RNA coming from non-Cre expressing cell types.

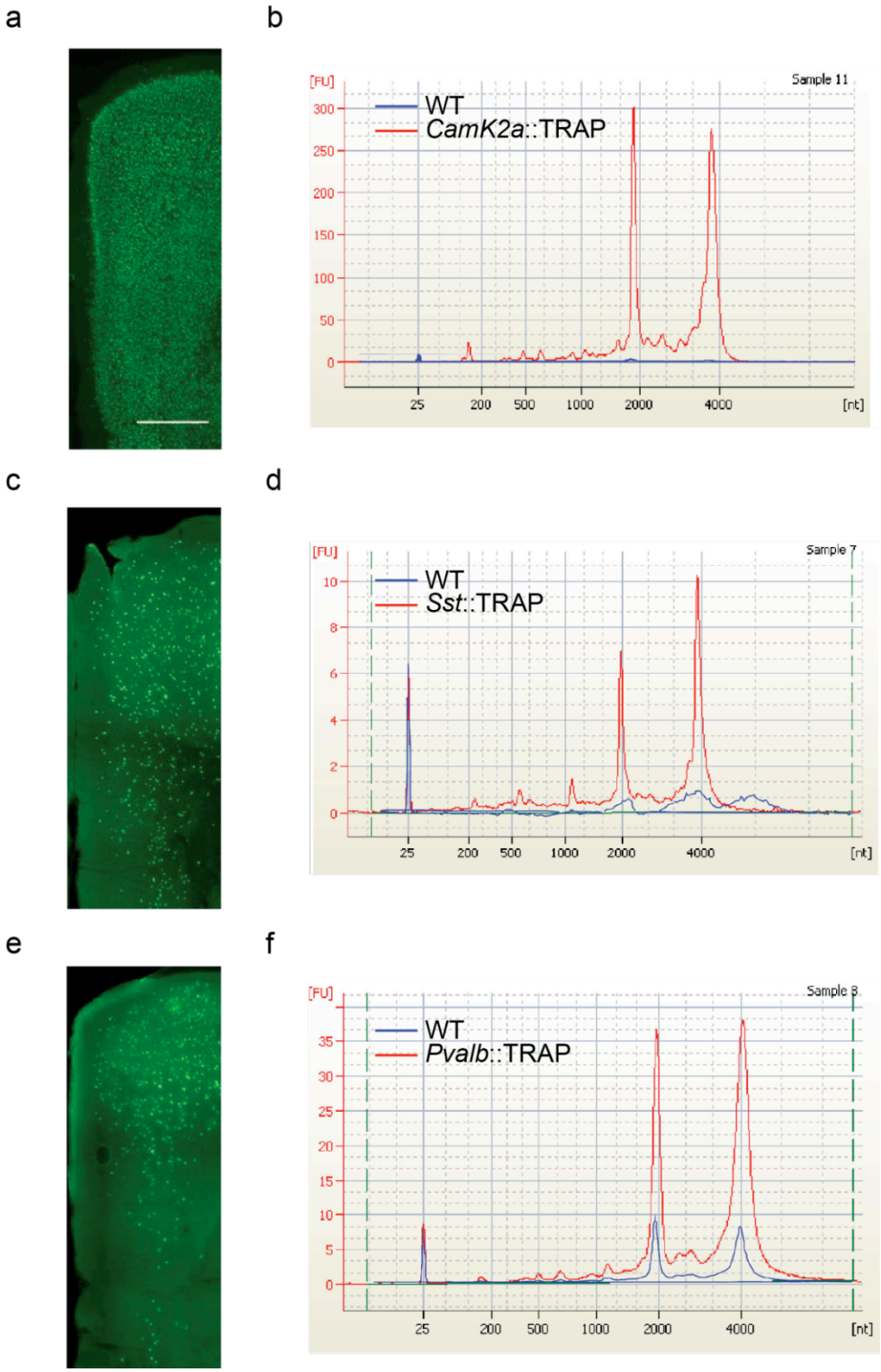

Figure 10. Setup of TRAP technique in CamK2a$^+$, Sst$^+$ and Pvalb$^+$neurons of the prefrontal cortex. Representative images of the prefrontal cortex of **(a)** *CamK2a*::TRAP, **(c)** *Sst*::TRAP, **(e)** *Pvalb*::TRAP animals showing the different abundance of, respectively, excitatory CamK2a$^+$, inhibitory Sst$^+$ and inhibitory Pvalb$^+$ neurons. The electropherograms represent total RNA immunoprecipitated from **(b)** *CamK2a*::TRAP, **(d)** *Sst*::TRAP and **(f)** *Pvalb*::TRAP compared to wild type animals, using anti-GFP antibodies. The two highest peaks represent 18S rRNA (~2000 bp) and 28S rRNA (~4000 bp). Fluorescence units are proportional to RNA abundance. Details are in text. Scale bar is 500 µm

Social defeat induces translational remodeling in PFC interneurons

To investigate the effects of the defeat on principal (glutamatergic, CamK2a^{+}) and inhibitory (Sst^{+} and Pvalb^{+}) neurons, we carried subchronic social defeat on *CamK2a*::TRAP, *Pvalb*::TRAP and *Sst*::TRAP animals. One day after the last defeat, we sacrificed mice and extracted and lysed PFC for ribosomal IP, RNA extraction and purification. We then evaluated gene expression changes by microarray analysis. Before looking at the expression differences between sensory and defeated animals, we assessed and confirmed cell type specificity of the isolated RNA by looking at the expression levels of some cell type specific genes (Sugino et al., 2006; Tasic et al., 2016) (Fig. 11). Based on levels of these genes, we set up an expression threshold for genes to be used for following analyses (see Materials and Methods for details) leading to a total of 7813, 6478 and 7781 genes, that were analyzed, respectively, for *CamK2a*::TRAP, *Sst*::TRAP and *Pvalb*::TRAP experiments.

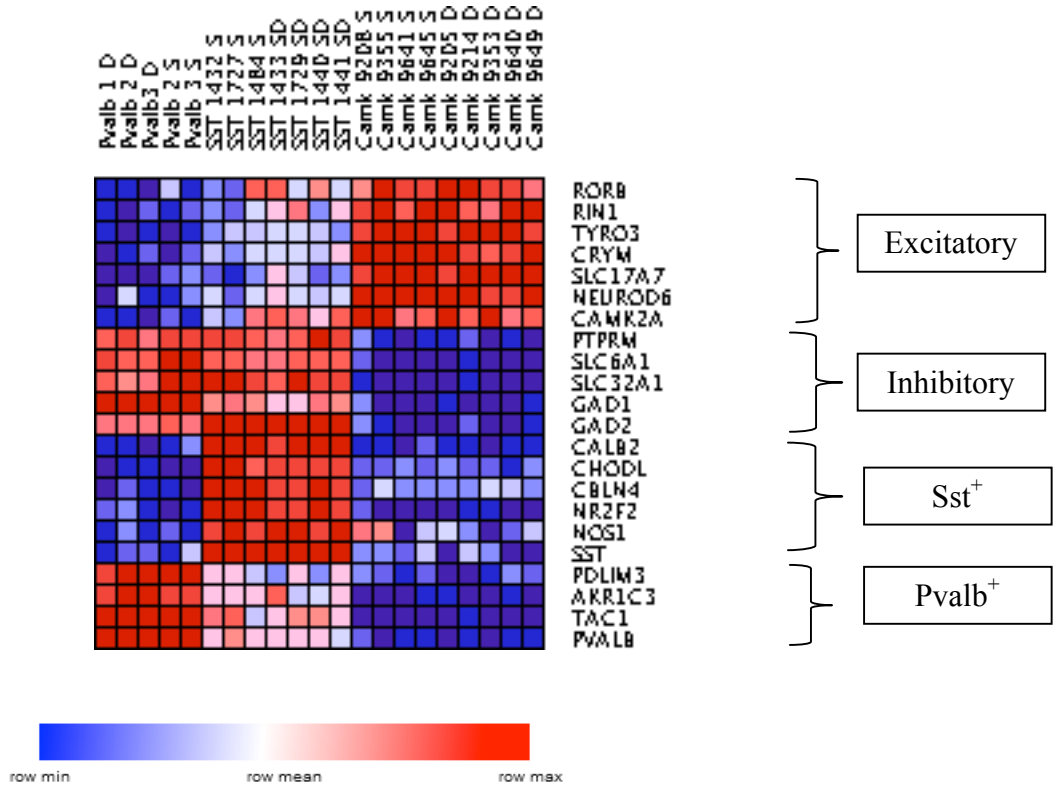

Figure 11. Cell-type specificity of TRAP technique. Heatmap representing GAPDH normalized log expression values of genes that are specific for excitatory, inhibitory, Sst^{+} and Pvalb^{+}neurons in *CamK2a*::TRAP, *Sst*::TRAP and *Pvalb*::TRAP samples. As evidenced from the legend, values are row normalized.

While no differences between sensory and defeated were found at the single gene level if considering an FDR<0.05, Gene Set Enrichment Analysis (GSEA) revealed that several gene sets were significantly differentially expressed (FDR<0.05) between sensory and defeated

animals in the three experiments. However, in *CamK2a*::TRAP samples, a more accurate analysis of the GSEA results (that returned 32 gene sets significantly enriched in defeated animals) revealed that, out of all the 224 genes that were leading the enrichment, only 1 gene had a p-value below 0.05 and a logFC>0.27 (FC>1.2) (*Eif2b2*, Table S1). We deduced that no reliable difference in gene expression could be inferred by GSEA results in the glutamatergic neuronal population.

In Somatostatin^{+} and Parvalbumin^{+} neurons, instead, much more prominent changes were detected. In Parvalbumin^{+} neurons of defeated animals, 162 gene sets were significantly downregulated (Table S2), while none of the upregulated gene sets had an FDR<0.05 (Fig.12).

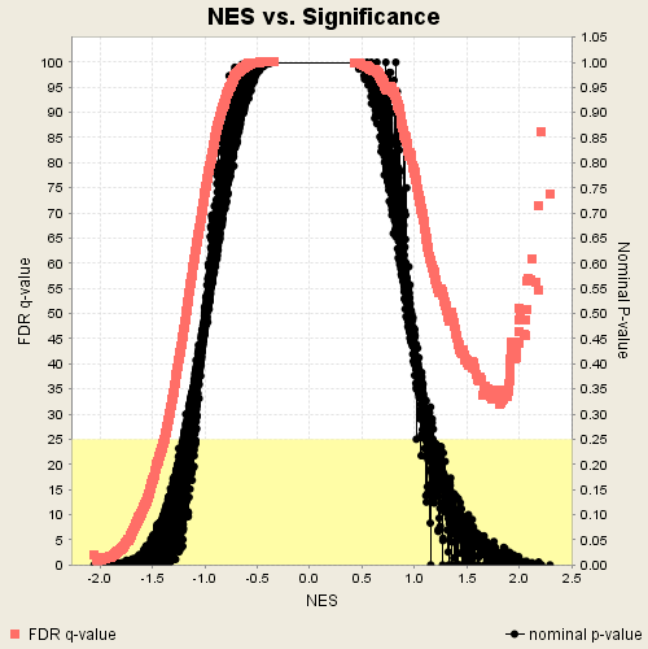

Figure 12. Overview of GSEA results from *Pvalb*::TRAP experiment. Gene sets are plotted according to their normalized enrichment score (NES) and FDR (in red) or P-value (in black). Considering that genes were previously ranked by t-test score, NES is the degree to which the gene set is overrepresented at the top or bottom of the ranked list of genes in the expression dataset, normalized across analyzed gene sets. Positive and negative NES indicate, respectively, up or down-regulation of gene set in defeated animals. Here, all significantly (FDR<0.05) enriched gene sets were downregulated in defeated animals.

Out of the 951 genes leading this negative enrichment, 161 had a p<0.05 and a logFC>0.27 (FC>1.2) (Table S3): these genes were represented in 161 of the 162 upregulated genesets (Tables S4-S5). To visualize these genes and their interactions as translated proteins, a protein-protein interaction network was built using STRING (Fig.13-14, see Methods for details).

Among the downregulated gene sets were found many related to electrical properties of the cells (e.g. GO_Regulation of ion transport, GO_regulation of membrane potential), to transmembrane transport in general (e.g. GO_transmembrane transporter activity), neurotransmitter transport and release (e.g. GO_Neurotransmitter transport and GO_exocytic vesicle, GO_synapse), receptors (e.g. GO_receptor activity, GO_G-protein coupled receptor activity) and perineuronal net (GO_amynoglycan biosynthetic process, GO_amynoglycan metabolic process, Reactome glycosaminoglycan metabolism). Genes that were part of the same or of similar gene sets tended to cluster in the protein-protein interaction network (Fig.13. and Tables S4-S5).

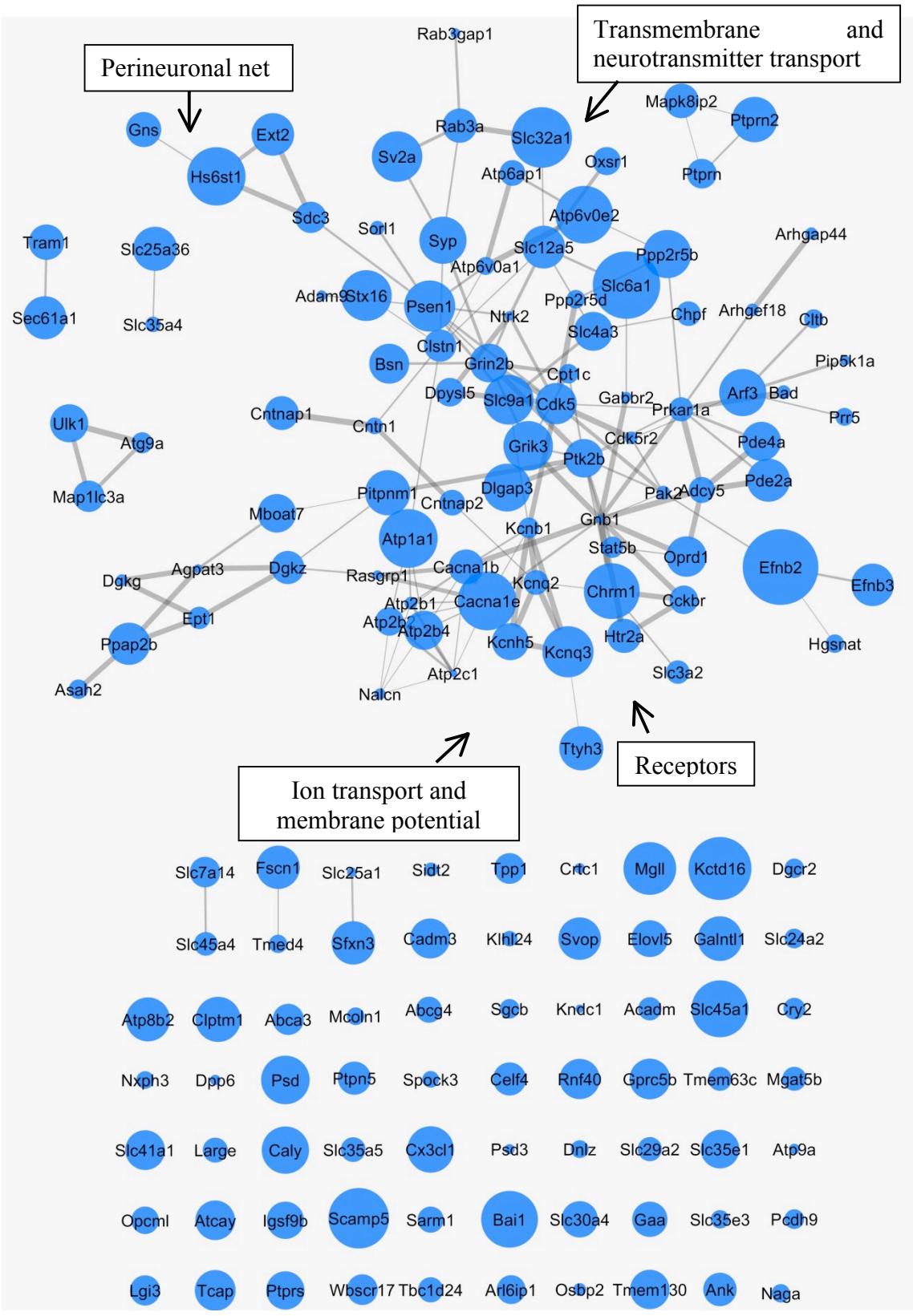

Figure 13. Network of downregulated genes leading GSEA results in Pvalb^{+} neurons of defeated animals. All genes (nodes) represented in the network are downregulated with a $p<0.05$ and a $logFC>0.27$ (see text for details). Network was built using STRING with a confidence score of 0.4. Genes interacting as proteins are connected. The arrows point examples of groups of genes that share similar function, process or subcellular localization and that show protein-protein interaction in the network. See Fig.14 for legend.

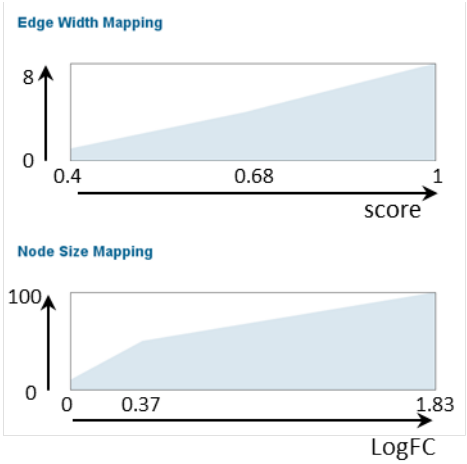

Figure 14. Legend for network in Fig. 13. Thickness of the edge reflects the strength of the interaction (score) and the size of the node reflects the fold change of the gene.

In Somatostatin^{+} neurons of defeated animals 163 gene sets were significantly upregulated (Table S6), while none of the gene sets that were downregulated in the defeated animals had an FDR<0.05 (Fig. 15).

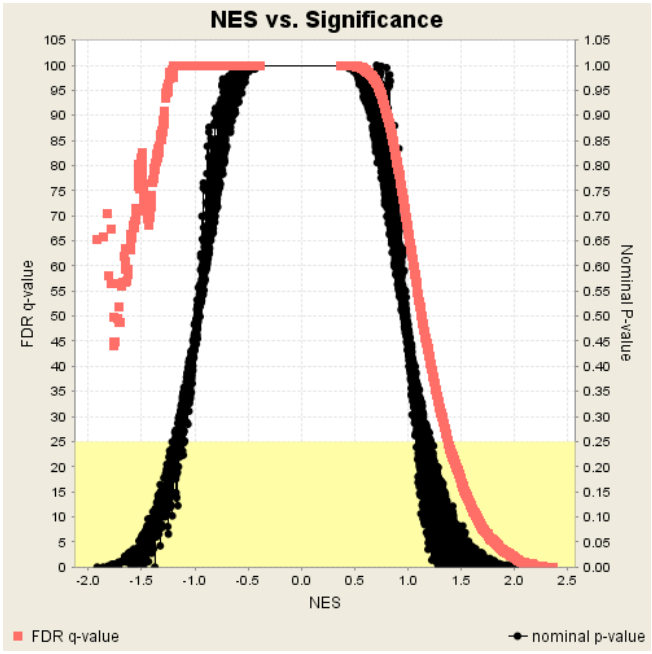

Figure 15. Overview of GSEA results from *Sst*::TRAP experiment. Gene sets are plotted according to their normalized enrichment score (NES) and FDR (in red) or P-value (in black). Considering that genes were previously ranked by t-test score, NES is the degree to which the gene set is overrepresented at the top or bottom of the ranked list of genes in the expression dataset, normalized across analyzed gene sets. Positive and negative NES indicate, respectively, up or down-regulation of gene set in defeated animals. Here, all significantly (FDR<0.05) enriched gene sets were upregulated in defeated animals.

Out of the 799 genes that were leading the enrichment of the upregulated gene sets only 109 had a p<0.05 and a logFC>0.27 (FC>1.2) (Table S7), that were represented in 155 of the 163 upregulated gene sets (Tables S8-S9). Again, these genes and their interactions as translated proteins, were visualized in a protein-protein interaction network using STRING (Fig. 16-17). Among the upregulated gene sets, were found gene sets related to the cytoskeleton and neuronal projections growth (e.g. GO_Structural constituent of cytoskeleton, GO_Movement of cellular or subcellular component, GO_Regulation of axonogenesis, Reactome_Axon guidance), but also gene sets related to spliceosome, (GO_U2 type prespliceosome and GO_catalytic step 2 spliceosome) and gene sets related to synaptic activity (e.g. GO_Synapse part, GO_postsynapse and GO_presynaptic active zone). Genes that were part of the same or of similar gene sets tended to be close in the protein-protein interaction network (Fig.16 and Tables S8-S9).

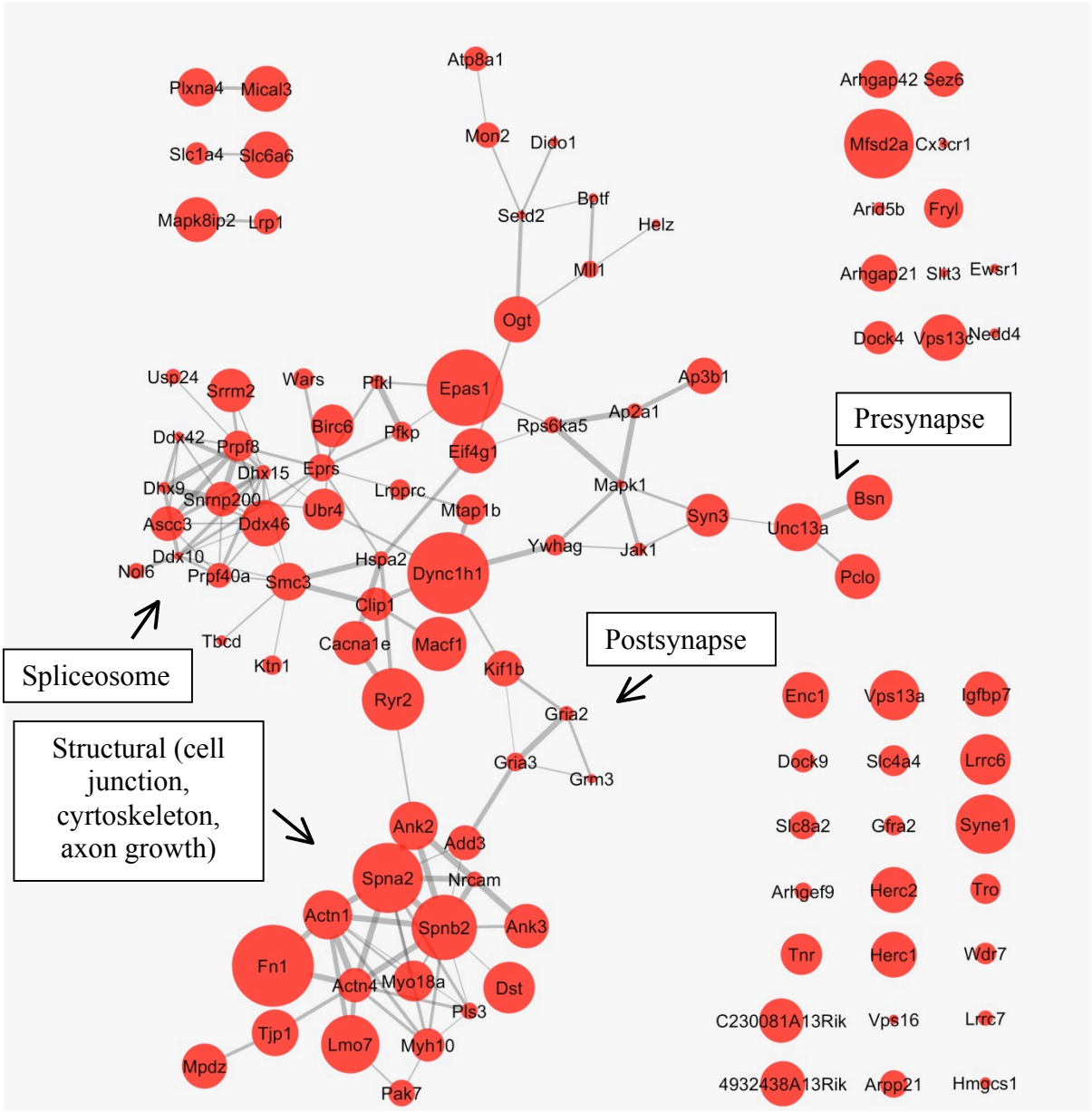

Figure 16. Network of upregulated genes leading GSEA results in Sst^{+} neurons of defeated animals. All genes (nodes) represented in the network are upregulated with a $p<0.05$ and a $logFC>0.27$ (see text for details). Network was built using STRING with a confidence score of 0.4. Genes interacting as proteins are connected. The arrows point examples of groups of genes that share similar function, process or subcellular localization and that show protein-protein interaction in the network. See Fig.17 for legend

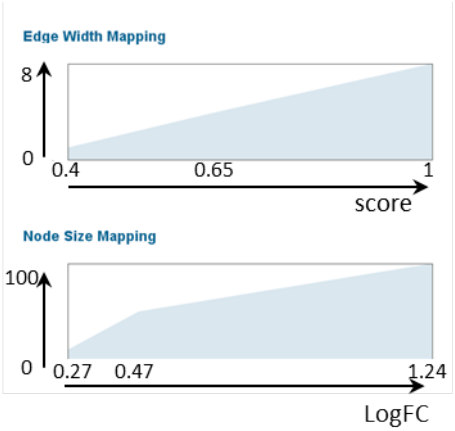

Figure 17. Legend for network in Fig. 16. Edge thickness reflects the strength of the interaction (score), while node size reflects the fold change.

Social defeat does not induce changes in the Chondroitin Sulfate Proteoglycans component of perineuronal net

Microarray results on PFC Parvalbumin^{+} neurons revealed, among the others, a downregulation of gene sets related to the synthesis and metabolism of perineuronal net in defeated animals (Fig. 13 and Table S2), suggesting a decrease in the amount of this specific extracellular matrix around these cells. Perineuronal net is composed by several proteoglycans, including chondroitin sulfate proteoglycans (CSPG) and Heparan sulfate proteoglycans (HSPG) (Maeda, 2015; McRae & Porter, 2012). The most common way to look at the perineuronal net is to use a lectin, Wisteria Floribunda Agglutinin (WFA), that binds the CSPG component. As a first test for the involvement of perineuronal net remodeling in the defeated phenotype, one day after the last defeat, we decided to costain the PFCs of wild type animals with anti-Parvalbumin and WFA (Fig. 18a, b and c).

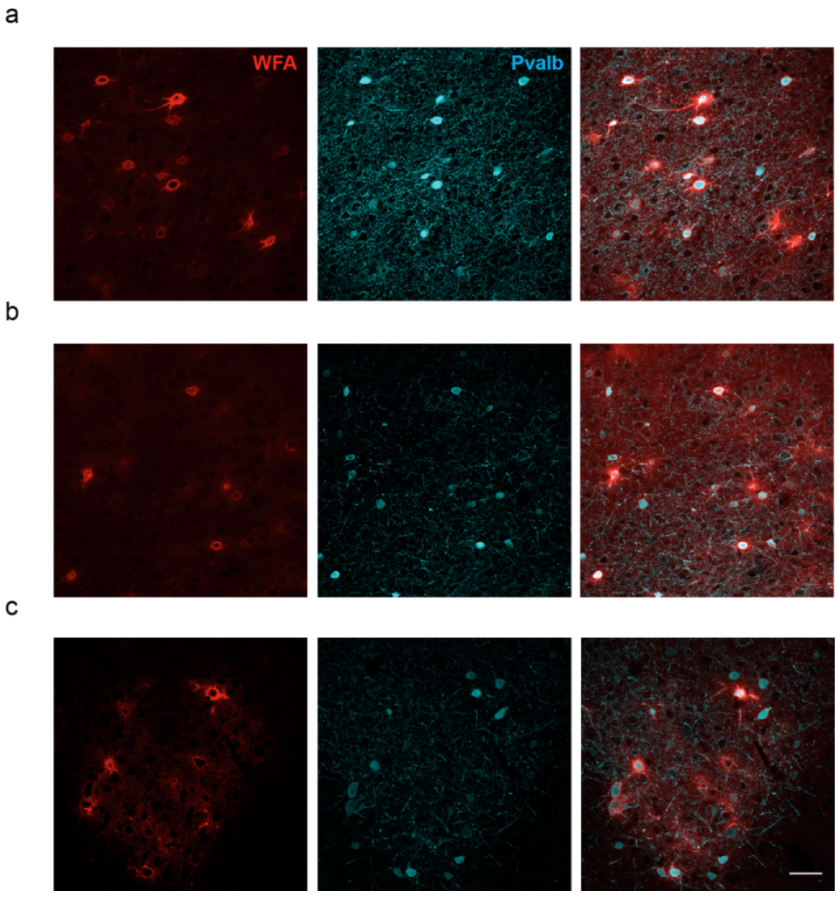

Figure 18. Staining for Parvalbumin and CSPGs (WFA). Representative pictures of **(a)** cingulate, **(b)** prelimbic and **(c)** infralimbic part of the prefrontal cortex showing high overlap of Parvalbumin positive and CSPG positive neurons. Scale bar is 50 µm.

The percentage of cells that were single or double positive for Parvalbumin and WFA was not affected by the defeat (Fig. 19), though more WFA^+neurons (and more $Pvalb^+$neurons colabeled with WFA) were present in cingulate, compared to prelimbic and infralimbic regions (Fig. 19b and c).

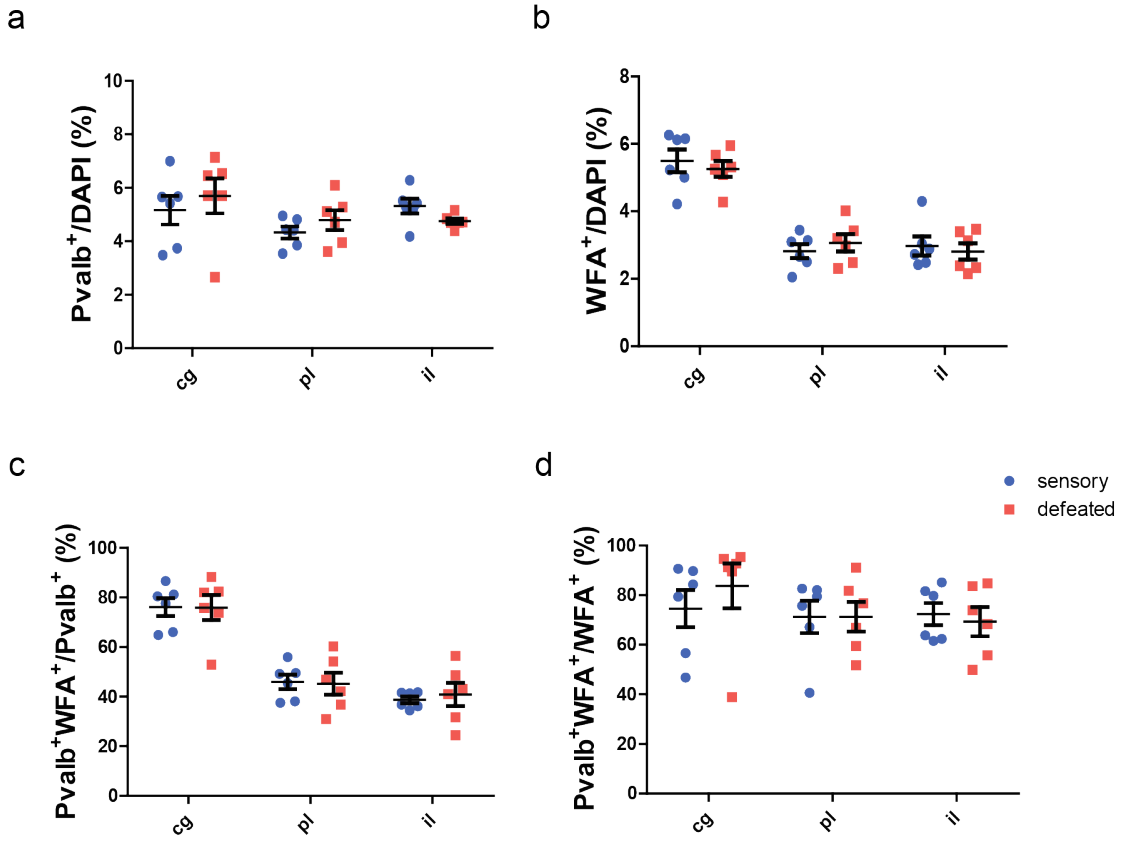

Figure 19. No changes in numbers of Parvalbumin$^+$ and WFA$^+$ neurons in the prefrontal cortex of defeated animals. (a) Parvalbumin$^+$ cell number is unaltered in cingulate, prelimbic and infralimbic parts of PFC after social defeat and **(b)** WFA$^+$neuronal numbers are unaltered after social defeat, but they are significantly higher in cingulate, compared to prelimbic and infralimbic (region, $p<0.0001$). **(c)** Percentage of Parvalbumin$^+$ neurons that are also positive for WFA is unaltered after social defeat, but is generally significantly higher in cingulate compared to prelimbic and infralimbic (region, $p<0.0001$). **(d)** Percentage of neurons surrounded by CSPG (WFA$^+$) that are also Parvalbumin$^+$ is also unaltered after social defeat. N=6 animals. All statistics were made by Two way ANOVA RM plus post-hoc Bonferroni correction.

Also the staining intensity of both Pvalb and WFA were unaltered in defeated animals (Fig.20 a-d) but were only changing by region, with higher intensity of both stainings in the cingulate cortex compared to prelimbic and infralimbic (Fig.20 a-d).

These results show that the CSPG component of the perineuronal net in the prefrontal cortex is not involved in the acquisition of the defeated phenotype.

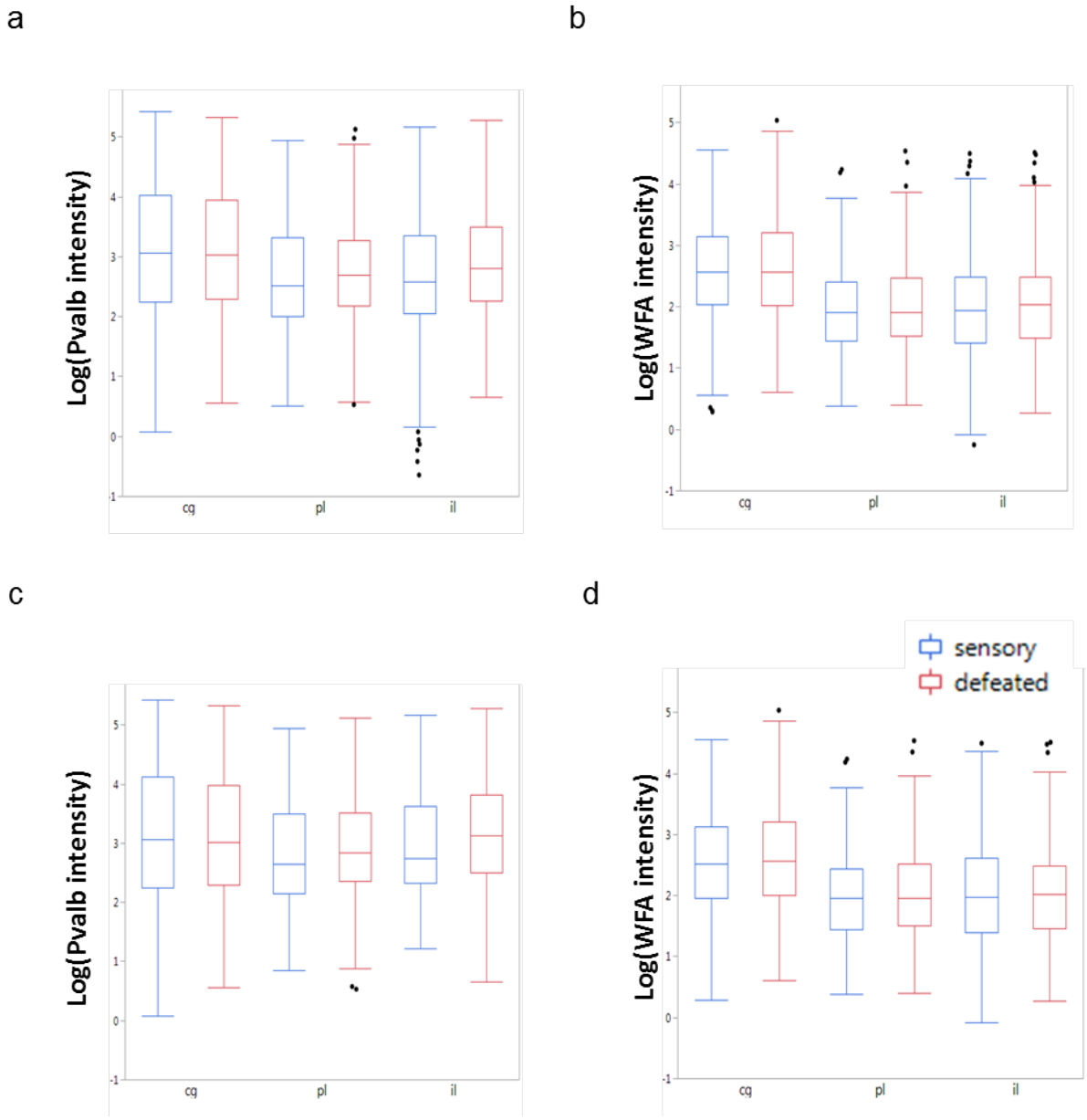

Figure 20. No changes in the intensity of either Pvalb or WFA in the PFC after social defeat. Pvalb **(a)** and WFA **(b)** intensities are not changing after social defeat, while cingulate region presents higher intensities of both in every condition (region, $p<0.0001$ in both). The same lack of effect of defeat is observable for both Pvalb **(c)** and WFA **(d)** intensities in double positive cells only, where anyway, again, cingulate shows the highest intensities (region, $p<0.0001$ in both). All analysis were made on all cells counted, using a mixed model with behavior, region and behavior*region as Fixed effects and animal as Random effect. N=6 animals, 2120-2256 total Pvalb$^+$cells in sensory and defeated, 1560-1623 total WFA$^+$ cells in sensory and defeated.

Sst$^+$neurons increase their presynaptic contacts in PFC layer I after social defeat

Sst::TRAP gene set enrichment analysis results (Fig.16 ad Table S6) raised the hypothesis that PFC Somatostatin$^+$ neurons might be growing and making more local presynaptic contacts following social defeat. To test this possibility, we used *Sst*::Syp-GFP mice, that express the vesicular presynaptic protein, synaptophysin (Syp), fused to GFP, only in

Sst$^+$neurons. Looking at the PFC of these animals it is clearly visible a higher level of Syp-GFP fluorescence in correspondance of layer I, where Martinotti cells, the largest Sst$^+$subpopulation, make inhibitory contacts (Fig. 21a). One day after the last social encounter, we then quantified number and volume of Syp-GFP boutons in this PFC layer. This analysis revealed that defeated animals presented an increased number of Syp-GFP presynaptic puncta in the cingulate part of PFC layer I (Fig. 21b), while increase in bouton volume was very small and not significant (Fig. 21c).

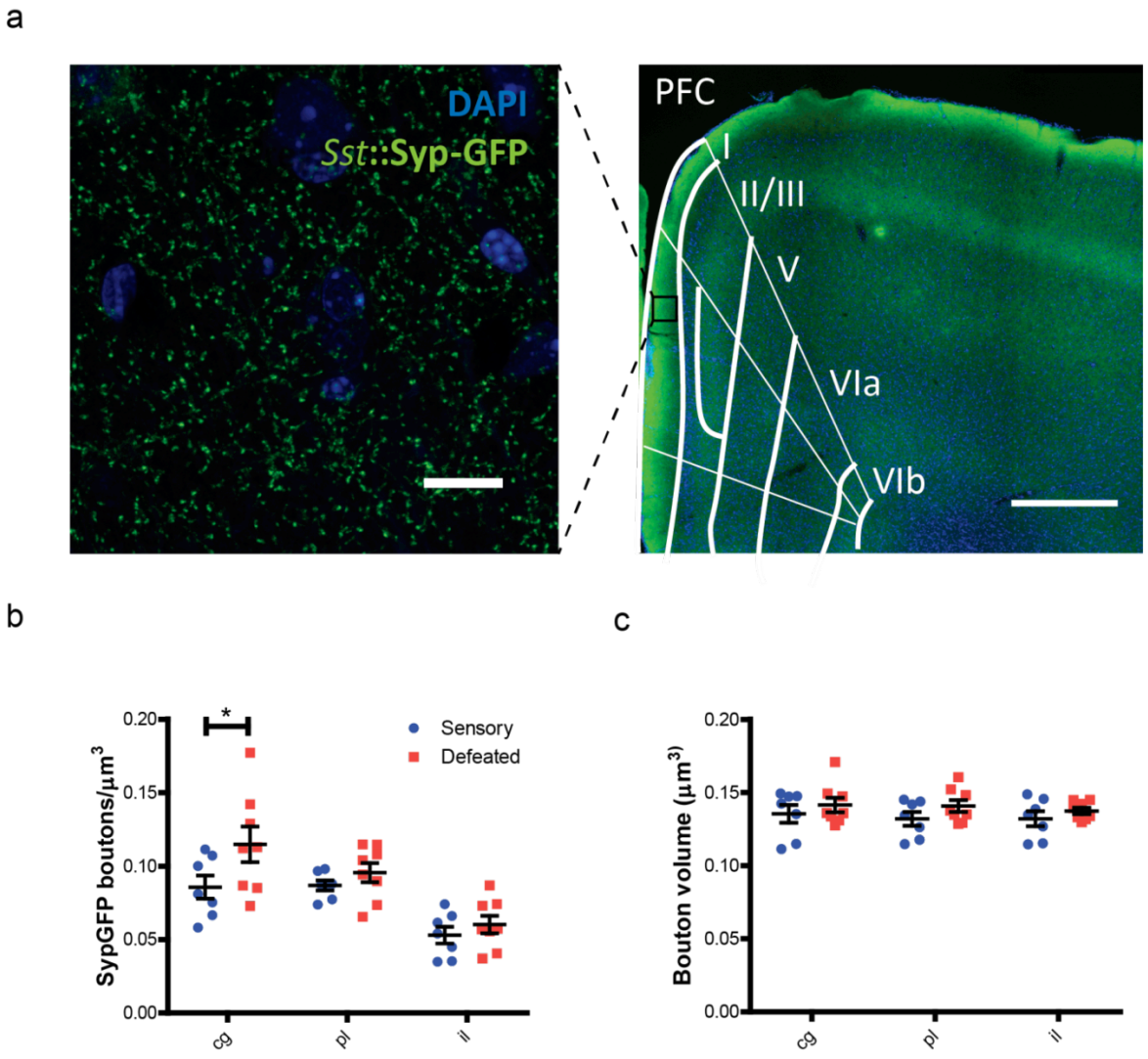

Figure 21. Increased number of presynaptic boutons from Sst$^+$neurons onto PFC layer I of defeated animals. (a) Representative pictures of prefrontal cortex from *Sst*::SypGFP mouse. Right: low magnification picture shows highest concentration of SypGFP in layer I, where Sst$^+$neurons make inhibitory contacts onto pyramidal neurons apical tufts. Left: high magnification picture of layer I. **(b)** Density of SypGFP boutons is different among prefrontal cortical regions (region: $p<0.0001$) and is significantly increased in cingulate cortex of defeated animals (behavior: $p=0.073$). **(c)** No significant changes are detected in bouton volume in any region after the defeat. All analyses were carried by two way ANOVA RM plus Bonferroni post-hoc correction. N= 7 sensory, 8 defeated animals. * $p<0.05$ Scale bars are 10 µm (left) and 500 µm (right).

Social defeat affects dendritic morphology, but not spine density, of PFC-dPAG projecting neurons

The absence of gene translation changes in the most abundant population of PFC neurons, the glutamatergic pyramidal CamK2a^{+} neurons, led us to investigate if instead the defeat was specifically and differentially affecting glutamatergic neurons projecting to different targets. We decided to investigate the structural plasticity of specifically PFC-dPAG projecting neurons, which are the ones who drive social behavior (Franklin et al., 2017). We chose to look at structural plasticity because morphological remodeling of PFC pyramidal neurons has extensively been shown after chronic restraint, but it has never been examined in social stress. To carry this experiment, we carried social defeat on *Thy1*::GFP animals, in which sparse cortical neurons express high levels of GFP. Four days before starting the behavioral paradigm, we injected the retrograde tracers CTB647 and CTB555 respectively in the dPAG to label PFC-dPAG projecting neurons (CTB647) and in the Nucleus Accumbens (NAc) to label PFC-NAc projecting neurons (CTB555) (Fig. 22a and b). Despite the recent surgery, sensory and defeated animal showed the expected approach/avoidance behavior during the social defeat days (Fig. 22c).

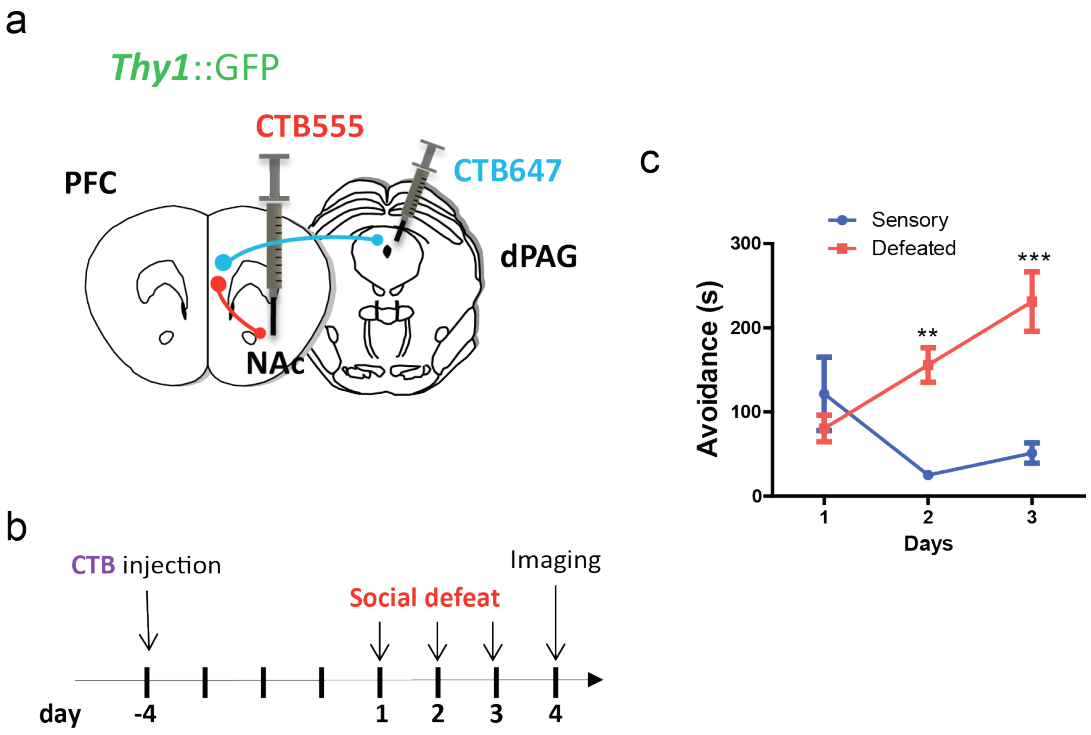

Figure 22. Experimental design for morphological study of PFC-dPAG neurons after social defeat. (a) Diagram representing injection sites of the tracers **(b)** Timeline of the experiment **(c)** Avoidance progression of the operated animals during social defeat (defeat, p=0.0044; defeat x day, p=0.0009). Data were analyzed by two way ANOVA RM plus post-hoc Bonferroni correction. N=5 animals ** p<0.01, *** p<0.001

One day after the last defeat, we sacrificed the animals to carry the morphological analysis. No PFC-NAc neurons were found that were also positive for GFP, probably because of the predominant presence of these cells in the layer II/III, where GFP neurons are not present (Fig. 23a and b). For this reason we could not reconstruct PFC-NAc neurons, but this labeling was used to better distinguish the different cortical layers (Fig. 23b).

In defeated animals, PFC-dPAG neurons had no changes in the number of branchings in either their basal or apical dendrites (Fig. 24b and d), but presented a general non-significant trend in the decrease of dendritic length in the apical arbor (Fig. 24a), appreciable also in the Sholl analysis (Fig. 24c). Layer specific analysis revealed then a significant decrease of dendritic length in the layer II/III apical dendrites after the defeat (Fig. 24e and f). Instead, no changes were found in the spine density at any level of the apical dendritic arbor, where only differences between dendritic compartments are detectable (Fig. 25a and b). These results reveal that a subchronic form of social defeat is sufficient to induce partial dendritic remodeling in mouse PFC-dPAG projecting neurons.

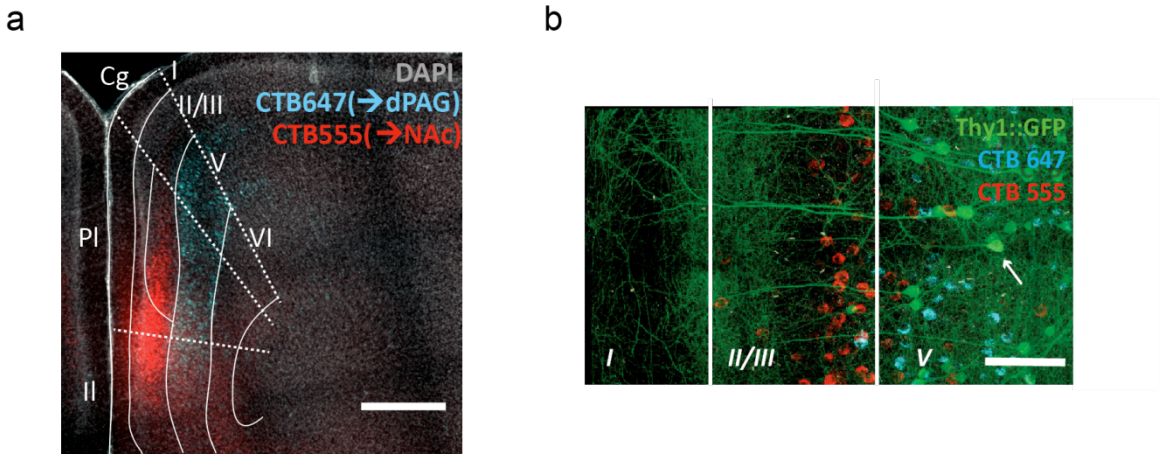

Figure 23. Layer specific segregation of PFC-dPAG and PFC-NAc projecting neurons. (a) Low magnification image of prefrontal cortex showing PFC-dPAG projecting neurons labelled by CTB647 (blue), located in layer V and PFC-NAc projecting neurons labelled by CTB555 (red), located predominantly in layer II/III. **(b)** High magnification image representing GFP labelled neurons of a *Thy1*::GFP animal located exclusively in layer V, where the minority of PFC-NAc neurons (red) is present. An example of *Thy1*::GFP positive neuron projecting to dPAG (as evidenced by colocalization with CTB647, blue) is pointed by an arrow. Scale bars are 500 µm in **(a)** and 50 µm in **(b).**

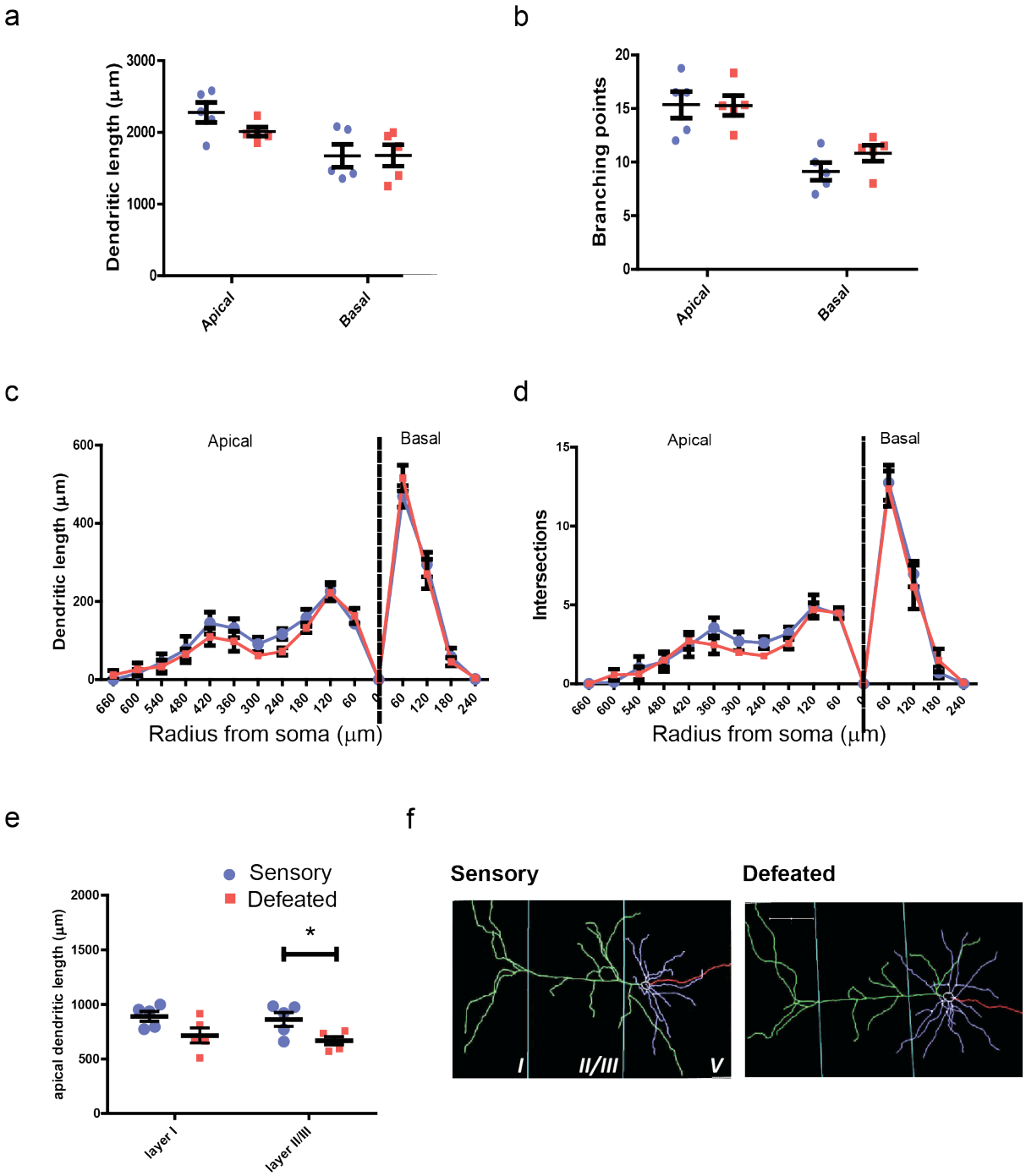

Figure 24. Partial dendritic retraction in PFC-dPAG projecting neurons of defeated animals. No significant changes are occurring in **(a)** total apical dendritic length (dendritic compartment p=0.0003) and **(b)** total number of branching points (dendritic compartment, p<0.0001). No significant changes are evidenced by Sholl analysis of **(c)** dendritic length and **(d)** number of intersections (radial distance from soma, p<0.0001). **(e)** Layer specific analysis of apical dendritic length reveals significant decrease (defeat p=0.0161) in length in layer II/III in defeated animals. **(f)** Representative images of reconstructed neurons from sensory and defeated animals. Scale bar is 100 µm. All analyses were made by Two way ANOVA RM plus post-hoc Bonferroni corrections. *p<0.05 N=5 animals

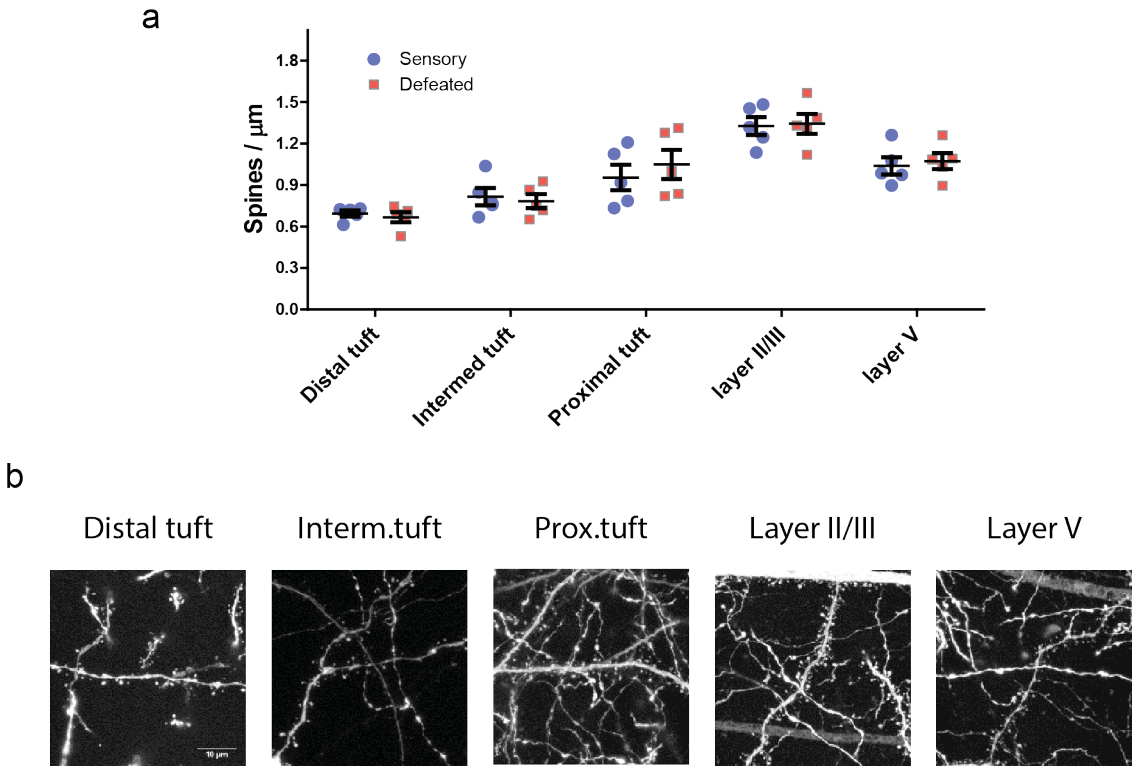

Figure 25. No changes in the spine density of PFC-dPAG neurons of defeated animals. (a) No significant changes are detectable in any part of the apical dendritic arbor after the defeat, but only differences between dendritic compartments themselves (dendritic compartment, $p<0.0001$) **(b)** Representative images showing different spine density in different compartments of apical dendritic arbor. Scale bar is 10 µm. All analyses were made by two way ANOVA RM plus post-hoc Bonferroni corrections. N=5 animals

A construct to tag AMPA receptors to visualize synaptic strength

To study synaptic strength of these neurons we made a new construct that would allow us to visualize AMPARs dynamics. To do so, we fused the sequence encoding for AMPAR's GluA1 subunit to a SNAP tag. SNAP is an engineered version of the mammalian enzyme O^6-alkylguanine-DNA-alkyltransferase (AGT). It can be fused to any protein of interest by molecular cloning, and labeling of the protein can then occur through administration of an engineered ligand, O^6-benzylguanine (BG), that can be conjugated for example with a fluorophore. BG covalently reacts with SNAP, labeling irreversibly the protein of interest (Gautier et al., 2008). In our construct, tdTomato was inserted, followed by the T2A peptide, before SNAPGluA1 (Fig. 26a), in order to visualize the infected cells in their entirety and to control for the expression of the vector. We cloned this sequence in a pCDNA expression vector that was used to transfect HEK cells, in order to check for functionality of the construct. One day after the transfection, cells became fluorescent for tdTomato and were additioned with BG, in order to label SNAP. Only in transfected cells, both reaction with the cell-penetrant SNAP-cell 505-Star (namely BG Cell 505) and with the non-cell penetrant

SNAP-Surface Alexa Fluor 488 (namely BG Alexa 488) resulted in green labeling of the cells, with an expression pattern that was different from tdTomato (Fig. 26b), demonstrating that the SNAP fused construct was correctly expressed. Non transfected cells, on the contrary, did not show any green labeling after addition of BG (Fig. 26c).

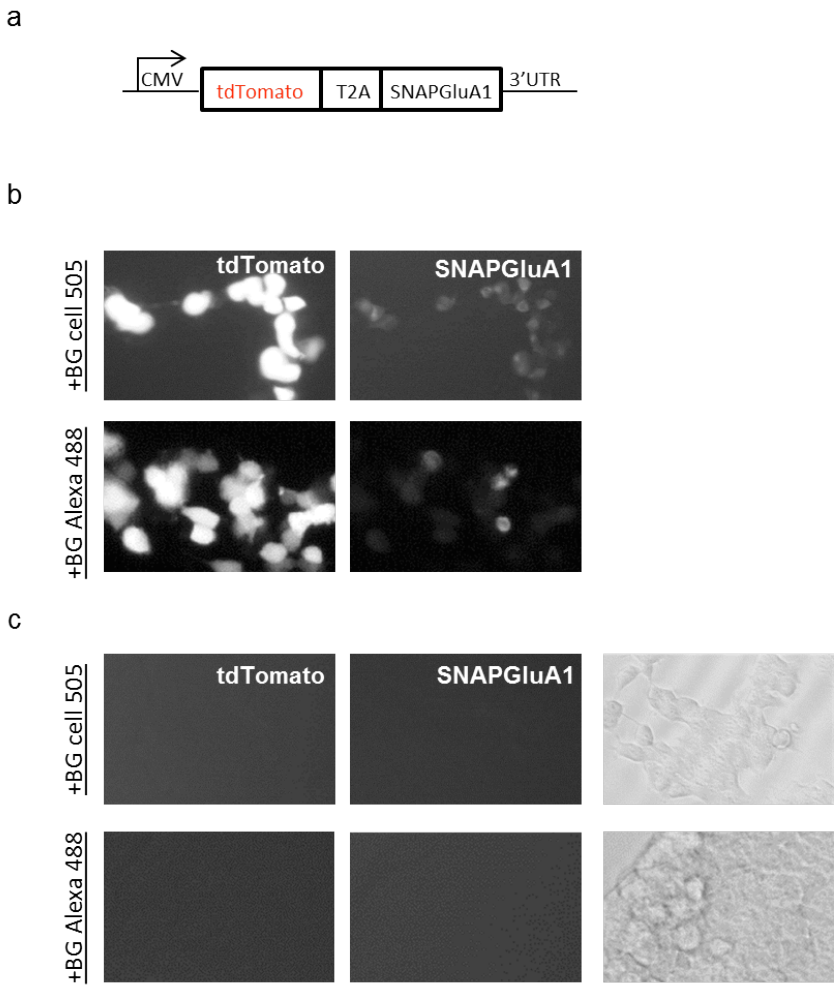

Figure 26. Expression and labeling of SNAPGluA1 in HEK cells. (a) Map of SNAPGluA1expressing plasmid. **(b)** The plasmid is correctly expressed in HEK cells and SNAPGluA1 labeling is evidenced by both cell penetrant BG cell 505 and non-cell penetrant BG Alexa 488. **(c)** The two BG ligands do not label aspecifically cells that do not express SNAP fused constructs. On the right, cells are visible in the brightfield channel.

Setup of SNAP tag labeling *in vivo* in the mouse brain

As a proof of principle for the feasibility of this technique in the mouse brain tissue, two AAV viral constructs were cloned and packaged in the lab, respectively AAV *hSyn*::SNAP and AAV *hSyn*::GPI-SNAP, that is exclusively transported and exposed on extracellular cell membrane. We first tested SNAP-BG reaction on fixed brain slices coming from a mouse infected bilaterally in the PFC with AAV *hSyn*::SNAP (Fig. 27a). Due to the nature of slices

and fixation, in this system cell membranes lose their impermeability to surface specific ligands such as SNAP Surface Alexa 647 (namely BG Alexa 647); so both this ligand and the cell penetrant SNAP Cell SiR 647 (namely BG cell SiR 647), gave a nice labeling of the cytoplasmic SNAP protein (Fig. 27b and c). As expected, labeling was more abundant in the emisphere where a larger amount of virus was injected.

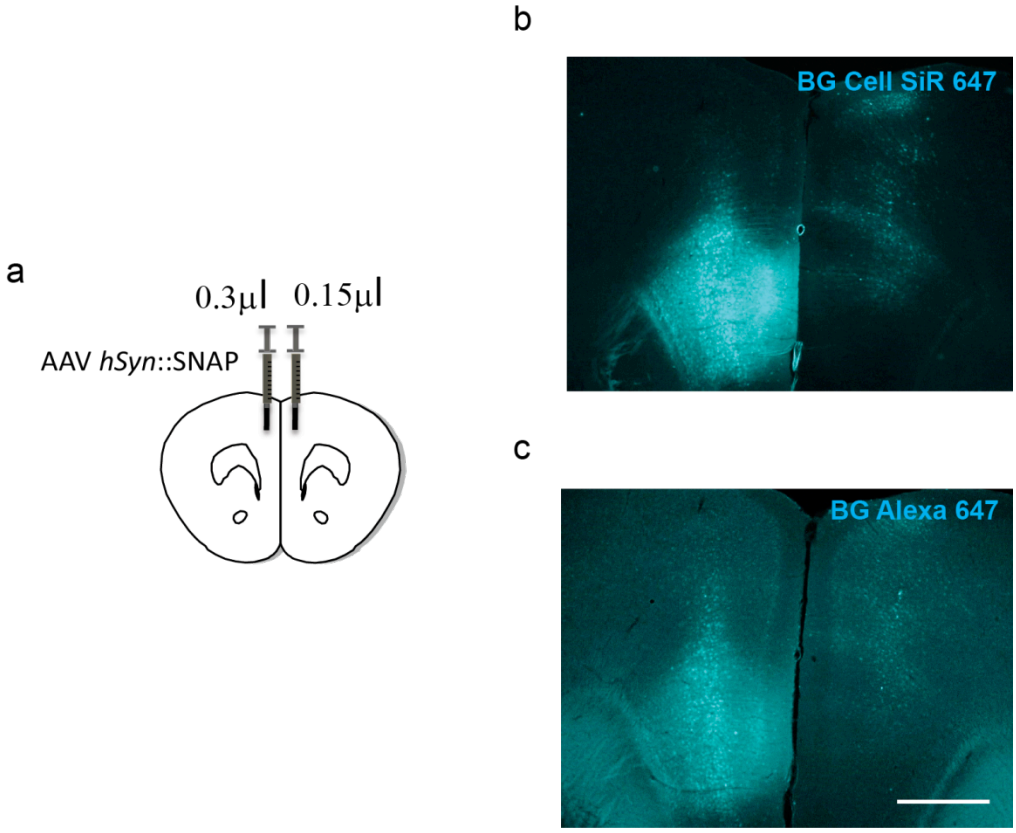

Figure 27. SNAP-BG labeling of virally expressed cytoplasmic SNAP on fixed mouse brain tissue. (a) Schematic of viral injection. Two different amounts of virus were used. **(b** and **c)** Representative pictures of SNAP-BG labeling on mouse brain slices with either BG Cell SiR 647 or BG Alexa 647, as indicated. Scale bar is 500 µm

To discriminate between cytoplasmic and surface labeling, we then tested BG surface Alexa 647 *in vivo* in a mouse injected with AAV *hSyn*::SNAP in the left PFC and AAV *hSyn*::GPI-SNAP in the right PFC. Briefly, we implanted a cannula in the lateral ventricle (Fig. 28a and i) of the mouse to get access to the cerebrospinal fluid flow when the two constructs would already be expressed. When the viruses were expressed, we injected BG *in vivo* i.c.v.in the awake animal (Fig.28b, see Methods for details). Decreasing concentrations (330 µM, 150 µM and 100 µM) of BG Alexa 647 were used (Fig. 28c-e), to test for sensitivity and specificity of the ligand. Mice were sacrificed 1h after injection, that demonstrated to be a sufficient amount of time to observe labeling in the PFC (Fig. 28b). Labeling with optimal

signal to background ratio was obtained with a concentration of 150 µM BG and was observable in perfused fixed mouse brain tissue only for GPI-SNAP, but not for cytoplasmic SNAP (Fig. 28c-h).

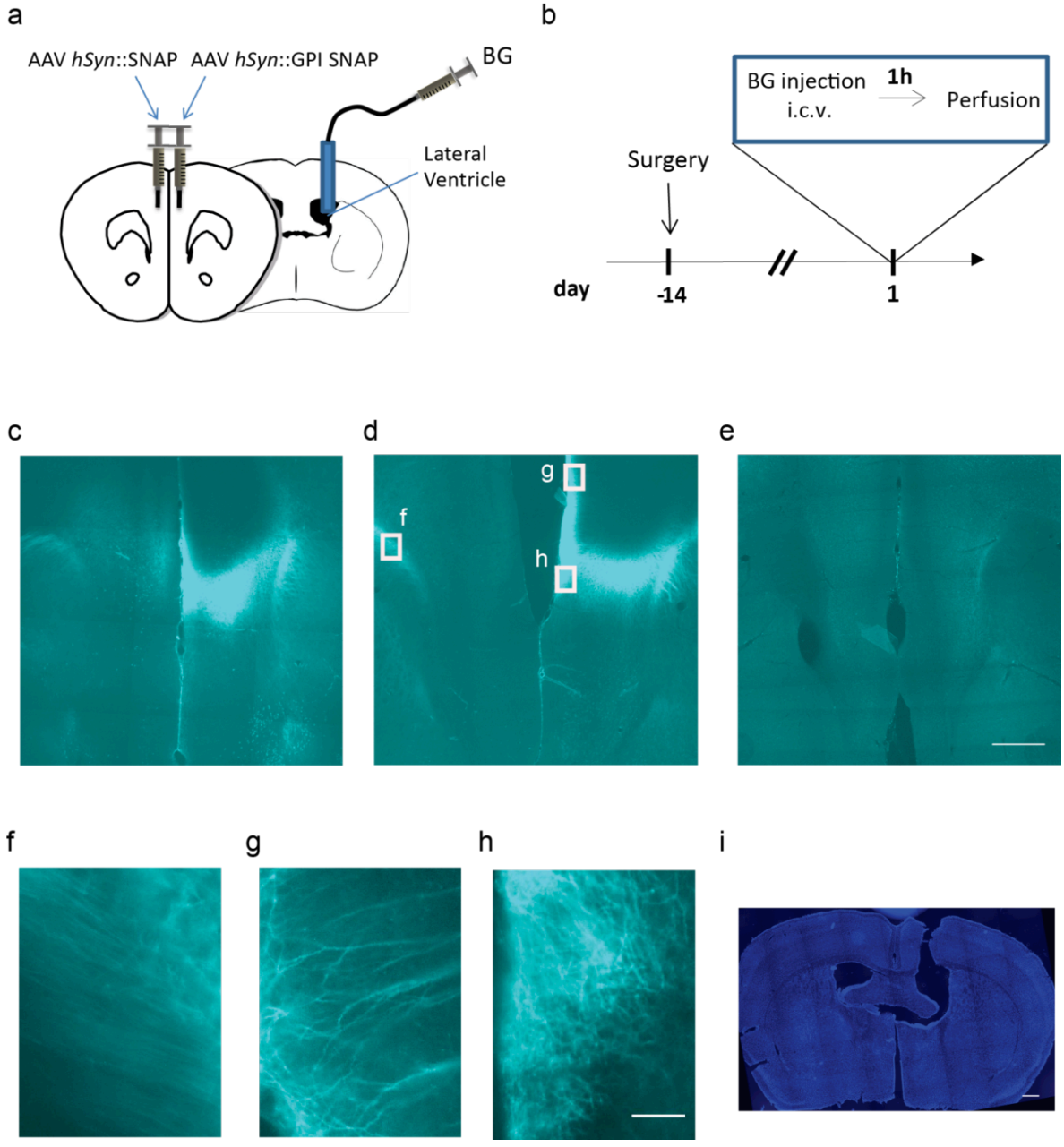

Figure 28. Setup of SNAP tag labeling *in vivo* in the mouse brain. (a) Schematic representation of surgical procedure including viral injection and cannula implantation. **(b)** Timeline of the experiments: BG administration was made i.c.v. through the cannula at least 2 weeks after surgery and animals were sacrificed 1h after i.c.v. injection. **(c)** 330 µM BG led prominently to labeling where AAV *hSyn*::GPI-SNAP was injected but labeled also aspecifically other locations. **(d)** 150 µM BG led only to specific labeling in GPI-SNAP expressing cells. **(e)** 100 µM BG led to very poor specific labeling at the GPI-SNAP injection site. **(f)** Membrane labeling coming from GPI-SNAP in corpus callosum fibers, controlaterally to viral injection. **(g)** Dendritic apical tufts coming from neurons infected with GPI SNAP ipsilaterally to the injection. **(h)** Fibers close to the site of injection of GPI-SNAP. **(i)** Representative picture of the site of implantation of the cannula in the lateral ventricle. Scale bars are 500 µm in **(e)** and **(i)** and 50 µm in **(h).**

To demonstrate that the labeling obtained in the side of AAV *hSyn*::SNAP injection was actually coming from axonal fibers of neurons infected controlaterally with AAV *hSyn*::GPI-SNAP and not from AAV *hSyn*::SNAP itself; we injected another mouse with AAV *hSyn*::SNAP only and later we carried *in vivo* labeling with BG Alexa 647 in the same way. No signal was detectable this time (Fig. 29a). As we did not manage to get SNAP labeling by i.c.v. injection of cell penetrant BG cell SiR 647 (data not shown), we injected BG Cell SiR 647 locally with a microcapillary in the PFC of an AAV *hSyn*::SNAP injected mouse. The same mouse was injected with BG Cell SiR 647 also in a region where SNAP was not present (anterior insula) as a control (Fig. 29b). This time, SNAP cytoplasmic labeling was observed in *post mortem* fixed mouse brain tissue only in the PFC (Fig. 29b), where AAV *hSyn*::SNAP had been injected, demonstrating even the feasibility of cytoplasmic SNAP fused proteins labeling *in vivo*, with the use of cell penetrant ligands.

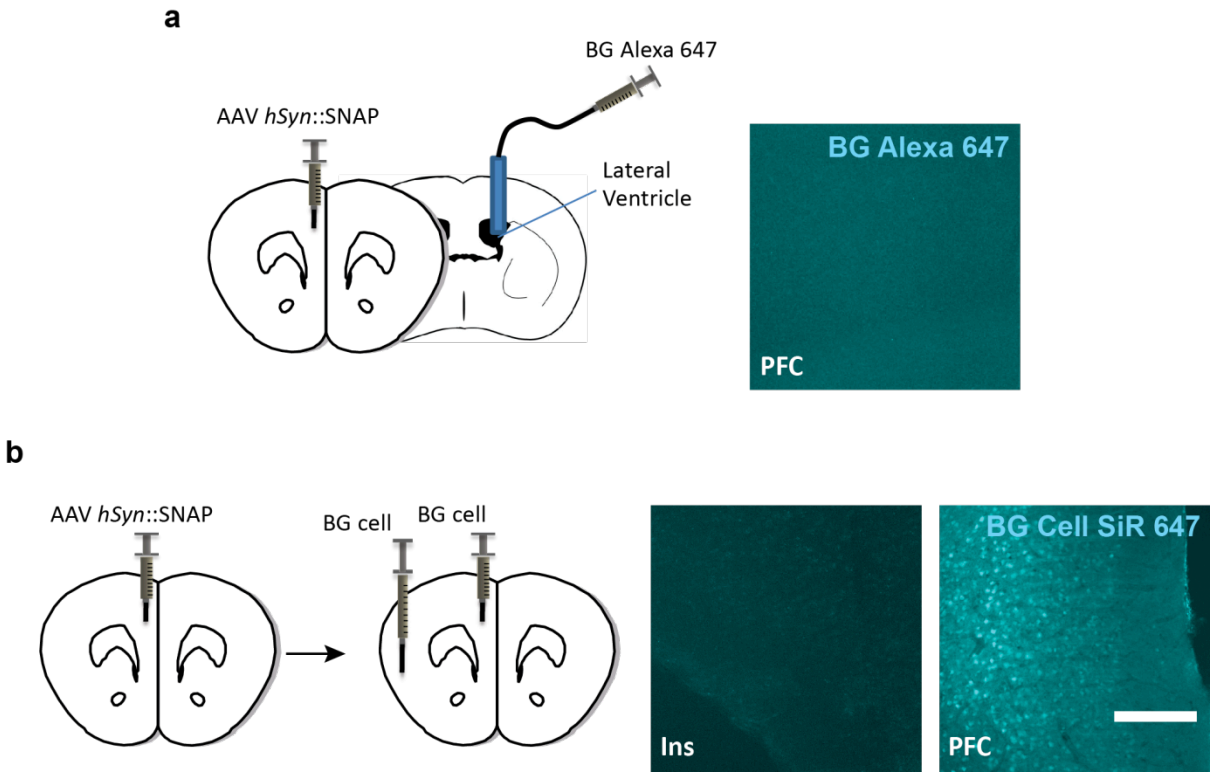

Figure 29. BG surface Alexa 647 does not lead to labeling of non-surface SNAP when injected i.c.v. (a) I.c.v. injection of BG Alexa 647 in a mouse previously infected with AAV *hSyn*::SNAP does not lead to labeling of cytoplasmic SNAP. **(b)** Local injection of BG Cell SiR 647 leads to specific labeling of cytoplasmic SNAP. Scale bar is 50 µm.

Setup of Halo tag labeling *in vivo* in the mouse brain

It would be useful for future applications to label more proteins contemporarily, in a different color, to study the dynamics of different components of synapses. For example, one could imagine to differentially label two different subunits of AMPA receptors or pre and postsynaptic components. For this purpose, another tag, called Halo, was tested for its functionality *in vivo* in the mouse brain. Like SNAP, Halo is an engineered form of an enzyme, haloalkane dehalogenase, that can be fused to a protein of interest by classical molecular cloning. The covalent reaction of Halo with its synthetic ligand, chloroalkane (CA), fused to a fluorescent reporter, would make the protein of interest turn fluorescent itself (Los et al., 2008). Also for this experiment, we used a non-cell penetrant version of the CA ligand, Halo Tag Alexa Fluor 488 ligand (here renamed CA Alexa 488). We injected mice with AAV *hSyn*::GPI-Halo, so that Halo would be exposed on the extracellular membrane, unilaterally in the PFC. Two weeks later we infused CA Alexa 488 (150 µM) in the lateral ventricle of the infected animals (Fig. 30a). A very strong labeling was obtained both in the site of injection, where even the apical dendrites of the infected pyramidal neurons were detectable, and in the controlateral side, where many axonal fibers were clearly visible (Fig. 30b) demonstrated the *in vivo* feasibility of Halo-tag labeling in the mouse brain.

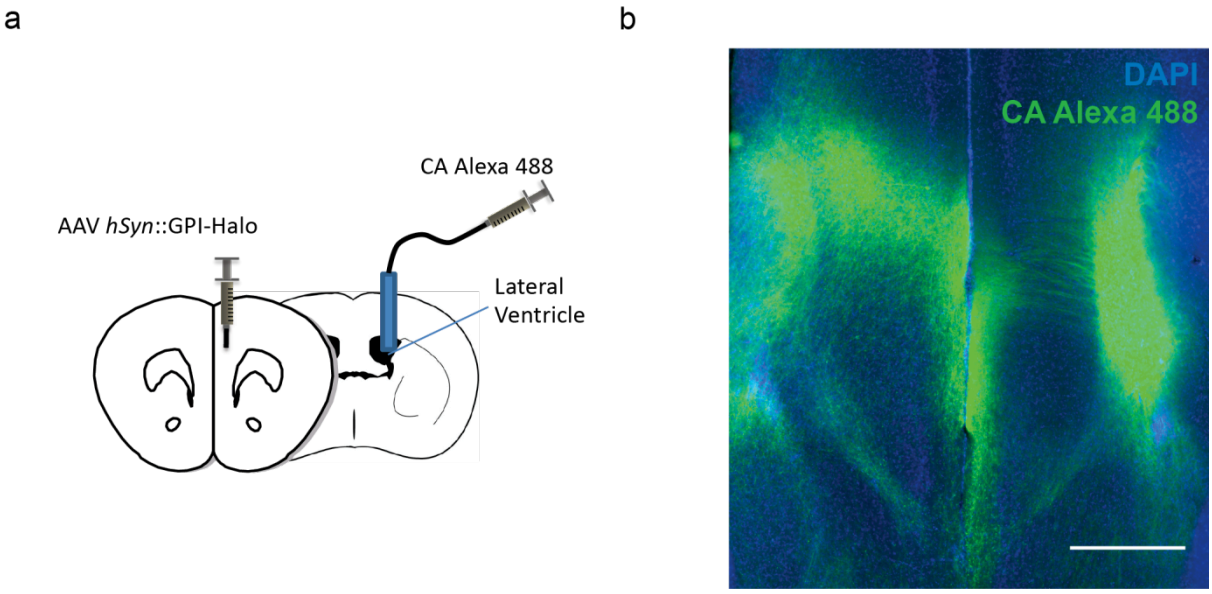

Figure 30. Feasibility of Halo-tag labeling of proteins *in vivo* in the mouse brain. (a) Schematic representation of surgical procedure, including viral injection and cannula implantation. **(b)** CA Alexa 488 labeling is evident both in the site of injection of the Halo construct (see apical dendrites) and in the fibers projecting to the controlateral side. Scale bar is 500um

HSV mediated retrograde labelling of PFC-PAG neurons for SNAPtag *in vivo* labelling of synapses

Once *in vivo* labeling of surface exposed proteins through SNAP and Halo tagging systems was established in the mouse brain, this was exploited to label surface exposed AMPA receptors. We transferred the tdTomT2ASNAPGluA1 construct in an entry vector for following packaging in a Herpes Simplex Viral Vector, a virus with higher capacity for DNA, compared to AAVs (Neve & Lim, 2013; Neve, Neve, Nestler, & Carlezon, 2005). HSV-1 is able to retrogradely migrate along neurons (Neve et al., 2005), so that sparse populations of specific projecting neurons can be visualized, making easier the imaging of single spines. In the virus, tdTomT2ASNAPGluA1 was expressed under the control of a strong hEF1α promoter and a Lox-STOP-Lox cassette, to drive Cre dependent expression (Fig. 31a). We injected the HSV in dPAG of *CamK2a*::Cre animals and 3 weeks after the injection we checked the expression in the PFC (Fig. 31b). We carried BG labeling *in vivo* by i.c.v. injection through a cannula, as previously done with AAV *hSyn*::GPI-SNAP. After the labeling, sparse neurons were detected in the prefrontal cortex, filled with tdTomato and labeled with BG in a different pattern (Fig. 31d). As expected, SNAPGluA1 was mainly located on the spines (Fig. 31c). The technique demonstrated then to be suitable for *in vivo* use and subsequent imaging of fixed slices.

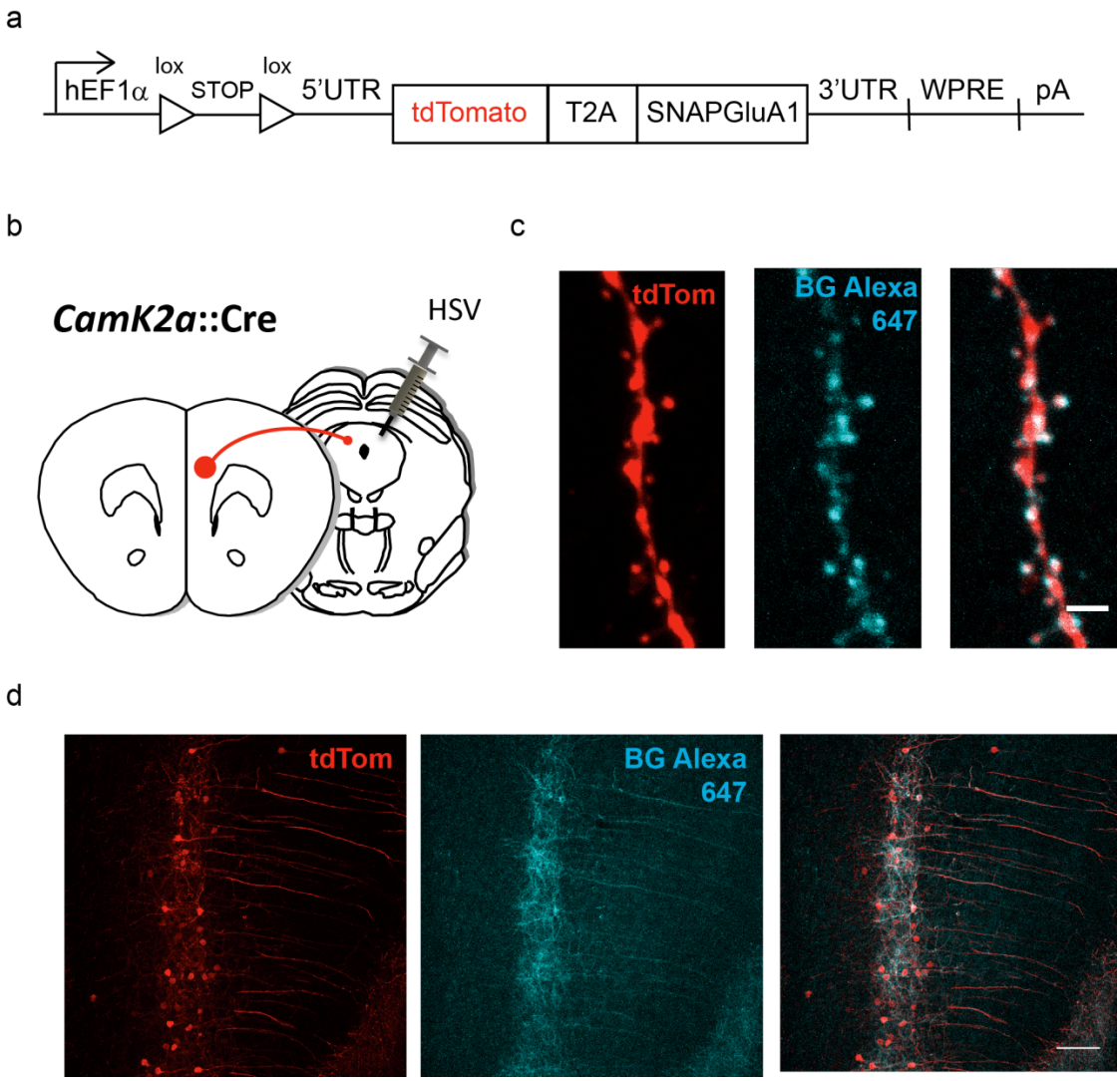

Figure 31. ***In vivo*** **expression of SNAPGluA1 construct through a retrograde HSV and** ***in vivo*** **labeling of the receptor in the mouse brain. (a)** Map of the construct that was cloned in the HSV. **(b)** Schematics of the surgery: the HSV was injected in the dPAG to elicit expression in PFC-dPAG projecting neurons. **(c)** High and **(d)** low magnification of PFC-dPAG projecting neurons expressing cytoplasmic tdTomato and SNAPGluA1 labeled by BG Alexa 647. SNAPGluA1 is concentrated on the dendrites and mainly on dendritic spines, as expected. Scale bars are 2 µm in **(c)** and 100 µm in **(d).**

Social defeat induces layer I-specific plasticity in PFC-dPAG projecting neurons, as visualized by surface SNAPGluA1

We used *in vivo* labeling of surface SNAPGluA1 to look at synaptic plasticity dynamics in the different parts of PFC-dPAG neurons dendritic arbor after social defeat.

To do so, we injected *CamK2a*::Cre mice with HSV *hEF1α*::LSL-tdTom-T2A-SNAPGluA1 in the dPAG and we implanted them with the cannula in the lateral ventricle respectively 4 weeks and 1 week before starting the behavioral paradigm. After the second surgery mice were isolated and then they were subjected to 3 days social defeat. On the 4th day we labeled

SNAPGluA1 with BG i.c.v. and perfused mice 1h later (Fig. 32a). As shown in Fig. 32b, exogenous expression of the AMPAR construct did not alter the normal behavioral outcome of social defeat.

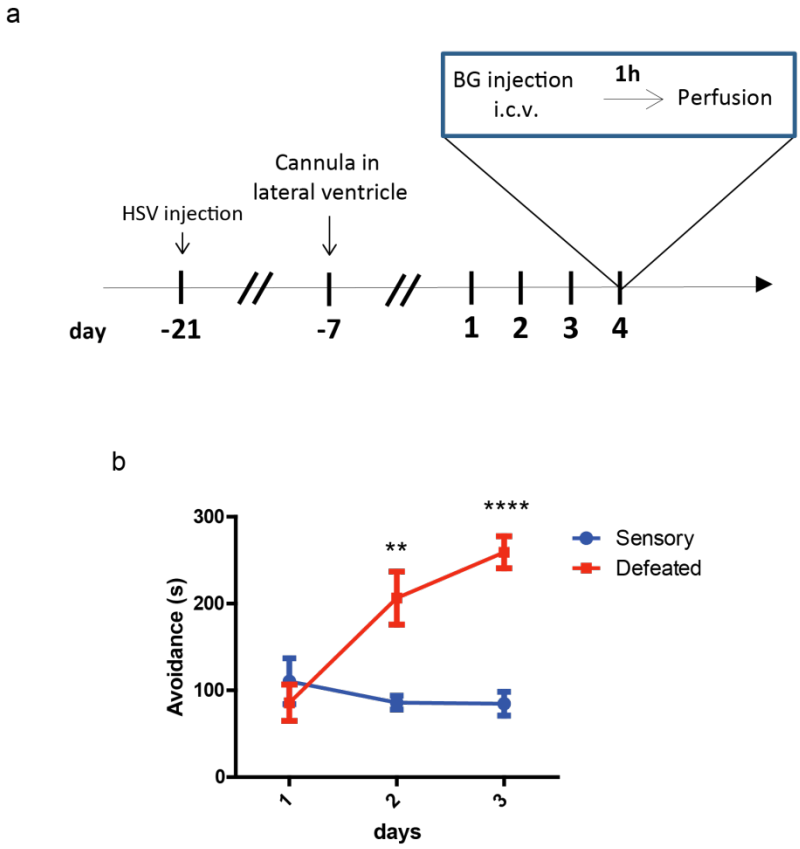

Figure 32. Experimental setup for SNAPGluA1 analysis following social defeat. (a) Timeline of the experiment. **(b)** Normal avoidance progression of sensory and defeated animals (defeat, p=0.0044; defeat x day, p=0.0009), all injected with the HSV *hEF1α*::LSL-tdTom-T2A-SNAPGluA1. Data were analyzed by two way ANOVA RM plus Bonferroni post-hoc corrections. N=6 sensory, 7 defeated ** p<0.01, **** p<0.0001

We imaged two parts of the dendritic arbor of PFC-dPAG neurons: the layer I proximal apical tuft (Fig. 33a) and the layer II/III oblique dendrites (Fig. 33b), to detect changes in synaptic strength for specific dendritic compartments. Intensity of tdTomato and SNAPGluA1 were used to estimate respectively size of the spines and content of surface GluA1, that was always normalized for viral expression and amount of BG background labeling. All analyses were carried on spines, keeping into account dendrite and animal of origin for the statistics (see Methods for details on both quantification and statistical analysis). In both dendritic compartments no changes between sensory and defeated animals were detected in spine size (Fig. 34a and b, 35a and b). However, spine surface GluA1 levels were significantly decreased in the apical tuft of defeated animals (Fig. 34c and d), but were not significantly altered in oblique dendrites (Fig. 35c and d). To measure synaptic strength,

we calculated surface GluA1 enrichment per spine, normalizing spine surface GluA1 levels for spine size (see Methods for details). Again, significant decrease of GluA1 enrichment was observed in the neuronal apical tufts (layer I) of defeated animals (Fig. 34e and f), but not in the oblique dendrites (Fig. 35e and f), showing that social defeat has an effect in decreasing synaptic strength selectively on the layer I dendrites of PFC-dPAG projecting neurons.

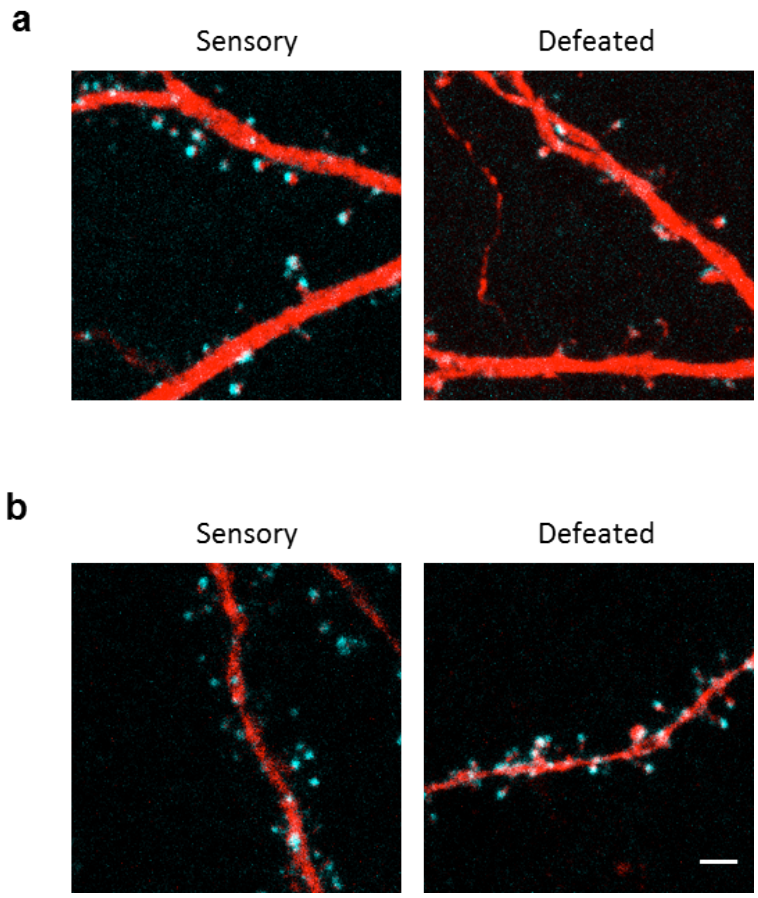

Figure 33. Representative pictures of the two imaged dendritic compartments. (a) Apical tuft and **(b)** Oblique layer II/III dendrites labeled with tdTomato (red) and BG Alexa 647 (cyan) labeling surface GluA1 receptor. Scale bar is 2µm

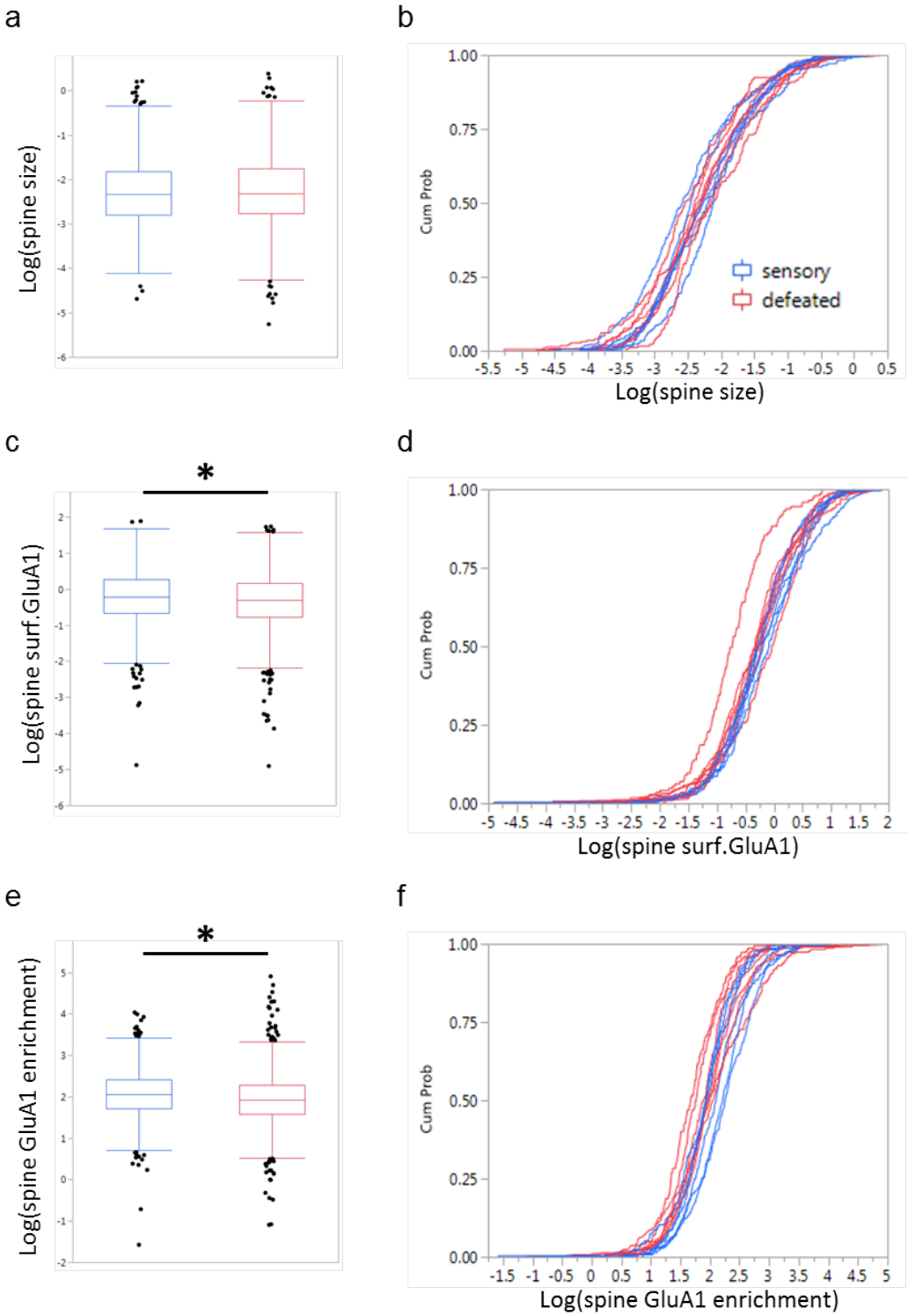

Figure 34. Decreased spine surface GluA1 and synaptic potentiation in apical tuft (layer I) of PFC-dPAG neurons after defeat. (a) No changes are detected in spine size. **(b)** Cumulative probability curves of spine size for each animal. **(c)** Significant decrease of surface GluA1 content in spines of defeated animals (behavior: p=0.047). **(d)** Cumulative probability curves of spine surface GluA1for each animal. **(e)** Significant decrease of GluA1enrichment in spines of defeated animals (behavior: p=0.0125). **(f)** Cumulative probability curves of spine GluA1 enrichment for each animal. Statistical analysis was made on single spines (log converted data) using a mixed model that took into account also animal and dendrite of origin, as described in methods. N=1578 spines, 28 tufts, 6 animals for sensory; 1966 spines, 35 tufts, 7 animals for defeated

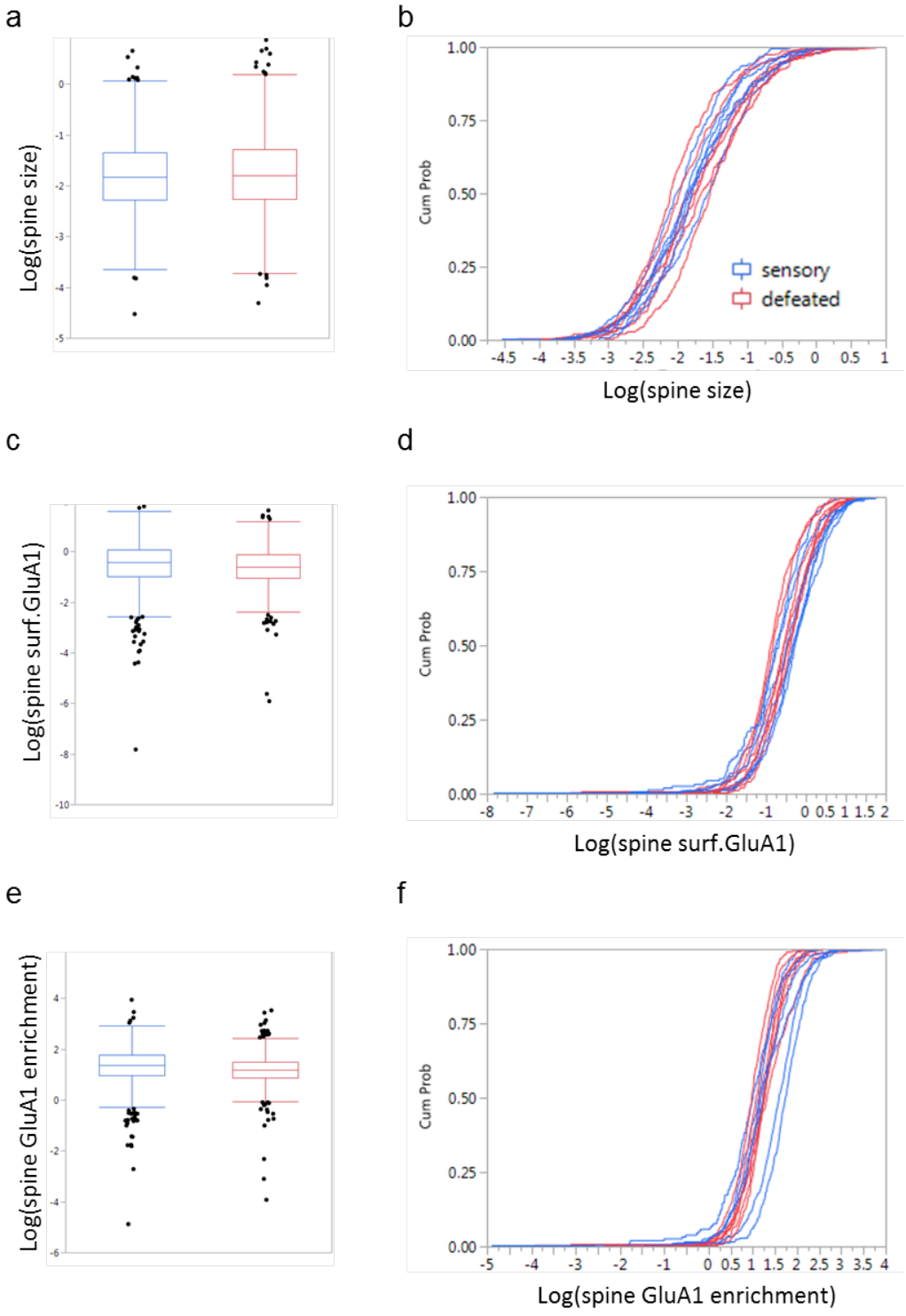

Figure 35. No significant changes are detected in either spine size or surface GluA1 in oblique layer II/III dendrites of PFC-dPAG neurons after defeat. (a) No changes are detected in spine size. **(b)** Cumulative probability curves of spine size for each animal. **(c)** Surface GluA1 content does not change significantly in spines of defeated animals. **(d)** Cumulative probability curves of spine surface GluA1for each animal. **(e)** GluA1enrichment is not significantly altered in spines of defeated animals. **(f)** Cumulative probability curves of spine GluA1 enrichment for each animal. Statistical analysis was made on single spines (log converted data) using a mixed model that took into account also animal and dendrite of origin, as described in methods. N=1807 spines, 40 dendrites, 6 animals, for sensory; 2180 spines, 49 dendrites , 7 animals for defeated.

Pharmacogenetic inhibition of Sst$^+$neurons during, but not after social defeat, impairs acquisition of social avoidance

Seen the postsynaptic weakening we observed in PFC-dPAG layer I dendrites and the increased presynaptic inputs that are made onto this layer by Sst$^+$neurons, we decided to assess if the activity of Sst$^+$neurons was promoting the acquisition of social avoidance in defeated animals. To do so, we inhibited their activity during the 3 days of social defeat and tested social interaction and avoidance on day 4. Briefly, we injected *Sst*::Cre animals with a Cre dependent virus (AAV *hSyn*::DIO-hM4D-mCherry) expressing the G_i coupled receptor hM4D (Fig. 36a and b), that induces neuronal silencing in presence of the inert ligand clozapine N-oxide (CNO) (Armbruster et al., 2007; Stachniak et al., 2014). Three weeks after surgery, mice were injected with saline and tested for their baseline social interaction. From the day after, all mice were subjected to 3 days social defeat, but each day CNO (3mg/kg) or saline was injected i.p. 1h before starting (as in Madroñal et al., 2016), finally on day 4 mice were tested again for social interaction, but all of them were injected with saline only (Fig. 36c). Furthermore, before starting the behavioral experiment mice were injected with saline for 1 week to habituate them to i.p.injections.

On day 1, regardless of their treatment (CNO or saline), mice did not show any significant change in either avoidance (Fig. 36d) or time spent interacting with the conspecific (Fig. 36e), compared to their avoidance or interaction measured at day 0: therefore acute inhibition of Sst$^+$neurons in non-previously defeated animals did not have any effect on social behavior.

On day 4, mice that had been treated with CNO were significantly less avoidant (Fig. 36f) and more interactive (Fig. 36g) than mice that had been treated with saline, demonstrating that chronic inhibition of Sst$^+$ neurons during the days of the defeat is sufficient to induce a more social approaching behavior after the stress and that the activity of Sst$^+$ neurons is then contributing to the process of behavioral adaptation to social defeat.

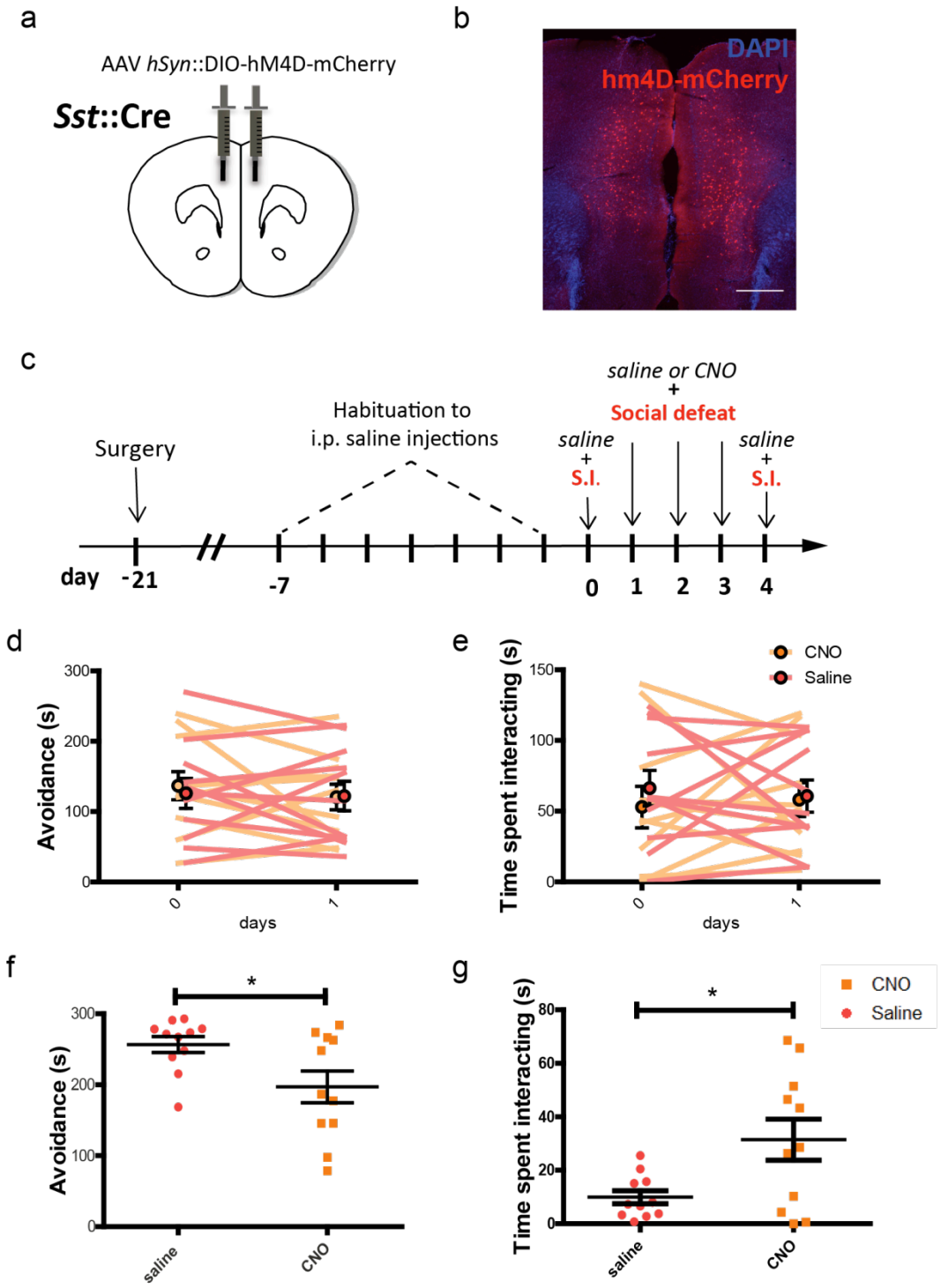

Figure 36. Inhibition of Sst$^+$ neurons during social defeat interferes with the remodeling of social behavior. **(a)** Schematic representation of surgical procedure. **(b)** Representative picture of *Sst*::Cre mouse PFC injected bilaterally with AAV *hSyn*::DIO-hM4D-mCherry. **(c)** Timeline of the experiment. Acute inhibition of Sst$^+$ neurons does not affect either **(d)** social avoidance or **(e)** social interaction in non-previously defeated mice. **(f)** Chronic inhibition of Sst$^+$ neurons during three days of repeated social defeat significantly decreases social avoidance and **(g)** increases social interaction in defeated mice on the day of social interaction test (day 4). Analyses were carried by Two way ANOVA RM plus post-hoc Bonferroni corrections in **(d)** and **(e)** and by t-test in **(f)** and **(g)**. N=11 animals. * $p<0.05$ Scale bar= 500µm

We repeated the experiment injecting the CNO each day right after the defeat (Fig. 37a), to identify if the activity of these neurons was essential in this process during or after the defeat. This time, when social behavior was tested after the social defeat paradigm (day 10), there was no effect of the inhibition on either social avoidance (Fig. 37b) or time spent interacting (Fig. 37c), demonstrating that the activity of Sst^{+}neurons is crucial during the defeat and not right after.

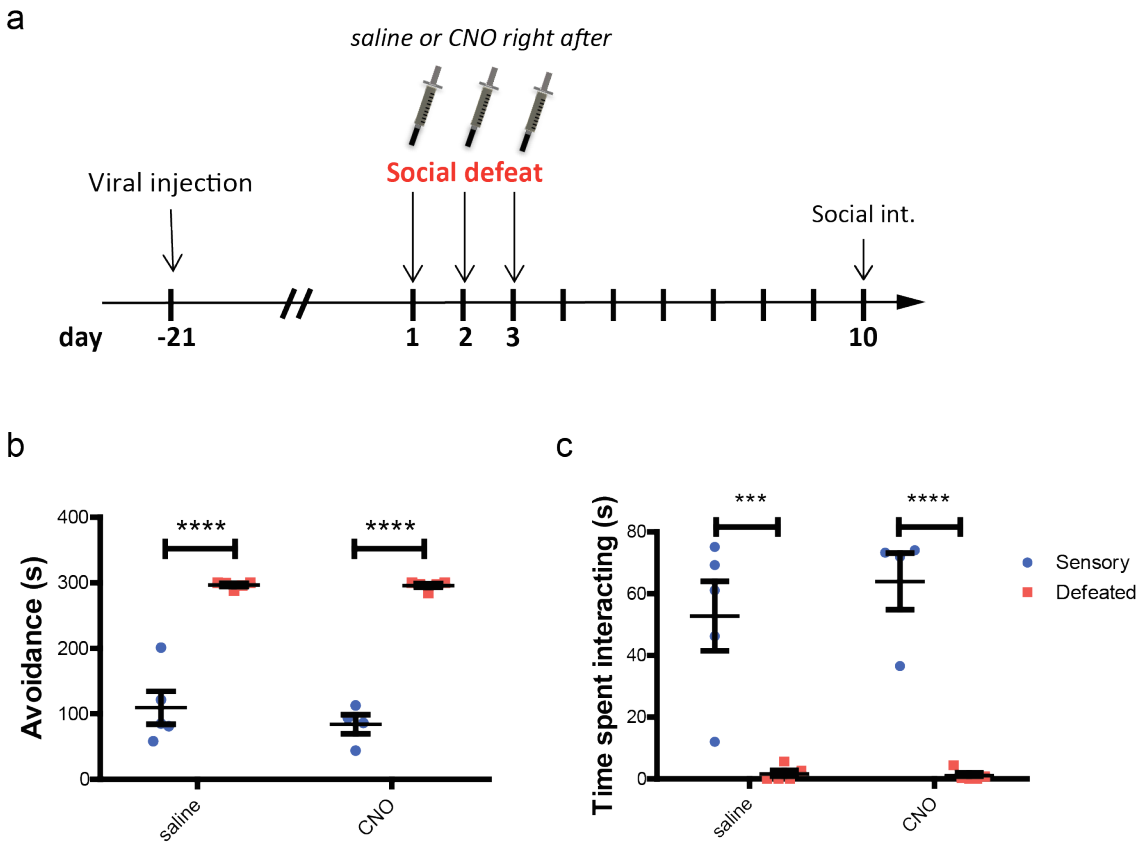

Figure 37. Inhibition of Sst^{+} neurons right after each defeat is not sufficient to affect the remodeling of social behavior. (a) Timeline of the experiment. **(b)** No effect of Sst^{+} neurons inhibition on either acquisition of social avoidance or decrease of **(c)** social interaction induced by the defeat and observed on the social interaction test day (day 10) (in both: behavior, $p<0.0001$) Data were analyzed by two way ANOVA plus post-hoc Bonferroni corrections. N=5 animals per group *** $p<0.001$, **** $p<0.0001$.

Discussion

In the present study, we integrated different approaches to identify plasticity mechanisms induced by negative social experiences in the PFC: among these, inhibiting the activity of Sst^+ interneurons revealed to be sufficient to impair acquisition of social avoidance in defeated animals. Our analysis revealed many other insights about plasticity events that are occurring in the PFC of defeated animals. First, looking at the whole PFC, we identified subtle perturbations of the levels of some translation-related markers of plasticity. Altered levels of several translated gene sets in PFC $Pvalb^+$ and Sst^+ neuronal subpopulations raised the hypothesis that Sst^+ neurons would be undergoing structural plasticity in defeated animals, which was confirmed by the observation of increased presynaptic inputs in the PFC layer I. We then revealed that PFC-dPAG neurons, namely the drivers of social behavior, were undergoing morphological remodelling and were decreasing levels of spine surface GluA1 specifically in layer I (where Sst^+neurons were making more synapses). We finally observed that artificially inhibiting the activity of Sst^+ neurons in the PFC during social defeat is sufficient to improve social interaction in defeated animals.

Translational and structural plasticity in the PFC microcircuit

Our first experiments aimed to establish if the molecular underpinnings of behavioural adaptation to social defeat actually resided in the PFC. The molecules we tested are transcriptional or translational plasticity markers, whose levels or phosphorylation state are altered while a neuron is undergoing some plastic adaptation. Results of these experiments confirmed that after the defeat the PFC was actually undergoing molecular remodelling, but detected changes were weak and pretty controversial. Indeed, we found increased levels of total eIF2α and GSK3β proteins (Fig. 9), but no changes in their phosphorylated fractions; therefore the question about their activation state remained unanswered. Increased expression of these two proteins (which was not reflected by parallel changes in TRAP experiments; data not shown) could be interpreted as enhanced ER stress in PFC cells and translational remodelling of these neurons. Indeed, eIF2α is important for translation initiation and its activation is observed in long term plasticity (Costa-Mattioli et al., 2009); while GSK3β inhibits and is inhibited by the mTORC1 pathway (Bradley et al., 2012). Interestingly, compromised eIF2 signaling is observable in Sst^+ neurons of mice which underwent chronic unpredictable stress (L. Lin & Sibille, 2015), while increased levels of GSK3β are found in

the brain of depressed patients and in the NAc of mice subjected to social defeat, in which context its inhibition has antidepressant effects (Li & Jope, 2010; Wilkinson et al., 2011). All of the other investigated plasticity markers resulted not to be changing in the whole PFC. Even in the case of pS6, a decrease was detected only by IF and not confirmed by WB (Fig. 8 and 9). We then hypothesized that subchronic social defeat was inducing cell type or projection specific alterations that could have only been detected by cell type specific techniques.

As a matter of fact, TRAP mediated gene expression analysis revealed cell-type specific translational plasticity in the PFC. The use of this technique had many advantages: first, cell type selectivity; second, the isolation of only translated mRNAs, including dendritic mRNAs, which play a relevant role in plasticity. Thanks to this tool and to the use of Gene Set Enrichment Analysis we detected changes in gene translation in both $Pvalb^+$ and Sst^+ neurons, but, surprisingly, not in glutamatergic neurons. Actually, few gene sets were upregulated in $CamK2a^+$glutamatergic neurons, but none of the genes contained in these gene sets had a $p<0.05$, except one: *Eif2b2* (Table S1).

Eif2b2 encodes for one of the five polypeptides composing eIF2β, a subunit of the eIF2 translation initiation complex. While eIF2α is the regulatory subunit of the complex, eIF2β is the Guanine nucleotide Exchange factor (Pavitt et al., 1998). Interestingly, eIF2β is inhibited when phosphorylated by GSK3β (Welsh, Miller, Loughlin, Price, & Proud, 1998), which was increased in our system. Therefore, although at this time point no major gene expression changes seem to be taking place in glutamatergic neurons; this result corroborates the hypothesis that also these neurons are undergoing a potential remodelling of translation.

Interestingly, gene expression changes observed in $Pvalb^+$ and Sst^+ neurons had opposite directions: while we observed only downregulation in $Pvalb^+$ neurons, the opposite was true for the Sst^+ population (Fig. 12 and 15). This bidirectionality is already suggestive of an opposite adaptation of these two subpopulations following social defeat, with Sst^+ neurons undergoing increased translation levels, probably due to increased activity and metabolism, and $Pvalb^+$ neurons decreasing their levels of translation, probably due to decreased activity. This interpretation is also reinforced by the observation that a substantial amount of Sst^+ neurons exerts inhibition also onto $Pvalb^+$ neuronal subpopulation (Pfeffer et al., 2013).

Changes observed in Pvalb$^+$ neurons were involving many aspects; the majority of the downregulated gene groups in Pvalb$^+$ neurons actually included membrane proteins and receptors, ranging from G-coupled receptors (mainly neuromodulator receptors, such as *Chrm1, Cckbr, Htr2a, Oprd1*) to ionotropic glutamate receptors (*Grik3* and *Grin2b*, encoding respectively for a subunit of kainate type receptors and NMDA receptors) and even the GABA receptor *Gabbr2* (Fig. 13 and Tables S2-S5). Downregulation of these receptors is not easy to explain, as each of them has different and even opposite roles in the neuron and its desensitization could drive its downregulation. The downregulation of groups of genes related to neurotransmitter transport, exocytic vesicles and neurotransmitter release could be instead directly linked to decreased activity of these neurons. In favour of this hypothesis, we know from previous literature that excitatory synaptic transmission onto Pvalb$^+$ neurons is decreased in mice that had shown susceptibility to learned helplessness (Perova et al., 2015). Furthermore, together with pyramidal neurons, Pvalb$^+$ neurons are targeted and activated by MDT projections in the PFC (Delevich, Tucciarone, Huang, & Li, 2015). These are the same projections whose stimulation induces a much weaker PFC response in defeated mice (Franklin et al., 2017). Interestingly, Pvalb$^+$ neurons downregulate also groups of genes related to membrane potential and ion channels: among these, changes in voltage-gated K^+ channels (Kv) are of notable interest. Kv are important regulators of neuronal excitability by promoting membrane repolarization after action potentials. Mutations in various Kv channels have been linked with epilepsy in humans (Villa & Combi, 2016): these include some genes that are present in our Pvalb network, namely *Kcnb1, Kcnq2* and *Kcnq3* (Fig.13, Table S3). The last two ones are at the basis of the so called M-currents, slowly activating K^+currents that are active at subthreshold potential and inactivate poorly, contributing to the stabilization of membrane potential (Robbins, 2001; J. Wang & Li, 2016). It has recently been shown that in Pvalb$^+$ neurons these currents can be activated by BDNF binding to TrkB receptor (Nieto-Gonzalez & Jensen, 2013), leading to depression of neuronal excitability. On the contrary, their inhibition can be triggered by acetylcholine binding to its muscarinic receptor 1 (M1-AchR, hence the name M-currents), encoded by *Chrm1*, also downregulated in our system (Fig. 13, Table S3). In this case, it must be noted that blockade of M-currents does not always lead to increased excitability of these neurons. Indeed, in a mouse model of schizophrenia it's been observed a decreased function of KCNQ2 channels, that seems to be at the basis of the decreased response of PFC Pvalb$^+$ neurons to dopaminergic stimulation, and renders these cells less capable to inhibit pyramidal neurons (Choi et al., 2017). Further investigation will

be needed to establish if this is the case also for PFC Pvalb$^+$ neurons of defeated animals. Finally, these neurons downregulate also three gene sets (GO_amynoglycan biosynthetic process, GO_amynoglycan metabolic process, Reactome glycosaminoglycan metabolism) including genes involved in the synthesis and metabolism of the so called perineuronal net (PNN). The PNN is a specialized extracellular matrix that aggregates mainly around the proximal neurite and cell body of Pvalb$^+$ interneurons (McRae & Porter, 2012). It is composed by several molecules including chondroitin sulfate proteoglycans (CSPGs) and heparan sulfate proteoglycans (HSPGs) (Deepa et al., 2006) and it has been shown to play important roles in axon guidance during development, synaptic stabilization, nerve repair and plasticity (McRae & Porter, 2012). Regarding plasticity, strong evidences exist about the role of the PNN formation, in particular the CSPG component, in the closure of the so called critical period in the mammalian CNS. During critical period, occurring in early postnatal life, plasticity is at a high level, so that neuronal circuits are shaped by experiences. Chondroitinase digestion of CSPGs reopens the critical period for several brain regions, for example reactivating ocular dominance plasticity (Pizzorusso, 2002). Recently, it has been demonstrated that in the adult brain the CSPG brevican controls plasticity in hippocampal Pvalb$^+$ cells by regulating the localization of potassium channels and AMPA receptors, a mechanism that is required for learning and memory (Favuzzi et al., 2017). Finally, the levels of both Parvalbumin and PNN labelling (measured again looking at the CSPG component) in the dlPFC of schizophrenic patients are lower (Enwright et al., 2016). However, when we used WFA labelling to test CSPG levels in the PFC of defeated animals, we detected no differences in either the number or the intensity of positive cells (Fig.19-20). This result can be explained by the observation that the genes involved in the downregulation are actually related to HSPGs: (*Sdc3*, encoding for syndecan3, a proteoglycan that may carry heparan sulphates and *Hs6st1, Ext2* encoding for enzymes required for HS biosynthesis, see Fig.13). The potential role of HSPGs in plasticity is not clear yet. However, there are studies showing that some types of HSPGs (glypicans 4 and 6) interact with AMPA receptors, and animals lacking glypican-4 have fewer AMPARs in hippocampal synapses (Allen et al., 2012). Also, knocking out Ext1, another enzyme for HS biosynthesis, leads to attenuation of excitatory neurotransmission, maybe due to decreased synaptically localized AMPARs, and leads to deficits in socio-communicative behavior (Irie, Badie-Mahdavi, & Yamaguchi, 2012). It will be important in the future to establish if similar mechanisms are occurring in the Pvalb$^+$ neurons of defeated animals.

Remodeling of gene expression in Sst^+ neurons was less diverse: the large majority of upregulated gene sets could be linked to increased activity and ongoing growth of this subpopulation. In favour of increased activity of these cells were the upregulation of gene sets related to both post and presynapse, in particular related to glutamate receptors (*Gria2*, encoding for GluA2) and components of the presynaptic active zone for neurotransmitter release (*Bsn* and *Pclo*, encoding for scaffolding proteins of the presynaptic active zone, and *Unc13a*, involved in synaptic vesicle priming; see Fig.16 Tables S6-S9). Growth was suggested by the large number of gene sets (and corresponding genes) related to axonogenesis, axon guidance and positive regulation of cell growth (Table S6; S8-S9). Our social defeat experiment on *Sst*::SypGFP animals confirmed this view, as we detected an increased number of presynaptic contacts made by Sst^+ neurons in layer I of PFC (Fig.21). Few evidences exist about interneuron structural plasticity in response to experience. Motor learning, for example, has been shown to induce decreased number of axonal boutons from Sst^+ neurons and increased number of boutons from $Pvalb^+$ neurons in the motor cortex of trained animals (S. X. Chen et al., 2016). Also, chronic restraint stress seems to induce dendritic hypertrophy in GABAergic interneurons (mainly characterized as Martinotti cells) of PFC (Gilabert-Juan, Castillo-Gomez, Guirado, Moltó, & Nacher, 2013). What is at the basis of the growth of these interneurons? Neurite outgrowth relies on the assembly, disassembly and stabilization of cytoskeletal elements, including actin filaments, through multiple interactions, that involve scaffold proteins, adhesion molecules and putative coreceptors (Maness & Schachner, 2007). Several scaffold proteins, mainly spectrins and ankyrins (e.g. *Spna2, Spnb2, Actn1, Actn4, Ank2, Ank3,* see Fig.16 and Table S7.), were upregulated in Sst^+ neurons of defeated animals. Many of these are known to be downstream interactors of neural cell adhesion molecule (NCAM), that belongs to the immunoglobulin superfamily (Maness & Schachner, 2007). NCAM has the ability to incorporate long polymeric chains of the sugar sialic acid (PSA-NCAM) which are negatively charged and highly hydrated, thus acquiring anti adhesive properties that facilitate structural plasticity. Though PSA-NCAM is mainly found in the brain during early developmental stages, it's been found also in the adult brain, where it is mainly surrounding soma and synapses of Sst^+ interneuron subclasses (Nacher, Guirado, & Castillo-Gómez, 2013). Thereby, PSA-NCAM could be a potential candidate for the Sst^+ neuron growth that we observe in the PFC of defeated animals. Also, NCAM can act through several coreceptors, such as GDNF family receptor α (Gfrα) proteins (Paratcha, Ledda, & Ibáñez, 2003), which can drive neuronal

growth and differentiation. One of these receptors, Gfrα2 *(Gfra2)*, which has a preferential binding for the neurotrophic factor neurturin, has been identified as a discriminating marker gene for Sst^+ neurons, according to recent single cell RNAseq experiments (Tasic et al., 2016). Actually, in our experiment, *Gfra2* appears to be also upregulated in Sst^+ neurons of defeated animals (Fig. 16, Table S7). Thus, it will be interesting in the future to determine the role of this receptor in the growth of this interneuron subclass that occurs following social defeat: in particular it would be intriguing to know if selectively blocking this growth can have any effect on behavioral adaptation.

Layer specific plasticity of PFC-dPAG neurons

Although we did not find significant changes in gene expression in the glutamatergic subpopulation, the choice to study specifically pyramidal neurons that drive social behavior, namely dPAG projecting PFC neurons, unraveled both structural and functional plasticity in this population. First, dendritic atrophy of these neurons confirmed the damaging effects of stress on the PFC. Though this phenomenon had been documented before; previously used behavioral models were chronic restraint stress or chronic unpredictable stress, which are less natural and induce a generalization of anxiety and depression symptoms, if compared with 3-days social defeat. Our study actually demonstrated that 3 days of negative social experiences are sufficient to change the dendritic structure of the PFC neurons that drive social behavior, while no effects can be observed in spine density (Fig.24-25). Unfortunately, this result does not exclude that also other pyramidal neurons, projecting to different targets, are undergoing the same remodelling, so further experiments will be needed to confirm that. Changes we observed were concentrated mainly on the proximal apical dendrites, the ones located in cortical layer II/III, while retraction of apical tuft dendrites was not significant (Fig.24). Also, functional changes in surface levels of AMPAR's GluA1, a more straightforward indication of synaptic strength, were layer specific. This time there were no significant alterations in layer II/III dendrites, while a significant decrease in surface GluA1 was detectable in layer I dendrites, also when normalized to the spine size, likely indicating a weakening of the synaptic transmission in this area. Like spine density, spine size was not altered by the defeat (Fig. 34-35).

This layer specific plasticity could depend on whether different inputs to the same neurons target different layers. These inputs can either be local or come from other brain regions. The MD, for example, targets preferentially layer I and deep layer III-layer V (Clascá, Rubio-

Garrido, & Jabaudon, 2012; Rubio-Garrido, Pérez-De-Manzo, Porrero, Galazo, & Clascá, 2009; Xiao, Zikopoulos, & Barbas, 2010) while avoiding the more superficial part of layer II/III. The previously observed weakening of PFC response to MDT stimulation in defeated animals (Franklin et al., 2017) is in line with a postsynaptic weakening of layer I dendrites, indicated by the decreased amount of surface AMPARs observed in there. Regarding rather local inputs, Sst^+ Martinotti cells target exclusively layer I dendrites. The parallel decrease in surface GluA1 and increase in Sst^+ presynaptic inputs, observed in the same layer, strongly suggests that the two phenomena could be interrelated in the acquisition of social avoidance, a theory that we wanted to pursue with our last manipulation experiment (see next section of Discussion).

It remains elusive why dendritic retraction of PFC-dPAG neurons is instead specific to layer II/III, where no significant changes were observed in surface AMPARs levels. One could for example speculate that while MDT-PFC circuit is disrupted, vHPC-PFC circuit is hyperactive: vHPC indeed projects abundantly to the PFC, but avoids layer I (Jay & Witter, 1991). One possibility could be that vHPC projections to PFC, which seem to have an essential role in the consolidation of social recognition memory (Tanimizu et al., 2017), are excessively active and causing excitotoxicity in layer II/III dendrites, that are consequently losing their branches. NMDAR dependent dendritic retraction has actually already been observed in other regions, such as CA3, following chronic stress (Christian, Miracle, Wellman, & Nakazawa, 2011). Of course, this is a speculation that should be explored with further experimentation.

A novel tool to image plasticity after behavior

The alteration of surface GluA1 levels in layer I dendrites of PFC-dPAG neurons was found using a novel tool, in which we adapted SNAP tagging technique to *in vivo* use in the mouse brain. This tool consists in the fusion of the AMPAR subunit GluA1 to the enzymatic tag SNAP, the following expression of this construct through a virus (in this case a retrograde HSV virus) in the mouse brain and, finally, the *in vivo* fluorescent labeling of extracellular SNAP through i.c.v. injection of a non cell penetrant BG ligand. By several control experiments we demonstrated that this tool was not only suitable for *in vivo* tagging of AMPARs, but also that the use of BG surface allowed selectively the labelling of surface exposed proteins (Fig. 28-29), a feature that was essential in the study of plasticity. Indeed, we know that increased and decreased synaptic strength are reflected, respectively, by

increased and decreased levels of surface AMPARs. Furthermore, thanks to the parallel expression of tdTomato, we were able to both estimate the spine size and to normalize surface AMPARs levels for this value, to get an estimation of synaptic strength, as we know that bigger spines contain also more AMPA receptors (Matsuzaki et al., 2001).

The use of a tool that allows to evaluate also the content in these receptors gives important information that are not always deducible by structural changes. Actually, experience does not always cause morphological alterations. For example, in our social defeat model we did not observe differences in either spine density (previously measured in *Thy1*::GFP animals) or spine size themselves. Moreover, compared to electrophysiology, which is the most reliable tool that is used to measure synaptic strength today, *in vivo* surface SNAPGluA1 tagging gives also information relatively to the localization (layer/dendritic branch) where the changes are occurring. Further, it can easily be used *in vivo*, after behavioral challenges.

One could argue that similar advantages were reached also by the use of SEP tagging of GluA1, another technique where fusion of GluA1 to a mutated GFP, that is fluorescent only at a neutral pH, allows to visualize only surface exposed AMPARs. Also this technique has been used *in vivo*. However, to visualize surface SEP-AMPARs levels after a behavioral challenge, other labs used either acute slices preparations (differences in pH between endosomes and extracellular space are lost by fixation) or *in vivo* two photon microscopy. Our technique allows, instead, to do the labelling *in vivo* and the imaging directly on fixed slices. This is more convenient than the preparation of acute slices, it can be applied in any region and with any behavioral challenge and it avoids the limits of tissue depth and head fixation that are imposed by *in vivo* two photon microscopy. Nevertheless, compared to two photon, it is not possible to follow spine dynamics during time, but only at one specific time point. Moreover, like for SEP, it would be preferable not to overexpress AMPAR subunits to avoid to alter mouse behavior. However, we showed that injected mice did not present any behavioral alteration in our social defeat challenge (Fig. 32) and the use of appropriate controls limits the possibility of wrong interpretations. Anyway, for future applications, an improvement could be to directly knock-in the construct in animals, avoiding the viral mediated overexpression.

SNAP tagging has a good potential for further development in the study of synapses. For example, it could be extended also to tagging of other glutamate receptor subunits (like SNAPGluA2, potentially useful to study homeostatic plasticity) or presynaptic components

(like Synaptophysin, to study presynaptic release). Together with SNAP tag, we also started to set up another labelling technique for *in vivo* use in the mouse brain, that is Halo tagging (Fig.30). In the future, one could imagine to couple SNAP and Halo tagging to contemporarily follow dynamics of pre and postsynaptic components, or to differentially tag two different subunits of the same receptors.

Disabling plasticity mechanisms in the PFC: inhibition of Sst^+ interneurons impairs social avoidance acquisition

Inhibiting Sst^+ interneurons activity in the PFC, we impaired the acquisition of social avoidance in defeated animals (Fig.36). The reason why we chose to inhibit these neurons was related to both the gene expression changes observed in these cells, the increased number of their presynaptic terminals found in PFC layer I and finally the decreased synaptic strength in PFC-dPAG neurons in the same layer. By the use of a pharmacogenetic tool we revealed that activity of these neurons was necessary during the behavioral challenge, but not right after, in order to acquire the defeated phenotype (Fig.37).

Our results are in line with a previous study where it had been shown that chronic inhibition of PFC Sst^+ interneurons had antidepressive and anxyolitic effects both under baseline conditions and after forms of chronic unpredictable stress (Soumier & Sibille, 2014). However, Soumier and Sibille had ablated neurons by the use of diphtheria toxin weeks before subjecting animals to stress, so that it was not possible to understand in which moment the contribution of these interneurons was actually necessary for the behavioral plasticity. Also, their study did not include any form of social stress or readout of social interaction, while we unraveled the role of these cells in influencing specifically adaptation of social behavior.

It remains to be understood what is driving the activity of Sst^+ interneurons during social defeat. One possibility could be the neuromodulator acetylcholine. For example, it seems that the antidepressant effects of scopolamine, an antagonist of muscarinic acetylcholine receptors, are actually mediated by Sst^+ neurons in the PFC. Indeed, knocking down the expression of M1-type muscarinic acetylcholine receptors (M1-AchR) selectively in Sst^+ neurons prevents the antidepressant effects of the drug (Wohleb et al., 2016). In this case, receptor knockdown might be expected to have the same antidepressant effects than scopolamine. However, the authors claim that shRNA knockdown reduces gradually M1-

AChR expression by approximately 50% and the timing of this change could potentially allow for compensatory neuronal adaptations. More importantly, by the use of optogenetics, it's been demonstrated in the visual cortex that acetylcholine causes desynchronization and decorrelation of cortical microcircuit by direct cholinergic activation of Sst^+ interneurons (N. Chen, Sugihara, & Sur, 2015). The effects of desynchronization and decorrelation on the circuit are due to the contemporary inhibition exerted by Sst^+ interneurons on both pyramidal and $Pvalb^+$ interneurons. Acetylcholine could then be a valid potential candidate for the activation of Sst^+ neurons during social defeat.

A last key question that will have to be answered is if there is a causality between hyperactivity of Sst^+ neurons and weakening of synaptic strength in the apical tuft of pyramidal neurons. This is a likely event because it has already been shown that activity of Sst^+ neurons is necessary to induce branch specific Ca^{2+} spikes when mice perform different motor learning tasks. In this case, the loss of branch specific generation of Ca^{2+} spikes reduces synaptic potentiation induced by one task when a different task is learned and it interferes with behavioral improvement (Cichon & Gan, 2015). This confirms the influence of Sst^+ neuronal activity on plasticity of pyramidal neurons.

Concluding remarks

With our study we identified plasticity mechanisms induced by social defeat in the different components of the PFC microcircuit and gave rise to some new questions that will need to be answered in the future (see summary model in Fig.38). After 3 days defeat $Pvalb^+$ neurons downregulated classes of genes related to membrane potential and electrical activity of these neurons and some enzymes related to synthesis and metabolism of HSPGs, while Sst^+neurons were upregulating groups of genes related to axonal growth and, likely, enhanced neuronal activity. Interestingly, Sst^+ neurons were forming more presynaptic contacts in PFC layer I after the defeat and inhibiting their activity was sufficient to impair acquisition of social avoidance. It will be interesting to determine which growth signaling pathway is upstream their axonal growth (Gfrα2?) and if blocking the formation of new presynaptic contacts is sufficient to get a behavioral effect. It will also be worth to determine if hyperactivity of Sst^+ neurons is also at the basis of a putative weakening of $Pvalb^+$ interneurons and/or if this hyperactivity is driven by the neuromodulator acetylcholine, that could also be responsible for the desensitization of its receptor (M1-AchR, encoded by *Chrm1*) and the downregulation of KCNQ channels in $Pvalb^+$ neurons. As to pyramidal PFC-dPAG neurons, we found

decreased branching selectively in layer II/III dendrites, that, we speculate, could be due to excitotoxicity caused by excessive stimulation of vHPC projections. In the same neurons we found decreased synaptic strength, as demonstrated by decreased surface SNAPGluA1 levels, selectively in layer I (apical tuft), that is putatively contacted by both MDT projections and Sst^+ neurons.

In conclusion, our results establish a central role for Sst^+ interneurons in plasticity of PFC microcircuitry during social defeat and acquisition of social avoidance. Further experiments and electrophysiological correlates will help to clarify the relationship between their function and the molecular and synaptic remodeling observed in the other cell types.

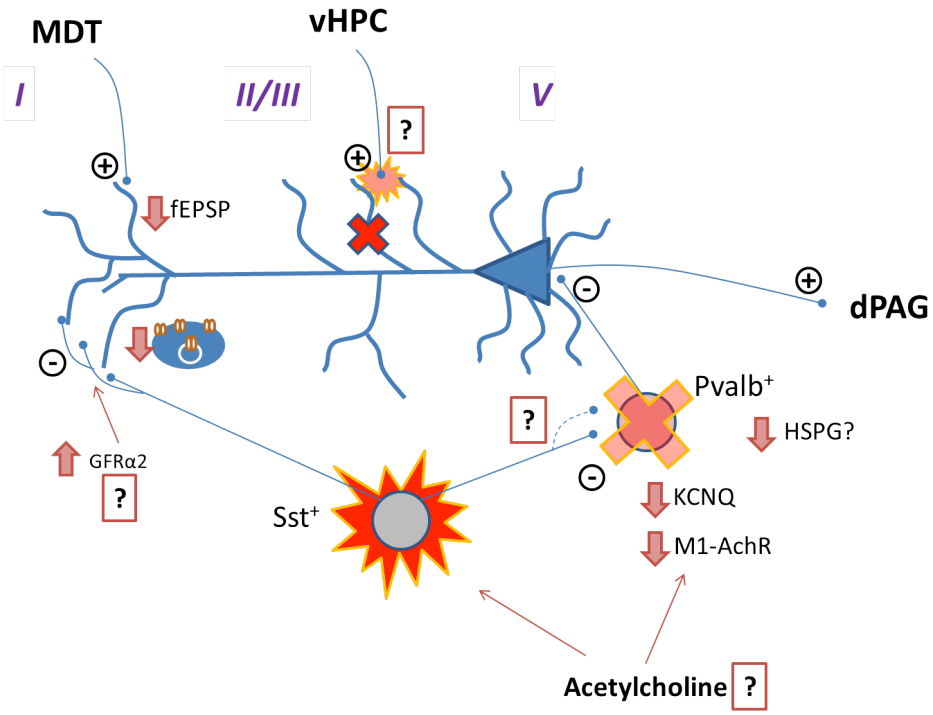

Figure 38. Model of plasticity mechanisms occurring in the PFC after the defeat. Sst^+neurons are growing, maybe in response to Gfrα2 activation, and their activity is inducing social avoidance. Enhanced inhibition from Sst^+ neurons in layer I could be contributing to the weakening of synaptic strength (decreased surface AMPARs) in the apical tuft of PFC-dPAG neurons, that are also decreasing their dendritic branching in layer II/III, putatively due to excitotoxicity in reponse to overstimulation from other afferents. Acetylcholine could be upstream the changes observed in both Sst^+ and $Pvalb^+$ neurons. A more detailed description of the model can be found in the text.

References

Aghajanian, G. K. (2013). BDNF Val66Met allele impairs basal and ketamine-stimulated synaptogenesis in prefrontal cortex. *PNAS*, *71*(11), 996–1005. doi:10.1016/j.biopsych.2011.09.030.

Alberini, C. M. (2009). Transcription Factors in Long-Term Memory and Synaptic Plasticity. *Physiol Rev*, 121–145. doi:10.1152/physrev.00017.2008.

Alexander, G. M., Rogan, S. C., Abbas, A. I., Armbruster, B. N., Pei, Y., Allen, J. A., … Roth, B. L. (2010). Remote control of neuronal activity in transgenic mice expressing evolved G protein-coupled receptors, *63*(1), 27–39. doi:10.1016/j.neuron.2009.06.014

Allen, N. J., Bennett, M. L., Foo, L. C., Wang, G. X., Chakraborty, C., Smith, S. J., & Barres, B. A. (2012). Astrocyte glypicans 4 and 6 promote formation of excitatory synapses via GluA1 AMPA receptors. *Nature*, *486*(7403), 410–4. doi:10.1038/nature11059

Antinone, S. E., & Smith, G. a. (2010). Retrograde Axon Transport of Herpes Simplex Virus and Pseudorabies Virus: a Live-Cell Comparative Analysis. *Journal of Virology*, *84*(3), 1504–1512. doi:10.1128/JVI.02029-09

Armbruster, B. N., Li, X., Pausch, M. H., Herlitze, S., & Roth, B. L. (2007). Evolving the lock to fit the key to create a family of G protein-coupled receptors potently activated by an inert ligand. *Proceedings of the National Academy of Sciences of the United States of America*, *104*(12), 5163–5168. Retrieved from http://www.pubmedcentral.nih.gov/articlerender.fcgi?artid=1829280&tool=pmcentrez&rendertype=abstract

Arnsten, A. F. T. (2009). Stress signalling pathways that impair prefrontal cortex structure and function. *Nature Reviews. Neuroscience*, *10*(6), 410–22. doi:10.1038/nrn2648

Aron, A. R., Monsell, S., Sahakian, B. J., & Robbins, T. W. (2004). A componential analysis of task-switching deficits associated with lesions of left and right frontal cortex. *Brain*, *127*(7), 1561–1573. doi:10.1093/brain/awh169

Avesar, D., & Gulledge, A. T. (2012). Selective serotonergic excitation of callosal projection neurons. *Frontiers in Neural Circuits*, *6*. doi:10.3389/fncir.2012.00012

Bats, C., Groc, L., & Choquet, D. (2007). The Interaction between Stargazin and PSD-95 Regulates AMPA Receptor Surface Trafficking. *Neuron*, *53*(5), 719–734. doi:10.1016/j.neuron.2007.01.030

Bicks, L. K., Koike, H., Akbarian, S., & Morishita, H. (2015). Prefrontal cortex and social cognition in mouse and man. *Frontiers in Psychology*, *6*(NOV), 1–15. doi:10.3389/fpsyg.2015.01805

Bliim, N., Leshchynska, I., Sytnyk, V., & Janitz, M. (2016). Transcriptional regulation of long-term potentiation. *Neurogenetics*, *17*(4), 201–210. doi:10.1007/s10048-016-0489-x

Bloss, E. B., Janssen, W. G., McEwen, B. S., & Morrison, J. H. (2010). Interactive effects of stress and aging on structural plasticity in the prefrontal cortex. *The Journal of Neuroscience : The Official Journal of the Society for Neuroscience*, *30*(19), 6726–31. doi:10.1523/JNEUROSCI.0759-10.2010

Boender, A. J., de Jong, J. W., Boekhoudt, L., Luijendijk, M. C. M., van der Plasse, G., & Adan, R. a H. (2014). Combined use of the canine adenovirus-2 and DREADD-technology to activate specific neural pathways in vivo. *PloS One*, *9*(4), e95392. doi:10.1371/journal.pone.0095392

Bolkan, S. S., Stujenske, J. M., Parnaudeau, S., Spellman, T., Rauffenbart, C., Abbas, A. I., … Kellendonk, C. (2017). Thalamic projections sustain prefrontal activity during working memory maintenance. *Nat Neurosci*, *20*(7), 987–998. doi:10.1038/nn.4568

Bourtchuladze, R., Frenguelli, B., Blendy, J., Cioffi, D., Schutz, G., & Silva, A. J. (1994). Deficient long-term memory in mice with a targeted mutation of the cAMP-responsive element-binding protein. *Cell*, *79*(1), 59–68. doi:10.1016/0092-8674(94)90400-6

Bozza, T., McGann, J. P., Mombaerts, P., & Wachowiak, M. (2004). In vivo imaging of neuronal activity by targeted expression of a genetically encoded probe in the mouse. *Neuron*, *42*(1), 9–21. doi:10.1016/S0896-6273(04)00144-8

Bradley, C. A., Peineau, S., Taghibiglou, C., Nicolas, C. S., Whitcomb, D. J., Bortolotto, Z. A., … Collingridge, G. L. (2012). A pivotal role of GSK-3 in synaptic plasticity. *Frontiers in Molecular Neuroscience*, *5*, 13. doi:10.3389/fnmol.2012.00013

Buffington, S., Huang, W., & Costa-Mattioli, M. (2015). Translational Control in Synaptic Plasticity and Cognitive Dysfunction. *Annu Rev Neurosci*, (37), 17–38. doi:10.1016/B978-0-12-386043-9.00005-0

Cajigas, I. J., Tushev, G., Will, T. J., Tom Dieck, S., Fuerst, N., & Schuman, E. M. (2012). The Local Transcriptome in the Synaptic Neuropil Revealed by Deep Sequencing and High-Resolution Imaging. *Neuron*, *74*(3), 453–466. doi:10.1016/j.neuron.2012.02.036

Calhoon, G. G., & O'Donnell, P. (2013). Closing the Gate in the Limbic Striatum: Prefrontal Suppression of Hippocampal and Thalamic Inputs. *Neuron*, *78*(1), 181–190. doi:10.1016/j.neuron.2013.01.032

Cannon, T. D., Chung, Y., He, G., Sun, D., Jacobson, A., Erp, T. G. M. Van, … Jeffries, C. (2016). Progressive Reduction in Cortical Thickness as Psychosis Develops: A Multisite Longitudinal Neuroimaging Study of Youth at Elevated Clinical Risk. *Biol Psychiatry*, *77*(2), 147–157. doi:10.1016/j.biopsych.2014.05.023.Progressive

Carrive, P. (1993). The periaqueductal gray and defensive behavior: Functional representation and neuronal organization. *Behavioural Brain Research*, *58*(1-2), 27–47. doi:10.1016/0166-4328(93)90088-8

Challis, C., Beck, S. G., & Berton, O. (2014). Optogenetic modulation of descending prefrontocortical inputs to the dorsal raphe bidirectionally bias socioaffective choices after social defeat. *Frontiers in Behavioral Neuroscience*, *8*(February), 43. doi:10.3389/fnbeh.2014.00043

Challis, C., Boulden, J., Veerakumar, A., Espallergues, J., Vassoler, F. M., Pierce, R. C., … Berton, O. (2013). Raphe GABAergic neurons mediate the acquisition of avoidance after social defeat. *The Journal of Neuroscience : The Official Journal of the Society for Neuroscience*, *33*(35), 13978–88, 13988a. doi:10.1523/JNEUROSCI.2383-13.2013

Chater, T. E., & Goda, Y. (2014). The role of AMPA receptors in postsynaptic mechanisms of synaptic plasticity. *Frontiers in Cellular Neuroscience*, *8*(November), 401. doi:10.3389/fncel.2014.00401

Chaudhury, D., Walsh, J. J., Friedman, A. K., Juarez, B., Ku, M., Koo, J. W., … Han, M. (2013). Rapid regulation of depression-related behaviours by control of midbrain dopamine neurons. *Nature*, *493*(7433), 532–536. doi:10.1038/nature11713

Chen, N., Sugihara, H., & Sur, M. (2015). An acetylcholine-activated microcircuit drives temporal dynamics of cortical activity. *Nature Neuroscience*, *18*(6), 892–902. doi:10.1038/nn.4002

Chen, S. X., Kim, A. N., Peters, A. J., Komiyama, T., Diego, S., Jolla, L., … Jolla, L. (2016). Subtype-specific plasticity of inhibitory circuits in motor cortex during motor learning. *Nat Neurosci*, *18*(8), 1109–1115. doi:10.1038/nn.4049

Cho, R. Y., Konecky, R. O., & Carter, C. S. (2006). Impairments in frontal cortical gamma synchrony and cognitive control in schizophrenia. *Proc Natl Acad Sci U S A*, *103*(52), 19878–19883. doi:0609440103 [pii]\r10.1073/pnas.0609440103

Choi, S. J., Mukai, J., Kvajo, M., Xu, B., Diamantopoulou, A., Pitychoutis, P. M., … Zhang, H. (2017). A Schizophrenia-Related Deletion Leads to KCNQ2-Dependent Abnormal Dopaminergic Modulation of Prefrontal Cortical Interneuron Activity. *Cerebral Cortex*, *19*, 1–17.

Chowdhury, S., Shepherd, J. D., Okuno, H., Lyford, G., Petralia, R. S., Plath, N., … Worley, P. F. (2006). Arc/Arg3.1 Interacts with the Endocytic Machinery to Regulate AMPA Receptor Trafficking. *Neuron*, *52*(3), 445–459. doi:10.1016/j.neuron.2006.08.033

Christian, K. M., Miracle, A. D., Wellman, C. L., & Nakazawa, K. (2011). Chronic stress-induced hippocampal dendritic retraction requires CA3 NMDA receptors. *Neuroscience*, *174*, 26–36. doi:10.1016/j.neuroscience.2010.11.033

Christoffel, D. J., Golden, S. a, Walsh, J. J., Guise, K. G., Heshmati, M., Friedman, A. K., … Russo, S. J. (2015). Excitatory transmission at thalamo-striatal synapses mediates susceptibility to social stress. *Nature Neuroscience*, *18*(7), 6–11. doi:10.1038/nn.4034

Cichon, J., & Gan, W. (2015). Branch-specific dendritic Ca2+ spikes cause persistent synaptic plasticity. *Nature*, *520*(7546), 180–185. doi:10.1038/nature14251

Cingolani, L. A., Thalhammer, A., Yu, L. M. Y., Catalano, M., Ramos, T., Colicos, M. A., & Goda, Y. (2008). Activity-dependent regulation of synaptic AMPA receptor composition and abundance by beta3 integrins. *Neuron*, *58*(5), 749–62. doi:10.1016/j.neuron.2008.04.011

Citri, A., & Malenka, R. C. (2008). Synaptic plasticity: multiple forms, functions, and mechanisms. *Neuropsychopharmacology : Official Publication of the American College of Neuropsychopharmacology*, *33*(1), 18–41. doi:10.1038/sj.npp.1301559

Clascá, F., Rubio-Garrido, P., & Jabaudon, D. (2012). Unveiling the diversity of thalamocortical neuron subtypes. *European Journal of Neuroscience*, *35*(10), 1524–1532. doi:10.1111/j.1460-9568.2012.08033.x

Cohen, S., Janicki-Deverts, D., & Miller, G. E. (2007). Psychological stress and disease. *JAMA : The Journal of the American Medical Association*, *298*(14), 1685–1687. doi:10.1001/jama.298.14.1685

Costa-Mattioli, M., Sossin, W. S., Klann, E., & Sonenberg, N. (2009). Translational Control of Long-Lasting Synaptic Plasticity and Memory. *Neuron*, *61*(1), 10–26. doi:10.1016/j.neuron.2008.10.055

Covington, H. E., Lobo, M. K., Maze, I., Vialou, V., Hyman, J. M., Zaman, S., … Nestler, E. J. (2010). Antidepressant effect of optogenetic stimulation of the medial prefrontal cortex. *The Journal of Neuroscience : The Official Journal of the Society for Neuroscience*, *30*(48), 16082–90. doi:10.1523/JNEUROSCI.1731-10.2010

Cruikshank, S. J., Ahmed, O. J., Stevens, T. R., Patrick, S. L., Gonzalez, A. N., Elmaleh, M., & Connors, B. W. (2012). Thalamic Control of Layer 1 Circuits in Prefrontal Cortex. *Journal of Neuroscience*, *32*(49), 17813–17823. doi:10.1523/JNEUROSCI.3231-12.2012

Curley, A. A., Arion, D., Volk, D. W., Asafu-Adjei, J. K., Sampson, A. R., Fish, K. N., & Lewis, D. A. (2011). Cortical deficits of glutamic acid decarboxylase 67 expression in schizophrenia: Clinical, protein, and cell type-specific features. *American Journal of Psychiatry*, *168*(9), 921–929. doi:10.1176/appi.ajp.2011.11010052

Damasio, H., Grabowski, T., Frank, R., Galaburda, A. M., & Damasio, A. R. (1994). The return of Phineas Gage: clues about the brain from the skull of a famous patient. *Science*, *264*(5162), 1102 LP – 1105. Retrieved from http://science.sciencemag.org/content/264/5162/1102.abstract

Dash, P. K., Hochner, B., & Kandel, E. R. (1990). Injection of the cAMP-responsive element into the nucleus of Aplysia sensory neurons blocks long-term facilitation. *Nature*, *345*(6277), 718–721. doi:10.1038/345718a0

De Roo, M., Klauser, P., & Muller, D. (2008). LTP promotes a selective long-term stabilization and clustering of dendritic spines. *PLoS Biology*, *6*(9), 1850–1860. doi:10.1371/journal.pbio.0060219

Deepa, S. S., Carulli, D., Galtrey, C., Rhodes, K., Fukuda, J., Mikami, T., … Fawcett, J. W. (2006). Composition of Perineuronal Net Extracellular Matrix in Rat Brain: A different disaccharide composition for the net-associated proteoglycans. *J Biol Chem*, *281*(26), 17789–17800. doi:10.1074/jbc.M600544200

Delevich, K., Tucciarone, J., Huang, Z. J., & Li, B. (2015). The Mediodorsal Thalamus Drives Feedforward Inhibition in the Anterior Cingulate Cortex via Parvalbumin Interneurons. *Journal of Neuroscience*, *35*(14), 5743–5753. doi:10.1523/JNEUROSCI.4565-14.2015

Dembrow, N., & Johnston, D. (2014). Subcircuit-specific neuromodulation in the prefrontal cortex. *Frontiers in Neural Circuits*, *8*(June), 54. doi:10.3389/fncir.2014.00054

Do-Monte, F. H., Quinones-Laracuente, K., & Quirk, G. J. (2015). A temporal shift in the circuits mediating retrieval of fear memory. *Nature*, *519*(7544), 460–463. Retrieved from http://dx.doi.org/10.1038/nature14030

Douglas, R. J., & Martin, K. A. C. (2004). NEURONAL CIRCUITS OF THE NEOCORTEX. *Annual Review of Neuroscience*, *27*(1), 419–451. doi:10.1146/annurev.neuro.27.070203.144152

Duman, R. S., Aghajanian, G. K., Sanacora, G., & Krystal, J. H. (2016). Synaptic plasticity and depression: new insights from stress and rapid-acting antidepressants. *Nature Medicine*, *22*(3), 238–249. doi:10.1038/nm.4050

Dwyer, J. M., Maldonado-Avilés, J. G., Lepack, A. E., DiLeone, R. J., & Duman, R. S. (2015). Ribosomal protein S6 kinase 1 signaling in prefrontal cortex controls depressive behavior. *Proceedings of the National Academy of Sciences*, *2015*, 1–6. doi:10.1073/pnas.1505289112

Enwright, J. F., Sanapala, S., Foglio, A., Berry, R., Fish, K. N., & Lewis, D. A. (2016). Reduced Labeling of Parvalbumin Neurons and Perineuronal Nets in the Dorsolateral Prefrontal Cortex of Subjects with Schizophrenia. *Neuropsychopharmacology : Official Publication of the American College of Neuropsychopharmacology*, *41*(9), 1–9. doi:10.1038/npp.2016.24

Farley, F. W., Soriano, P., Steffen, L. S., & Dymecki, S. M. (2000). Widespread recombinase expression using FLPeR (Flipper) mice. *Genesis*, *28*(3-4), 106–110. doi:10.1002/1526-968X(200011/12)28:3/4<106::AID-GENE30>3.0.CO;2-T

Fatt, P., & Katz, B. (1952). Spontaneous subthreshold activity at motor nerve endings. *The Journal of Physiology*, *117*, 109–128. doi:10.1113/jphysiol.1952.sp004735

Favuzzi, E., Marques-Smith, A., Deogracias, R., Winterflood, C. M., Sánchez-Aguilera, A., Mantoan, L., … Rico, B. (2017). Activity-Dependent Gating of Parvalbumin Interneuron Function by the Perineuronal Net Protein Brevican. *Neuron*, 1–17. doi:10.1016/j.neuron.2017.06.028

Feng, G., Mellor, R. H., Bernstein, M., Keller-Peck, C., Nguyen, Q. T., Wallace, M., … Sanes, J. R. (2000). Imaging neuronal subsets in transgenic mice expressing multiple spectral variants of GFP. *Neuron*, *28*(1), 41–51. doi:10.1016/S0896-6273(00)00084-2

Fenno, L., Yizhar, O., & Deisseroth, K. (2011). The development and application of optogenetics. *Annual Review of Neuroscience*, *34*, 389–412. doi:10.1146/annurev-neuro-061010-113817

Franklin, T. B., Silva, B. A., Perova, Z., Marrone, L., Masferrer, M. E., Zhan, Y., … Gross, C. T. (2017). Prefrontal cortical control of a brainstem social behavior circuit. *Nat Neurosci*, *20*(2), 260–270. Retrieved from http://dx.doi.org/10.1038/nn.4470

Friedman, A. K., Walsh, J. J., Juarez, B., Ku, S. M., Chaudhury, D., Wang, J., … Han, M.-H. (2014). Enhancing depression mechanisms in midbrain dopamine neurons achieves homeostatic resilience. *Science (New York, N.Y.)*, *344*(6181), 313–9. doi:10.1126/science.1249240

Fuster, J. M. (2008). Anatomy of the Prefrontal Cortex. In *The Prefrontal Cortex* (pp. 7–58). Elsevier. doi:10.1016/B978-0-12-373644-4.00002-5

Gainey, M. A., Hurvitz-Wolff, J. R., Lambo, M. E., & Turrigiano, G. G. (2009). Synaptic scaling requires the GluR2 subunit of the AMPA receptor. *The Journal of Neuroscience : The Official Journal of the Society for Neuroscience*, *29*(20), 6479–89. doi:10.1523/JNEUROSCI.3753-08.2009

Gautier, A., Juillerat, A., Heinis, C., Corrêa, I. R., Kindermann, M., Beaufils, F., & Johnsson, K. (2008). An Engineered Protein Tag for Multiprotein Labeling in Living Cells. *Chemistry and Biology*, *15*(2), 128–136. doi:10.1016/j.chembiol.2008.01.007

Gilabert-Juan, J., Castillo-Gomez, E., Guirado, R., Moltó, M. D., & Nacher, J. (2013). Chronic stress alters inhibitory networks in the medial prefrontal cortex of adult mice. *Brain Structure & Function*, *218*(6), 1591–605. doi:10.1007/s00429-012-0479-1

Golden, S. a, Covington, H. E., Berton, O., & Russo, S. J. (2011). A standardized protocol for repeated social defeat stress in mice. *Nature Protocols*, *6*(8), 1183–1191. doi:10.1038/nprot.2011.361

Goldman-Rakic, P., Cools, A., & Srivastava, K. (1996). The Prefrontal Landscape: Implications of Functional Architecture for …. *Philosophical Transactions: ...*. Retrieved from http://www.ncbi.nlm.nih.gov/entrez/query.fcgi?db=pubmed&cmd=Retrieve&dopt=AbstractPlus&list_uids=17207235949104919 99related:X-VFJ_484RcJ

Goldwater, D. S., Pavlides, C., Hunter, R. G., Bloss, E. B., Patrick, R., Mcewen, B. S., … Hof, P. R. (2010). Structural and functional alterations to rat medial prefrontal cortex following chronic restraint stress and recovery. *Neuroscience*, *164*(2), 798–808. doi:10.1016/j.neuroscience.2009.08.053.Structural

Gomez, J. L., Bonaventura, J., Lesniak, W., Mathews, W. B., Sysa-Shah, P., Rodriguez, L. a., … Michaelides, M. (2017). Chemogenetics revealed: DREADD occupancy and activation via converted clozapine. *Science*, *357*(6350), 503–507. doi:10.1126/science.aan2475

Gordon, J. a. (2016). On being a circuit psychiatrist. *Nature Neuroscience*, *19*(11), 1385–1386. doi:10.1038/nn.4419

Grooms, S. Y., Noh, K.-M., Regis, R., Bassell, G. J., Bryan, M. K., Carroll, R. C., & Zukin, R. S. (2006). Activity bidirectionally regulates AMPA receptor mRNA abundance in dendrites of hippocampal neurons. *The Journal of Neuroscience : The Official Journal of the Society for Neuroscience*, *26*(32), 8339–8351. doi:10.1523/JNEUROSCI.0472-06.2006

Guldin, W. O., Pritzel, M., & Markowitsch, H. J. (1981). Prefrontal cortex of the mouse defined as cortical projection area of the thalamic mediodorsal nucleus. *Brain, Behavior and Evolution*, *19*(3-4), 93–107. doi:10.1159/000121636

Gunaydin, L. A., Grosenick, L., Finkelstein, J. C., Kauvar, I. V., Fenno, L. E., Adhikari, A., … Deisseroth, K. (2014). Natural neural projection dynamics underlying social behavior. *Cell*, *157*(7), 1535–1551. doi:10.1016/j.cell.2014.05.017

Haas, K., Li, J., & Cline, H. T. (2006). AMPA receptors regulate experience-dependent dendritic arbor growth in vivo. *Proceedings of the National Academy of Sciences of the United States of America*, *103*(32), 12127–31. doi:10.1073/pnas.0602670103

Hames, J. L., Hagan, C. R., & Joiner, T. E. (2013). Interpersonal Processes in Depression. *Annual Review of Clinical Psychology*, *9*(1), 355–377. doi:10.1146/annurev-clinpsy-050212-185553

Han, Y., Kaeser, P. S., Südhof, T. C., & Schneggenburger, R. (2011). RIM determines Ca2+ channel density and vesicle docking at the presynaptic active zone. *Neuron*, *69*(2), 304–316. doi:10.1016/j.neuron.2010.12.014

Harlow, J. M. (1993). Recovery from the passage of an iron bar through the head. *History of Psychiatry*, *4*(14), 274–281. doi:10.1177/0957154X9300401407

Hebb, D. . (1949). *The Organization of Behavior. A neuropsychological theory*. *The Organization of Behavior* (Vol. 911). doi:10.2307/1418888

Heiman, M., Kulicke, R., Fenster, R. J., Greengard, P., & Heintz, N. (2014). Cell type-specific mRNA purification by translating ribosome affinity purification (TRAP). *Nature Protocols*, *9*(6), 1282–91. doi:10.1038/nprot.2014.085

Holtmaat, A., Randall, J., & Cane, M. (2013). Optical imaging of structural and functional synaptic plasticity in vivo. *European Journal of Pharmacology*, 1–9. doi:10.1016/j.ejphar.2013.07.020

Hoover, W. B., & Vertes, R. P. (2007). Anatomical analysis of afferent projections to the medial prefrontal cortex in the rat. *Brain Structure and Function*, *212*(2), 149–179. doi:10.1007/s00429-007-0150-4

Huganir, R. L., & Nicoll, R. a. (2013). AMPARs and synaptic plasticity: the last 25 years. *Neuron*, *80*(3), 704–17. doi:10.1016/j.neuron.2013.10.025

Irie, F., Badie-Mahdavi, H., & Yamaguchi, Y. (2012). Autism-like socio-communicative deficits and stereotypies in mice lacking heparan sulfate. *Proceedings of the National Academy of Sciences of the United States of America*, *109*(13), 5052–6. doi:10.1073/pnas.1117881109

Jay, T. M., & Witter, M. P. (1991). Distribution of hippocampal CA1 and subicular efferents in the prefrontal cortex of the rat studied by means of anterograde transport of Phaseolus vulgaris???leucoagglutinin. *Journal of Comparative Neurology*, *313*(4), 574–586. doi:10.1002/cne.903130404

Jung, H., Gkogkas, C. G., Sonenberg, N., & Holt, C. E. (2014). Remote control of gene function by local translation. *Cell*. doi:10.1016/j.cell.2014.03.005

Kalivas, P. W. (2009). The glutamate homeostasis hypothesis of addiction. *Nature Reviews Neuroscience*, *10*(8), 561–572. doi:10.1038/nrn2515

Kaneko, M., Stellwagen, D., Malenka, R. C., & Stryker, M. P. (2008). Tumor Necrosis Factor-alpha Mediates One Component of Competitive, Experience-Dependent Plasticity in Developing Visual Cortex. *Neuron*, *58*(5), 673–680. doi:10.1016/j.neuron.2008.04.023

Kang, H. J., Voleti, B., Hajszan, T., Rajkowska, G., Stockmeier, C. a, Licznerski, P., … Duman, R. S. (2012). Decreased expression of synapse-related genes and loss of synapses in major depressive disorder. *Nature Medicine*, *18*(9), 1413–1417. doi:10.1038/nm.2886

Klann, E., & Dever, T. E. (2004). Biochemical mechanisms for translational regulation in synaptic plasticity. *Nature Reviews. Neuroscience*, *5*(12), 931–42. doi:10.1038/nrn1557

Koenigs, M., & Tranel, D. (2007). Irrational economic decision-making after ventromedial prefrontal damage: evidence from the Ultimatum Game. *The Journal of Neuroscience : The Official Journal of the Society for Neuroscience*, *27*(4), 951–956. doi:10.1523/JNEUROSCI.4606-06.2007

Kolb, B., & Gibb, R. (2015). Plasticity in the prefrontal cortex of adult rats. *Frontiers in Cellular Neuroscience*, *9*(February), 15. doi:10.3389/fncel.2015.00015

Kolluri, N., Sun, Z., Sampson, A. R., & Lewis, D. A. (2005). Lamina-specific reductions in dendritic spine density in the prefrontal cortex of subjects with schizophrenia. *American Journal of Psychiatry*, *162*(6), 1200–1202. doi:10.1176/appi.ajp.162.6.1200

Kühn, S., & Gallinat, J. (2013). Gray matter correlates of posttraumatic stress disorder: A quantitative meta-analysis. *Biological Psychiatry*, *73*(1), 70–74. doi:10.1016/j.biopsych.2012.06.029

Kumar, S., Black, S. J., Hultman, R., Szabo, S. T., DeMaio, K. D., Du, J., … Dzirasa, K. (2013). Cortical control of affective networks. *The Journal of Neuroscience*, *33*(3), 1116–29. doi:10.1523/JNEUROSCI.0092-12.2013

Kvitsiani, D., Ranade, S., Hangya, B., Taniguchi, H., Huang, J. Z., & Kepecs, a. (2013). Distinct behavioural and network correlates of two interneuron types in prefrontal cortex. *Nature*, *498*(7454), 363–6. doi:10.1038/nature12176

Lammel, S., Ion, D. I., Roeper, J., & Malenka, R. C. (2011). Projection-Specific Modulation of Dopamine Neuron Synapses by Aversive and Rewarding Stimuli. *Neuron*, *70*(5), 855–862. doi:10.1016/j.neuron.2011.03.025

Lee, A., Gee, S., Vogt, D., Patel, T., Rubenstein, J., & Sohal, V. (2014). Pyramidal neurons in prefrontal cortex receive subtype-specific forms of excitation and inhibition. *Neuron*, *81*(1), 61–68. doi:10.1016/j.neuron.2013.10.031

Lee, E., Rhim, I., Lee, J. W., Ghim, J.-W., Lee, S., Kim, E., & Jung, M. W. (2016). Enhanced Neuronal Activity in the Medial Prefrontal Cortex during Social Approach Behavior. *Journal of Neuroscience*, *36*(26), 6926–6936. doi:10.1523/JNEUROSCI.0307-16.2016

Lee, K. J., Park, I. S., Kim, H., Greenough, W. T., Pak, D. T. S., & Rhyu, I. J. (2013). Motor Skill Training Induces Coordinated Strengthening and Weakening between Neighboring Synapses. *The Journal of Neuroscience*, *33*(23), 9794–9799. doi:10.1523/JNEUROSCI.0848-12.2013

Lehmann, M. L., Weigel, T. K., Elkahloun, A. G., & Herkenham, M. (2017). Chronic social defeat reduces myelination in the mouse medial prefrontal cortex. *Nature Publishing Group*, (April), 1–13. doi:10.1038/srep46548

Lewis, D. A., Cruz, D. A., Melchitzky, D. S., & Pierri, J. N. (2001). Lamina-specific deficits in parvalbumin-immunoreactive varicosities in the prefrontal cortex of subjects with schizophrenia: Evidence for fewer projections from the thalamus. *American Journal of Psychiatry*, *158*(9), 1411–1422. doi:10.1176/appi.ajp.158.9.1411

Lewis, D. A., Curley, A. A., Glausier, J. R., & Volk, D. W. (2012). Cortical parvalbumin interneurons and cognitive dysfunction in schizophrenia. *Trends in Neurosciences*, *35*(1), 57–67. doi:10.1016/j.tins.2011.10.004

Li, X., & Jope, R. S. (2010). Is glycogen synthase kinase-3 a central modulator in mood regulation? *Neuropsychopharmacology : Official Publication of the American College of Neuropsychopharmacology*, *35*(11), 2143–54. doi:10.1038/npp.2010.105

Likhtik, E., Stujenske, J. M., Topiwala, M. A., Harris, A. Z., & Gordon, J. A. (2013). Prefrontal entrainment of amygdala activity signals safety in learned fear and innate anxiety. *Nature Publishing Group*, *17*(1), 106–113. doi:10.1038/nn.3582

Lin, L., & Sibille, E. (2015). Somatostatin, neuronal vulnerability and behavioral emotionality. *Molecular Psychiatry*, *20*(3), 377–387. doi:10.1038/mp.2014.184

Lin, M. Z., & Schnitzer, M. J. (2016). Genetically encoded indicators of neuronal activity. *Nature Neuroscience*, *19*(9). doi:10.1038/nn.4359

Liston, C., Miller, M. M., Goldwater, D. S., Radley, J. J., Rocher, A. B., Hof, P. R., … McEwen, B. S. (2006). Stress-induced alterations in prefrontal cortical dendritic morphology predict selective impairments in perceptual attentional set-shifting. *The Journal of Neuroscience : The Official Journal of the Society for Neuroscience*, *26*(30), 7870–4. doi:10.1523/JNEUROSCI.1184-06.2006

Liu, R.-J., & Aghajanian, G. K. (2008). Stress blunts serotonin- and hypocretin-evoked EPSCs in prefrontal cortex: role of corticosterone-mediated apical dendritic atrophy. *Proceedings of the National Academy of Sciences of the United States of America*, *105*(1), 359–64. doi:10.1073/pnas.0706679105

Los, G. V., Encell, L. P., McDougall, M. G., Hartzell, D. D., Karassina, N., Zimprich, C., … Wood, K. V. (2008). HaloTag: A novel protein labeling technology for cell imaging and protein analysis. *ACS Chemical Biology*, *3*(6), 373–382. doi:10.1021/cb800025k

Luchkina, N. V, Huupponen, J., Clarke, V. R. J., Coleman, S. K., Keinänen, K., Taira, T., & Lauri, S. E. (2014). Developmental switch in the kinase dependency of long-term potentiation depends on expression of GluA4 subunit-containing AMPA receptors. *Proceedings of the National Academy of Sciences of the United States of America*, *111*(11), 4321–6. doi:10.1073/pnas.1315769111

Lüthi, A., & Lüscher, C. (2014). Pathological circuit function underlying addiction and anxiety disorders. *Nature Neuroscience*, *17*(12), 1635–1643. doi:10.1038/nn.3849

Ma, X. M., & Blenis, J. (2009). Molecular mechanisms of mTOR-mediated translational control. *Nature Reviews Molecular Cell Biology*, *10*(5), 307–318. doi:10.1038/nrm2672

Madroñal, N., Delgado-García, J. M., Fernández-Guizán, A., Chatterjee, J., Köhn, M., Mattucci, C., … Gruart, A. (2016). Rapid erasure of hippocampal memory following inhibition of dentate gyrus granule cells. *Nature Communications*, *7*, 10923. doi:10.1038/ncomms10923

Maeda, N. (2015). Proteoglycans and neuronal migration in the cerebral cortex during development and disease. *Frontiers in Neuroscience*, *9*(MAR), 1–15. doi:10.3389/fnins.2015.00098

Makino, H., & Li, B. (2013). Monitoring synaptic plasticity by imaging AMPA receptor content and dynamics on dendritic spines. *Methods in Molecular Biology (Clifton, N.J.)*, *1018*, 269–75. doi:10.1007/978-1-62703-444-9_25

Makino, H., & Malinow, R. (2011). Compartmentalized versus Global Synaptic Plasticity on Dendrites Controlled by Experience. *Neuron*, *72*(6), 1001–1011. doi:10.1016/j.neuron.2011.09.036

Maness, P. F., & Schachner, M. (2007). Neural recognition molecules of the immunoglobulin superfamily: signaling transducers of axon guidance and neuronal migration. *Nature Neuroscience*, *10*(1), 19–26. doi:10.1038/nn1827

Matsuzaki, M., Ellis-Davies, G. C., Nemoto, T., Miyashita, Y., Iino, M., & Kasai, H. (2001). Dendritic spine geometry is critical for AMPA receptor expression in hippocampal CA1 pyramidal neurons. *Nature Neuroscience*, *4*(11), 1086–92. doi:10.1038/nn736

McClung, C. a, Ulery, P. G., Perrotti, L. I., Zachariou, V., Berton, O., & Nestler, E. J. (2004). DeltaFosB: a molecular switch for long-term adaptation in the brain. *Brain Research. Molecular Brain Research*, *132*(2), 146–54. doi:10.1016/j.molbrainres.2004.05.014

McEwen, B. S., & Morrison, J. H. (2013). The brain on stress: vulnerability and plasticity of the prefrontal cortex over the life course. *Neuron*, *79*(1), 16–29. doi:10.1016/j.neuron.2013.06.028

McRae, P. a., & Porter, B. E. (2012). The perineuronal net component of the extracellular matrix in plasticity and epilepsy. *Neurochemistry International*, *61*(7), 963–972. doi:10.1016/j.neuint.2012.08.007

Miesenböck, G., De Angelis, D. a, & Rothman, J. E. (1998). Visualizing secretion and synaptic transmission with pH-sensitive green fluorescent proteins. *Nature*, *394*(6689), 192–5. doi:10.1038/28190

Milad, M., & Quirk, G. (2002). Neurons in medial prefrontal cortex signal memory for fear extinction. *Nature*, *420*(6911), 70–74. doi:10.1038/nature01138

Milner, B. (1963). Effects of different brain lesions on card sorting: The role of the frontal lobes. *Arch Neurol*, *9*(1), 90–100. doi:10.1001/archneur.1963.00460070100010

Minichiello, L., Korte, M., Wolfer, D., Kühn, R., Unsicker, K., Cestari, V., … Klein, R. (1999). Essential role for TrkB receptors in hippocampus-mediated learning. *Neuron*, *24*(2), 401–414. doi:10.1016/S0896-6273(00)80853-3

Morris, H. M., Hashimoto, T., & Lewis, D. A. (2008). Alterations in Somatostatin mRNA Expression in the Dorsolateral Prefrontal Cortex of Subjects with Schizophrenia or Schizoaffective Disorder. *Cerebral Cortex (New York, N.Y. : 1991)*, *18*(7), 1575–1587. doi:10.1093/cercor/bhm186

Moy, S. S., Nadler, J. J., Perez, A., Barbaro, R. P., Johns, J. M., Magnuson, T. R., … Crawley, J. N. (2004). Sociability and preference for social novelty in five inbred strains: An approach to assess autistic-like behavior in mice. *Genes, Brain and Behavior*, *3*(5), 287–302. doi:10.1111/j.1601-1848.2004.00076.x

Müller, M., Pym, E. C. G., Tong, A., & Davis, G. W. (2011). Rab3-GAP Controls the Progression of Synaptic Homeostasis at a Late Stage of Vesicle Release. *Neuron*, *69*(4), 749–762. doi:10.1016/j.neuron.2011.01.025

Murray, A. J., Woloszynowska-Fraser, M. U., Ansel-Bollepalli, L., Cole, K. L. H., Foggetti, A., Crouch, B., … Wulff, P. (2015). Parvalbumin-positive interneurons of the prefrontal cortex support working memory and cognitive flexibility. *Nature Scientific Reports*, *5*(October), 16778. doi:10.1038/srep16778

Murrough, J. W., Iacoviello, B., Neumeister, A., Charney, D. S., & Iosifescu, D. V. (2011). Cognitive dysfunction in depression: Neurocircuitry and new therapeutic strategies. *Neurobiology of Learning and Memory*, *96*(4), 553–563. doi:10.1016/j.nlm.2011.06.006

Murthy, V. N., Schikorski, T., Stevens, C. F., & Zhu, Y. (2001). Inactivity produces increases in neurotransmitter release and synapse size. *Neuron*, *32*(4), 673–682. doi:10.1016/S0896-6273(01)00500-1

Nacher, J., Guirado, R., & Castillo-Gómez, E. (2013). Structural plasticity of interneurons in the adult brain: Role of PSA-NCAM and implications for psychiatric disorders. *Neurochemical Research*, *38*(6), 1122–1133. doi:10.1007/s11064-013-0977-4

Neve, R. L., & Lim, F. (2013). Generation of high-titer defective HSV-1 vectors. *Current Protocols in Neuroscience / Editorial Board, Jacqueline N. Crawley ... [et Al.]*, *Chapter 4*, Unit 4.13. doi:10.1002/0471142301.ns0413s62

Neve, R. L., Neve, K. A., Nestler, E. J., & Carlezon, W. A. (2005). Use of herpes virus amplicon vectors to study brain disorders. *Biotechniques*, *39*(3), 2–3. doi:10.2144/05393PS01

Niederkofler, V., Asher, T. E., Okaty, B. W., Rood, B. D., Narayan, A., Hwa, L. S., … Dymecki, S. M. (2016). Identification of Serotonergic Neuronal Modules that Affect Aggressive Behavior. *Cell Reports*, *17*(8), 1934–1949. doi:10.1016/j.celrep.2016.10.063

Nieto-Gonzalez, J. L., & Jensen, K. (2013). BDNF Depresses Excitability of Parvalbumin-Positive Interneurons through an M-Like Current in Rat Dentate Gyrus. *PLoS ONE*, *8*(6). doi:10.1371/journal.pone.0067318

Opazo, P., Labrecque, S., Tigaret, C. M., Frouin, A., Wiseman, P. W., De Koninck, P., & Choquet, D. (2010). CaMKII triggers the diffusional trapping of surface AMPARs through phosphorylation of stargazin. *Neuron*, *67*(2), 239–252. doi:10.1016/j.neuron.2010.06.007

Ota, K. T., Liu, R. J., Voleti, B., Maldonado-Aviles, J. G., Duric, V., Iwata, M., … Duman, R. S. (2014). REDD1 is essential for stress-induced synaptic loss and depressive behavior. *Nat Med*, *20*(5), 531–535. doi:10.1038/nm.3513

Paratcha, G., Ledda, F., & Ibáñez, C. F. (2003). The neural cell adhesion molecule NCAM is an alternative signaling receptor for GDNF family ligands. *Cell*, *113*(7), 867–879. doi:10.1016/S0092-8674(03)00435-5

Pavitt, G. D., Ramaiah, K. V. A., Kimball, S. R., & Hinnebusch, A. G. (1998). eIF2 independently binds two distinct eIF2b subcomplexes that catalyze and regulate

guanine-nucleotide exchange. *Genes and Development*, *12*(4), 514–526. doi:10.1101/gad.12.4.514

Paxinos, G., & Franklin, K. (2012). The Mouse Brain in Stereotaxic Coordinates. *São Paulo, Academic Press*. Retrieved from https://www.elsevier.com/books/paxinos-and-franklins-the-mouse-brain-in-stereotaxic-coordinates/paxinos/978-0-12-391057-8

Peineau, S., Taghibiglou, C., Bradley, C., Wong, T. P., Liu, L., Lu, J., … Collingridge, G. L. (2007). LTP Inhibits LTD in the Hippocampus via Regulation of GSK3β. *Neuron*, *53*(5), 703–717. doi:10.1016/j.neuron.2007.01.029

Perova, Z., Delevich, K., & Li, B. (2015). Depression of Excitatory Synapses onto Parvalbumin Interneurons in the Medial Prefrontal Cortex in Susceptibility to Stress. *Journal of Neuroscience*, *35*(7), 3201–3206. doi:10.1523/JNEUROSCI.2670-14.2015

Pfeffer, C. K., Xue, M., He, M., Huang, Z. J., & Scanziani, M. (2013). Inhibition of inhibition in visual cortex: the logic of connections between molecularly distinct interneurons. *Nature Neuroscience*, *16*(8), 1068–76. doi:10.1038/nn.3446

Pi, H.-J., Hangya, B., Kvitsiani, D., Sanders, J. I., Huang, Z. J., & Kepecs, A. (2013). Cortical interneurons that specialize in disinhibitory control. *Nature*, *503*(7477), 521–4. doi:10.1038/nature12676

Piochon, C., Kano, M., & Hansel, C. (2016). LTD-like molecular pathways in developmental synaptic pruning. *Nature Neuroscience*, *19*(10), 1299–1310. doi:10.1038/nn.4389

Pizzorusso, T. (2002). Reactivation of Ocular Dominance Plasticity in the Adult Visual Cortex. *Science*, *298*(5596), 1248–1251. doi:10.1126/science.1072699

Plant, K., Pelkey, K. a, Bortolotto, Z. a, Morita, D., Terashima, A., McBain, C. J., … Isaac, J. T. R. (2006). Transient incorporation of native GluR2-lacking AMPA receptors during hippocampal long-term potentiation. *Nature Neuroscience*, *9*(5), 602–604. doi:10.1038/nn1678

Pozo, K., & Goda, Y. (2010). Unraveling mechanisms of homeostatic synaptic plasticity. *Neuron*, *66*(3), 337–51. doi:10.1016/j.neuron.2010.04.028

Queenan, B. N., Lee, K. J., & Pak, D. T. S. (2012). Wherefore Art thou, homeo(stasis)? Functional diversity in homeostatic synaptic plasticity. *Neural Plasticity*, *2012*. doi:10.1155/2012/718203

Radley, J. J., Rocher, A. B., Miller, M., Janssen, W. G. M., Liston, C., Hof, P. R., … Morrison, J. H. (2006). Repeated stress induces dendritic spine loss in the rat medial prefrontal cortex. *Cerebral Cortex (New York, N.Y. : 1991)*, *16*(3), 313–20. doi:10.1093/cercor/bhi104

Rajkowska, G., O'Dwyer, G., Teleki, Z., Stockmeier, C. A., & Miguel-Hidalgo, J. J. (2007). GABAergic neurons immunoreactive for calcium binding proteins are reduced in the prefrontal cortex in major depression. *Neuropsychopharmacology : Official Publication*

of the American College of Neuropsychopharmacology, *32*(2), 471–482. doi:10.1038/sj.npp.1301234

Ratiu, P., Talos, I.-F., Haker, S., Lieberman, D., & Everett, P. (2004). The tale of Phineas Gage, Digitally Remastered. *Journal of Neurotrauma*, *21*, 637–643. doi:10.1007/s11999-007-0109-z

Riga, D., Matos, M. R., Glas, A., Smit, A. B., Spijker, S., & Van den Oever, M. C. (2014). Optogenetic dissection of medial prefrontal cortex circuitry. *Frontiers in Systems Neuroscience*, *8*(December), 1–19. doi:10.3389/fnsys.2014.00230

Robbins, J. (2001). KCNQ potassium channels : physiology , pathophysiology , and pharmacology. *Pharmacology and Therapeutics*, *90*, 1–19.

Roth, R. H., Zhang, Y., & Huganir, R. L. (2017). Dynamic imaging of AMPA receptor trafficking in vitro and in vivo. *Current Opinion in Neurobiology*, *45*, 51–58. doi:10.1016/j.conb.2017.03.008

Rubio-Garrido, P., Pérez-De-Manzo, F., Porrero, C., Galazo, M. J., & Clascá, F. (2009). Thalamic input to distal apical dendrites in neocortical layer 1 is massive and highly convergent. *Cerebral Cortex*, *19*(10), 2380–2395. doi:10.1093/cercor/bhn259

Salas, C. E., Castro, O., Yuen, K. S. L., Radovic, D., d'Avossa, G., & Turnbull, O. H. (2016). "Just can"t hide it': A behavioral and lesion study on emotional response modulation after right prefrontal damage. *Social Cognitive and Affective Neuroscience*, *11*(10), 1528–1540. doi:10.1093/scan/nsw075

Schoenenberger, P., Schärer, Y.-P. Z., & Oertner, T. G. (2011). Channelrhodopsin as a tool to investigate synaptic transmission and plasticity. *Experimental Physiology*, *96*(1), 34–9. doi:10.1113/expphysiol.2009.051219

Senn, V., Wolff, S. B. E., Herry, C., Grenier, F., Ehrlich, I., Gr??ndemann, J., … L??thi, A. (2014). Long-range connectivity defines behavioral specificity of amygdala neurons. *Neuron*, *81*(2), 428–437. doi:10.1016/j.neuron.2013.11.006

Shansky, R. M., Hamo, C., Hof, P. R., McEwen, B. S., & Morrison, J. H. (2009). Stress-induced dendritic remodeling in the prefrontal cortex is circuit specific. *Cerebral Cortex*, *19*(10), 2479–2484. doi:10.1093/cercor/bhp003

Shepherd, J. D., Rumbaugh, G., Wu, J., Chowdhury, S., Plath, N., Kuhl, D., … Worley, P. F. (2006). Arc/Arg3.1 Mediates Homeostatic Synaptic Scaling of AMPA Receptors. *Neuron*, *52*(3), 475–484. doi:10.1016/j.neuron.2006.08.034

Shi, S., Hayashi, Y., Esteban, J. a, & Malinow, R. (2001). Subunit-specific rules governing AMPA receptor trafficking to synapses in hippocampal pyramidal neurons. *Cell*, *105*(3), 331–343. doi:10.1126/science.284.5421.1811

Silva, B. a, Mattucci, C., Krzywkowski, P., Murana, E., Illarionova, A., Grinevich, V., … Gross, C. T. (2013). Independent hypothalamic circuits for social and predator fear. *Nature Neuroscience*, (November), 1–5. doi:10.1038/nn.3573

Sotres-bayon, F., Sierra-mercado, D., Pardilla-delgado, E., & Quirk, G. (2013). Gating of fear in prelimbic cortex by hippocampal and amygdala inputs. *Neuron*, *76*(4), 804–812. doi:10.1016/j.neuron.2012.09.028.Gating

Soumier, A., & Sibille, E. (2014). Opposing effects of acute versus chronic blockade of frontal cortex somatostatin-positive inhibitory neurons on behavioral emotionality in mice. *Neuropsychopharmacology : Official Publication of the American College of Neuropsychopharmacology*, *39*(9), 2252–62. doi:10.1038/npp.2014.76

Spellman, T., Rigotti, M., Ahmari, S. E., Fusi, S., Joseph, A., & Gordon, J. a. (2015). Hippocampal-prefrontal input supports spatial encoding in working memory. *Nature*, *522*(7556), 309–314. doi:10.1038/nature14445

Stachniak, T. J., Ghosh, A., & Sternson, S. M. (2014). Chemogenetic Synaptic Silencing of Neural Circuits Localizes a Hypothalamus→Midbrain Pathway for Feeding Behavior. *Neuron*, 1–12. doi:10.1016/j.neuron.2014.04.008

Steinmetz, C. C., & Turrigiano, G. G. (2010). Tumor necrosis factor-α signaling maintains the ability of cortical synapses to express synaptic scaling. *The Journal of Neuroscience : The Official Journal of the Society for Neuroscience*, *30*(44), 14685–14690. doi:10.1523/JNEUROSCI.2210-10.2010

Stellwagen, D., & Malenka, R. C. (2006). Synaptic scaling mediated by glial TNF-alpha. *Nature*, *440*(7087), 1054–1059. doi:10.1038/nature04671

Sugino, K., Hempel, C. M., Miller, M. N., Hattox, A. M., Shapiro, P., Wu, C., … Nelson, S. B. (2006). Molecular taxonomy of major neuronal classes in the adult mouse forebrain. *Nature Neuroscience*, *9*(1), 99–107. doi:10.1038/nn1618

Sun, Q., & Turrigiano, G. G. (2011). PSD-95 and PSD-93 Play Critical But Distinct Roles in Synaptic Scaling Up and Down. *The Journal of Neuroscience : The Official Journal of the Society for Neuroscience*, *31*(18), 6800–6808. doi:10.1523/JNEUROSCI.5616-10.2011

Sutton, M. A., Taylor, A. M., Ito, H. T., Pham, A., & Schuman, E. M. (2007). Postsynaptic Decoding of Neural Activity: eEF2 as a Biochemical Sensor Coupling Miniature Synaptic Transmission to Local Protein Synthesis. *Neuron*, *55*(4), 648–661. doi:10.1016/j.neuron.2007.07.030

Szklarczyk, D., Morris, J. H., Cook, H., Kuhn, M., Wyder, S., Simonovic, M., … Mering, C. Von. (2017). The STRING database in 2017 : quality-controlled protein – protein association networks , made broadly accessible. *Nucleic Acids Research*, *45*(October 2016), 362–368. doi:10.1093/nar/gkw937

Tamura, R., Eifuku, S., Uwano, T., Sugimori, M., Uchiyama, K., & Ono, T. (2011). A method for recording evoked local field potentials in the primate dentate gyrus in vivo. *Hippocampus*, *21*(5), 565–574. doi:10.1002/hipo.20773

Taniguchi, H., Lu, J., Huang, Z. J., Markram, H., Gelman, D. M., Marín, O., … Gandhi, S. P. (2013). The spatial and temporal origin of chandelier cells in mouse neocortex. *Science (New York, N.Y.)*, *339*(6115), 70–4. doi:10.1126/science.1227622

Tanimizu, T., Kenney, J. W., Okano, E., Kadoma, K., Frankland, P. W., & Kida, S. (2017). Functional connectivity of multiple brain regions required for the consolidation of social recognition memory. *The Journal of Neuroscience*, 3451–16. doi:10.1523/JNEUROSCI.3451-16.2017

Tasic, B., Menon, V., Nguyen, T. N., Kim, T. K., Jarsky, T., Yao, Z., … Zeng, H. (2016). Adult mouse cortical cell taxonomy revealed by single cell transcriptomics. *Nature Neuroscience*, *19*(2), 335–346. doi:10.1038/nn.4216

Thiagarajan, T. C., Lindskog, M., & Tsien, R. W. (2005). Adaptation to synaptic inactivity in hippocampal neurons. *Neuron*, *47*(5), 725–737. doi:10.1016/j.neuron.2005.06.037

Thor, D. H., & Holloway, W. R. (1982). Social memory of the male laboratory rat. *Journal of Comparative and Physiological Psychology*, *96*(6), 1000–1006. doi:10.1037/0735-7036.96.6.1000

Tovote, P., Esposito, M. S., Botta, P., Chaudun, F., & Jonathan, P. (2016). Midbrain circuits for defensive behaviour. *Nature*, 1–17. doi:10.1038/nature17996

Tripp, A., Kota, R. S., Lewis, D. A., & Sibille, E. (2011). Reduced somatostatin in subgenual anterior cingulate cortex in major depression. *Neurobiology of Disease*, *42*(1), 116–124. doi:10.1016/j.nbd.2011.01.014

Tsetsenis, T., Younts, T. J., Chiu, C. Q., Kaeser, P. S., Castillo, P. E., & Südhof, T. C. (2011). Rab3B protein is required for long-term depression of hippocampal inhibitory synapses and for normal reversal learning. *Proceedings of the National Academy of Sciences of the United States of America*, *108*(34), 14300–5. doi:10.1073/pnas.1112237108

Turrigiano, G. G., & Nelson, S. B. (2000). Hebb and homeostasis in neuronal plasticity. *Current Opinion in Neurobiology*, *10*(3), 358–64. Retrieved from http://www.ncbi.nlm.nih.gov/pubmed/10851171

Tye, K. M., Prakash, R., Kim, S., Fenno, L. E., Grosenick, L., Zarabi, H., … Ramakrishnan, C. (2011). Amygdala circuitry mediating reversible and bidirectional control of anxiety. *Nature*, *471*(7338), 358–362. doi:10.1038/nature09820.Amygdala

Uylings, H. B., & van Eden, C. G. (1990). Qualitative and quantitative comparison of the prefrontal cortex in rat and in primates, including humans. *Progress in Brain Research*. doi:10.1016/S0079-6123(08)62675-8

Vertes, R. P. (2004). Differential projections of the infralimbic and prelimbic cortex in the rat. *Synapse (New York, N.Y.)*, *51*(1), 32–58. doi:10.1002/syn.10279

Vertes, R. P. (2006). Interactions among the medial prefrontal cortex, hippocampus and midline thalamus in emotional and cognitive processing in the rat. *Neuroscience*. doi:10.1016/j.neuroscience.2006.06.027

Vialou, V., Bagot, R. C., Cahill, M. E., Ferguson, D., Robison, a. J., Dietz, D. M., … Nestler, E. J. (2014). Prefrontal Cortical Circuit for Depression- and Anxiety-Related Behaviors Mediated by Cholecystokinin: Role of FosB. *Journal of Neuroscience*, *34*(11), 3878–3887. doi:10.1523/JNEUROSCI.1787-13.2014

Villa, C., & Combi, R. (2016). Potassium Channels and Human Epileptic Phenotypes: An Updated Overview. *Frontiers in Cellular Neuroscience*, *10*, 81. doi:10.3389/fncel.2016.00081

Wallis, J. D. (2012). Cross-species studies of orbitofrontal cortex and value-based decision-making. *Nature Neuroscience*, *15*(1), 13–9. doi:10.1038/nn.2956

Wang, F., Zhu, J., Zhu, H., Zhang, Q., Lin, Z., & Hu, H. (2011). Bidirectional control of social hierarchy by synaptic efficacy in medial prefrontal cortex. *Science (New York, N.Y.)*, *334*(6056), 693–7. doi:10.1126/science.1209951

Wang, J., & Li, Y. (2016). KCNQ potassium channels in sensory system and neural circuits. *Acta Pharmacologica Sinica*, *37*(1), 25–33. doi:10.1038/aps.2015.131

Warden, M. R., Selimbeyoglu, A., Mirzabekov, J. J., Lo, M., Thompson, K. R., Kim, S.-Y., … Deisseroth, K. (2012). A prefrontal cortex-brainstem neuronal projection that controls response to behavioural challenge. *Nature*, *492*(7429), 428–32. doi:10.1038/nature11617

Welsh, G. I., Miller, C. M., Loughlin, A. J., Price, N. T., & Proud, C. G. (1998). Regulation of eukaryotic initiation factor eIF2B: Glycogen synthase kinase-3 phosphorylates a conserved serine which undergoes dephosphorylation in response to insulin. *FEBS Letters*, *421*(2), 125–130. doi:10.1016/S0014-5793(97)01548-2

Wilkinson, M. B., Dias, C., Magida, J., Mazei-Robison, M., Lobo, M., Kennedy, P., … Nestler, E. J. (2011). A novel role of the WNT-dishevelled-GSK3β signaling cascade in the mouse nucleus accumbens in a social defeat model of depression. *The Journal of Neuroscience : The Official Journal of the Society for Neuroscience*, *31*(25), 9084–92. doi:10.1523/JNEUROSCI.0039-11.2011

Wise, S. P. (2008). Forward frontal fields: phylogeny and fundamental function. *Trends in Neurosciences*, *31*(12), 599–608. doi:10.1016/j.tins.2008.08.008

Wohleb, E. S., Wu, M., Gerhard, D. M., Taylor, S. R., Picciotto, M. R., Alreja, M., & Duman, R. S. (2016). GABA interneurons mediate the rapid antidepressant- like effects of scopolamine, *126*(7), 1–13. doi:10.1172/JCI85033

Xiao, Zikopoulos, B., & Barbas, H. (2010). Laminar and modular organization of prefrontal projections to multiple thalamic nuclei. *Neuroscience*, *36*(3), 490–499. doi:10.1124/dmd.107.016501

Yang, G., de Castro Reis, F., Sundukova, M., Pimpinella, S., Asaro, A., Castaldi, L., … Heppenstall, P. a. (2015). Genetic targeting of chemical indicators in vivo. *Nature Methods*, *12*(2), 137–9. doi:10.1038/nmeth.3207

Yizhar, O., Fenno, L. E., Prigge, M., Schneider, F., Davidson, T. J., O'Shea, D. J., … Deisseroth, K. (2011). Neocortical excitation/inhibition balance in information processing and social dysfunction. *Nature*, *477*(7363), 171–178. doi:10.1038/nature10360

Yuen, E. Y., Liu, W., Karatsoreos, I. N., Feng, J., Mcewen, B. S., & Yan, Z. (2009). Acute stress enhances glutamatergic transmission in prefrontal cortex and facilitates working memory, *106*(33), 14075–14079.

Yuen, E. Y., Wei, J., Liu, W., Zhong, P., Li, X., & Yan, Z. (2012). Repeated stress causes cognitive impairment by suppressing glutamate receptor expression and function in prefrontal cortex. *Neuron*, *73*(5), 962–77. doi:10.1016/j.neuron.2011.12.033

Yuste, R., & Bonhoeffer, T. (2001). Morphological changes in dendritic spines associated with long-term synaptic plasticity. *Annual Review of Neuroscience*, *24*(1862), 1071–89. doi:10.1146/annurev.neuro.24.1.1071

Zamanillo, D., Sprengel, R., Hvalby, O., Jensen, V., Burnashev, N., Rozov, A., … Sakmann, B. (1999). Importance of AMPA receptors for hippocampal synaptic plasticity but not for spatial learning. *Science*, *284*(5421), 1805–11. doi:10.1126/science.284.5421.1805

Zhang, W., Zhang, L., Liang, B., Schroeder, D., Zhang, Z.-W., Cox, G. a, … Lin, D.-T. (2016). Hyperactive somatostatin interneurons contribute to excitotoxicity in neurodegenerative disorders. *Nature Neuroscience*, *19*(4), 2–6. doi:10.1038/nn.4257

Zhang, Y., Cudmore, R. H., Lin, D.-T., Linden, D. J., & Huganir, R. L. (2015). Visualization of NMDA receptor–dependent AMPA receptor synaptic plasticity in vivo. *Nature Neuroscience*, *18*(3), 402–407. doi:10.1038/nn.3936

Zhou, P., Zhang, Y., Ma, Q., Gu, F., Day, D. S., He, A., … Pu, W. T. (2013). Interrogating translational efficiency and lineage-specific transcriptomes using ribosome affinity purification. *Proceedings of the National Academy of Sciences of the United States of America*, *110*(38), 15395–400. doi:10.1073/pnas.1304124110

Zhou, T., Zhu, H., Fan, Z., Wang, F., Chen, Y., Liang, H., … Hu, H. (2017). History of winning remodels thalamo-PFC circuit to reinforce social dominance. *Science*, *357*(6347), 162 LP – 168. Retrieved from http://science.sciencemag.org/content/357/6347/162.abstract

Zikopoulos, B., & Barbas, H. (2013). Altered neural connectivity in excitatory and inhibitory cortical circuits in autism. *Frontiers in Human Neuroscience*, *7*, 609. doi:10.3389/fnhum.2013.00609

Acknowledgements

I would like to express my most sincere gratitude to my supervisor Cornelius Gross, for being a great mentor, but also for giving me the freedom to explore many different paths while carrying this research. I would also like to thank all the members of my Thesis Advisory Committee; Paul Heppenstall, Christoph Schuster and Yannick Schwab, for carefully following my progress and always giving great advice.

This work would have not been possible without the support of all EMBL services and facilities and all the members of the lab. I want to thank, in particular, Angelo Raggioli, who made the AAVs and helped me in a part of molecular cloning, Alessandro Ciccarelli, who helped me to set up the analysis in Fiji for SNAPGluA1, Maria Esteban Masferrer, who taught me stereotactic surgeries in my first year and my students Poornemaa Natarajan and Phoebe Tate, who gave a great help for some TRAP experiments and for the Sst manipulation experiment. I am also very grateful to Andreas Buness for frequent discussion and especially for explaining how to do the statistics for the SNAPGluA1 experiment.

Finally, I want to thank for their constant support all my family and friends and in particular Filippo, who kept being present and understanding, even if far away.

Supplementary tables

	Score	Rank	Feature P	Log Fold Change	FDR (BH)	Q Value	defeated Mean	defeated Std	sensory Mean	sensory Std
Eif2b2	3.045	106	0.036	0.285	0.999	0.999	7.873	0.087	7.588	0.171

Table S1. Statistical properties of the only gene coming from the leading edge analysis of GSEA results for the *CamK2a*::TRAP experiment. *Eif2b2* is upregulated in CamK2a^{+}neurons of defeated animals and is the only gene leading GSEA results that has a p value<0.05 and a LogFC>0.27. Gene sets annotations related to this gene were GO_Methionine Metabolic process and Reactome_Translation. Score is the score in the t-test, Rank is the position in the ranking of all genes analyzed according to the score. Feature P is the p-value, while Q value is the p-value adjusted by FDR. Std=standard deviation.

NAME	SIZE	ES	NES	NOM p-val	FDR q-val	FWER p-val	RANK AT MAX	LEADING EDGE
GO SIGNALING RECEPTOR ACTIVITY	211	-0.54553	-2.01577	0	0.007	0.052	1766	tags=40%, list=23%, signal=50%
GO INTRINSIC COMPONENT OF PLASMA MEMBRANE	451	-0.53098	-2.01926	0	0.008	0.049	2065	tags=47%, list=27%, signal=61%
GO SECONDARY ACTIVE TRANSMEMBRANE TRANSPORTER ACTIVITY	66	-0.62486	-2.02091	0	0.009	0.047	1610	tags=56%, list=21%, signal=70%
GO G PROTEIN COUPLED RECEPTOR ACTIVITY	68	-0.61875	-2.02938	0	0.009	0.039	1719	tags=46%, list=22%, signal=58%
GO RECEPTOR ACTIVITY	288	-0.5287	-1.99996	0	0.009	0.078	1836	tags=41%, list=24%, signal=51%
GO PRESYNAPSE	188	-0.5541	-1.99518	0	0.009	0.087	2380	tags=54%, list=31%, signal=76%
GO REGULATION OF MEMBRANE POTENTIAL	175	-0.54791	-1.98842	0	0.010	0.108	2316	tags=53%, list=30%, signal=74%
GO EXOCYTIC VESICLE MEMBRANE	40	-0.64996	-1.99036	0	0.010	0.101	1529	tags=55%, list=20%, signal=68%
GO MODULATION OF SYNAPTIC TRANSMISSION	197	-0.53435	-1.97505	0	0.011	0.139	2378	tags=54%, list=31%, signal=76%
GO TERMINAL BOUTON	46	-0.66165	-2.03458	0	0.012	0.037	1315	tags=46%, list=17%, signal=55%
GO REGULATION OF SYNAPTIC TRANSMISSION GLUTAMATERGIC	31	-0.67627	-1.96792	0	0.012	0.153	1087	tags=39%, list=14%, signal=45%
GO NEURON PROJECTION MEMBRANE	26	-0.69052	-1.94699	0	0.013	0.233	1531	tags=62%, list=20%, signal=76%
GO EXOCYTIC VESICLE	95	-0.56878	-1.94896	0	0.013	0.224	1697	tags=47%, list=22%,

								signal=60%
KEGG NEUROACTIVE LIGAND RECEPTOR INTERACTION	60	-0.60674	-1.95061	0	0.013	0.216	1683	tags=47%, list=22%, signal=59%
GO CALCIUM ION TRANSMEMBRANE TRANSPORT	62	-0.59538	-1.9415	0	0.014	0.252	2371	tags=68%, list=30%, signal=97%
GO SYNAPSE PART	408	-0.5125	-1.93912	0	0.014	0.266	2536	tags=53%, list=33%, signal=75%
GO SYNAPSE	486	-0.50587	-1.95131	0	0.014	0.216	2536	tags=52%, list=33%, signal=73%
GO REGULATION OF CALCIUM ION DEPENDENT EXOCYTOSIS	40	-0.64383	-1.93486	0	0.014	0.277	1315	tags=52%, list=17%, signal=63%
GO AMINOGLYCAN METABOLIC PROCESS	56	-0.60399	-1.95674	0	0.014	0.19	1747	tags=52%, list=22%, signal=66%
GO CELL CELL SIGNALING	296	-0.51513	-1.95299	0	0.014	0.21	2399	tags=51%, list=31%, signal=70%
GO IONOTROPIC GLUTAMATE RECEPTOR SIGNALING PATHWAY	18	-0.7445	-1.92198	0	0.015	0.343	1535	tags=72%, list=20%, signal=90%
GO MAIN AXON	45	-0.61871	-1.92204	0	0.015	0.343	1435	tags=49%, list=18%, signal=60%
GO REGULATION OF POSTSYNAPTIC MEMBRANE POTENTIAL	32	-0.65309	-1.92476	0	0.015	0.319	1442	tags=56%, list=19%, signal=69%
GO SODIUM ION TRANSMEMBRANE TRANSPORTER ACTIVITY	51	-0.60271	-1.92281	0	0.016	0.335	1513	tags=55%, list=19%, signal=68%
GO NUCLEOBASE CONTAINING COMPOUND TRANSMEMBRANE TRANSPORTER	15	-0.76723	-1.92661	0.001292	0.016	0.312	530	tags=33%, list=7%, signal=36%

ACTIVITY								
GO METAL ION TRANSMEMBRANE TRANSPORTER ACTIVITY	168	-0.52906	-1.89636	0	0.016	0.476	1375	tags=42%, list=18%, signal=50%
GO NEUROTRANSMITTER RECEPTOR ACTIVITY	26	-0.68217	-1.90243	0	0.016	0.438	1267	tags=46%, list=16%, signal=55%
GO SYNAPTIC SIGNALING	221	-0.55176	-2.0377	0	0.016	0.034	2399	tags=56%, list=31%, signal=78%
GO AXON PART	159	-0.53027	-1.90037	0	0.016	0.449	1375	tags=35%, list=18%, signal=42%
REACTOME NEURONAL SYSTEM	174	-0.52232	-1.89388	0	0.016	0.493	2395	tags=55%, list=31%, signal=77%
REACTOME TRANSPORT OF INORGANIC CATIONS ANIONS AND AMINO ACIDS OLIGOPEPTIDES	34	-0.64039	-1.8966	0.001208	0.016	0.475	1590	tags=59%, list=20%, signal=74%
GO GLUTAMATE RECEPTOR ACTIVITY	17	-0.73742	-1.90301	0	0.016	0.434	421	tags=41%, list=5%, signal=43%
GO SYNAPTIC MEMBRANE	169	-0.51859	-1.89791	0	0.016	0.468	2024	tags=43%, list=26%, signal=56%
GO POSITIVE REGULATION OF SYNAPSE ASSEMBLY	38	-0.63498	-1.91148	0	0.016	0.396	1465	tags=39%, list=19%, signal=48%
GO DIVALENT INORGANIC CATION TRANSMEMBRANE TRANSPORTER ACTIVITY	69	-0.57795	-1.90601	0	0.016	0.425	2748	tags=75%, list=35%, signal=115%
GO POSITIVE REGULATION OF CELL CELL ADHESION	64	-0.57763	-1.88924	0	0.016	0.518	879	tags=27%, list=11%, signal=30%
REACTOME TRANSMISSION ACROSS CHEMICAL SYNAPSES	124	-0.53333	-1.89065	0	0.017	0.511	2094	tags=52%, list=27%, signal=71%
GO	29	-0.65899	-1.90319	0	0.017	0.434	1688	tags=55%,

REGULATION OF CARDIAC CONDUCTION								list=22%, signal=70%
GO REGULATION OF NEUROTRANSMITTER LEVELS	110	-0.55763	-1.90827	0	0.017	0.413	2380	tags=57%, list=31%, signal=81%
GO CALCIUM ION TRANSMEMBRANE TRANSPORTER ACTIVITY	52	-0.60755	-1.91322	0	0.017	0.391	1338	tags=50%, list=17%, signal=60%
GO AMINO ACID TRANSPORT	61	-0.58602	-1.90613	0	0.017	0.425	1774	tags=49%, list=23%, signal=63%
GO GLUTAMATE RECEPTOR SIGNALING PATHWAY	26	-0.67525	-1.8855	0	0.017	0.546	1535	tags=58%, list=20%, signal=72%
GO PRESYNAPTIC MEMBRANE	40	-0.62294	-1.88119	0	0.018	0.573	1106	tags=43%, list=14%, signal=49%
GO ACTIVE TRANSMEMBRANE TRANSPORTER ACTIVITY	123	-0.53331	-1.87989	0	0.018	0.588	1652	tags=49%, list=21%, signal=61%
GO NEURON PROJECTION TERMINUS	88	-0.60114	-2.05519	0	0.019	0.02	2563	tags=60%, list=33%, signal=89%
GO GATED CHANNEL ACTIVITY	128	-0.53218	-1.87658	0	0.019	0.614	2195	tags=55%, list=28%, signal=75%
GO PASSIVE TRANSMEMBRANE TRANSPORTER ACTIVITY	167	-0.51989	-1.86831	0	0.020	0.67	2536	tags=59%, list=33%, signal=86%
REACTOME TRIGLYCERIDE BIOSYNTHESIS	23	-0.67901	-1.86881	0.001285	0.020	0.666	1660	tags=52%, list=21%, signal=66%
GO EXTRACELLULAR GLUTAMATE GATED ION CHANNEL ACTIVITY	14	-0.76137	-1.87152	0	0.020	0.65	1535	tags=71%, list=20%, signal=89%
GO AUTOPHAGOSOME MEMBRANE	20	-0.71002	-1.86988	0	0.020	0.66	496	tags=35%, list=6%, signal=37%
GO L AMINO ACID	26	-0.66166	-1.86323	0	0.021	0.695	1513	tags=58%, list=19%,

TRANSPORT								signal=71%
GO POSTSYNAPSE	263	-0.49458	-1.85916	0	0.022	0.712	2536	tags=52%, list=33%, signal=75%
GO CATION CHANNEL COMPLEX	86	-0.54041	-1.86016	0	0.022	0.707	2195	tags=56%, list=28%, signal=77%
GO SYMPORTER ACTIVITY	36	-0.62503	-1.85658	0	0.022	0.72	1610	tags=58%, list=21%, signal=73%
GO SOLUTE CATION SYMPORTER ACTIVITY	26	-0.65956	-1.8572	0.001271	0.022	0.715	1610	tags=62%, list=21%, signal=77%
GO DIVALENT INORGANIC CATION TRANSPORT	109	-0.53409	-1.85329	0	0.022	0.743	2704	tags=66%, list=35%, signal=100 %
GO TRANSMEMBRANE TRANSPORTER ACTIVITY	385	-0.4859	-1.84659	0	0.024	0.784	1535	tags=38%, list=20%, signal=45%
GO CALCIUM ION TRANSPORT	91	-0.53957	-1.84666	0	0.025	0.783	1338	tags=42%, list=17%, signal=50%
GO REGULATION OF SYNAPSE ASSEMBLY	46	-0.58976	-1.83688	0.001198	0.025	0.842	1465	tags=37%, list=19%, signal=45%
GO NEGATIVE REGULATION OF SYNAPTIC TRANSMISSION	39	-0.61125	-1.83875	0.001209	0.025	0.829	1203	tags=41%, list=15%, signal=48%
GO REGULATION OF SYNAPTIC PLASTICITY	107	-0.53367	-1.84381	0	0.025	0.803	2557	tags=60%, list=33%, signal=88%
GO PHOSPHOLIPASE C ACTIVITY	12	-0.78586	-1.84023	0.001359	0.025	0.821	359	tags=25%, list=5%, signal=26%
GO REGULATION OF SYNAPSE STRUCTURE OR ACTIVITY	159	-0.50323	-1.83744	0	0.025	0.839	2378	tags=50%, list=31%, signal=71%
GO TRANSMITTER GATED CHANNEL ACTIVITY	16	-0.73236	-1.84134	0.001361	0.025	0.818	421	tags=44%, list=5%, signal=46%
GO ACIDIC AMINO ACID	12	-0.77434	-1.83884	0.001357	0.025	0.827	1513	tags=67%, list=19%,

TRANSPORT								signal=83%
KEGG TASTE TRANSDUCTION	11	-0.80507	-1.84151	0	0.026	0.817	651	tags=45%, list=8%, signal=50%
GO ANCHORED COMPONENT OF MEMBRANE	35	-0.62029	-1.8318	0.00365	0.026	0.865	1471	tags=46%, list=19%, signal=56%
GO EXCITATORY SYNAPSE	155	-0.51131	-1.83244	0	0.027	0.863	2536	tags=56%, list=33%, signal=82%
GO SYNAPSE ORGANIZATION	87	-0.54377	-1.8302	0	0.027	0.871	2675	tags=60%, list=34%, signal=90%
GO RESPONSE TO MECHANICAL STIMULUS	78	-0.55256	-1.82624	0	0.027	0.878	1696	tags=44%, list=22%, signal=55%
GO G PROTEIN COUPLED RECEPTOR SIGNALING PATHWAY	189	-0.50043	-1.82707	0	0.027	0.877	1820	tags=39%, list=23%, signal=50%
GO REGULATION OF CELL CELL ADHESION	109	-0.52464	-1.8246	0	0.028	0.889	879	tags=24%, list=11%, signal=27%
KEGG CALCIUM SIGNALING PATHWAY	76	-0.54041	-1.82338	0	0.028	0.898	1835	tags=41%, list=24%, signal=53%
GO CATION CHANNEL ACTIVITY	107	-0.52549	-1.82198	0	0.028	0.904	2371	tags=60%, list=30%, signal=85%
GO POSTSYNAPTIC MEMBRANE	129	-0.51345	-1.81779	0	0.028	0.919	2450	tags=47%, list=31%, signal=68%
GO NEUROTRANSMITTER TRANSPORT	89	-0.53376	-1.81908	0	0.028	0.911	2105	tags=51%, list=27%, signal=69%
GO UDP GLYCOSYLTRANSFERASE ACTIVITY	52	-0.56834	-1.81666	0	0.028	0.923	1728	tags=50%, list=22%, signal=64%
GO POSITIVE REGULATION OF SYNAPTIC TRANSMISSION	69	-0.55249	-1.81981	0	0.028	0.908	2378	tags=54%, list=31%, signal=77%
GO L ALPHA AMINO ACID TRANSMEMBRANE TRANSPORT	14	-0.73268	-1.81788	0.001337	0.029	0.919	1774	tags=71%, list=23%, signal=92%
GO AMINO ACID TRANSMEMBRA	30	-0.63083	-1.81278	0	0.030	0.932	1774	tags=67%, list=23%,

NE TRANSPORTER ACTIVITY								signal=86%
GO REGULATION OF HOMOTYPIC CELL CELL ADHESION	84	-0.5361	-1.81054	0	0.031	0.934	876	tags=26%, list=11%, signal=29%
GO PLASMA MEMBRANE REGION	398	-0.47302	-1.80575	0	0.031	0.943	2027	tags=40%, list=26%, signal=51%
REACTOME PEPTIDE LIGAND BINDING RECEPTORS	18	-0.68648	-1.80932	0.001279	0.031	0.937	29	tags=17%, list=0%, signal=17%
GO REGULATION OF AMINE TRANSPORT	33	-0.61832	-1.8061	0	0.031	0.943	1004	tags=36%, list=13%, signal=42%
GO ION TRANSMEMBRANE TRANSPORT	333	-0.47837	-1.8064	0	0.031	0.941	2195	tags=49%, list=28%, signal=66%
GO REGULATION OF ION TRANSPORT	273	-0.4809	-1.79876	0	0.031	0.959	2272	tags=48%, list=29%, signal=65%
GO VOLTAGE GATED CATION CHANNEL ACTIVITY	60	-0.55409	-1.80367	0	0.031	0.949	2195	tags=60%, list=28%, signal=83%
GO REGULATION OF SENSORY PERCEPTION OF PAIN	15	-0.70988	-1.79702	0.00133	0.031	0.961	824	tags=33%, list=11%, signal=37%
GO ADENYLATE CYCLASE MODULATING G PROTEIN COUPLED RECEPTOR SIGNALING PATHWAY	41	-0.58677	-1.80644	0.001196	0.032	0.941	1683	tags=49%, list=22%, signal=62%
KEGG CELL ADHESION MOLECULES CAMS	34	-0.61456	-1.79778	0	0.032	0.959	1766	tags=50%, list=23%, signal=64%
GO SODIUM ION TRANSMEMBRANE TRANSPORT	38	-0.59761	-1.79879	0	0.032	0.959	1466	tags=53%, list=19%, signal=65%
GO AXON	292	-0.47816	-1.80053	0	0.032	0.956	2399	tags=50%, list=31%, signal=70%

GO METAL ION TRANSPORT	246	-0.48308	-1.80244	0	0.032	0.951	2195	tags=50%, list=28%, signal=67%
REACTOME NEUROTRANSMITTER RELEASE CYCLE	24	-0.6451	-1.80155	0.0025	0.032	0.951	1697	tags=67%, list=22%, signal=85%
GO PRESYNAPTIC PROCESS INVOLVED IN SYNAPTIC TRANSMISSION	71	-0.54647	-1.79911	0	0.032	0.959	2380	tags=58%, list=31%, signal=82%
GO CELL SURFACE RECEPTOR SIGNALING PATHWAY INVOLVED IN CELL CELL SIGNALING	31	-0.61744	-1.80065	0	0.032	0.956	1353	tags=45%, list=17%, signal=54%
GO ACID SECRETION	30	-0.6187	-1.79922	0	0.032	0.958	1697	tags=50%, list=22%, signal=64%
GO REGULATION OF AMINO ACID TRANSPORT	13	-0.75174	-1.79428	0.00428	0.032	0.965	1003	tags=54%, list=13%, signal=62%
GO POSITIVE REGULATION OF CALCIUM ION DEPENDENT EXOCYTOSIS	12	-0.76734	-1.79095	0.00146	0.033	0.971	1013	tags=67%, list=13%, signal=77%
REACTOME CLASS A1 RHODOPSIN LIKE RECEPTORS	34	-0.60388	-1.79439	0	0.033	0.965	1683	tags=38%, list=22%, signal=49%
GO AMINOGLYCAN BIOSYNTHETIC PROCESS	39	-0.58201	-1.79133	0.001217	0.033	0.97	1694	tags=49%, list=22%, signal=62%
GO CELL CELL ADHESION VIA PLASMA MEMBRANE ADHESION MOLECULES	55	-0.55303	-1.79175	0	0.033	0.969	1788	tags=40%, list=23%, signal=52%
GO SIGNAL TRANSDUCER ACTIVITY	386	-0.46314	-1.79223	0	0.033	0.968	1871	tags=35%, list=24%, signal=44%
GO POSITIVE REGULATION OF LYMPHOCYTE	16	-0.70555	-1.78818	0.001299	0.034	0.975	163	tags=25%, list=2%, signal=25%

DIFFERENTIATION								
GO LEADING EDGE MEMBRANE	79	-0.53662	-1.78657	0	0.034	0.976	1693	tags=42%, list=22%, signal=53%
GO LEARNING	80	-0.5284	-1.78698	0	0.034	0.976	2378	tags=52%, list=31%, signal=75%
GO LIGAND GATED CHANNEL ACTIVITY	54	-0.56189	-1.78521	0	0.034	0.979	2513	tags=63%, list=32%, signal=92%
REACTOME TRAFFICKING OF AMPA RECEPTORS	25	-0.63911	-1.78226	0.002591	0.035	0.98	2372	tags=76%, list=30%, signal=109%
REACTOME AMINO ACID AND OLIGOPEPTIDE SLC TRANSPORTERS	16	-0.69153	-1.7826	0.001333	0.035	0.98	1590	tags=69%, list=20%, signal=86%
GO SODIUM ION TRANSPORT	53	-0.55789	-1.78123	0.001195	0.035	0.98	1590	tags=51%, list=20%, signal=64%
REACTOME ION TRANSPORT BY P TYPE ATPASES	14	-0.73792	-1.77977	0	0.036	0.981	1186	tags=71%, list=15%, signal=84%
BIOCARTA NOS1 PATHWAY	16	-0.69298	-1.77822	0.001326	0.036	0.983	1297	tags=50%, list=17%, signal=60%
GO REGULATION OF BLOOD CIRCULATION	115	-0.50452	-1.77668	0	0.036	0.986	2153	tags=50%, list=28%, signal=69%
GO COGNITION	146	-0.49388	-1.77704	0	0.036	0.985	2378	tags=51%, list=31%, signal=72%
REACTOME TRAFFICKING OF GLUR2 CONTAINING AMPA RECEPTORS	15	-0.70699	-1.77464	0	0.037	0.988	2094	tags=80%, list=27%, signal=109%
GO SIGNAL RELEASE	92	-0.51393	-1.77278	0	0.038	0.989	2423	tags=52%, list=31%, signal=75%
GO ANION TRANSMEMBRANE TRANSPORTER ACTIVITY	93	-0.51901	-1.76707	0	0.039	0.993	1625	tags=44%, list=21%, signal=55%
GO	19	-0.66616	-1.77003	0.0052	0.039	0.992	1819	tags=63%,

PHOSPHOLIPASE C ACTIVATING G PROTEIN COUPLED RECEPTOR SIGNALING PATHWAY				08				list=23%, signal=82%
GO REGULATION OF SENSORY PERCEPTION	15	-0.70988	-1.76815	0.001377	0.039	0.993	824	tags=33%, list=11%, signal=37%
GO ANTIPORTER ACTIVITY	26	-0.63676	-1.76857	0.001209	0.039	0.993	1508	tags=58%, list=19%, signal=71%
GO FEEDING BEHAVIOR	26	-0.62751	-1.76727	0	0.039	0.993	135	tags=15%, list=2%, signal=16%
GO ANION TRANSPORT	182	-0.48668	-1.76891	0	0.039	0.993	2057	tags=45%, list=26%, signal=60%
REACTOME INTERACTION BETWEEN L1 AND ANKYRINS	15	-0.70333	-1.76481	0.001357	0.040	0.995	2027	tags=73%, list=26%, signal=99%
GO LIPID TRANSPORTER ACTIVITY	37	-0.5841	-1.76252	0.001199	0.040	0.995	2230	tags=62%, list=29%, signal=87%
GO NEUROMUSCULAR JUNCTION DEVELOPMENT	21	-0.65832	-1.76278	0.001264	0.041	0.995	1992	tags=57%, list=26%, signal=77%
GO EXCITATORY POSTSYNAPTIC POTENTIAL	18	-0.67821	-1.76004	0.003937	0.042	0.996	1353	tags=61%, list=17%, signal=74%
GO NEUTRAL LIPID BIOSYNTHETIC PROCESS	12	-0.73467	-1.75478	0.001387	0.044	0.997	1095	tags=42%, list=14%, signal=48%
GO G PROTEIN COUPLED RECEPTOR SIGNALING PATHWAY COUPLED TO CYCLIC NUCLEOTIDE SECOND MESSENGER	45	-0.57581	-1.75244	0	0.045	0.998	1683	tags=47%, list=22%, signal=59%
GO PHOSPHATE TRANSMEMBRANE TRANSPORTER ACTIVITY	15	-0.70627	-1.75394	0.0014	0.045	0.998	770	tags=40%, list=10%, signal=44%

REACTOME PLATELET HOMEOSTASIS	40	-0.58398	-1.75162	0.001242	0.045	0.998	1335	tags=38%, list=17%, signal=45%
REACTOME PKA MEDIATED PHOSPHORYLATION OF CREB	12	-0.74903	-1.75267	0	0.045	0.998	943	tags=58%, list=12%, signal=66%
GO L AMINO ACID TRANSMEMBRANE TRANSPORTER ACTIVITY	22	-0.63983	-1.75298	0.003745	0.045	0.998	1774	tags=64%, list=23%, signal=82%
GO TRANSPORTER COMPLEX	157	-0.48649	-1.74752	0	0.045	0.998	2195	tags=49%, list=28%, signal=67%
GO DENDRITE MEMBRANE	12	-0.73303	-1.74937	0.004016	0.045	0.998	1531	tags=67%, list=20%, signal=83%
GO ROUGH ENDOPLASMIC RETICULUM	39	-0.56946	-1.74832	0.003695	0.045	0.998	1504	tags=38%, list=19%, signal=47%
GO INORGANIC ION TRANSMEMBRANE TRANSPORT	236	-0.47212	-1.7476	0	0.045	0.998	2195	tags=50%, list=28%, signal=68%
GO TRANSMEMBRANE TRANSPORT	443	-0.45964	-1.74947	0	0.045	0.998	2195	tags=47%, list=28%, signal=62%
GO EXCITATORY EXTRACELLULAR LIGAND GATED ION CHANNEL ACTIVITY	19	-0.6648	-1.74832	0.009186	0.045	0.998	1535	tags=53%, list=20%, signal=65%
GO MUCOPOLYSACCHARIDE METABOLIC PROCESS	38	-0.58064	-1.74951	0	0.046	0.998	1694	tags=50%, list=22%, signal=64%
REACTOME GLYCOSAMINOGLYCAN METABOLISM	39	-0.57966	-1.74439	0	0.047	1	1497	tags=44%, list=19%, signal=54%
GO CELL BODY	301	-0.46358	-1.74004	0	0.048	1	2103	tags=46%, list=27%, signal=60%
REACTOME GPCR LIGAND BINDING	54	-0.55282	-1.74204	0.001176	0.048	1	1683	tags=35%, list=22%, signal=45%
GO MECHANORECE	18	-0.67699	-1.74131	0.001289	0.048	1	910	tags=33%, list=12%,

PTOR DIFFERENTIATION								signal=38%
GO ACTION POTENTIAL	50	-0.55864	-1.74007	0.001198	0.048	1	2261	tags=52%, list=29%, signal=73%
GO DICARBOXYLIC ACID TRANSPORT	33	-0.59153	-1.7406	0.004975	0.048	1	1697	tags=45%, list=22%, signal=58%
GO HOMOPHILIC CELL ADHESION VIA PLASMA MEMBRANE ADHESION MOLECULES	42	-0.56105	-1.73118	0.002356	0.049	1	1788	tags=40%, list=23%, signal=52%
GO ADENYLATE CYCLASE INHIBITING G PROTEIN COUPLED RECEPTOR SIGNALING PATHWAY	24	-0.62994	-1.7376	0.005038	0.049	1	1331	tags=42%, list=17%, signal=50%
REACTOME PHOSPHOLIPID METABOLISM	103	-0.5015	-1.73552	0	0.049	1	2171	tags=48%, list=28%, signal=65%
GO ORGANIC ACID TRANSPORT	99	-0.50518	-1.73127	0	0.049	1	2105	tags=45%, list=27%, signal=62%
GO INORGANIC ANION TRANSPORT	37	-0.57901	-1.73795	0.00237	0.049	1	1399	tags=46%, list=18%, signal=56%
GO REGULATION OF SYNAPTIC VESICLE TRANSPORT	25	-0.62236	-1.73005	0.005096	0.049	1	2316	tags=76%, list=30%, signal=108%
GO PHOSPHORIC DIESTER HYDROLASE ACTIVITY	35	-0.58494	-1.73157	0.001227	0.049	1	1274	tags=31%, list=16%, signal=37%
GO COLUMNAR CUBOIDAL EPITHELIAL CELL DEVELOPMENT	20	-0.6497	-1.73608	0.001277	0.049	1	884	tags=30%, list=11%, signal=34%
GO SECRETORY VESICLE	192	-0.4728	-1.73563	0	0.049	1	2119	tags=43%, list=27%, signal=57%
GO ORGANIC ANION TRANSPORT	141	-0.48553	-1.72805	0	0.049	1	2057	tags=45%, list=26%, signal=60%

GO CAMP METABOLIC PROCESS	14	-0.70265	-1.73627	0.004065	0.049	1	1178	tags=50%, list=15%, signal=59%
GO TRANSMISSION OF NERVE IMPULSE	27	-0.62401	-1.73158	0.002535	0.049	1	2195	tags=67%, list=28%, signal=93%
GO CATION TRANSMEMBRANE TRANSPORTER ACTIVITY	242	-0.46655	-1.7339	0	0.049	1	2298	tags=51%, list=30%, signal=70%
GO SOMATODENDRITIC COMPARTMENT	429	-0.45126	-1.72813	0	0.049	1	2115	tags=43%, list=27%, signal=56%
GO PLASMA MEMBRANE PROTEIN COMPLEX	208	-0.47004	-1.72871	0	0.049	1	2195	tags=43%, list=28%, signal=59%
KEGG LYSOSOME	70	-0.5283	-1.73179	0	0.049	1	1927	tags=49%, list=25%, signal=64%
GO LONG TERM SYNAPTIC DEPRESSION	11	-0.75048	-1.73208	0	0.050	1	1042	tags=64%, list=13%, signal=73%

Table S2 *(pages 116-128)*. List of gene sets significantly downregulated (FDR<0.05) in Pvalb^{+}neurons of defeated animals. Gene sets are ordered by FDR. Size indicates the number of genes in the gene set after filtering out those not present in the dataset. ES is the enrichment score: the degree to which the gene set is overrepresented at the top or bottom of the ranked list of genes in the expression dataset. NES is the normalized enrichment score, that is, the enrichment score for the gene set after it has been normalized across analyzed gene sets. Rank at max is the position in the ranked list at which the maximum enrichment score occurred (genes are ranked according to the t-test score). In the leading edge column: "tags" is the percentage of genes of the gene set contributing to the enrichment score; "list" is the percentage of genes in the ranked gene list before (for positive ES, like in *Sst*::TRAP experiment) or after (for negative ES, like in this case) the peak in the running enrichment score (this gives an indication of where in the list the enrichment score is attained); "signal" is the enrichment signal strength and results from a combination of the previous two statistics (the higher the better).

Name	Score	Rank	Feature P	Log Fold Change	FDR (BH)	Q Value	defeated Mean	defeated Std	sensory Mean	sensory Std
Abca3	-3.763	644	0.035	0.379	0.591	0.356	6.366	0.153	6.744	0.069
Abcg4	-3.527	764	0.046	0.355	0.591	0.356	8.481	0.124	8.836	0.101
Acadm	-11.947	18	0.002	0.343	0.591	0.356	7.721	0.045	8.064	0.018
Adam9	-3.549	750	0.038	0.283	0.591	0.356	7.305	0.114	7.589	0.064
Adcy5	-3.787	628	0.039	0.355	0.591	0.356	6.387	0.148	6.742	0.055
Agpat3	-24.701	4	0.001	0.276	0.591	0.356	7.327	0.019	7.603	0.003
Ank	-3.814	617	0.045	0.389	0.591	0.356	9.138	0.167	9.527	0.047
Arf3	-6.617	142	0.022	0.529	0.591	0.356	7.946	0.139	8.475	0.002
Arhgap44	-5.462	227	0.032	0.292	0.591	0.356	10.013	0.093	10.305	0.002
Arhgef18	-5.914	189	0.011	0.294	0.591	0.356	6.654	0.076	6.948	0.034
Arl6ip1	-5.293	243	0.014	0.368	0.591	0.356	10.278	0.103	10.647	0.051
Asah2	-4.470	411	0.024	0.325	0.591	0.356	7.523	0.112	7.848	0.048
Atcay	-4.588	386	0.027	0.432	0.591	0.356	8.892	0.151	9.324	0.050
Atg9a	-8.257	73	0.005	0.333	0.591	0.356	7.732	0.063	8.065	0.025
Atp1a1	-6.621	141	0.022	0.679	0.591	0.356	8.649	0.177	9.328	0.009
Atp2b1	-3.780	634	0.046	0.294	0.591	0.356	9.626	0.089	9.920	0.083
Atp2b2	-4.071	534	0.034	0.366	0.591	0.356	8.827	0.143	9.193	0.050
Atp2b4	-6.379	157	0.022	0.426	0.591	0.356	6.242	0.115	6.668	0.012
Atp2c1	-5.649	210	0.011	0.271	0.591	0.356	8.270	0.069	8.541	0.037
Atp6ap1	-4.456	416	0.029	0.354	0.591	0.356	9.256	0.127	9.609	0.042
Atp6v0a1	-3.720	670	0.041	0.319	0.591	0.356	9.442	0.105	9.760	0.086
Atp6v0e2	-3.853	607	0.039	0.665	0.591	0.356	10.159	0.274	10.824	0.097
Atp8b2	-5.623	214	0.014	0.489	0.591	0.356	5.987	0.109	6.476	0.085
Atp9a	-5.174	268	0.026	0.284	0.591	0.356	7.878	0.091	8.162	0.022
Bad	-5.998	184	0.010	0.300	0.591	0.356	7.500	0.068	7.801	0.044
Bai1	-5.229	258	0.029	0.653	0.591	0.356	6.870	0.212	7.524	0.035
Bsn	-3.421	815	0.045	0.436	0.591	0.356	6.969	0.193	7.405	0.088
Cacna1b	-4.060	539	0.028	0.395	0.591	0.356	6.610	0.130	7.005	0.088
Cacna1e	-4.195	496	0.042	0.679	0.591	0.356	6.634	0.271	7.314	0.057
Cadm	-5.155	272	0.016	0.437	0.591	0.356	9.786	0.130	10.223	0.056

3										
Caly	-5.855	194	0.010	0.532	0.591	0.356	8.943	0.127	9.475	0.075
Cckbr	-12.141	16	0.001	0.367	0.591	0.356	6.263	0.040	6.630	0.028
Cdk5	-3.285	875	0.047	0.453	0.591	0.356	9.324	0.204	9.777	0.102
Cdk5r2	-13.280	12	0.002	0.294	0.591	0.356	8.885	0.027	9.179	0.023
Celf4	-3.999	558	0.030	0.388	0.591	0.356	8.896	0.128	9.284	0.089
Chpf	-3.631	713	0.045	0.349	0.591	0.356	6.913	0.154	7.262	0.052
Chrm1	-8.435	66	0.041	0.641	0.591	0.356	7.073	0.049	7.714	0.100
Clptm1	-7.510	95	0.026	0.503	0.591	0.356	10.103	0.059	10.606	0.081
Clstn1	-4.857	321	0.022	0.384	0.591	0.356	10.215	0.125	10.599	0.045
Cltb	-4.410	436	0.041	0.324	0.591	0.356	9.732	0.124	10.056	0.022
Cntn1	-4.664	369	0.033	0.313	0.591	0.356	10.007	0.074	10.320	0.073
Cntnap1	-7.069	114	0.016	0.391	0.591	0.356	8.517	0.058	8.908	0.062
Cntnap2	-3.789	626	0.040	0.354	0.591	0.356	9.311	0.114	9.665	0.094
Cpt1c	-3.653	703	0.036	0.325	0.591	0.356	7.763	0.129	8.088	0.069
Crtc1	-4.188	498	0.025	0.285	0.591	0.356	8.238	0.098	8.522	0.053
Cry2	-3.541	752	0.048	0.336	0.591	0.356	8.234	0.151	8.569	0.052
Cx3cl1	-12.762	14	0.002	0.520	0.591	0.356	9.252	0.066	9.772	0.020
Dgcr2	-6.063	180	0.009	0.325	0.591	0.356	6.191	0.079	6.517	0.039
Dgkg	-6.791	132	0.025	0.292	0.591	0.356	7.919	0.041	8.210	0.051
Dgkz	-7.479	96	0.007	0.388	0.591	0.356	8.436	0.081	8.824	0.032
Dlgap3	-5.874	193	0.012	0.539	0.591	0.356	7.121	0.117	7.659	0.088
Dnlz	-3.901	586	0.047	0.318	0.591	0.356	8.201	0.135	8.518	0.032
Dpp6	-4.414	433	0.038	0.284	0.591	0.356	8.090	0.108	8.374	0.023
Dpysl5	-3.226	904	0.049	0.367	0.591	0.356	6.933	0.157	7.300	0.098
Efnb2	-9.653	45	0.005	0.898	0.591	0.356	6.078	0.150	6.975	0.048
Efnb3	-4.716	358	0.019	0.469	0.591	0.356	6.292	0.148	6.761	0.072
Elovl5	-8.123	79	0.004	0.404	0.591	0.356	7.858	0.068	8.262	0.043
Ept1	-4.426	427	0.032	0.339	0.591	0.356	8.594	0.125	8.933	0.037
Ext2	-8.206	75	0.008	0.470	0.591	0.356	6.427	0.094	6.896	0.025
Fscn1	-3.572	743	0.039	0.480	0.591	0.356	7.243	0.200	7.723	0.096
Gaa	-4.498	407	0.031	0.398	0.591	0.356	8.918	0.144	9.315	0.042
Gabbr2	-5.252	256	0.018	0.285	0.591	0.356	9.951	0.066	10.235	0.055
Galntl1	-7.125	112	0.006	0.498	0.591	0.356	6.930	0.093	7.428	0.063
Gnb1	-4.768	341	0.019	0.276	0.591	0.356	10.691	0.087	10.967	0.041
Gns	-4.291	466	0.033	0.397	0.591	0.356	8.470	0.150	8.866	0.046
Gprc5b	-4.449	422	0.026	0.446	0.591	0.356	8.269	0.157	8.715	0.060

Grik3	-11.157	27	0.002	0.560	0.591	0.356	7.659	0.071	8.219	0.041
Grin2b	-4.296	465	0.045	0.419	0.591	0.356	6.752	0.102	7.171	0.110
Hgsnat	-10.404	36	0.006	0.321	0.591	0.356	7.917	0.052	8.238	0.011
Hs6st1	-6.568	144	0.022	0.674	0.591	0.356	7.035	0.177	7.709	0.010
Htr2a	-3.899	587	0.033	0.392	0.591	0.356	9.000	0.154	9.392	0.067
Igsf9b	-4.410	437	0.048	0.407	0.591	0.356	6.270	0.160	6.676	0.002
Kcnb1	-6.336	161	0.024	0.330	0.591	0.356	6.676	0.090	7.006	0.002
Kcnh5	-3.515	766	0.044	0.405	0.591	0.356	6.985	0.178	7.391	0.074
Kcnq2	-28.887	2	0.001	0.349	0.591	0.356	7.323	0.013	7.673	0.013
Kcnq3	-7.142	111	0.016	0.581	0.591	0.356	8.046	0.138	8.628	0.022
Kctd16	-7.308	103	0.012	0.734	0.591	0.356	6.932	0.168	7.667	0.038
Klhl24	-6.852	126	0.035	0.307	0.591	0.356	8.517	0.037	8.825	0.056
Kndc1	-5.167	270	0.015	0.275	0.591	0.356	7.199	0.079	7.474	0.040
Large	-4.458	414	0.021	0.350	0.591	0.356	7.971	0.108	8.322	0.068
Lgi3	-5.725	204	0.012	0.374	0.591	0.356	8.923	0.099	9.298	0.045
Map1lc3a	-4.660	371	0.023	0.380	0.591	0.356	7.360	0.128	7.740	0.049
Mapk8ip2	-3.958	571	0.039	0.395	0.591	0.356	8.299	0.118	8.694	0.103
Mboat7	-5.177	267	0.014	0.418	0.591	0.356	7.252	0.117	7.669	0.062
Mcoln1	-3.593	732	0.048	0.317	0.591	0.356	8.239	0.142	8.556	0.046
Mgat5b	-8.029	82	0.012	0.346	0.591	0.356	6.966	0.073	7.312	0.011
Mgll	-3.574	741	0.038	0.601	0.591	0.356	6.835	0.246	7.436	0.127
Naga	-9.082	52	0.003	0.320	0.591	0.356	6.621	0.046	6.941	0.033
Nalcn	-4.853	322	0.026	0.288	0.591	0.356	7.044	0.097	7.332	0.029
Ntrk2	-20.000	8	0.000	0.280	0.591	0.356	9.392	0.021	9.672	0.010
Nxph3	-3.676	695	0.039	0.317	0.591	0.356	6.296	0.133	6.613	0.055
Opcml	-8.331	69	0.004	0.362	0.591	0.356	8.372	0.062	8.734	0.035
Oprd1	-10.228	39	0.016	0.443	0.591	0.356	7.319	0.038	7.762	0.053
Osbp2	-6.692	139	0.016	0.295	0.591	0.356	7.839	0.074	8.133	0.015
Oxsr1	-3.763	643	0.034	0.365	0.591	0.356	6.216	0.130	6.581	0.086
Pak2	-5.005	295	0.023	0.300	0.591	0.356	7.396	0.097	7.696	0.030
Pcdh9	-6.721	137	0.019	0.326	0.591	0.356	7.822	0.083	8.149	0.010
Pde2a	-5.780	200	0.013	0.476	0.591	0.356	8.199	0.128	8.676	0.052
Pde4a	-3.578	740	0.038	0.426	0.591	0.356	7.654	0.175	8.080	0.089
Pip5k1a	-5.273	249	0.027	0.283	0.591	0.356	7.642	0.091	7.925	0.017
Pitpnm1	-3.793	624	0.034	0.504	0.591	0.356	7.332	0.198	7.836	0.096
Ppap2b	-4.155	504	0.042	0.465	0.591	0.356	6.863	0.187	7.328	0.042
Ppp2r5b	-11.040	31	0.005	0.543	0.591	0.356	8.562	0.083	9.105	0.017

Ppp2r5d	-3.480	790	0.042	0.322	0.591	0.356	9.328	0.122	9.649	0.085
Prkar1a	-3.740	656	0.036	0.347	0.591	0.356	8.792	0.121	9.138	0.086
Prr5	-4.833	326	0.019	0.318	0.591	0.356	6.192	0.101	6.510	0.043
Psd	-3.657	699	0.037	0.548	0.591	0.356	6.728	0.223	7.276	0.108
Psd3	-4.266	470	0.026	0.283	0.591	0.356	6.531	0.087	6.814	0.062
Psen1	-4.413	435	0.029	0.581	0.591	0.356	7.225	0.211	7.806	0.070
Ptk2b	-5.151	273	0.036	0.418	0.591	0.356	7.811	0.141	8.229	0.003
Ptpn5	-9.131	50	0.005	0.388	0.591	0.356	7.433	0.069	7.821	0.021
Ptprn	-7.219	106	0.011	0.372	0.591	0.356	8.826	0.059	9.198	0.054
Ptprn2	-7.375	101	0.008	0.507	0.591	0.356	8.922	0.109	9.429	0.040
Ptprs	-3.826	613	0.031	0.415	0.591	0.356	7.915	0.152	8.330	0.090
Rab3a	-3.758	648	0.041	0.393	0.591	0.356	11.435	0.166	11.828	0.059
Rab3gap1	-7.322	102	0.017	0.282	0.591	0.356	7.710	0.066	7.992	0.006
Rasgrp1	-10.150	40	0.010	0.281	0.591	0.356	9.362	0.027	9.643	0.032
Rnf40	-4.775	337	0.017	0.441	0.591	0.356	6.623	0.132	7.064	0.074
Sarm1	-4.449	421	0.026	0.356	0.591	0.356	6.323	0.125	6.679	0.049
Scamp5	-3.835	610	0.047	0.702	0.591	0.356	10.108	0.303	10.810	0.077
Sdc3	-4.447	423	0.034	0.379	0.591	0.356	7.836	0.141	8.215	0.036
Sec61a1	-5.273	250	0.026	0.477	0.591	0.356	7.081	0.152	7.558	0.033
Sfxn3	-5.783	199	0.028	0.480	0.591	0.356	8.568	0.143	9.048	0.010
Sgcb	-8.646	60	0.006	0.326	0.591	0.356	7.418	0.061	7.744	0.019
Sidt2	-16.201	11	0.001	0.300	0.591	0.356	7.393	0.025	7.693	0.016
Slc12a5	-4.618	381	0.031	0.474	0.591	0.356	8.184	0.169	8.657	0.044
Slc24a2	-3.994	561	0.034	0.326	0.591	0.356	9.764	0.101	10.090	0.081
Slc25a1	-5.511	224	0.024	0.280	0.591	0.356	8.101	0.085	8.382	0.018
Slc25a36	-9.450	48	0.003	0.490	0.591	0.356	6.585	0.074	7.075	0.042
Slc29a2	-4.875	317	0.018	0.347	0.591	0.356	6.808	0.092	7.154	0.066
Slc30a4	-5.272	251	0.014	0.402	0.591	0.356	6.779	0.104	7.181	0.066
Slc32a1	-4.377	445	0.025	0.703	0.591	0.356	7.199	0.246	7.902	0.106
Slc35a4	-9.547	47	0.007	0.307	0.591	0.356	7.788	0.035	8.095	0.035
Slc35a5	-4.261	472	0.042	0.349	0.591	0.356	6.273	0.138	6.622	0.028
Slc35e1	-10.718	33	0.002	0.419	0.591	0.356	7.949	0.055	8.368	0.033
Slc35e3	-4.752	346	0.020	0.320	0.591	0.356	7.710	0.102	8.031	0.046

Slc3a2	-4.383	443	0.041	0.343	0.591	0.356	7.433	0.132	7.776	0.024
Slc41a1	-4.128	511	0.036	0.434	0.591	0.356	6.880	0.124	7.314	0.109
Slc45a1	-5.981	185	0.016	0.655	0.591	0.356	7.220	0.178	7.875	0.053
Slc45a4	-4.736	353	0.040	0.344	0.591	0.356	6.757	0.074	7.102	0.083
Slc4a3	-4.895	314	0.023	0.423	0.591	0.356	7.702	0.138	8.125	0.047
Slc6a1	-4.300	464	0.023	0.791	0.591	0.356	10.133	0.253	10.924	0.159
Slc7a14	-4.084	529	0.045	0.376	0.591	0.356	9.116	0.100	9.492	0.101
Slc9a1	-5.088	281	0.030	0.563	0.591	0.356	7.052	0.187	7.615	0.034
Sorl1	-11.124	28	0.002	0.302	0.591	0.356	7.695	0.039	7.996	0.022
Spock3	-4.865	318	0.019	0.313	0.591	0.356	9.133	0.099	9.445	0.042
Stat5b	-5.600	219	0.016	0.334	0.591	0.356	6.475	0.095	6.809	0.034
Stx16	-10.585	35	0.002	0.576	0.591	0.356	7.567	0.084	8.144	0.035
Sv2a	-5.195	264	0.035	0.573	0.591	0.356	9.979	0.191	10.552	0.003
Svop	-4.630	378	0.019	0.469	0.591	0.356	6.148	0.146	6.617	0.080
Syp	-8.533	64	0.004	0.530	0.591	0.356	10.476	0.095	11.006	0.042
Tbc1d24	-11.721	21	0.004	0.351	0.591	0.356	7.368	0.033	7.719	0.032
Tcap	-4.457	415	0.021	0.448	0.591	0.356	8.211	0.146	8.659	0.077
Tmed4	-5.289	244	0.014	0.320	0.591	0.356	8.740	0.089	9.060	0.045
Tmem130	-6.146	175	0.011	0.429	0.591	0.356	9.436	0.087	9.865	0.068
Tmem63c	-4.547	394	0.026	0.345	0.591	0.356	6.730	0.092	7.075	0.077
Tpp1	-6.932	123	0.008	0.377	0.591	0.356	8.342	0.084	8.718	0.035
Tram1	-3.638	709	0.039	0.398	0.591	0.356	8.013	0.167	8.411	0.073
Ttyh3	-4.065	536	0.031	0.490	0.591	0.356	9.572	0.187	10.062	0.075
Ulk1	-4.704	363	0.042	0.412	0.591	0.356	8.294	0.152	8.706	0.002
Wbscr17	-6.367	158	0.012	0.377	0.591	0.356	6.793	0.070	7.170	0.061

Table S3 ***(pages 129-133)*** **. Statistical properties of genes leading the enrichment of downregulated gene sets in Pvalb^{+} neurons of defeated animals.** Only genes with $p<0.05$ and LogFC>0.27 were considered and are listed. Genes are listed in alphabetical order. See caption of Table S1 for the meaning of each column.

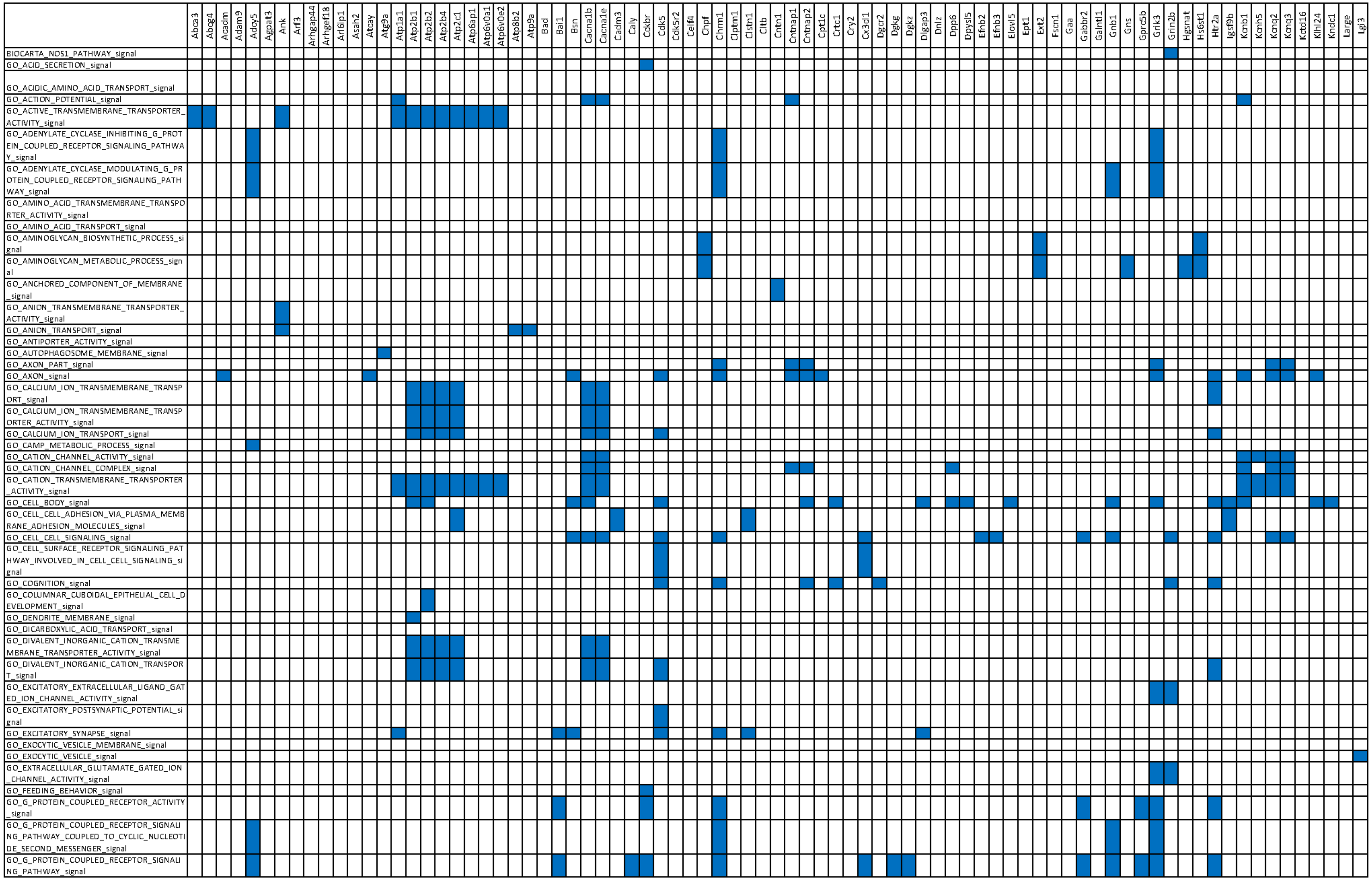
Abca3
Abcg4
Acadm
Adam9
Adcy5
Agpat3
Ank
Arf3
Arhgap44
Arhgef18
Arl6ip1
Asah2
Atcay
Atg9a
Atp1a1
Atp2b1
Atp2b2
Atp2b4
Atp2c1
Atp6ap1
Atp6v0a1
Atp6v0e2
Atp8b2
Atp9a
Bad
Bai1
Bsn
Cacna1b
Cacna1e
Cadm3
Caly
Cckbr
Cdk5
Cdk5r2
Celf4
Chpf
Chrm1
Clptm1
Clstn1
Cltb
Cntn1
Cntnap1
Cntnap2
Cpt1c
Crtc1
Cry2
Cx3cl1
Dgcr2
Dgkg
Dgkz
Dlgap3
Dnlz
Dpp6
Dpysl5
Efnb2
Efnb3
Elovl5
Ept1
Ext2
Fscn1
Gaa
Gabbr2
Galntl1
Gnb1
Gns
Gprc5b
Grik3
Grin2b
Hgsnat
Hs6st1
Htr2a
Igsf9b
Kcnb1
Kcnh5
Kcnq2
Kcnq3
Kctd16
Klhl24
Kndc1
Large
Lgi3
BIOCARTA_NOS1_PATHWAY_signal
GO_ACID_SECRETION_signal
GO_ACIDIC_AMINO_ACID_TRANSPORT_signal
GO_ACTION_POTENTIAL_signal
GO_ACTIVE_TRANSMEMBRANE_TRANSPORTER_ACTIVITY_signal
GO_ADENYLATE_CYCLASE_INHIBITING_G_PROTEIN_COUPLED_RECEPTOR_SIGNALING_PATHWAY_signal
GO_ADENYLATE_CYCLASE_MODULATING_G_PROTEIN_COUPLED_RECEPTOR_SIGNALING_PATHWAY_signal
GO_AMINO_ACID_TRANSMEMBRANE_TRANSPORTER_ACTIVITY_signal
GO_AMINO_ACID_TRANSPORT_signal
GO_AMINOGLYCAN_BIOSYNTHETIC_PROCESS_signal
GO_AMINOGLYCAN_METABOLIC_PROCESS_signal
GO_ANCHORED_COMPONENT_OF_MEMBRANE_signal
GO_ANION_TRANSMEMBRANE_TRANSPORTER_ACTIVITY_signal
GO_ANION_TRANSPORT_signal
GO_ANTIPORTER_ACTIVITY_signal
GO_AUTOPHAGOSOME_MEMBRANE_signal
GO_AXON_PART_signal
GO_AXON_signal
GO_CALCIUM_ION_TRANSMEMBRANE_TRANSPORT_signal
GO_CALCIUM_ION_TRANSMEMBRANE_TRANSPORTER_ACTIVITY_signal
GO_CALCIUM_ION_TRANSPORT_signal
GO_CAMP_METABOLIC_PROCESS_signal
GO_CATION_CHANNEL_ACTIVITY_signal
GO_CATION_CHANNEL_COMPLEX_signal
GO_CATION_TRANSMEMBRANE_TRANSPORTER_ACTIVITY_signal
GO_CELL_BODY_signal
GO_CELL_CELL_ADHESION_VIA_PLASMA_MEMBRANE_ADHESION_MOLECULES_signal
GO_CELL_CELL_SIGNALING_signal
GO_CELL_SURFACE_RECEPTOR_SIGNALING_PATHWAY_INVOLVED_IN_CELL_CELL_SIGNALING_signal
GO_COGNITION_signal
GO_COLUMNAR_CUBOIDAL_EPITHELIAL_CELL_DEVELOPMENT_signal
GO_DENDRITE_MEMBRANE_signal
GO_DICARBOXYLIC_ACID_TRANSPORT_signal
GO_DIVALENT_INORGANIC_CATION_TRANSMEMBRANE_TRANSPORTER_ACTIVITY_signal
GO_DIVALENT_INORGANIC_CATION_TRANSPORT_signal
GO_EXCITATORY_EXTRACELLULAR_LIGAND_GATED_ION_CHANNEL_ACTIVITY_signal
GO_EXCITATORY_POSTSYNAPTIC_POTENTIAL_signal
GO_EXCITATORY_SYNAPSE_signal
GO_EXOCYTIC_VESICLE_MEMBRANE_signal
GO_EXOCYTIC_VESICLE_signal
GO_EXTRACELLULAR_GLUTAMATE_GATED_ION_CHANNEL_ACTIVITY_signal
GO_FEEDING_BEHAVIOR_signal
GO_G_PROTEIN_COUPLED_RECEPTOR_ACTIVITY_signal
GO_G_PROTEIN_COUPLED_RECEPTOR_SIGNALING_PATHWAY_COUPLED_TO_CYCLIC_NUCLEOTIDE_SECOND_MESSENGER_signal
GO_G_PROTEIN_COUPLED_RECEPTOR_SIGNALING_PATHWAY_signal

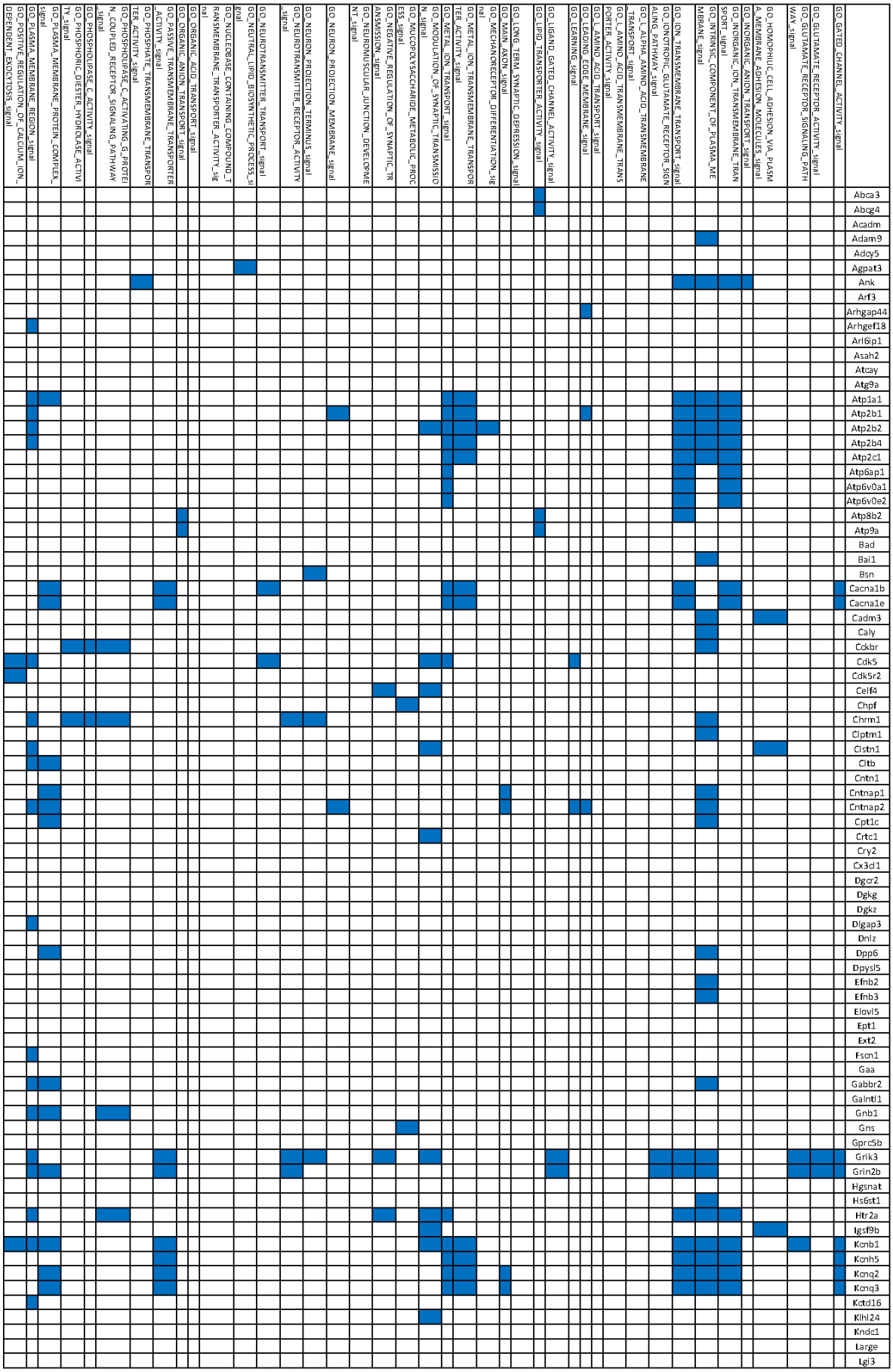
GO_GATED_CHANNEL_ACTIVITY_signal
GO_GLUTAMATE_RECEPTOR_ACTIVITY_signal
GO_GLUTAMATE_RECEPTOR_SIGNALING_PATHWAY_signal
GO_HOMOPHILIC_CELL_ADHESION_VIA_PLASMA_MEMBRANE_ADHESION_MOLECULES_signal
GO_INORGANIC_ANION_TRANSPORT_signal
GO_INORGANIC_ION_TRANSMEMBRANE_TRANSPORT_signal
GO_INTRINSIC_COMPONENT_OF_PLASMA_MEMBRANE_signal
GO_ION_TRANSMEMBRANE_TRANSPORT_signal
GO_IONOTROPIC_GLUTAMATE_RECEPTOR_SIGNALING_PATHWAY_signal
GO_L_ALPHA_AMINO_ACID_TRANSMEMBRANE_TRANSPORT_signal
GO_L_AMINO_ACID_TRANSMEMBRANE_TRANSPORTER_ACTIVITY_signal
GO_L_AMINO_ACID_TRANSPORT_signal
GO_LEADING_EDGE_MEMBRANE_signal
GO_LEARNING_signal
GO_LIGAND_GATED_CHANNEL_ACTIVITY_signal
GO_LIPID_TRANSPORTER_ACTIVITY_signal
GO_LONG_TERM_SYNAPTIC_DEPRESSION_signal
GO_MAIN_AXON_signal
GO_MECHANORECEPTOR_DIFFERENTIATION_signal
GO_METAL_ION_TRANSMEMBRANE_TRANSPORTER_ACTIVITY_signal
GO_METAL_ION_TRANSPORT_signal
GO_MODULATION_OF_SYNAPTIC_TRANSMISSION_signal
GO_MUCOPOLYSACCHARIDE_METABOLIC_PROCESS_signal
GO_NEGATIVE_REGULATION_OF_SYNAPTIC_TRANSMISSION_signal
GO_NEUROMUSCULAR_JUNCTION_DEVELOPMENT_signal
GO_NEURON_PROJECTION_MEMBRANE_signal
GO_NEURON_PROJECTION_TERMINUS_signal
GO_NEUROTRANSMITTER_RECEPTOR_ACTIVITY_signal
GO_NEUROTRANSMITTER_TRANSPORT_signal
GO_NEUTRAL_LIPID_BIOSYNTHETIC_PROCESS_signal
GO_NUCLEOBASE_CONTAINING_COMPOUND_TRANSMEMBRANE_TRANSPORTER_ACTIVITY_signal
GO_ORGANIC_ACID_TRANSPORT_signal
GO_ORGANIC_ANION_TRANSPORT_signal
GO_PASSIVE_TRANSMEMBRANE_TRANSPORTER_ACTIVITY_signal
GO_PHOSPHATE_TRANSMEMBRANE_TRANSPORTER_ACTIVITY_signal
GO_PHOSPHOLIPASE_C_ACTIVATING_G_PROTEIN_COUPLED_RECEPTOR_SIGNALING_PATHWAY_signal
GO_PHOSPHOLIPASE_C_ACTIVITY_signal
GO_PHOSPHORIC_DIESTER_HYDROLASE_ACTIVITY_signal
GO_PLASMA_MEMBRANE_PROTEIN_COMPLEX_signal
GO_PLASMA_MEMBRANE_REGION_signal
GO_POSITIVE_REGULATION_OF_CALCIUM_ION_DEPENDENT_EXOCYTOSIS_signal
Abca3
Abcg4
Acadm
Adam9
Adcy5
Agpat3
Ank
Arf3
Arhgap44
Arhgef18
Arl6ip1
Asah2
Atcay
Atg9a
Atp1a1
Atp2b1
Atp2b2
Atp2b4
Atp2c1
Atp6ap1
Atp6v0a1
Atp6v0e2
Atp8b2
Atp9a
Bad
Bai1
Bsn
Cacna1b
Cacna1e
Cadm3
Caly
Cckbr
Cdk5
Cdk5r2
Celf4
Chpf
Chrm1
Clptm1
Clstn1
Citb
Cntn1
Cntnap1
Cntnap2
Cpt1c
Crtc1
Cry2
Cx3cl1
Dgcr2
Dgkg
Dgkz
Dlgap3
Dnlz
Dpp6
Dpysl5
Efnb2
Efnb3
Elovl5
Ept1
Ext2
Fscn1
Gaa
Gabbr2
Galntl1
Gnb1
Gns
Gprc5b
Grik3
Grin2b
Hgsnat
Hs6st1
Htr2a
Igsf9b
Kcnb1
Kcnh5
Kcnq2
Kcnq3
Kctd16
Klhl24
Kndc1
Large
Lgi3

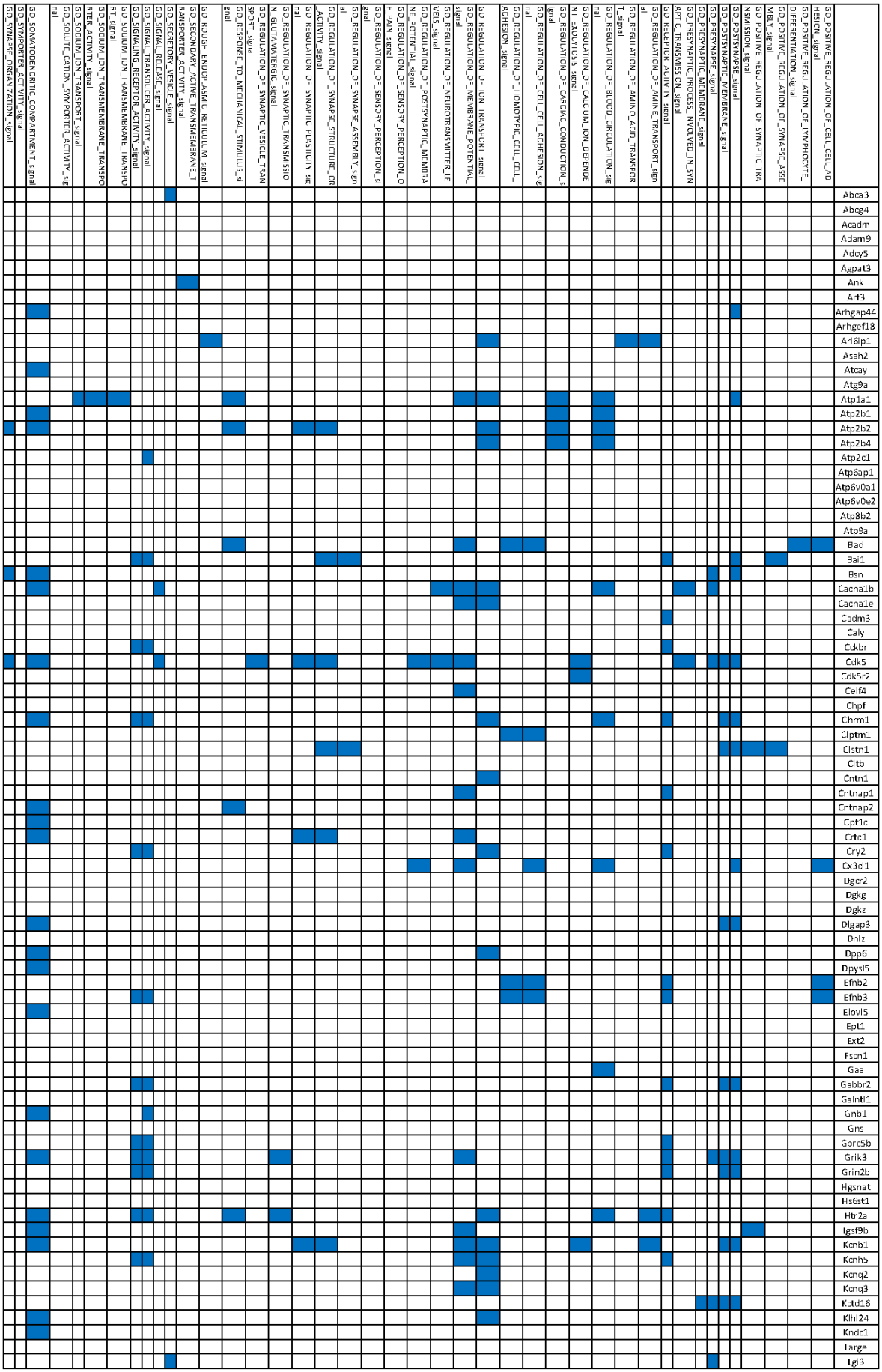
GO_POSITIVE_REGULATION_OF_CELL_CELL_ADHESION_signal
GO_POSITIVE_REGULATION_OF_LYMPHOCYTE_DIFFERENTIATION_signal
GO_POSITIVE_REGULATION_OF_SYNAPSE_ASSEMBLY_signal
GO_POSITIVE_REGULATION_OF_SYNAPTIC_TRANSMISSION_signal
GO_POSTSYNAPSE_signal
GO_POSTSYNAPTIC_MEMBRANE_signal
GO_PRESYNAPSE_signal
GO_PRESYNAPTIC_MEMBRANE_signal
GO_PRESYNAPTIC_PROCESS_INVOLVED_IN_SYNAPTIC_TRANSMISSION_signal
GO_RECEPTOR_ACTIVITY_signal
GO_REGULATION_OF_AMINE_TRANSPORT_signal
GO_REGULATION_OF_AMINO_ACID_TRANSPORT_signal
GO_REGULATION_OF_BLOOD_CIRCULATION_signal
GO_REGULATION_OF_CALCIUM_ION_DEPENDENT_EXOCYTOSIS_signal
GO_REGULATION_OF_CARDIAC_CONDUCTION_signal
GO_REGULATION_OF_CELL_CELL_ADHESION_signal
GO_REGULATION_OF_HOMOTYPIC_CELL_CELL_ADHESION_signal
GO_REGULATION_OF_ION_TRANSPORT_signal
GO_REGULATION_OF_MEMBRANE_POTENTIAL_signal
GO_REGULATION_OF_NEUROTRANSMITTER_LEVELS_signal
GO_REGULATION_OF_POSTSYNAPTIC_MEMBRANE_POTENTIAL_signal
GO_REGULATION_OF_SENSORY_PERCEPTION_OF_PAIN_signal
GO_REGULATION_OF_SENSORY_PERCEPTION_signal
GO_REGULATION_OF_SYNAPSE_ASSEMBLY_signal
GO_REGULATION_OF_SYNAPSE_STRUCTURE_OR_ACTIVITY_signal
GO_REGULATION_OF_SYNAPTIC_PLASTICITY_signal
GO_REGULATION_OF_SYNAPTIC_TRANSMISSION_GLUTAMATERGIC_signal
GO_REGULATION_OF_SYNAPTIC_VESICLE_TRANSPORT_signal
GO_RESPONSE_TO_MECHANICAL_STIMULUS_signal
GO_ROUGH_ENDOPLASMIC_RETICULUM_signal
GO_SECONDARY_ACTIVE_TRANSMEMBRANE_TRANSPORTER_ACTIVITY_signal
GO_SECRETORY_VESICLE_signal
GO_SIGNAL_RELEASE_signal
GO_SIGNAL_TRANSDUCER_ACTIVITY_signal
GO_SIGNALING_RECEPTOR_ACTIVITY_signal
GO_SODIUM_ION_TRANSMEMBRANE_TRANSPORTER_signal
GO_SODIUM_ION_TRANSMEMBRANE_TRANSPORTER_ACTIVITY_signal
GO_SODIUM_ION_TRANSPORT_signal
GO_SOLUTE_CATION_SYMPORTER_ACTIVITY_signal
GO_SOMATODENDRITIC_COMPARTMENT_signal
GO_SYMPORTER_ACTIVITY_signal
GO_SYNAPSE_ORGANIZATION_signal
Abca3
Abcg4
Acadm
Adam9
Adcy5
Agpat3
Ank
Arf3
Arhgap44
Arhgef18
Arl6ip1
Asah2
Atcay
Atg9a
Atp1a1
Atp2b1
Atp2b2
Atp2b4
Atp2c1
Atp6ap1
Atp6v0a1
Atp6v0e2
Atp8b2
Atp9a
Bad
Bai1
Bsn
Cacna1b
Cacna1e
Cadm3
Caly
Cckbr
Cdk5
Cdk5r2
Celf4
Chpf
Chrm1
Clptm1
Clstn1
Cltb
Cntn1
Cntnap1
Cntnap2
Cpt1c
Crtc1
Cry2
Cx3cl1
Dgcr2
Dgkg
Dgkz
Dlgap3
Dnlz
Dpp6
Dpysl5
Efnb2
Efnb3
Elovl5
Ept1
Ext2
Fscn1
Gaa
Gabbr2
Galntl1
Gnb1
Gns
Gprc5b
Grik3
Grin2b
Hgsnat
Hs6st1
Htr2a
Igsf9b
Kcnb1
Kcnh5
Kcnq2
Kcnq3
Kctd16
Klhl24
Kndc1
Large
Lgi3

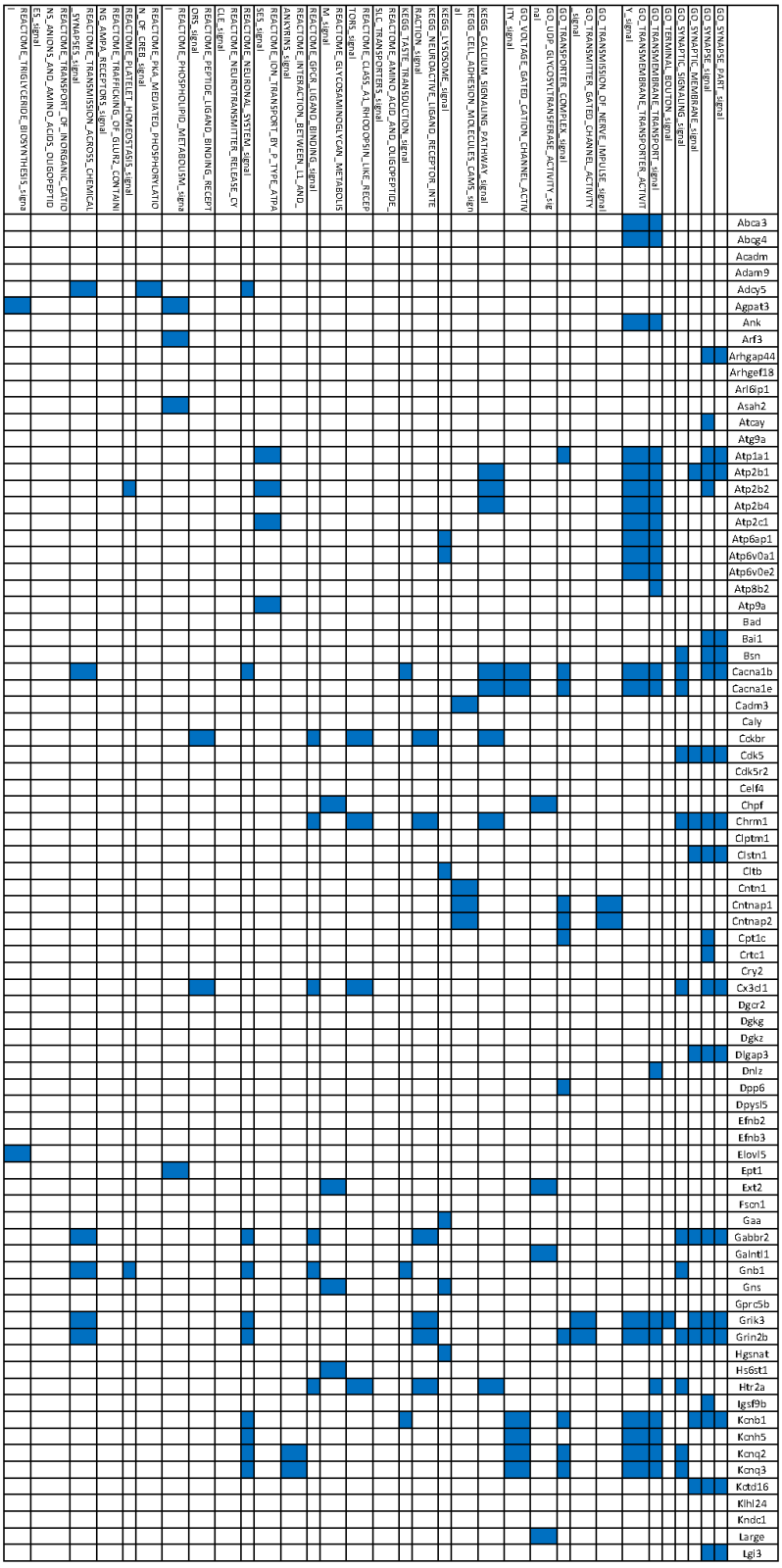

Table S4 ***(pages 134-137).*** **Heatmap of significantly downregulated gene sets and corresponding leading genes (alphabetically ordered, A-L) in Pvalb^{+} neurons of defeated animals.** Columns are downregulated gene sets in defeated animals. Rows are the downregulated genes that are leading the impoverishment of the gene sets (from GSEA leading edge analysis results). Only genes with also $p<0.05$ and $logFC>0.27$ are listed. When a gene is leading the impoverishment of a specific gene set the square at the cross is blue.

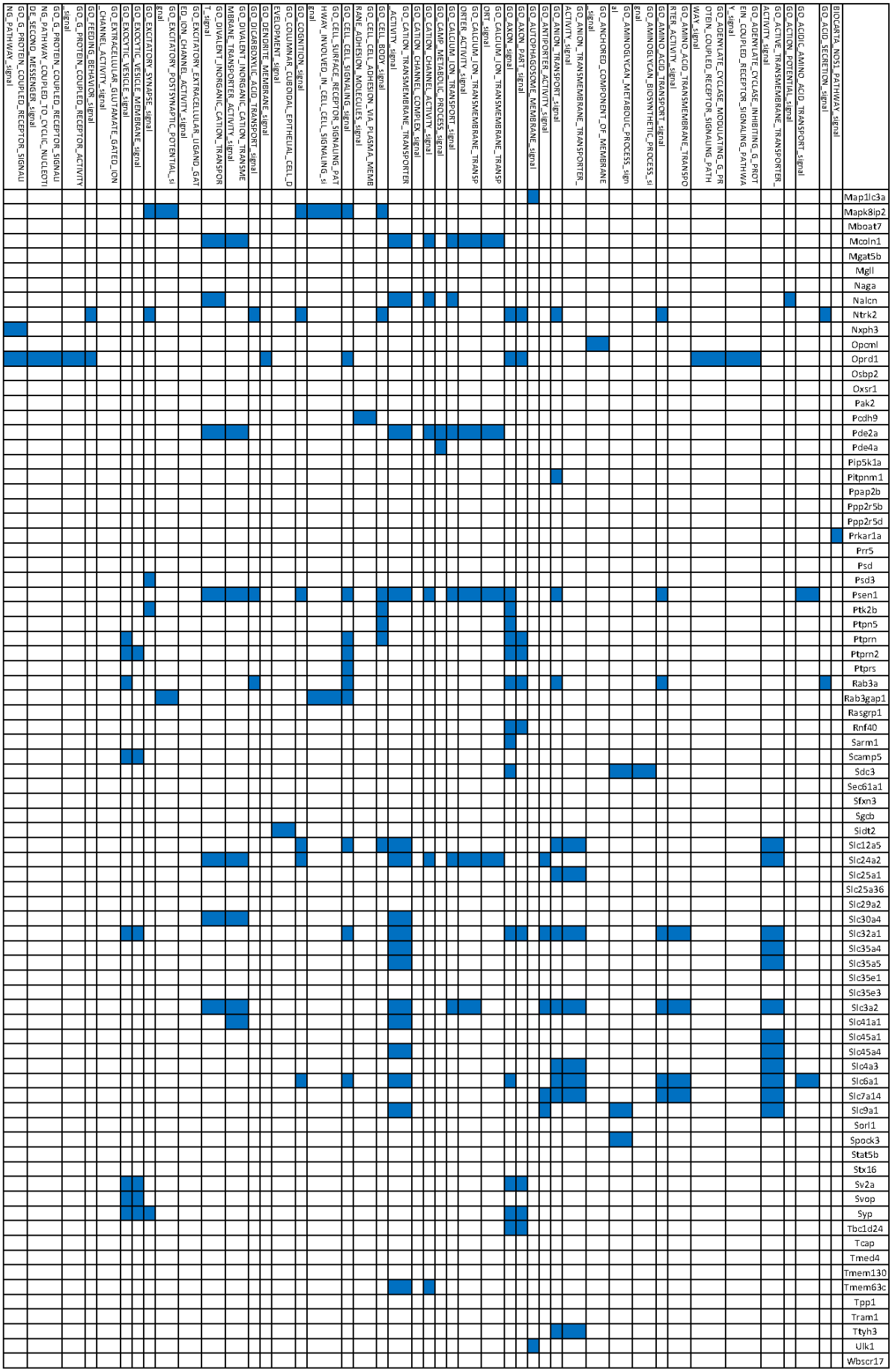
BIOCARTA_NOS1_PATHWAY_signal
GO_ACID_SECRETION_signal
GO_ACIDIC_AMINO_ACID_TRANSPORT_signal
GO_ACTION_POTENTIAL_signal
GO_ACTIVE_TRANSMEMBRANE_TRANSPORTER_ACTIVITY_signal
GO_ADENYLATE_CYCLASE_INHIBITING_G_PROTEIN_COUPLED_RECEPTOR_SIGNALING_PATHWAY_signal
GO_ADENYLATE_CYCLASE_MODULATING_G_PROTEIN_COUPLED_RECEPTOR_SIGNALING_PATHWAY_signal
GO_AMINO_ACID_TRANSMEMBRANE_TRANSPORTER_ACTIVITY_signal
GO_AMINO_ACID_TRANSPORT_signal
GO_AMINOGLYCAN_BIOSYNTHETIC_PROCESS_signal
GO_AMINOGLYCAN_METABOLIC_PROCESS_signal
GO_ANCHORED_COMPONENT_OF_MEMBRANE_signal
GO_ANION_TRANSMEMBRANE_TRANSPORTER_ACTIVITY_signal
GO_ANION_TRANSPORT_signal
GO_ANTIPORTER_ACTIVITY_signal
GO_AUTOPHAGOSOME_MEMBRANE_signal
GO_AXON_PART_signal
GO_CALCIUM_ION_TRANSMEMBRANE_TRANSPORT_signal
GO_CALCIUM_ION_TRANSMEMBRANE_TRANSPORTER_ACTIVITY_signal
GO_CALCIUM_ION_TRANSPORT_signal
GO_CAMP_METABOLIC_PROCESS_signal
GO_CATION_CHANNEL_ACTIVITY_signal
GO_CATION_CHANNEL_COMPLEX_signal
GO_CATION_TRANSMEMBRANE_TRANSPORTER_ACTIVITY_signal
GO_CELL_BODY_signal
GO_CELL_CELL_ADHESION_VIA_PLASMA_MEMBRANE_ADHESION_MOLECULES_signal
GO_CELL_SURFACE_RECEPTOR_SIGNALING_PATHWAY_INVOLVED_IN_CELL_CELL_SIGNALING_signal
GO_COGNITION_signal
GO_COLUMNAR_CUBOIDAL_EPITHELIAL_CELL_DEVELOPMENT_signal
GO_DENDRITE_MEMBRANE_signal
GO_DICARBOXYLIC_ACID_TRANSPORT_signal
GO_DIVALENT_INORGANIC_CATION_TRANSMEMBRANE_TRANSPORTER_ACTIVITY_signal
GO_DIVALENT_INORGANIC_CATION_TRANSPORT_signal
GO_EXCITATORY_EXTRACELLULAR_LIGAND_GATED_ION_CHANNEL_ACTIVITY_signal
GO_EXCITATORY_POSTSYNAPTIC_POTENTIAL_signal
GO_EXCITATORY_SYNAPSE_signal
GO_EXOCYTIC_VESICLE_MEMBRANE_signal
GO_EXOCYTIC_VESICLE_signal
GO_EXTRACELLULAR_GLUTAMATE_GATED_ION_CHANNEL_ACTIVITY_signal
GO_FEEDING_BEHAVIOR_signal
GO_G_PROTEIN_COUPLED_RECEPTOR_ACTIVITY_signal
GO_G_PROTEIN_COUPLED_RECEPTOR_SIGNALING_PATHWAY_COUPLED_TO_CYCLIC_NUCLEOTIDE_SECOND_MESSENGER_signal
GO_G_PROTEIN_COUPLED_RECEPTOR_SIGNALING_PATHWAY_signal
Map1lc3a
Mapk8ip2
Mboat7
Mcoln1
Mgat5b
Mgll
Naga
Nalcn
Ntrk2
Nxph3
Opcml
Oprd1
Osbp2
Oxsr1
Pak2
Pcdh9
Pde2a
Pde4a
Pip5k1a
Pitpnm1
Ppap2b
Ppp2r5b
Ppp2r5d
Prkar1a
Prr5
Psd
Psd3
Psen1
Ptk2b
Ptpn5
Ptprn
Ptprn2
Ptprs
Rab3a
Rab3gap1
Rasgrp1
Rnf40
Sarm1
Scamp5
Sdc3
Sec61a1
Sfxn3
Sgcb
Sidt2
Slc12a5
Slc24a2
Slc25a1
Slc25a36
Slc29a2
Slc30a4
Slc32a1
Slc35a4
Slc35a5
Slc35e1
Slc35e3
Slc3a2
Slc41a1
Slc45a1
Slc45a4
Slc4a3
Slc6a1
Slc7a14
Slc9a1
Sorl1
Spock3
Stat5b
Stx16
Sv2a
Svop
Syp
Tbc1d24
Tcap
Tmed4
Tmem130
Tmem63c
Tpp1
Tram1
Ttyh3
Ulk1
Wbscr17

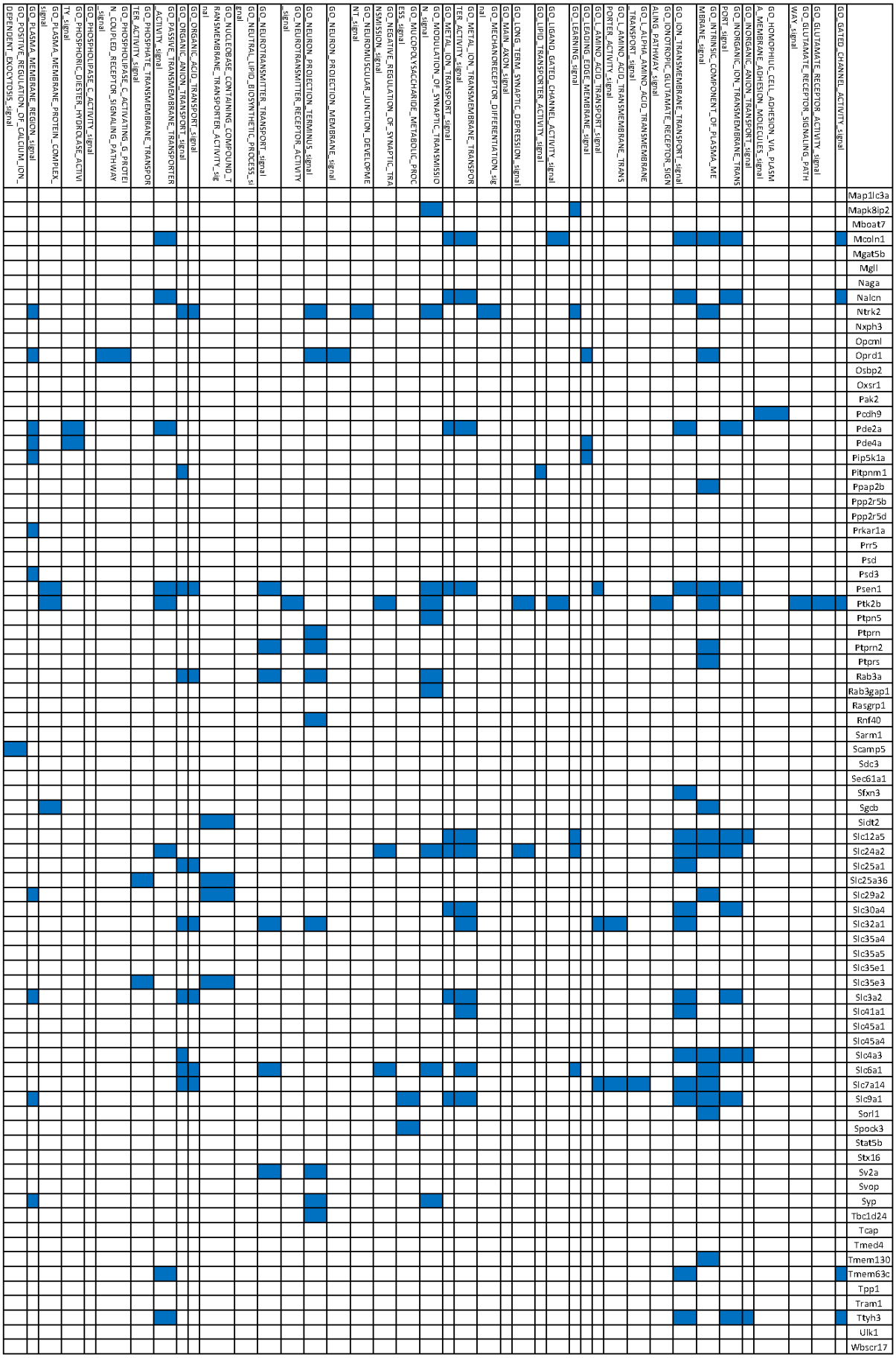
GO_GATED_CHANNEL_ACTIVITY_signal
GO_GLUTAMATE_RECEPTOR_ACTIVITY_signal
GO_GLUTAMATE_RECEPTOR_SIGNALING_PATHWAY_signal
GO_HOMOPHILIC_CELL_ADHESION_VIA_PLASMA_MEMBRANE_ADHESION_MOLECULES_signal
GO_INORGANIC_ANION_TRANSPORT_signal
GO_INORGANIC_ION_TRANSMEMBRANE_TRANSPORT_signal
GO_INTRINSIC_COMPONENT_OF_PLASMA_MEMBRANE_signal
GO_ION_TRANSMEMBRANE_TRANSPORT_signal
GO_IONOTROPIC_GLUTAMATE_RECEPTOR_SIGNALING_PATHWAY_signal
GO_L_ALPHA_AMINO_ACID_TRANSMEMBRANE_TRANSPORT_signal
GO_L_AMINO_ACID_TRANSMEMBRANE_TRANSPORTER_ACTIVITY_signal
GO_L_AMINO_ACID_TRANSPORT_signal
GO_LEADING_EDGE_MEMBRANE_signal
GO_LEARNING_signal
GO_LIGAND_GATED_CHANNEL_ACTIVITY_signal
GO_LIPID_TRANSPORTER_ACTIVITY_signal
GO_LONG_TERM_SYNAPTIC_DEPRESSION_signal
GO_MAIN_AXON_signal
GO_MECHANORECEPTOR_DIFFERENTIATION_signal
GO_METAL_ION_TRANSMEMBRANE_TRANSPORTER_ACTIVITY_signal
GO_METAL_ION_TRANSPORT_signal
GO_MODULATION_OF_SYNAPTIC_TRANSMISSION_signal
GO_MUCOPOLYSACCHARIDE_METABOLIC_PROCESS_signal
GO_NEGATIVE_REGULATION_OF_SYNAPTIC_TRANSMISSION_signal
GO_NEUROMUSCULAR_JUNCTION_DEVELOPMENT_signal
GO_NEURON_PROJECTION_MEMBRANE_signal
GO_NEURON_PROJECTION_TERMINUS_signal
GO_NEUROTRANSMITTER_RECEPTOR_ACTIVITY_signal
GO_NEUROTRANSMITTER_TRANSPORT_signal
GO_NEUTRAL_LIPID_BIOSYNTHETIC_PROCESS_signal
GO_NUCLEOBASE_CONTAINING_COMPOUND_TRANSMEMBRANE_TRANSPORTER_ACTIVITY_signal
GO_ORGANIC_ACID_TRANSPORT_signal
GO_ORGANIC_ANION_TRANSPORT_signal
GO_PASSIVE_TRANSMEMBRANE_TRANSPORTER_ACTIVITY_signal
GO_PHOSPHATE_TRANSMEMBRANE_TRANSPORTER_ACTIVITY_signal
GO_PHOSPHOLIPASE_C_ACTIVATING_G_PROTEIN_COUPLED_RECEPTOR_SIGNALING_PATHWAY_signal
GO_PHOSPHOLIPASE_C_ACTIVITY_signal
GO_PHOSPHORIC_DIESTER_HYDROLASE_ACTIVITY_signal
GO_PLASMA_MEMBRANE_PROTEIN_COMPLEX_signal
GO_PLASMA_MEMBRANE_REGION_signal
GO_POSITIVE_REGULATION_OF_CALCIUM_ION_DEPENDENT_EXOCYTOSIS_signal
Map1lc3a
Mapk8ip2
Mboat7
Mcoln1
Mgat5b
Mgll
Naga
Nalcn
Ntrk2
Nxph3
Opcml
Oprd1
Osbp2
Oxsr1
Pak2
Pcdh9
Pde2a
Pde4a
Pip5k1a
Pitpnm1
Ppap2b
Ppp2r5b
Ppp2r5d
Prkar1a
Prr5
Psd
Psd3
Psen1
Ptk2b
Ptpn5
Ptprn
Ptprn2
Ptprs
Rab3a
Rab3gap1
Rasgrp1
Rnf40
Sarm1
Scamp5
Sdc3
Sec61a1
Sfxn3
Sgcb
Sidt2
Slc12a5
Slc24a2
Slc25a1
Slc25a36
Slc29a2
Slc30a4
Slc32a1
Slc35a4
Slc35a5
Slc35e1
Slc35e3
Slc3a2
Slc41a1
Slc45a1
Slc45a4
Slc4a3
Slc6a1
Slc7a14
Slc9a1
Sorl1
Spock3
Stat5b
Stx16
Sv2a
Svop
Syp
Tbc1d24
Tcap
Tmed4
Tmem130
Tmem63c
Tpp1
Tram1
Ttyh3
Ulk1
Wbscr17

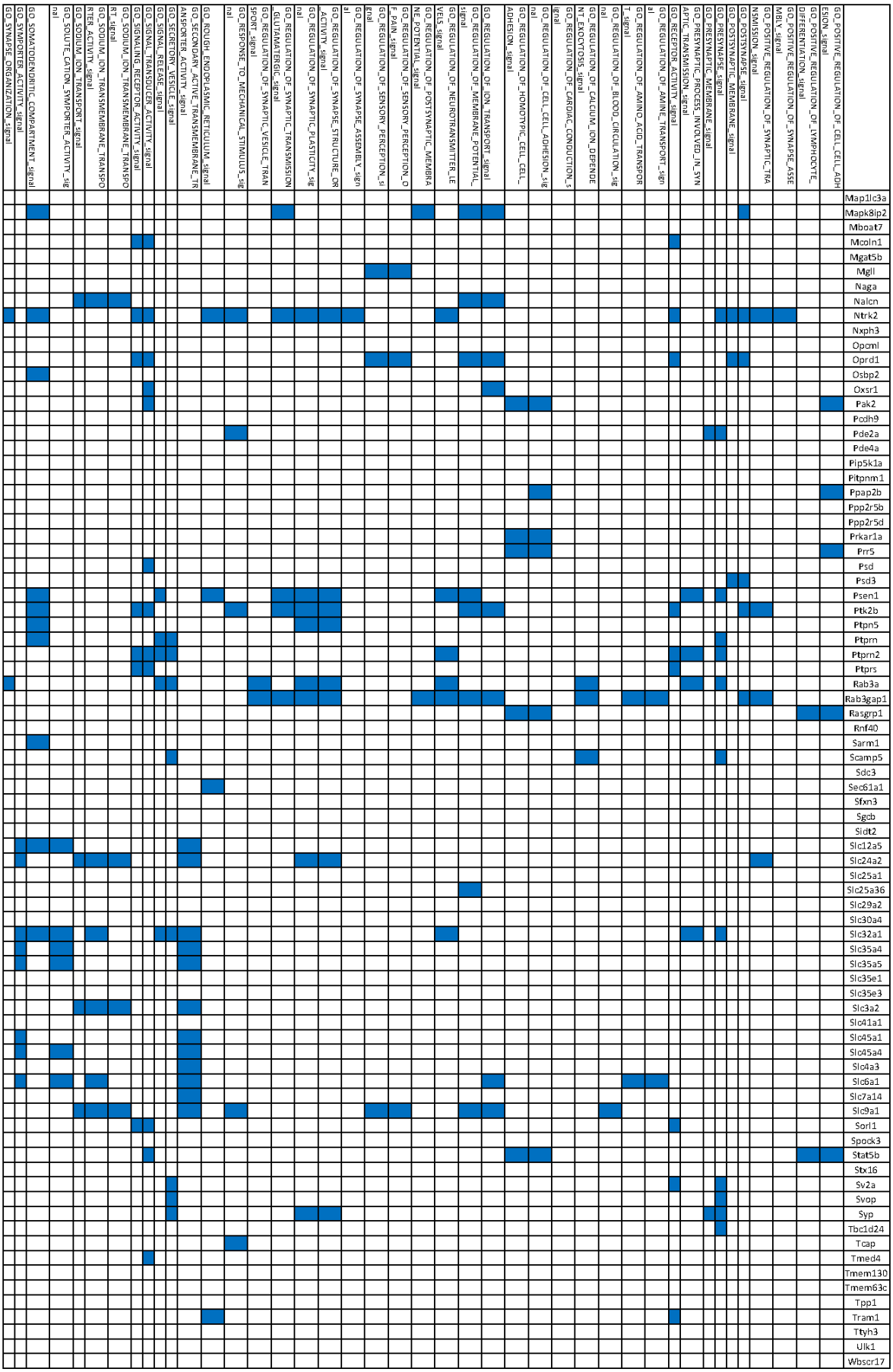
GO_POSITIVE_REGULATION_OF_CELL_CELL_ADHESION_signal
GO_POSITIVE_REGULATION_OF_LYMPHOCYTE_DIFFERENTIATION_signal
GO_POSITIVE_REGULATION_OF_SYNAPSE_ASSEMBLY_signal
GO_POSITIVE_REGULATION_OF_SYNAPTIC_TRANSMISSION_signal
GO_POSTSYNAPSE_signal
GO_POSTSYNAPTIC_MEMBRANE_signal
GO_PRESYNAPSE_signal
GO_PRESYNAPTIC_MEMBRANE_signal
GO_PRESYNAPTIC_PROCESS_INVOLVED_IN_SYNAPTIC_TRANSMISSION_signal
GO_RECEPTOR_ACTIVITY_signal
GO_REGULATION_OF_AMINE_TRANSPORT_signal
GO_REGULATION_OF_AMINO_ACID_TRANSPORT_signal
GO_REGULATION_OF_BLOOD_CIRCULATION_signal
GO_REGULATION_OF_CALCIUM_ION_DEPENDENT_EXOCYTOSIS_signal
GO_REGULATION_OF_CARDIAC_CONDUCTION_signal
GO_REGULATION_OF_CELL_CELL_ADHESION_signal
GO_REGULATION_OF_HOMOTYPIC_CELL_CELL_ADHESION_signal
GO_REGULATION_OF_ION_TRANSPORT_signal
GO_REGULATION_OF_MEMBRANE_POTENTIAL_signal
GO_REGULATION_OF_NEUROTRANSMITTER_LEVELS_signal
GO_REGULATION_OF_POSTSYNAPTIC_MEMBRANE_POTENTIAL_signal
GO_REGULATION_OF_SENSORY_PERCEPTION_OF_PAIN_signal
GO_REGULATION_OF_SENSORY_PERCEPTION_signal
GO_REGULATION_OF_SYNAPSE_ASSEMBLY_signal
GO_REGULATION_OF_SYNAPSE_STRUCTURE_OR_ACTIVITY_signal
GO_REGULATION_OF_SYNAPTIC_PLASTICITY_signal
GO_REGULATION_OF_SYNAPTIC_TRANSMISSION_GLUTAMATERGIC_signal
GO_REGULATION_OF_SYNAPTIC_VESICLE_TRANSPORT_signal
GO_RESPONSE_TO_MECHANICAL_STIMULUS_signal
GO_ROUGH_ENDOPLASMIC_RETICULUM_signal
GO_SECONDARY_ACTIVE_TRANSMEMBRANE_TRANSPORTER_ACTIVITY_signal
GO_SECRETORY_VESICLE_signal
GO_SIGNAL_RELEASE_signal
GO_SIGNAL_TRANSDUCER_ACTIVITY_signal
GO_SIGNALING_RECEPTOR_ACTIVITY_signal
GO_SODIUM_ION_TRANSMEMBRANE_TRANSPORTER_signal
GO_SODIUM_ION_TRANSMEMBRANE_TRANSPORTER_ACTIVITY_signal
GO_SODIUM_ION_TRANSPORT_signal
GO_SOLUTE_CATION_SYMPORTER_ACTIVITY_signal
GO_SOMATODENDRITIC_COMPARTMENT_signal
GO_SYMPORTER_ACTIVITY_signal
GO_SYNAPSE_ORGANIZATION_signal
Map1lc3a
Mapk8ip2
Mboat7
Mcoln1
Mgat5b
Mgll
Naga
Nalcn
Ntrk2
Nxph3
Opcml
Oprd1
Osbp2
Oxsr1
Pak2
Pcdh9
Pde2a
Pde4a
Pip5k1a
Pitpnm1
Ppap2b
Ppp2r5b
Ppp2r5d
Prkar1a
Prr5
Psd
Psd3
Psen1
Ptk2b
Ptpn5
Ptprn
Ptprn2
Ptprs
Rab3a
Rab3gap1
Rasgrp1
Rnf40
Sarm1
Scamp5
Sdc3
Sec61a1
Sfxn3
Sgcb
Sidt2
Slc12a5
Slc24a2
Slc25a1
Slc25a36
Slc29a2
Slc30a4
Slc32a1
Slc35a4
Slc35a5
Slc35e1
Slc35e3
Slc3a2
Slc41a1
Slc45a1
Slc45a4
Slc4a3
Slc6a1
Slc7a14
Slc9a1
Sorl1
Spock3
Stat5b
Stx16
Sv2a
Svop
Syp
Tbc1d24
Tcap
Tmed4
Tmem130
Tmem63c
Tpp1
Tram1
Ttyh3
Ulk1
Wbscr17

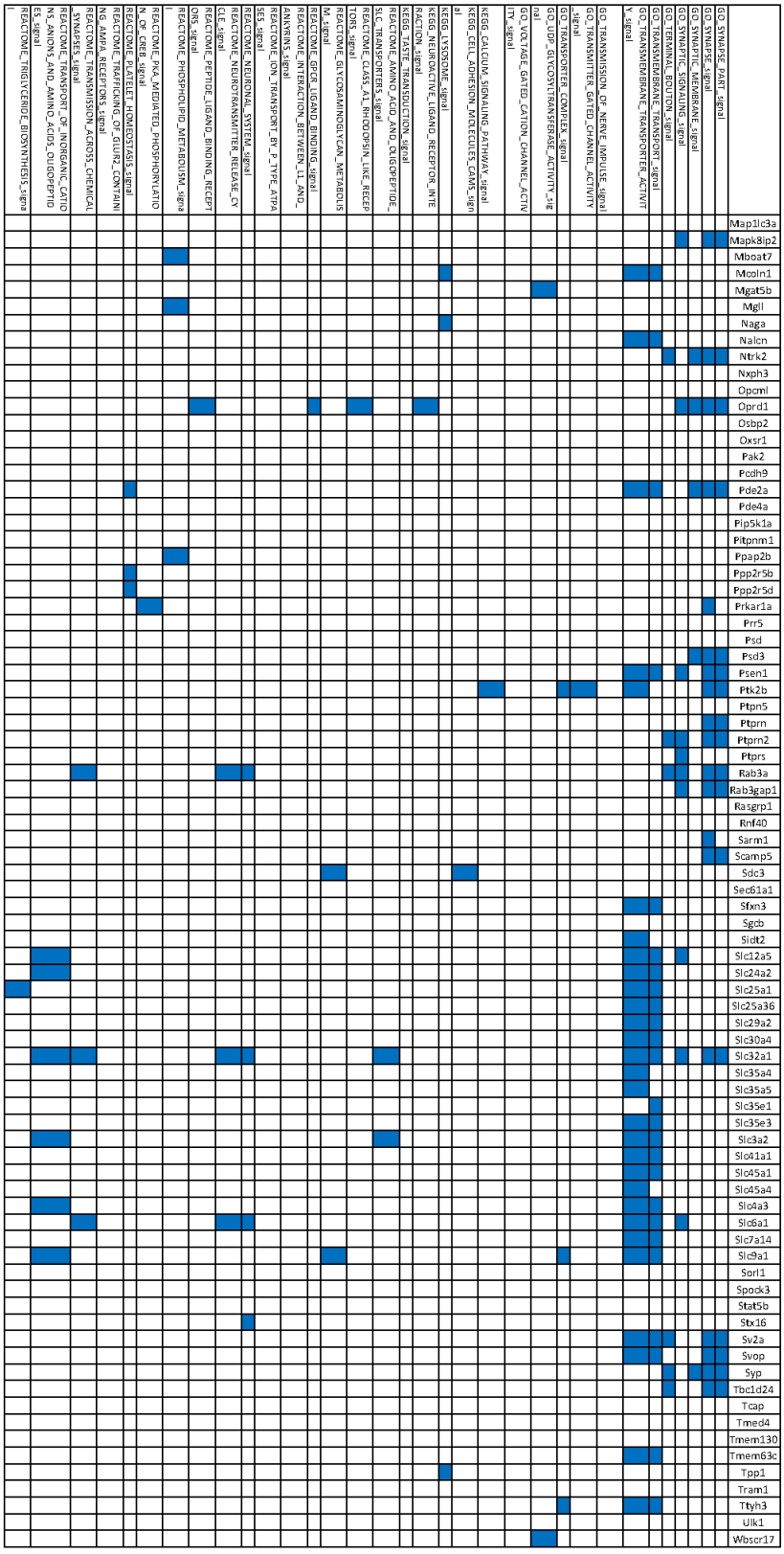

Table S5 ***(pages 138-141).*** **Heatmap of significantly downregulated gene sets and corresponding leading genes (alphabetically ordered, M-Z) in Pvalb^{+} neurons of defeated animals.** Columns are downregulated gene sets in defeated animals. Rows are the downregulated genes that are leading the impoverishment of the gene sets (from GSEA leading edge analysis results). Only genes with also $p<0.05$ and $logFC>0.27$ are listed. When a gene is leading the impoverishment of a specific gene set the square at the cross is blue.

NAME	SIZE	ES	NES	NOM p-val	FDR q-val	FWER p-val	RANK AT MAX	LEADING EDGE
GO NEURONAL POSTSYNAPTIC DENSITY	47	0.634761	2.358562	0	0.000	0.000	1032	tags=53%, list=16%, signal=63%
REACTOME CYTOSOLIC TRNA AMINOACYLATION	19	0.767393	2.316367	0	0.000	0.000	603	tags=58%, list=9%, signal=64%
GO INTERCALATED DISC	24	0.694719	2.217309	0	0.002	0.009	838	tags=58%, list=13%, signal=67%
GO COATED PIT	37	0.625529	2.219736	0	0.002	0.008	1047	tags=49%, list=16%, signal=58%
GO CELL JUNCTION ASSEMBLY	46	0.624142	2.268542	0	0.002	0.004	915	tags=41%, list=14%, signal=48%
GO NAD METABOLIC PROCESS	23	0.715424	2.248243	0	0.002	0.006	1167	tags=61%, list=18%, signal=74%
GO HELICASE ACTIVITY	75	0.559799	2.223406	0	0.002	0.008	1218	tags=49%, list=19%, signal=60%
REACTOME LYSOSOME VESICLE BIOGENESIS	18	0.741178	2.176919	0	0.004	0.024	1047	tags=56%, list=16%, signal=66%
REACTOME ACTIVATION OF NMDA RECEPTOR UPON GLUTAMATE BINDING AND POSTSYNAPTIC EVENTS	26	0.666347	2.18019	0	0.004	0.023	988	tags=54%, list=15%, signal=63%
GO ENDOCYTIC VESICLE MEMBRANE	62	0.555345	2.145842	0	0.005	0.047	870	tags=35%, list=13%, signal=41%
GO EXCITATORY SYNAPSE	151	0.482484	2.153417	0	0.005	0.042	1324	tags=46%, list=20%, signal=56%
GO REGULATION OF SODIUM ION TRANSMEMBRANE TRANSPORTER ACTIVITY	22	0.70106	2.148993	0	0.005	0.046	593	tags=50%, list=9%, signal=55%
REACTOME TRNA AMINOACYLATION	24	0.693595	2.157752	0	0.006	0.041	603	tags=46%, list=9%, signal=50%

GO CLATHRIN COATED VESICLE MEMBRANE	36	0.615614	2.136222	0	0.006	0.054	876	tags=42%, list=14%, signal=48%
GO ATPASE ACTIVITY	192	0.467412	2.16256	0	0.006	0.040	1218	tags=38%, list=19%, signal=45%
GO REGULATION OF NEURON PROJECTION DEVELOPMENT	228	0.44244	2.130403	0	0.006	0.062	1074	tags=34%, list=17%, signal=39%
KEGG AMINOACYL TRNA BIOSYNTHESIS	22	0.678211	2.118762	0	0.007	0.078	603	tags=50%, list=9%, signal=55%
GO NADH METABOLIC PROCESS	20	0.709781	2.119439	0	0.007	0.077	1167	tags=65%, list=18%, signal=79%
GO REGULATION OF SODIUM ION TRANSMEMBRANE TRANSPORT	28	0.658597	2.113636	0	0.007	0.087	608	tags=46%, list=9%, signal=51%
GO POSTSYNAPSE	246	0.441112	2.093613	0	0.008	0.115	1324	tags=42%, list=20%, signal=51%
GO CLATHRIN COATED VESICLE	64	0.530533	2.088064	0	0.008	0.124	966	tags=38%, list=15%, signal=44%
GO ATPASE ACTIVITY COUPLED	145	0.46528	2.093994	0	0.008	0.115	1218	tags=39%, list=19%, signal=46%
GO PRESYNAPTIC ACTIVE ZONE	23	0.661097	2.086099	0	0.008	0.129	1029	tags=52%, list=16%, signal=62%
GO LIGASE ACTIVITY FORMING CARBON OXYGEN BONDS	23	0.667388	2.083497	0	0.008	0.135	603	tags=48%, list=9%, signal=53%
GO GOLGI TO VACUOLE TRANSPORT	19	0.690665	2.080018	0	0.008	0.141	778	tags=47%, list=12%, signal=54%
GO CLATHRIN COATED ENDOCYTIC VESICLE	20	0.691802	2.095782	0	0.008	0.112	851	tags=60%, list=13%, signal=69%
GO REGULATION OF SYNAPTIC PLASTICITY	104	0.488706	2.076155	0	0.008	0.145	1481	tags=46%, list=23%, signal=59%
GO CONDENSED NUCLEAR CHROMOSOME	20	0.695044	2.096388	0	0.008	0.111	704	tags=50%, list=11%, signal=56%
GO CLATHRIN COAT OF COATED	13	0.782621	2.097094	0	0.009	0.111	778	tags=62%, list=12%,

PIT								signal=70%
GO CELL SUBSTRATE JUNCTION ASSEMBLY	16	0.728474	2.061855	0	0.010	0.178	673	tags=50%, list=10%, signal=56%
GO CLATHRIN COATED ENDOCYTIC VESICLE MEMBRANE	16	0.723163	2.049042	0	0.011	0.206	850	tags=63%, list=13%, signal=72%
GO CELL JUNCTION ORGANIZATION	69	0.516234	2.04762	0	0.011	0.217	915	tags=32%, list=14%, signal=37%
GO CELL CELL CONTACT ZONE	31	0.616105	2.042166	0	0.012	0.232	838	tags=45%, list=13%, signal=52%
GO RAS GUANYL NUCLEOTIDE EXCHANGE FACTOR ACTIVITY	81	0.502054	2.028673	0	0.013	0.279	1457	tags=49%, list=22%, signal=63%
GO GOLGI TO ENDOSOME TRANSPORT	12	0.756908	2.029045	0	0.013	0.277	778	tags=67%, list=12%, signal=76%
REACTOME UNBLOCKING OF NMDA RECEPTOR GLUTAMATE BINDING AND ACTIVATION	12	0.77069	2.030028	0	0.013	0.274	988	tags=75%, list=15%, signal=88%
GO ANTIGEN PROCESSING AND PRESENTATION OF PEPTIDE ANTIGEN VIA MHC CLASS II	52	0.528872	2.033432	0	0.013	0.261	850	tags=35%, list=13%, signal=40%
GO POSITIVE REGULATION OF CELL PROJECTION ORGANIZATION	174	0.439516	2.030076	0	0.014	0.274	1922	tags=52%, list=30%, signal=72%
GO EXCITATORY POSTSYNAPTIC POTENTIAL	18	0.693964	2.023206	0	0.014	0.306	1324	tags=72%, list=20%, signal=91%
GO REGULATION OF EXTENT OF CELL GROWTH	56	0.52737	2.020474	0	0.014	0.315	842	tags=32%, list=13%, signal=37%
GO REGULATION OF CELL GROWTH	166	0.446403	2.018413	0	0.014	0.323	1424	tags=39%, list=22%, signal=49%
GO POSITIVE REGULATION OF TRANSPORTER	35	0.594362	2.002821	0	0.017	0.388	950	tags=43%, list=15%, signal=50%

ACTIVITY								
GO REGULATION OF SMOOTH MUSCLE CELL MIGRATION	16	0.683924	1.992769	0	0.020	0.442	1256	tags=56%, list=19%, signal=70%
GO ATPASE ACTIVITY COUPLED TO MOVEMENT OF SUBSTANCES	47	0.546154	1.988866	0	0.021	0.454	827	tags=34%, list=13%, signal=39%
GO ACTIN BINDING	158	0.434036	1.983982	0	0.021	0.480	1070	tags=35%, list=17%, signal=41%
GO ACTIN FILAMENT BASED MOVEMENT	36	0.575241	1.981822	0.002169	0.021	0.489	737	tags=39%, list=11%, signal=44%
GO CATION TRANSPORTING ATPASE ACTIVITY	33	0.581218	1.984438	0	0.022	0.476	760	tags=33%, list=12%, signal=38%
GO REGULATION OF NEURON DIFFERENTIATION	269	0.403753	1.972618	0	0.023	0.533	1354	tags=36%, list=21%, signal=43%
REACTOME POST NMDA RECEPTOR ACTIVATION EVENTS	22	0.647242	1.9769	0	0.023	0.512	988	tags=55%, list=15%, signal=64%
GO ANTIGEN PROCESSING AND PRESENTATION OF PEPTIDE OR POLYSACCHARIDE ANTIGEN VIA MHC CLASS II	52	0.528872	1.969437	0	0.023	0.546	850	tags=35%, list=13%, signal=40%
GO CARDIAC MUSCLE CELL CONTRACTION	12	0.75876	1.973509	0.002096	0.023	0.526	617	tags=58%, list=10%, signal=64%
GO STRIATED MUSCLE CONTRACTION	38	0.567296	1.967059	0	0.023	0.553	748	tags=37%, list=12%, signal=41%
REACTOME TRAFFICKING OF AMPA RECEPTORS	24	0.634087	1.974379	0.002151	0.023	0.520	838	tags=46%, list=13%, signal=52%
GO REGULATION OF SODIUM ION TRANSPORT	40	0.555249	1.964922	0	0.023	0.566	838	tags=43%, list=13%, signal=49%
GO CELLULAR RESPONSE TO ALCOHOL	33	0.57144	1.969741	0	0.023	0.545	758	tags=33%, list=12%, signal=38%
GO REGULATION OF RHO PROTEIN	43	0.542259	1.960057	0	0.024	0.594	1426	tags=51%, list=22%,

SIGNAL TRANSDUCTION								signal=65%
REACTOME RECYCLING PATHWAY OF L1	19	0.660883	1.961058	0	0.024	0.591	639	tags=47%, list=10%, signal=52%
GO SYNAPSE PART	387	0.388746	1.946911	0	0.026	0.655	1363	tags=36%, list=21%, signal=43%
GO REGULATION OF CELL PROJECTION ORGANIZATION	292	0.400055	1.950257	0	0.026	0.644	1380	tags=36%, list=21%, signal=43%
BIOCARTA PTDINS PATHWAY	17	0.682455	1.947053	0	0.026	0.654	1044	tags=59%, list=16%, signal=70%
GO CLATHRIN COAT	31	0.592262	1.948105	0	0.026	0.650	850	tags=42%, list=13%, signal=48%
GO AP TYPE MEMBRANE COAT ADAPTOR COMPLEX	25	0.609807	1.950562	0	0.026	0.643	876	tags=48%, list=14%, signal=55%
GO ACTIN FILAMENT BINDING	52	0.524308	1.94224	0.00198	0.027	0.686	703	tags=35%, list=11%, signal=39%
REACTOME MEIOSIS	18	0.670168	1.950598	0	0.027	0.643	531	tags=39%, list=8%, signal=42%
GO EXTRACELLULAR MATRIX COMPONENT	18	0.659323	1.940114	0	0.027	0.698	139	tags=28%, list=2%, signal=28%
GO CELL SUBSTRATE ADHESION	41	0.54359	1.942387	0	0.027	0.685	758	tags=34%, list=12%, signal=38%
GO SYNAPSE	458	0.370712	1.925932	0	0.028	0.750	1150	tags=31%, list=18%, signal=35%
GO MYELIN SHEATH	117	0.447959	1.934643	0	0.028	0.718	1551	tags=44%, list=24%, signal=57%
REACTOME MHC CLASS II ANTIGEN PRESENTATION	54	0.508891	1.924283	0	0.028	0.756	850	tags=33%, list=13%, signal=38%
GO U2 TYPE PRESPLICEOSOME	14	0.695041	1.927556	0.004264	0.028	0.748	871	tags=50%, list=13%, signal=58%
GO CALMODULIN BINDING	83	0.473835	1.929159	0	0.028	0.745	880	tags=29%, list=14%, signal=33%
KEGG LONG TERM	48	0.522209	1.926219	0	0.028	0.750	988	tags=42%, list=15%,

POTENTIATION								signal=49%
GO ATPASE COUPLED ION TRANSMEMBRANE TRANSPORTER ACTIVITY	35	0.564229	1.931338	0	0.028	0.732	760	tags=31%, list=12%, signal=35%
GO REGULATION OF CELL SIZE	81	0.472104	1.929553	0	0.029	0.742	1378	tags=40%, list=21%, signal=50%
GO REGULATION OF SYNAPSE STRUCTURE OR ACTIVITY	149	0.4267	1.932159	0	0.029	0.725	1687	tags=45%, list=26%, signal=59%
GO AXON INITIAL SEGMENT	11	0.740222	1.931423	0	0.029	0.730	605	tags=45%, list=9%, signal=50%
GO POSITIVE REGULATION OF CELL GROWTH	73	0.477136	1.921065	0	0.029	0.769	1646	tags=47%, list=25%, signal=62%
GO ATP HYDROLYSIS COUPLED TRANSMEMBRANE TRANSPORT	21	0.624074	1.913538	0	0.030	0.791	492	tags=33%, list=8%, signal=36%
GO REGULATION OF DENDRITE DEVELOPMENT	78	0.473588	1.914611	0	0.030	0.791	1350	tags=46%, list=21%, signal=58%
GO ACTIN BASED CELL PROJECTION	66	0.501081	1.915315	0	0.030	0.788	1355	tags=48%, list=21%, signal=61%
GO NEGATIVE REGULATION OF PROTEIN COMPLEX DISASSEMBLY	72	0.483544	1.917603	0	0.030	0.781	1087	tags=40%, list=17%, signal=48%
GO CELL CELL JUNCTION ASSEMBLY	24	0.600356	1.915346	0	0.030	0.788	915	tags=38%, list=14%, signal=44%
GO ACTIVE TRANSMEMBRANE TRANSPORTER ACTIVITY	98	0.450386	1.915816	0	0.031	0.786	1181	tags=36%, list=18%, signal=43%
GO REGULATION OF RECEPTOR MEDIATED ENDOCYTOSIS	47	0.525838	1.908889	0	0.031	0.813	1256	tags=45%, list=19%, signal=55%
GO REGULATION OF NERVOUS SYSTEM DEVELOPMENT	345	0.383545	1.896519	0	0.031	0.852	1354	tags=34%, list=21%, signal=41%
GO SISTER CHROMATID COHESION	43	0.535656	1.897244	0	0.031	0.851	1436	tags=53%, list=22%, signal=68%

GO CARDIAC MUSCLE CELL ACTION POTENTIAL	16	0.690869	1.895691	0	0.032	0.853	617	tags=56%, list=10%, signal=62%
GO POSITIVE REGULATION OF LIPID KINASE ACTIVITY	11	0.738196	1.90744	0.002105	0.032	0.815	1256	tags=64%, list=19%, signal=79%
GO RECEPTOR MEDIATED ENDOCYTOSIS	73	0.478608	1.897986	0	0.032	0.848	1443	tags=40%, list=22%, signal=51%
GO REGULATION OF CALCIUM ION IMPORT	39	0.535104	1.898495	0.002037	0.032	0.848	763	tags=38%, list=12%, signal=43%
GO DNA HELICASE ACTIVITY	20	0.629054	1.898725	0.00202	0.032	0.846	1087	tags=50%, list=17%, signal=60%
GO REGULATION OF CATION TRANSMEMBRANE TRANSPORT	90	0.458767	1.89944	0	0.032	0.846	950	tags=32%, list=15%, signal=37%
GO REGULATION OF SHORT TERM NEURONAL SYNAPTIC PLASTICITY	11	0.749067	1.901794	0.001984	0.032	0.837	647	tags=64%, list=10%, signal=71%
GO RHO GUANYL NUCLEOTIDE EXCHANGE FACTOR ACTIVITY	26	0.587186	1.902537	0	0.032	0.836	1389	tags=58%, list=21%, signal=73%
GO REGULATION OF CELL SUBSTRATE ADHESION	65	0.488571	1.903995	0	0.032	0.827	1482	tags=48%, list=23%, signal=61%
GO CYTOPLASMIC REGION	140	0.42624	1.892946	0	0.032	0.862	1200	tags=40%, list=19%, signal=48%
REACTOME L1CAM INTERACTIONS	50	0.50598	1.899681	0	0.032	0.845	838	tags=42%, list=13%, signal=48%
GO CORTICAL CYTOSKELETON	41	0.529493	1.892238	0	0.032	0.865	1069	tags=44%, list=17%, signal=52%
REACTOME CREB PHOSPHORYLATION THROUGH THE ACTIVATION OF RAS	18	0.652252	1.90289	0	0.032	0.836	988	tags=56%, list=15%, signal=65%
GO HEART PROCESS	35	0.549562	1.904596	0	0.033	0.826	639	tags=34%, list=10%, signal=38%
GO MOVEMENT	430	0.375008	1.900071	0	0.033	0.843	1540	tags=37%,

OF CELL OR SUBCELLULAR COMPONENT								list=24%, signal=46%
REACTOME RAS ACTIVATION UOPN CA2 INFUX THROUGH NMDA RECEPTOR	11	0.736446	1.885011	0.004024	0.035	0.891	1324	tags=82%, list=20%, signal=103%
GO EMBRYONIC ORGAN DEVELOPMENT	103	0.444086	1.885736	0	0.035	0.888	1150	tags=35%, list=18%, signal=42%
GO REGULATION OF GTPASE ACTIVITY	283	0.383026	1.876358	0	0.035	0.918	1681	tags=42%, list=26%, signal=55%
GO BASOLATERAL PLASMA MEMBRANE	60	0.487547	1.873896	0	0.035	0.923	1069	tags=38%, list=17%, signal=45%
GO REGULATION OF PHOSPHATIDYLINOSITOL 3 KINASE ACTIVITY	12	0.72453	1.881358	0.002114	0.035	0.903	1256	tags=58%, list=19%, signal=72%
GO INTERMEDIATE FILAMENT CYTOSKELETON	41	0.528197	1.875349	0	0.035	0.919	1123	tags=37%, list=17%, signal=44%
REACTOME GOLGI ASSOCIATED VESICLE BIOGENESIS	34	0.549895	1.878802	0	0.035	0.912	567	tags=38%, list=9%, signal=42%
GO INTERMEDIATE FILAMENT	22	0.619855	1.877608	0.004032	0.035	0.914	1481	tags=55%, list=23%, signal=70%
REACTOME MEIOTIC SYNAPSIS	15	0.682752	1.874395	0	0.035	0.922	531	tags=40%, list=8%, signal=43%
GO POSITIVE REGULATION OF DENDRITE DEVELOPMENT	43	0.519289	1.876385	0.002242	0.035	0.917	1420	tags=47%, list=22%, signal=59%
GO ACTION POTENTIAL	42	0.521311	1.879769	0	0.035	0.909	617	tags=33%, list=10%, signal=37%
GO CELL CORTEX	104	0.441426	1.881562	0	0.035	0.902	1200	tags=39%, list=19%, signal=48%
GO PURINE NTP DEPENDENT HELICASE ACTIVITY	53	0.506809	1.878831	0	0.035	0.912	1449	tags=47%, list=22%, signal=60%
GO POSITIVE	141	0.425096	1.88188	0	0.035	0.902	1057	tags=32%,

REGULATION OF NEURON PROJECTION DEVELOPMENT								list=16%, signal=37%
GO EMBRYONIC PLACENTA DEVELOPMENT	25	0.595116	1.880024	0	0.035	0.908	633	tags=36%, list=10%, signal=40%
GO CLATHRIN ADAPTOR COMPLEX	19	0.6369	1.869829	0.002174	0.036	0.935	850	tags=53%, list=13%, signal=60%
GO ANCHORING JUNCTION	224	0.390779	1.867374	0	0.037	0.939	922	tags=25%, list=14%, signal=29%
GO ACTIVE ION TRANSMEMBRANE TRANSPORTER ACTIVITY	57	0.498001	1.866645	0	0.037	0.942	829	tags=33%, list=13%, signal=38%
GO SECOND MESSENGER MEDIATED SIGNALING	56	0.490261	1.86393	0	0.037	0.950	1032	tags=39%, list=16%, signal=46%
GO POSITIVE REGULATION OF NEURON DIFFERENTIATION	160	0.410731	1.864714	0	0.037	0.948	1900	tags=50%, list=29%, signal=69%
GO REGULATION OF CELL MATRIX ADHESION	38	0.533121	1.862587	0.002183	0.038	0.952	1482	tags=55%, list=23%, signal=71%
GO REGULATION OF NEURONAL SYNAPTIC PLASTICITY	37	0.542675	1.859471	0.002151	0.039	0.962	1015	tags=41%, list=16%, signal=48%
GO REGULATION OF CARDIAC MUSCLE CONTRACTION BY REGULATION OF THE RELEASE OF SEQUESTERED CALCIUM ION	10	0.747411	1.857853	0	0.039	0.964	492	tags=60%, list=8%, signal=65%
GO NEGATIVE REGULATION OF DNA REPLICATION	26	0.571792	1.858479	0	0.039	0.963	1459	tags=50%, list=23%, signal=64%
REACTOME TRAFFICKING OF GLUR2 CONTAINING AMPA RECEPTORS	14	0.688776	1.856592	0	0.039	0.967	1286	tags=64%, list=20%, signal=80%
GO REGULATION OF	31	0.550688	1.853819	0.006667	0.040	0.972	1324	tags=52%, list=20%,

POSTSYNAPTIC MEMBRANE POTENTIAL								signal=65%
GO GLYCOPROTEIN BINDING	30	0.558709	1.854154	0.002137	0.040	0.971	957	tags=37%, list=15%, signal=43%
GO MITOTIC SPINDLE ORGANIZATION	28	0.566633	1.851469	0	0.041	0.973	836	tags=39%, list=13%, signal=45%
GO SUBSTRATE ADHESION DEPENDENT CELL SPREADING	10	0.756523	1.851984	0	0.041	0.973	705	tags=60%, list=11%, signal=67%
REACTOME AXON GUIDANCE	124	0.421768	1.848728	0	0.041	0.974	866	tags=32%, list=13%, signal=37%
GO REGULATION OF TRANSPORTER ACTIVITY	102	0.432369	1.849587	0	0.041	0.974	950	tags=29%, list=15%, signal=34%
GO PLASMA MEMBRANE REGION	357	0.366852	1.848729	0	0.041	0.974	1324	tags=35%, list=20%, signal=41%
GO MEMBRANE REGION	442	0.361765	1.847556	0	0.041	0.975	1131	tags=29%, list=17%, signal=33%
REACTOME TRANS GOLGI NETWORK VESICLE BUDDING	39	0.520438	1.844108	0.004098	0.042	0.981	567	tags=33%, list=9%, signal=36%
GO GROWTH FACTOR BINDING	28	0.565663	1.838549	0	0.042	0.983	1232	tags=50%, list=19%, signal=61%
REACTOME PROCESSING OF CAPPED INTRON CONTAINING PRE MRNA	111	0.432367	1.844329	0	0.042	0.981	1536	tags=45%, list=24%, signal=58%
GO REGULATION OF SYNAPTIC TRANSMISSION GLUTAMATERGIC	31	0.543144	1.838884	0.004329	0.042	0.983	1029	tags=45%, list=16%, signal=53%
GO T TUBULE	22	0.608663	1.841903	0.002146	0.043	0.982	617	tags=45%, list=10%, signal=50%
REACTOME NRAGE SIGNALS DEATH THROUGH JNK	24	0.577602	1.841186	0.002151	0.043	0.982	1127	tags=50%, list=17%, signal=60%
GO CATALYTIC STEP 2 SPLICEOSOME	70	0.465218	1.842335	0	0.043	0.982	1375	tags=46%, list=21%, signal=57%
GO REGULATION	32	0.543377	1.838907	0.002	0.043	0.983	575	tags=38%,

OF RELEASE OF SEQUESTERED CALCIUM ION INTO CYTOSOL				222				list=9%, signal=41%
GO ACTIN MEDIATED CELL CONTRACTION	29	0.554403	1.839925	0	0.043	0.982	617	tags=34%, list=10%, signal=38%
GO REGULATION OF MUSCLE ADAPTATION	29	0.551945	1.839241	0.004202	0.043	0.982	834	tags=38%, list=13%, signal=43%
GO RNA HELICASE ACTIVITY	40	0.522129	1.833714	0.00432	0.045	0.989	1147	tags=45%, list=18%, signal=54%
GO NEURON PROJECTION GUIDANCE	89	0.448817	1.832358	0	0.045	0.989	580	tags=22%, list=9%, signal=24%
KEGG TYPE II DIABETES MELLITUS	20	0.614136	1.831237	0.002058	0.045	0.990	1503	tags=55%, list=23%, signal=71%
GO NITRIC OXIDE SYNTHASE BINDING	10	0.749418	1.829303	0.004175	0.045	0.992	1518	tags=90%, list=23%, signal=117%
GO STRUCTURAL CONSTITUENT OF CYTOSKELETON	49	0.495823	1.825045	0	0.046	0.992	1123	tags=43%, list=17%, signal=51%
GO CELL MORPHOGENESIS INVOLVED IN DIFFERENTIATION	212	0.388741	1.825798	0	0.046	0.992	1378	tags=36%, list=21%, signal=44%
GO ADP BINDING	21	0.606584	1.826042	0.002079	0.047	0.992	392	tags=29%, list=6%, signal=30%
GO REGULATION OF AXONOGENESIS	90	0.43773	1.822226	0	0.048	0.994	1378	tags=39%, list=21%, signal=49%
GO FILOPODIUM	46	0.498733	1.816064	0	0.048	0.994	1355	tags=50%, list=21%, signal=63%
GO REGULATION OF ACTION POTENTIAL	15	0.657098	1.820485	0.006276	0.048	0.994	760	tags=47%, list=12%, signal=53%
GO NEGATIVE REGULATION OF ACTIN FILAMENT DEPOLYMERIZATION	15	0.646359	1.820754	0.008316	0.048	0.994	1032	tags=53%, list=16%, signal=63%
GO NEGATIVE REGULATION OF CYTOSKELETON ORGANIZATION	99	0.422904	1.817608	0.002165	0.048	0.994	838	tags=31%, list=13%, signal=35%
GO PLACENTA	38	0.520266	1.816088	0	0.048	0.994	866	tags=34%,

DEVELOPMENT								list=13%, signal=39%
GO NEUROMUSCULAR JUNCTION DEVELOPMENT	19	0.622737	1.819443	0	0.048	0.994	324	tags=26%, list=5%, signal=28%
GO COATED MEMBRANE	56	0.477668	1.81482	0.002141	0.048	0.994	946	tags=39%, list=15%, signal=46%
GO MODULATION OF SYNAPTIC TRANSMISSION	190	0.391963	1.817674	0	0.048	0.994	1261	tags=32%, list=19%, signal=39%
GO POSITIVE REGULATION OF NERVOUS SYSTEM DEVELOPMENT	211	0.384718	1.816327	0	0.048	0.994	1902	tags=47%, list=29%, signal=64%
GO SODIUM CHANNEL REGULATOR ACTIVITY	12	0.713295	1.817864	0.002132	0.049	0.994	799	tags=50%, list=12%, signal=57%
REACTOME RETROGRADE NEUROTROPHIN SIGNALLING	10	0.719222	1.813374	0.004193	0.049	0.994	544	tags=50%, list=8%, signal=54%

Table S6 ***(pages 142-153).*** **List of gene sets significantly upregulated (FDR<0.05) in Sst^{+}neurons of defeated animals.** Gene sets are ordered by FDR. See caption of Table S2 for the meaning of each column

Name	Score	Rank	Feature P	Log Fold Change	FDR (BH)	Q Value	defeated Mean	defeated Std	sensory Mean	sensory Std
4932438A13Rik	3.321	390	0.025	0.548	0.504	0.385	7.879	0.288	7.331	0.139
Actn1	2.871	569	0.037	0.620	0.507	0.387	7.736	0.300	7.116	0.270
Actn4	3.105	470	0.035	0.427	0.507	0.387	7.928	0.168	7.501	0.189
Add3	3.452	358	0.034	0.430	0.507	0.387	7.488	0.242	7.058	0.052
Ank2	6.749	20	0.003	0.605	0.488	0.373	9.033	0.166	8.428	0.058
Ank3	4.012	205	0.010	0.533	0.488	0.373	8.859	0.206	8.326	0.145
Ap2a1	3.716	273	0.033	0.314	0.507	0.387	8.745	0.077	8.431	0.130
Ap3b1	4.129	185	0.028	0.441	0.507	0.387	8.560	0.089	8.119	0.168
Arhgap21	3.693	285	0.014	0.443	0.488	0.373	8.927	0.186	8.483	0.131
Arhgap42	2.645	733	0.046	0.448	0.513	0.392	7.208	0.258	6.759	0.191
Arhgef9	3.540	328	0.034	0.326	0.507	0.387	10.116	0.089	9.790	0.140
Arid5b	6.977	16	0.004	0.297	0.488	0.373	8.011	0.042	7.714	0.064
Arpp21	2.906	550	0.037	0.387	0.507	0.387	7.008	0.228	6.621	0.119
Ascc3	4.520	123	0.007	0.429	0.488	0.373	7.676	0.138	7.247	0.113
Atp8a1	3.179	442	0.028	0.369	0.507	0.387	8.378	0.202	8.009	0.098
Birc6	4.384	144	0.009	0.501	0.488	0.373	7.617	0.155	7.115	0.146
Bptf	3.725	269	0.022	0.278	0.504	0.385	9.000	0.140	8.722	0.045
Bsn	3.745	265	0.013	0.555	0.488	0.373	7.134	0.234	6.578	0.158
C230081A13Rik	5.666	48	0.002	0.533	0.488	0.373	8.581	0.146	8.048	0.103
Cacna1e	3.903	234	0.015	0.522	0.488	0.373	8.299	0.172	7.777	0.177
Clip1	4.496	126	0.006	0.423	0.488	0.373	8.906	0.143	8.483	0.106
Cx3cr1	5.489	60	0.003	0.276	0.488	0.373	7.294	0.071	7.018	0.062
Ddx10	3.787	261	0.015	0.273	0.488	0.373	7.358	0.097	7.085	0.092
Ddx42	3.551	320	0.028	0.282	0.507	0.387	7.750	0.086	7.469	0.115
Ddx46	5.351	65	0.017	0.568	0.488	0.373	9.539	0.080	8.971	0.170
Dhx15	3.371	378	0.023	0.308	0.504	0.385	9.165	0.123	8.857	0.118
Dhx9	6.083	31	0.002	0.289	0.488	0.373	9.940	0.074	9.651	0.052
Dido1	2.851	582	0.036	0.278	0.507	0.387	7.816	0.148	7.538	0.111
Dock4	2.699	691	0.043	0.421	0.507	0.387	8.245	0.235	7.825	0.177
Dock9	3.802	256	0.013	0.363	0.488	0.373	8.073	0.155	7.710	0.097
Dst	7.756	7	0.003	0.667	0.488	0.373	8.717	0.169	8.050	0.029
Dync1h1	4.980	91	0.008	1.235	0.488	0.373	10.164	0.459	8.929	0.163
Eif4g1	4.966	94	0.006	0.549	0.488	0.373	8.985	0.197	8.436	0.087
Enc1	2.682	699	0.046	0.572	0.515	0.394	10.911	0.296	10.339	0.266

Epas1	4.277	159	0.022	1.137	0.504	0.385	7.282	0.527	6.146	0.062
Eprs	3.303	395	0.022	0.386	0.502	0.384	8.278	0.187	7.892	0.121
Ewsr1	4.197	172	0.010	0.278	0.488	0.373	7.922	0.114	7.644	0.059
Fn1	3.961	220	0.024	1.237	0.504	0.385	6.600	0.611	5.363	0.113
Fryl	2.768	644	0.042	0.457	0.507	0.387	7.343	0.228	6.886	0.207
Gfra2	3.025	498	0.036	0.343	0.507	0.387	9.213	0.143	8.871	0.152
Gria2	3.573	315	0.034	0.311	0.507	0.387	10.101	0.172	9.790	0.025
Gria3	3.676	290	0.015	0.334	0.488	0.373	9.916	0.149	9.582	0.090
Grm3	3.494	345	0.026	0.278	0.504	0.385	8.132	0.147	7.854	0.053
Helz	4.968	93	0.005	0.274	0.488	0.373	8.421	0.079	8.147	0.067
Herc1	3.168	448	0.042	0.559	0.507	0.387	8.776	0.341	8.217	0.078
Herc2	3.325	389	0.021	0.562	0.500	0.382	8.288	0.248	7.726	0.199
Hmgcs1	2.866	573	0.037	0.289	0.507	0.387	10.159	0.168	9.870	0.097
Hspa2	2.581	792	0.050	0.310	0.518	0.396	7.701	0.177	7.391	0.141
Igfbp7	3.645	302	0.015	0.544	0.488	0.373	6.868	0.245	6.324	0.148
Jak1	4.164	178	0.016	0.301	0.488	0.373	9.739	0.136	9.438	0.043
Kif1b	4.983	90	0.014	0.437	0.488	0.373	10.094	0.173	9.657	0.023
Ktn1	3.295	402	0.039	0.338	0.507	0.387	7.801	0.104	7.462	0.153
Lmo7	3.127	465	0.026	0.795	0.506	0.386	7.492	0.404	6.697	0.268
Lrp1	5.393	62	0.008	0.374	0.488	0.373	7.509	0.133	7.135	0.033
Lrpprc	3.698	283	0.015	0.346	0.488	0.373	8.493	0.133	8.147	0.114
Lrrc6	3.137	461	0.028	0.649	0.507	0.387	7.212	0.285	6.562	0.260
Lrrc7	2.706	683	0.049	0.314	0.517	0.395	9.504	0.206	9.190	0.093
Macf1	5.667	47	0.004	0.720	0.488	0.373	8.361	0.163	7.641	0.168
Mapk1	3.414	371	0.025	0.271	0.504	0.385	10.802	0.098	10.530	0.108
Mapk8ip2	3.973	214	0.012	0.540	0.488	0.373	8.855	0.184	8.315	0.173
Mfsd2a	3.905	233	0.016	1.009	0.488	0.373	6.749	0.466	5.740	0.193
Mical3	3.665	294	0.018	0.561	0.488	0.373	7.645	0.202	7.084	0.199
Mll1	6.011	33	0.003	0.325	0.488	0.373	8.511	0.068	8.186	0.073
Mon2	2.828	599	0.038	0.374	0.507	0.387	8.032	0.217	7.657	0.132
Mpdz	3.707	279	0.017	0.545	0.488	0.373	7.022	0.260	6.477	0.120
Mtap1b	3.742	266	0.029	0.404	0.507	0.387	11.793	0.212	11.389	0.037
Myh10	2.865	576	0.044	0.421	0.510	0.390	9.234	0.266	8.813	0.108
Myo18a	2.848	583	0.044	0.466	0.510	0.390	7.245	0.202	6.779	0.223
Nedd4	6.809	18	0.001	0.281	0.488	0.373	10.460	0.064	10.178	0.045
Nol6	4.501	125	0.012	0.318	0.488	0.373	8.877	0.082	8.559	0.100
Nrcam	3.536	330	0.037	0.315	0.507	0.387	8.319	0.177	8.003	0.018
Ogt	3.230	423	0.047	0.565	0.517	0.395	8.743	0.161	8.178	0.269
Pak7	3.969	217	0.013	0.381	0.488	0.373	7.610	0.129	7.229	0.123
Pclo	2.761	649	0.040	0.548	0.507	0.387	8.293	0.312	7.745	0.213

Pfkl	2.981	516	0.032	0.308	0.507	0.387	7.423	0.151	7.114	0.123
Pfkp	5.761	43	0.002	0.343	0.488	0.373	9.631	0.096	9.289	0.061
Pls3	3.815	250	0.020	0.322	0.489	0.374	9.134	0.156	8.812	0.055
Plxna4	3.912	231	0.025	0.452	0.504	0.385	7.980	0.115	7.528	0.173
Prpf40a	6.793	19	0.001	0.371	0.488	0.373	8.328	0.074	7.957	0.069
Prpf8	3.262	414	0.035	0.406	0.507	0.387	10.306	0.138	9.900	0.180
Rps6ka5	3.273	411	0.029	0.322	0.507	0.387	6.861	0.121	6.539	0.134
Ryr2	5.528	58	0.003	0.867	0.488	0.373	8.763	0.222	7.896	0.192
Setd2	3.648	301	0.016	0.276	0.488	0.373	8.430	0.106	8.154	0.093
Sez6	3.453	357	0.025	0.436	0.504	0.385	7.362	0.229	6.926	0.092
Slc1a4	2.843	587	0.041	0.357	0.507	0.387	6.814	0.165	6.457	0.164
Slc4a4	3.762	264	0.033	0.407	0.507	0.387	7.345	0.096	6.938	0.168
Slc6a6	3.953	222	0.011	0.580	0.488	0.373	8.211	0.217	7.631	0.171
Slc8a2	2.983	514	0.049	0.390	0.517	0.395	7.161	0.252	6.771	0.059
Slit3	2.715	674	0.043	0.276	0.507	0.387	6.915	0.149	6.639	0.120
Smc3	3.722	271	0.016	0.448	0.488	0.373	9.695	0.162	9.247	0.155
Snrnp200	6.978	15	0.001	0.429	0.488	0.373	9.035	0.107	8.607	0.052
Spna2	3.543	326	0.036	1.014	0.507	0.387	10.838	0.267	9.824	0.439
Spnb2	3.486	349	0.038	0.924	0.507	0.387	9.776	0.245	8.851	0.407
Srrm2	9.684	3	0.000	0.516	0.488	0.373	11.652	0.094	11.135	0.044
Syn3	3.866	245	0.012	0.504	0.488	0.373	7.280	0.190	6.776	0.155
Syne1	2.804	613	0.049	0.816	0.517	0.395	7.696	0.346	6.880	0.405
Tbcd	2.892	556	0.042	0.286	0.507	0.387	11.318	0.123	11.032	0.134
Tjp1	3.866	246	0.018	0.574	0.488	0.373	8.729	0.179	8.155	0.205
Tnr	6.461	24	0.001	0.475	0.488	0.373	8.084	0.114	7.609	0.080
Tro	3.507	342	0.027	0.404	0.507	0.387	8.204	0.215	7.800	0.071
Ubr4	4.061	192	0.010	0.477	0.488	0.373	7.978	0.187	7.501	0.123
Unc13a	8.144	6	0.002	0.601	0.488	0.373	9.582	0.081	8.981	0.107
Usp24	3.418	370	0.024	0.315	0.504	0.385	7.298	0.164	6.983	0.072
Vps13a	3.493	346	0.036	0.640	0.507	0.387	7.301	0.362	6.660	0.053
Vps13c	4.670	111	0.012	0.574	0.488	0.373	7.366	0.232	6.792	0.070
Vps16	5.003	86	0.006	0.279	0.488	0.373	8.415	0.098	8.136	0.046
Wars	3.902	235	0.020	0.347	0.489	0.374	9.132	0.167	8.784	0.053
Wdr7	3.518	338	0.034	0.351	0.507	0.387	10.023	0.098	9.672	0.151
Ywhag	3.207	433	0.041	0.347	0.507	0.387	12.008	0.112	11.661	0.161

Table S7 ***(pages 154-156).*** **Statistical properties of genes leading the enrichment of upregulated gene sets in Sst$^+$ neurons of defeated animals.** Only genes with $p<0.05$ and LogFC>0.27 were considered and are listed. Genes are listed in alphabetical order. See caption of Table S1 for meaning of each column.

BIOCARTA_PTDINS_PATHWAY_signal
GO_ACTIN_BASED_CELL_PROJECTION_signal
GO_ACTIN_BINDING_signal
GO_ACTIN_FILAMENT_BASED_MOVEMENT_signal
GO_ACTIN_FILAMENT_BINDING_signal
GO_ACTIN_MEDIATED_CELL_CONTRACTION_signal
GO_ACTION_POTENTIAL_signal
GO_ACTIVE_ION_TRANSMEMBRANE_TRANSPORTER_ACTIVITY_signal
GO_ACTIVE_TRANSMEMBRANE_TRANSPORTER_ACTIVITY_signal
GO_ADP_BINDING_signal
GO_ANCHORING_JUNCTION_signal
GO_ANTIGEN_PROCESSING_AND_PRESENTATION_OF_PEPTIDE_ANTIGEN_V
IA_MHC_CLASS_II_signal
GO_ANTIGEN_PROCESSING_AND_PRESENTATION_OF_PEPTIDE_OR_POLYSA
CCHARIDE_ANTIGEN_VIA_MHC_CLASS_II_signal
GO_AP_TYPE_MEMBRANE_COAT_ADAPTOR_COMPLEX_signal
GO_ATPASE_ACTIVITY_COUPLED_signal
GO_ATPASE_ACTIVITY_COUPLED_TO_MOVEMENT_OF_SUBSTANCES_signal
GO_ATPASE_ACTIVITY_signal
GO_ATPASE_COUPLED_ION_TRANSMEMBRANE_TRANSPORTER_ACTIVITY_si
gnal
GO_AXON_INITIAL_SEGMENT_signal
GO_BASOLATERAL_PLASMA_MEMBRANE_signal
GO_CALMODULIN_BINDING_signal
GO_CARDIAC_MUSCLE_CELL_ACTION_POTENTIAL_signal
GO_CARDIAC_MUSCLE_CELL_CONTRACTION_signal
GO_CATALYTIC_STEP_2_SPLICEOSOME_signal
GO_CATION_TRANSPORTING_ATPASE_ACTIVITY_signal
GO_CELL_CELL_CONTACT_ZONE_signal
GO_CELL_CELL_JUNCTION_ASSEMBLY_signal
GO_CELL_CORTEX_signal
GO_CELL_JUNCTION_ASSEMBLY_signal
GO_CELL_JUNCTION_ORGANIZATION_signal
GO_CELL_MORPHOGENESIS_INVOLVED_IN_DIFFERENTIATION_signal
GO_CELL_SUBSTRATE_ADHESION_signal
GO_CELL_SUBSTRATE_JUNCTION_ASSEMBLY_signal
GO_CELLULAR_RESPONSE_TO_ALCOHOL_signal
GO_CLATHRIN_ADAPTOR_COMPLEX_signal
GO_CLATHRIN_COAT_OF_COATED_PIT_signal
GO_CLATHRIN_COAT_signal
GO_CLATHRIN_COATED_ENDOCYTIC_VESICLE_MEMBRANE_signal
GO_CLATHRIN_COATED_ENDOCYTIC_VESICLE_signal
GO_CLATHRIN_COATED_VESICLE_MEMBRANE_signal
GO_CLATHRIN_COATED_VESICLE_signal
GO_COATED_MEMBRANE_signal
GO_COATED_PIT_signal
GO_CONDENSED_NUCLEAR_CHROMOSOME_signal
GO_CORTICAL_CYTOSKELETON_signal
GO_CYTOPLASMIC_REGION_signal
4932438A13Rik
Actn1
Actn4
Add3
Ank2
Ank3
Ap2a1
Ap3b1
Arhgap21
Arhgap42
Arhgef9
Arid5b
Arpp21
Ascc3
Atp8a1
Birc6
Bptf
Bsn
C23 81A13Rik
Cacna1e
Clip1
Cx3cr1
Ddx1
Ddx42
Ddx46
Dhx15
Dhx9
Dido1
Dock4
Dock9
Dst
Dync1h1
Eif4g1
Enc1
Epas1
Eprs
Ewsr1
Fn1
Fryl
Gfra2
Gria2
Gria3
Grm3
Helz
Herc1
Herc2
Hmgcs1
Hspa2
Igfbp7
Jak1
Kif1b
Ktn1
Lmo7
Lrp1
Lrpprc

GO_DNA_HELICASE_ACTIVITY_signal
GO_EMBRYONIC_ORGAN_DEVELOPMENT_signal
GO_EMBRYONIC_PLACENTA_DEVELOPMENT_signal
GO_ENDOCYTIC_VESICLE_MEMBRANE_signal
GO_EXCITATORY_POSTSYNAPTIC_POTENTIAL_signal
GO_EXCITATORY_SYNAPSE_signal
GO_EXTRACELLULAR_MATRIX_COMPONENT_signal
GO_FILOPODIUM_signal
GO_GOLGI_TO_ENDOSOME_TRANSPORT_signal
GO_GOLGI_TO_VACUOLE_TRANSPORT_signal
GO_GROWTH_FACTOR_BINDING_signal
GO_HEART_PROCESS_signal
GO_HELICASE_ACTIVITY_signal
GO_INTERCALATED_DISC_signal
GO_INTERMEDIATE_FILAMENT_CYTOSKELETON_signal
GO_INTERMEDIATE_FILAMENT_signal
GO_LIGASE_ACTIVITY_FORMING_CARBON_OXYGEN_BONDS_signal
GO_MEMBRANE_REGION_signal
GO_MITOTIC_SPINDLE_ORGANIZATION_signal
GO_MODULATION_OF_SYNAPTIC_TRANSMISSION_signal
GO_MOVEMENT_OF_CELL_OR_SUBCELLULAR_COMPONENT_signal
GO_MYELIN_SHEATH_signal
GO_NAD_METABOLIC_PROCESS_signal
GO_NADH_METABOLIC_PROCESS_signal
GO_NEGATIVE_REGULATION_OF_ACTIN_FILAMENT_DEPOLYMERIZATION_signal
GO_NEGATIVE_REGULATION_OF_CYTOSKELETON_ORGANIZATION_signal
GO_NEGATIVE_REGULATION_OF_DNA_REPLICATION_signal
GO_NEGATIVE_REGULATION_OF_PROTEIN_COMPLEX_DISASSEMBLY_signal
GO_NEUROMUSCULAR_JUNCTION_DEVELOPMENT_signal
GO_NEURON_PROJECTION_GUIDANCE_signal
GO_NEURONAL_POSTSYNAPTIC_DENSITY_signal
GO_PLACENTA_DEVELOPMENT_signal
GO_PLASMA_MEMBRANE_REGION_signal
GO_POSITIVE_REGULATION_OF_CELL_GROWTH_signal
GO_POSITIVE_REGULATION_OF_CELL_PROJECTION_ORGANIZATION_signal
GO_POSITIVE_REGULATION_OF_DENDRITE_DEVELOPMENT_signal
GO_POSITIVE_REGULATION_OF_NERVOUS_SYSTEM_DEVELOPMENT_signal
GO_POSITIVE_REGULATION_OF_NEURON_DIFFERENTIATION_signal
GO_POSITIVE_REGULATION_OF_NEURON_PROJECTION_DEVELOPMENT_signal
GO_POSITIVE_REGULATION_OF_TRANSPORTER_ACTIVITY_signal
GO_POSTSYNAPSE_signal
GO_PRESYNAPTIC_ACTIVE_ZONE_signal
GO_PURINE_NTP_DEPENDENT_HELICASE_ACTIVITY_signal
GO_RAS_GUANYL_NUCLEOTIDE_EXCHANGE_FACTOR_ACTIVITY_signal
GO_RECEPTOR_MEDIATED_ENDOCYTOSIS_signal
4932438A13Rik
Actn1
Actn4
Add3
Ank2
Ank3
Ap2a1
Ap3b1
Arhgap21
Arhgap42
Arhgef9
Arid5b
Arpp21
Ascc3
Atp8a1
Birc6
Bptf
Bsn
C23_81A13Rik
Cacna1e
Clip1
Cx3cr1
Ddx1
Ddx42
Ddx46
Dhx15
Dhx9
Dido1
Dock4
Dock9
Dst
Dync1h1
Eif4g1
Enc1
Epas1
Eprs
Ewsr1
Fn1
Fryl
Gfra2
Gria2
Gria3
Grm3
Helz
Herc1
Herc2
Hmgcs1
Hspa2
Igfbp7
Jak1
Kif1b
Ktn1
Lmo7
Lrp1
Lrpprc

GO_REGULATION_OF_ACTION_POTENTIAL_signal
GO_REGULATION_OF_AXONOGENESIS_signal
GO_REGULATION_OF_CALCIUM_ION_IMPORT_signal
GO_REGULATION_OF_CARDIAC_MUSCLE_CONTRACTION_BY_REGULATION_OF_THE_RELEASE_OF_SEQUESTERED_CALCIUM_ION_signal
GO_REGULATION_OF_CATION_TRANSMEMBRANE_TRANSPORT_signal
GO_REGULATION_OF_CELL_GROWTH_signal
GO_REGULATION_OF_CELL_MATRIX_ADHESION_signal
GO_REGULATION_OF_CELL_PROJECTION_ORGANIZATION_signal
GO_REGULATION_OF_CELL_SIZE_signal
GO_REGULATION_OF_CELL_SUBSTRATE_ADHESION_signal
GO_REGULATION_OF_DENDRITE_DEVELOPMENT_signal
GO_REGULATION_OF_EXTENT_OF_CELL_GROWTH_signal
GO_REGULATION_OF_GTPASE_ACTIVITY_signal
GO_REGULATION_OF_MUSCLE_ADAPTATION_signal
GO_REGULATION_OF_NERVOUS_SYSTEM_DEVELOPMENT_signal
GO_REGULATION_OF_NEURON_DIFFERENTIATION_signal
GO_REGULATION_OF_NEURON_PROJECTION_DEVELOPMENT_signal
GO_REGULATION_OF_NEURONAL_SYNAPTIC_PLASTICITY_signal
GO_REGULATION_OF_POSTSYNAPTIC_MEMBRANE_POTENTIAL_signal
GO_REGULATION_OF_RELEASE_OF_SEQUESTERED_CALCIUM_ION_INTO_CYTOSOL_signal
GO_REGULATION_OF_RHO_PROTEIN_SIGNAL_TRANSDUCTION_signal
GO_REGULATION_OF_SHORT_TERM_NEURONAL_SYNAPTIC_PLASTICITY_signal
GO_REGULATION_OF_SMOOTH_MUSCLE_CELL_MIGRATION_signal
GO_REGULATION_OF_SODIUM_ION_TRANSMEMBRANE_TRANSPORT_signal
GO_REGULATION_OF_SODIUM_ION_TRANSMEMBRANE_TRANSPORTER_ACTIVITY_signal
GO_REGULATION_OF_SODIUM_ION_TRANSPORT_signal
GO_REGULATION_OF_SYNAPSE_STRUCTURE_OR_ACTIVITY_signal
GO_REGULATION_OF_SYNAPTIC_PLASTICITY_signal
GO_REGULATION_OF_SYNAPTIC_TRANSMISSION_GLUTAMATERGIC_signal
GO_REGULATION_OF_TRANSPORTER_ACTIVITY_signal
GO_RHO_GUANYL_NUCLEOTIDE_EXCHANGE_FACTOR_ACTIVITY_signal
GO_RNA_HELICASE_ACTIVITY_signal
GO_SECOND_MESSENGER_MEDIATED_SIGNALING_signal
GO_SISTER_CHROMATID_COHESION_signal
GO_SODIUM_CHANNEL_REGULATOR_ACTIVITY_signal
GO_STRIATED_MUSCLE_CONTRACTION_signal
GO_STRUCTURAL_CONSTITUENT_OF_CYTOSKELETON_signal
GO_SUBSTRATE_ADHESION_DEPENDENT_CELL_SPREADING_signal
GO_SYNAPSE_PART_signal
4932438A13Rik
Actn1
Actn4
Add3
Ank2
Ank3
Ap2a1
Ap3b1
Arhgap21
Arhgap42
Arhgef9
Arid5b
Arpp21
Ascc3
Atp8a1
Birc6
Bptf
Bsn
C23 81A13Rik
Cacna1e
Clip1
Cx3cr1
Ddx1
Ddx42
Ddx46
Dhx15
Dhx9
Dido1
Dock4
Dock9
Dst
Dync1h1
Eif4g1
Enc1
Epas1
Eprs
Ewsr1
Fn1
Fryl
Gfra2
Gria2
Gria3
Grm3
Helz
Herc1
Herc2
Hmgcs1
Hspa2
Igfbp7
Jak1
Kif1b
Ktn1
Lmo7
Lrp1
Lrpprc

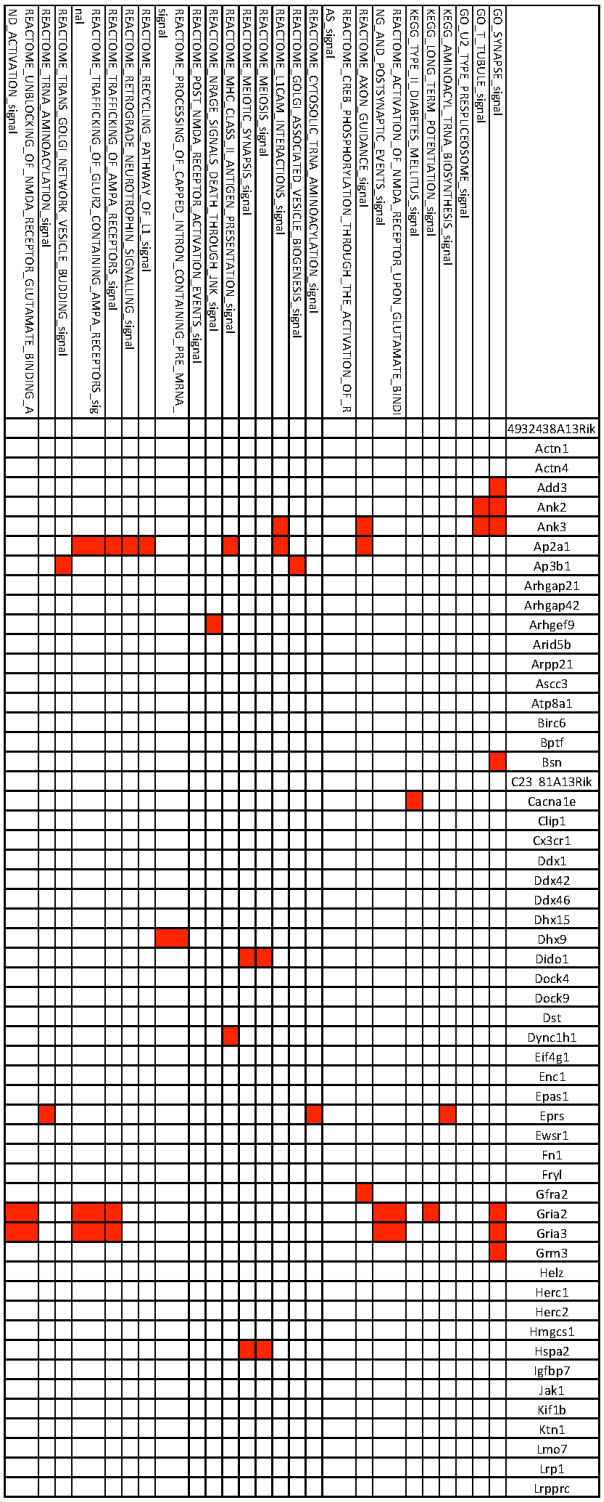

Table S8 ***(pages 157-160).*** **Heatmap of significantly upregulated gene sets and corresponding leading genes (alphabetically ordered, A-Lrpprc) in Sst^{+} neurons of defeated animals.** Columns are upregulated gene sets in defeated animals. Rows are the upregulated genes that are leading the enrichment of the gene sets (from GSEA leading edge analysis results). Only genes with also $p<0.05$ and $logFC>0.27$ are listed. When a gene is leading the enrichment of a specific gene set the square at the cross is red.

BIOCARTA_PTDINS_PATHWAY_signal
GO_ACTIN_BASED_CELL_PROJECTION_signal
GO_ACTIN_BINDING_signal
GO_ACTIN_FILAMENT_BASED_MOVEMENT_signal
GO_ACTIN_FILAMENT_BINDING_signal
GO_ACTIN_MEDIATED_CELL_CONTRACTION_signal
GO_ACTION_POTENTIAL_signal
GO_ACTIVE_ION_TRANSMEMBRANE_TRANSPORTER_ACTIVITY_signal
GO_ACTIVE_TRANSMEMBRANE_TRANSPORTER_ACTIVITY_signal
GO_ADP_BINDING_signal
GO_ANCHORING_JUNCTION_signal
GO_ANTIGEN_PROCESSING_AND_PRESENTATION_OF_PEPTIDE_ANTIGEN_VIA_MHC_CLASS_II_signal
GO_ANTIGEN_PROCESSING_AND_PRESENTATION_OF_PEPTIDE_OR_POLYSACCHARIDE_ANTIGEN_VIA_MHC_CLASS_II_signal
GO_AP_TYPE_MEMBRANE_COAT_ADAPTOR_COMPLEX_signal
GO_ATPASE_ACTIVITY_COUPLED_signal
GO_ATPASE_ACTIVITY_COUPLED_TO_MOVEMENT_OF_SUBSTANCES_signal
GO_ATPASE_ACTIVITY_signal
GO_ATPASE_COUPLED_ION_TRANSMEMBRANE_TRANSPORTER_ACTIVITY_signal
GO_AXON_INITIAL_SEGMENT_signal
GO_BASOLATERAL_PLASMA_MEMBRANE_signal
GO_CALMODULIN_BINDING_signal
GO_CARDIAC_MUSCLE_CELL_ACTION_POTENTIAL_signal
GO_CARDIAC_MUSCLE_CELL_CONTRACTION_signal
GO_CATALYTIC_STEP_2_SPLICEOSOME_signal
GO_CATION_TRANSPORTING_ATPASE_ACTIVITY_signal
GO_CELL_CELL_CONTACT_ZONE_signal
GO_CELL_CELL_JUNCTION_ASSEMBLY_signal
GO_CELL_CORTEX_signal
GO_CELL_JUNCTION_ASSEMBLY_signal
GO_CELL_JUNCTION_ORGANIZATION_signal
GO_CELL_MORPHOGENESIS_INVOLVED_IN_DIFFERENTIATION_signal
GO_CELL_SUBSTRATE_ADHESION_signal
GO_CELL_SUBSTRATE_JUNCTION_ASSEMBLY_signal
GO_CELLULAR_RESPONSE_TO_ALCOHOL_signal
GO_CLATHRIN_ADAPTOR_COMPLEX_signal
GO_CLATHRIN_COAT_OF_COATED_PIT_signal
GO_CLATHRIN_COAT_signal
GO_CLATHRIN_COATED_ENDOCYTIC_VESICLE_MEMBRANE_signal
GO_CLATHRIN_COATED_ENDOCYTIC_VESICLE_signal
GO_CLATHRIN_COATED_VESICLE_MEMBRANE_signal
GO_CLATHRIN_COATED_VESICLE_signal
GO_COATED_MEMBRANE_signal
GO_COATED_PIT_signal
GO_CONDENSED_NUCLEAR_CHROMOSOME_signal
GO_CORTICAL_CYTOSKELETON_signal
GO_CYTOPLASMIC_REGION_signal
GO_DNA_HELICASE_ACTIVITY_signal
Lrrc6
Lrrc7
Macf1
Mapk1
Mapk8ip2
Mfsd2a
Mical3
Mll1
Mon2
Mpdz
Mtap1b
Myh1
Myo18a
Nedd4
Nol6
Nrcam
Ogt
Pak7
Pclo
Pfkl
Pfkp
Pls3
Plxna4
Prpf4 a
Prpf8
Rps6ka5
Ryr2
Setd2
Sez6
Slc1a4
Slc4a4
Slc6a6
Slc8a2
Slit3
Smc3
Snrnp2
Spna2
Spnb2
Srrm2
Syn3
Syne1
Tbcd
Tjp1
Tnr
Tro
Ubr4
Unc13a
Usp24
Vps13a
Vps13c
Vps16
Wars
Wdr7
Ywhag

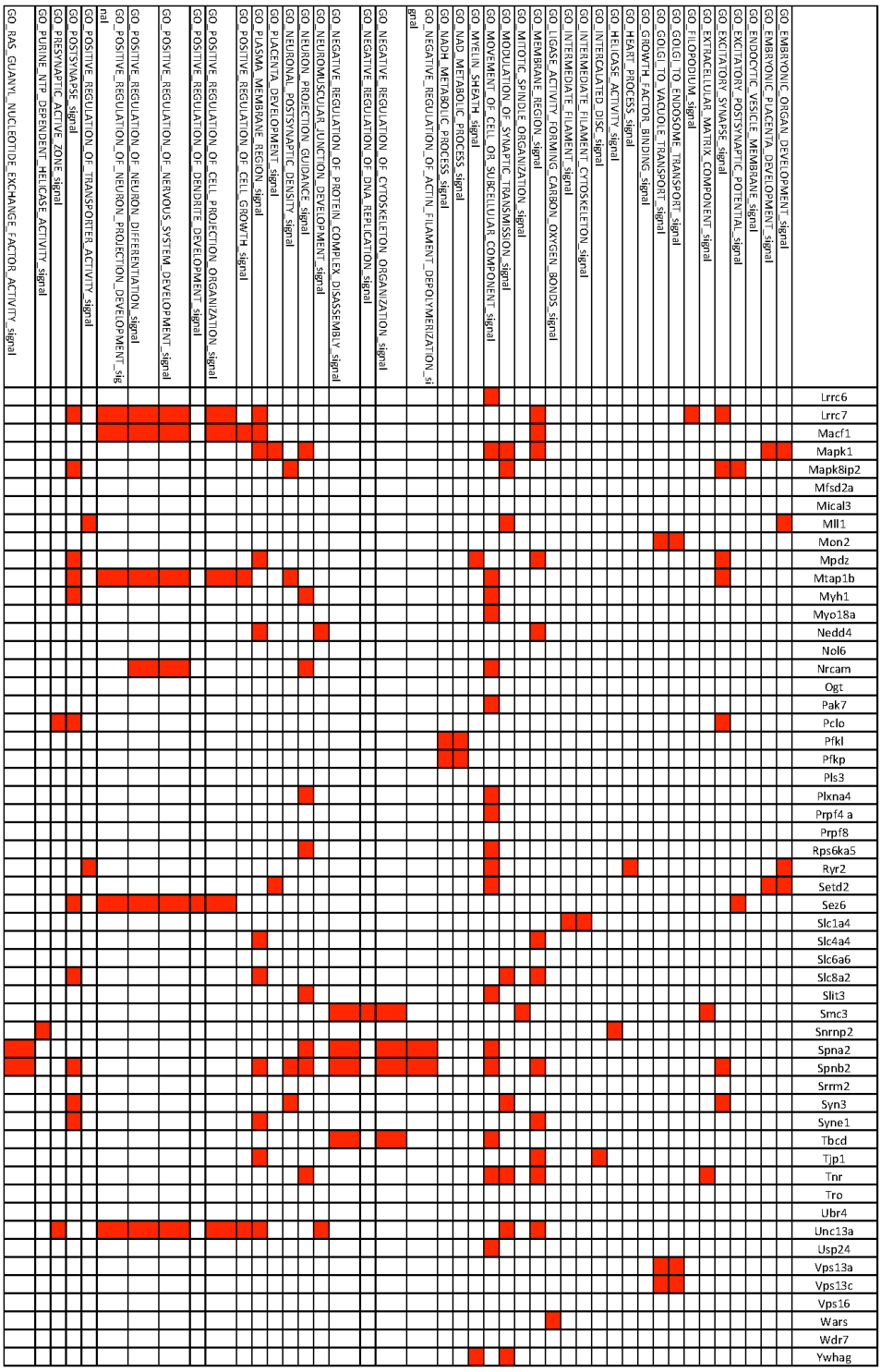
GO_EMBRYONIC_ORGAN_DEVELOPMENT_signal
GO_EMBRYONIC_PLACENTA_DEVELOPMENT_signal
GO_ENDOCYTIC_VESICLE_MEMBRANE_signal
GO_EXCITATORY_POSTSYNAPTIC_POTENTIAL_signal
GO_EXCITATORY_SYNAPSE_signal
GO_EXTRACELLULAR_MATRIX_COMPONENT_signal
GO_FILOPODIUM_signal
GO_GOLGI_TO_ENDOSOME_TRANSPORT_signal
GO_GOLGI_TO_VACUOLE_TRANSPORT_signal
GO_GROWTH_FACTOR_BINDING_signal
GO_HEART_PROCESS_signal
GO_HELICASE_ACTIVITY_signal
GO_INTERCALATED_DISC_signal
GO_INTERMEDIATE_FILAMENT_CYTOSKELETON_signal
GO_INTERMEDIATE_FILAMENT_signal
GO_LIGASE_ACTIVITY_FORMING_CARBON_OXYGEN_BONDS_signal
GO_MEMBRANE_REGION_signal
GO_MITOTIC_SPINDLE_ORGANIZATION_signal
GO_MODULATION_OF_SYNAPTIC_TRANSMISSION_signal
GO_MOVEMENT_OF_CELL_OR_SUBCELLULAR_COMPONENT_signal
GO_MYELIN_SHEATH_signal
GO_NAD_METABOLIC_PROCESS_signal
GO_NADH_METABOLIC_PROCESS_signal
GO_NEGATIVE_REGULATION_OF_ACTIN_FILAMENT_DEPOLYMERIZATION_signal
GO_NEGATIVE_REGULATION_OF_CYTOSKELETON_ORGANIZATION_signal
GO_NEGATIVE_REGULATION_OF_DNA_REPLICATION_signal
GO_NEGATIVE_REGULATION_OF_PROTEIN_COMPLEX_DISASSEMBLY_signal
GO_NEUROMUSCULAR_JUNCTION_DEVELOPMENT_signal
GO_NEURON_PROJECTION_GUIDANCE_signal
GO_NEURONAL_POSTSYNAPTIC_DENSITY_signal
GO_PLACENTA_DEVELOPMENT_signal
GO_PLASMA_MEMBRANE_REGION_signal
GO_POSITIVE_REGULATION_OF_CELL_GROWTH_signal
GO_POSITIVE_REGULATION_OF_CELL_PROJECTION_ORGANIZATION_signal
GO_POSITIVE_REGULATION_OF_DENDRITE_DEVELOPMENT_signal
GO_POSITIVE_REGULATION_OF_NERVOUS_SYSTEM_DEVELOPMENT_signal
GO_POSITIVE_REGULATION_OF_NEURON_DIFFERENTIATION_signal
GO_POSITIVE_REGULATION_OF_NEURON_PROJECTION_DEVELOPMENT_signal
GO_POSITIVE_REGULATION_OF_TRANSPORTER_ACTIVITY_signal
GO_POSTSYNAPSE_signal
GO_PRESYNAPTIC_ACTIVE_ZONE_signal
GO_PURINE_NTP_DEPENDENT_HELICASE_ACTIVITY_signal
GO_RAS_GUANYL_NUCLEOTIDE_EXCHANGE_FACTOR_ACTIVITY_signal
Lrrc6
Lrrc7
Macf1
Mapk1
Mapk8ip2
Mfsd2a
Mical3
Mll1
Mon2
Mpdz
Mtap1b
Myh1
Myo18a
Nedd4
Nol6
Nrcam
Ogt
Pak7
Pclo
Pfkl
Pfkp
Pls3
Plxna4
Prpf4 a
Prpf8
Rps6ka5
Ryr2
Setd2
Sez6
Slc1a4
Slc4a4
Slc6a6
Slc8a2
Slit3
Smc3
Snrnp2
Spna2
Spnb2
Srrm2
Syn3
Syne1
Tbcd
Tjp1
Tnr
Tro
Ubr4
Unc13a
Usp24
Vps13a
Vps13c
Vps16
Wars
Wdr7
Ywhag

GO_RECEPTOR_MEDIATED_ENDOCYTOSIS_signal
GO_REGULATION_OF_ACTION_POTENTIAL_signal
GO_REGULATION_OF_AXONOGENESIS_signal
GO_REGULATION_OF_CALCIUM_ION_IMPORT_signal
GO_REGULATION_OF_CARDIAC_MUSCLE_CONTRACTION_BY_REGULATION_OF_THE_RELEASE_OF_SEQUESTERED_CALCIUM_ION_signal
GO_REGULATION_OF_CATION_TRANSMEMBRANE_TRANSPORT_signal
GO_REGULATION_OF_CELL_GROWTH_signal
GO_REGULATION_OF_CELL_MATRIX_ADHESION_signal
GO_REGULATION_OF_CELL_PROJECTION_ORGANIZATION_signal
GO_REGULATION_OF_CELL_SIZE_signal
GO_REGULATION_OF_CELL_SUBSTRATE_ADHESION_signal
GO_REGULATION_OF_DENDRITE_DEVELOPMENT_signal
GO_REGULATION_OF_EXTENT_OF_CELL_GROWTH_signal
GO_REGULATION_OF_GTPASE_ACTIVITY_signal
GO_REGULATION_OF_MUSCLE_ADAPTATION_signal
GO_REGULATION_OF_NERVOUS_SYSTEM_DEVELOPMENT_signal
GO_REGULATION_OF_NEURON_DIFFERENTIATION_signal
GO_REGULATION_OF_NEURON_PROJECTION_DEVELOPMENT_signal
GO_REGULATION_OF_NEURONAL_SYNAPTIC_PLASTICITY_signal
GO_REGULATION_OF_POSTSYNAPTIC_MEMBRANE_POTENTIAL_signal
GO_REGULATION_OF_RELEASE_OF_SEQUESTERED_CALCIUM_ION_INTO_CYTOSOL_signal
GO_REGULATION_OF_RHO_PROTEIN_SIGNAL_TRANSDUCTION_signal
GO_REGULATION_OF_SHORT_TERM_NEURONAL_SYNAPTIC_PLASTICITY_signal
GO_REGULATION_OF_SMOOTH_MUSCLE_CELL_MIGRATION_signal
GO_REGULATION_OF_SODIUM_ION_TRANSMEMBRANE_TRANSPORTER_ACTIVITY_signal
GO_REGULATION_OF_SODIUM_ION_TRANSMEMBRANE_TRANSPORT_signal
GO_REGULATION_OF_SODIUM_ION_TRANSPORT_signal
GO_REGULATION_OF_SYNAPSE_STRUCTURE_OR_ACTIVITY_signal
GO_REGULATION_OF_SYNAPTIC_PLASTICITY_signal
GO_REGULATION_OF_SYNAPTIC_TRANSMISSION_GLUTAMATERGIC_signal
GO_REGULATION_OF_TRANSPORTER_ACTIVITY_signal
GO_RHO_GUANYL_NUCLEOTIDE_EXCHANGE_FACTOR_ACTIVITY_signal
GO_RNA_HELICASE_ACTIVITY_signal
GO_SECOND_MESSENGER_MEDIATED_SIGNALING_signal
GO_SISTER_CHROMATID_COHESION_signal
GO_SODIUM_CHANNEL_REGULATOR_ACTIVITY_signal
GO_STRIATED_MUSCLE_CONTRACTION_signal
GO_STRUCTURAL_CONSTITUENT_OF_CYTOSKELETON_signal
GO_SUBSTRATE_ADHESION_DEPENDENT_CELL_SPREADING_signal
GO_SYNAPSE_PART_signal
Lrrc6
Lrrc7
Macf1
Mapk1
Mapk8ip2
Mfsd2a
Mical3
Mll1
Mon2
Mpdz
Mtap1b
Myh1
Myo18a
Nedd4
Nol6
Nrcam
Ogt
Pak7
Pclo
Pfkl
Pfkp
Pls3
Plxna4
Prpf4 a
Prpf8
Rps6ka5
Ryr2
Setd2
Sez6
Slc1a4
Slc4a4
Slc6a6
Slc8a2
Slit3
Smc3
Snrnp2
Spna2
Spnb2
Srrm2
Syn3
Syne1
Tbcd
Tjp1
Tnr
Tro
Ubr4
Unc13a
Usp24
Vps13a
Vps13c
Vps16
Wars
Wdr7
Ywhag

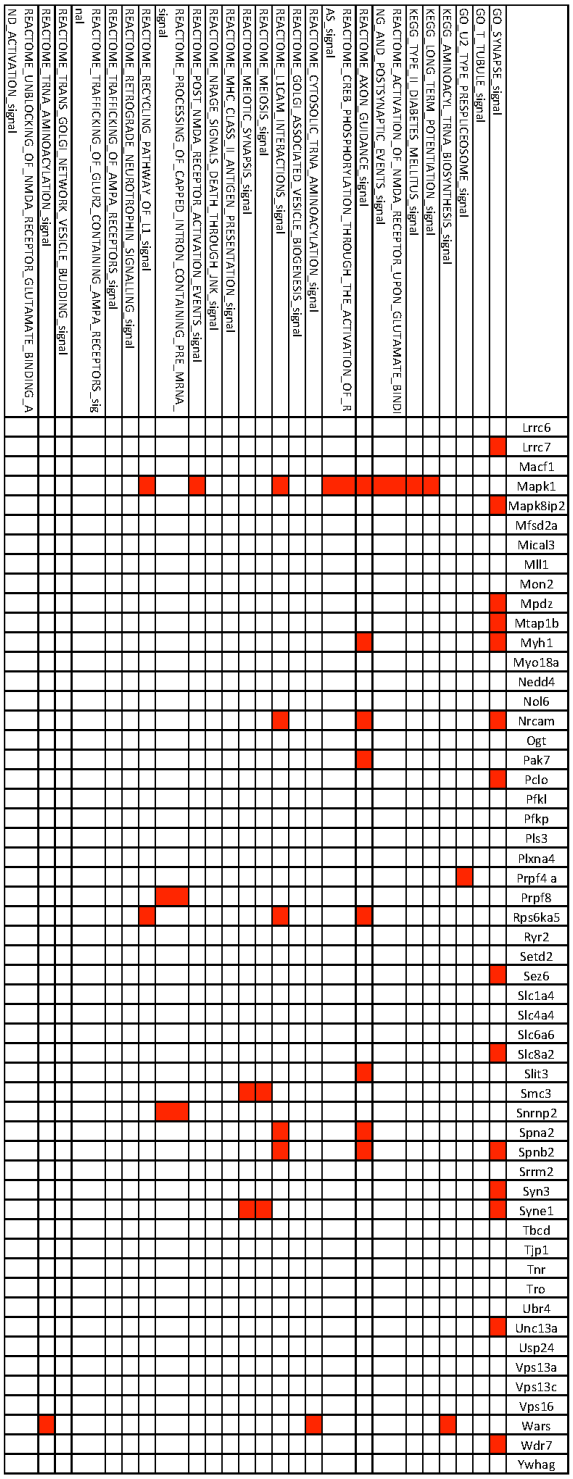

Table S9 ***(pages 161-164).*** **Heatmap of significantly upregulated gene sets and corresponding leading genes (alphabetically ordered, Lrrc6-Z)) in Sst^{+} neurons of defeated animals.** Columns are upregulated gene sets in defeated animals. Rows are the upregulated genes that are leading the enrichment of the gene sets (from GSEA leading edge analysis results). Only genes with also $p<0.05$ and $logFC>0.27$ are listed. When a gene is leading the enrichment of a specific gene set the square at the cross is red.